



**HAL**  
open science

# Synthesis of monolayer graphene on polycrystalline Ni and Ni-Cu bimetallic catalyst and study toward reuse of catalyst

Choon-Ming Seah

► **To cite this version:**

Choon-Ming Seah. Synthesis of monolayer graphene on polycrystalline Ni and Ni-Cu bimetallic catalyst and study toward reuse of catalyst. Other. Université de Lorraine, 2015. English. NNT : 2015LORR0281 . tel-01752204

**HAL Id: tel-01752204**

**<https://hal.univ-lorraine.fr/tel-01752204v1>**

Submitted on 29 Mar 2018

**HAL** is a multi-disciplinary open access archive for the deposit and dissemination of scientific research documents, whether they are published or not. The documents may come from teaching and research institutions in France or abroad, or from public or private research centers.

L'archive ouverte pluridisciplinaire **HAL**, est destinée au dépôt et à la diffusion de documents scientifiques de niveau recherche, publiés ou non, émanant des établissements d'enseignement et de recherche français ou étrangers, des laboratoires publics ou privés.



## AVERTISSEMENT

Ce document est le fruit d'un long travail approuvé par le jury de soutenance et mis à disposition de l'ensemble de la communauté universitaire élargie.

Il est soumis à la propriété intellectuelle de l'auteur. Ceci implique une obligation de citation et de référencement lors de l'utilisation de ce document.

D'autre part, toute contrefaçon, plagiat, reproduction illicite encourt une poursuite pénale.

Contact : [ddoc-theses-contact@univ-lorraine.fr](mailto:ddoc-theses-contact@univ-lorraine.fr)

## LIENS

Code de la Propriété Intellectuelle. articles L 122. 4

Code de la Propriété Intellectuelle. articles L 335.2- L 335.10

[http://www.cfcopies.com/V2/leg/leg\\_droi.php](http://www.cfcopies.com/V2/leg/leg_droi.php)

<http://www.culture.gouv.fr/culture/infos-pratiques/droits/protection.htm>



**UNIVERSITÉ  
DE LORRAINE**

Université de Lorraine  
Secteur Physique Géosciences Chimie Mécanique  
Faculté des Sciences et Technologies  
Institut Jean Lamour-CP2S-équipe 205  
Ecole doctorale EMMA

---

**Thèse**

Présentée pour l'obtention du titre de  
**Docteur de l'Université de Lorraine**  
En Chimie spécialité Sciences des matériaux

Par **Choon-Ming SEAH**

**Synthesis of monolayer graphene on polycrystalline Ni and Ni-Cu  
bimetallic catalyst and study toward reuse of catalyst**

Soutenance publique le 15 décembre 2015 :  
(Thèse en Co-Tutelle avec Universiti Sains Malaysia)

Membres du jury :

<b>Rapporteurs :</b>	Prof. Noraishah Saidina AMIN (président du jury)	Professeur, Faculty of Chemical Engineering, Universiti Teknologi Malaysia, Johor, Malaysia
	Dr. Johann CORAUX	Chargé de Recherche (CNRS), Institut NÉEL, Grenoble, France
<b>Directeurs de thèse :</b>	Prof. Abdul Rahman MOHAMED	Professeur, School of Chemical Engineering, Universiti Sains Malaysia, Nibong Tebal, Malaysia
	Dr. Brigitte VIGOLO	Chargée de Recherche (CNRS), Institut Jean Lamour, Nancy, France
<b>Invité :</b>	Dr. Chai Siang PIAO	Professeur Assistant, Monash University Sunway Campus, Malaysia



**SYNTHESIS OF MONOLAYER GRAPHENE ON POLYCRYSTALLINE  
NICKEL AND NICKEL-COPPER BIMETALLIC CATALYST AND STUDY  
TOWARD THE REUSE OF NICKEL CATALYST**

**by**

**SEAH CHOON MING**

**Thesis submitted in fulfillment of the requirements**

**for the degree of**

**Doctor of Philosophy**

**February 2016**

## ACKNOWLEDGMENT

This thesis is the end of my journey in obtaining my PhD degree. Throughout the journey, I have worked with a great number of peoples whose contribution deserved special mention. It is a pleasure to deliver my gratitude to them all in my humble acknowledgement.

Foremost, I would like to thank my parents and family members for their encouragement and support throughout my pursuance of PhD degree in Universiti Sains Malaysia (USM) and Université de Lorraine. Words failed me to express my appreciation to my family members. They deserve special mention for their inseparable support and persistent confidence in me.

My deepest appreciation also goes to all of my dedicated supervisors, Prof. Abdul Rahman Mohamed, Dr Brigitte Vigolo and Dr Chai Siang Piao for the continuous support of my study and research. I thank them for the unflinching support in various ways, which greatly inspire and enrich my growth as a student and researcher. Their patient, enthusiasm, motivation and guidance helped me in all the time of research and thesis writing, their advices, supervisions, and suggestions, which made them a backbone of this research. Their involvement with his originality has inspired and kindled me. In addition to that, I am much indebted for their valuable advice and critical comment, which I grateful in every possible way

During this research work, I have collaborated with many colleagues, and I wish to extend my warmest thank to all those who have helped me with my research work. Many thanks to Assoc. Prof. Satoshi Ichikawa and from Osaka University, who kindly granted me his time to perform HR-TEM observation on my samples, and for answering some of my questions about the HR-TEM images captured. I also thank Professor Tadashi Itoh for giving me the opportunity to work on their HR-

TEM equipment in the Institute of NanoScience Design, Osaka University. I greatly benefited from their advice, and I thank for their willingness to share their bright though with me. The visit to Osaka University was really a great and memorable experience, which was very fruitful for shaping up my ideas and research.

Special thanks to Dr Jaafar Ghanbaja from Institut Jean Lamour, for his technical assistance in HRTEM characterization. To Dr Jérôme Gleize and Pascal Franchetti from Laboratoire de Chimie Physique-Approche Multi-échelle de Milieux Complexes-Université de Lorraine, for the kind technical help and expertise during Raman measurements. To Dr François Le Normand and Mr Fitsum Aweke from ICUDE, CNRS-Université de Strasbourg in XPS and sheet resistance measurement and to Dr Pascal Boulet from École des Mines in XRD measurement. I gratefully thank all the staffs of School of Chemical Engineering, USM and colleague in Group 205, Institut Jean Lamour, Université de Lorraine for all the kind supports and advices.

Collective and individual acknowledgement are also owed to my colleagues and friends whose present in some manner perpetually refreshed, helpful and memorable. Many thanks to all my friends for their unparalleled help, kindness and moral supports towards me. I enjoyed and treasured the time we spent together and my journey will be totally different without you all. I thank everybody who was important to the successful realization of this thesis, as well as expressing my apology that I forgot to mention personally one by one.

Last but not least, the financial support provided by USM Fellowship and Les Bourses du Gouvernement Français are greatly acknowledged.

Thank you very Much!  
Merci Beaucoup!  
SEAH CHOON MING  
February 2016

## TABLE OF CONTENTS

Acknowledgement.....	ii
Table of Content.....	iv
List of Tables .....	viii
List of Figures.....	ix
List of Abbreviations.....	xvi
List of Symbol.....	xvii
Abstrak .....	xx
Abstract.....	xxii
Résumé.....	xxiv
 CHAPTER 1 - INTRODUCTION	
1.1 Nanotechnology .....	1
1.2 Carbon element.....	3
1.3 Graphene.....	4
1.4 Methane.....	5
1.5 Problem statement.....	7
1.6 Objectives.....	9
1.7 Scope of study.....	9
1.8 Organization of the thesis.....	11
 CHAPTER 2 - LITERATURE REVIEW	
2.1 Introduction.....	13
2.2 Properties of graphene.....	14
2.3 Methods of graphene synthesis.....	15



2.3.1	Mechanical exfoliation.....	16
2.3.2	Wet chemical exfoliation.....	16
2.3.3	Sublimation of SiC.....	17
2.3.4	Chemical vapour deposition.....	19
	2.3.4(a) Hydrogen .....	21
	2.3.4(b) Temperature.....	22
	2.3.4(c) Carbon precursor.....	24
	2.3.4(d) Pressure.....	25
2.4	Catalysts.....	26
	2.4.1 Ruthenium (Ru).....	27
	2.4.2 Iridium (Ir).....	29
	2.4.3 Platinum (Pt).....	30
	2.4.4 Nickel (Ni).....	32
	2.4.5 Copper (Cu).....	36
	2.4.6 Nickel-Copper Bicycatalyst (Ni-Cu) .....	43
2.5	Transfer of graphene.....	44
	2.5.1 Mechanical exfoliation.....	44
	2.5.2 Wet chemical etching.....	49
	2.5.2(a) Etchants.....	55
	2.5.2(b) Protective layers.....	57
2.6	Reuse of catalyst.....	61
2.7	Summary.....	63
<b>CHAPTER 3 - MATERIALS AND METHODS</b>		
3.1	Materials and Chemicals.....	64

3.2	Experimental equipment and rig set-up.....	66
3.2.1	Graphene growth rig.....	66
3.2.1(a)	Gas mixing section.....	66
3.2.1(b)	Reaction section.....	67
3.3	Experimental steps.....	74
3.3.1	Catalyst preparation.....	75
3.3.2	Production of graphene by CVD and process study.....	75
3.3.3	Controlled experiment for bilayer catalyst.....	77
3.3.4	Graphene separation.....	78
3.3.5	Study on the reuse and recycle of catalyst.....	79
3.4	Characterization.....	79
3.4.1	Raman spectroscopy.....	79
3.4.2	Atomic force microscopy.....	81
3.4.3	X-ray Diffraction .....	81
3.4.4	High Resolution Transmission Electron Microscopy (HRTEM), electron diffraction and Energy Dispersive Spectrometer (EDS).....	82

## CHAPTER 4 - RESULTS AND DISCUSSIONS

4.1	Preliminary studies.....	84
4.1.1	Blank test on methane decomposition and preliminary studies of Ni and Cu foil for graphene formation.....	84
4.1.2	Preliminary test of graphene separation from Ni and Cu .....	87
4.2	Graphene formation on polycrystalline Cu foil.....	89

4.2.1	Temperature.....	89
4.2.2	Growth duration.....	91
4.2.3	Methane partial pressure.....	92
4.2.4	Summary.....	94
4.3	Graphene formation on polycrystalline Ni foil.....	94
4.3.1	Temperature.....	95
4.3.2	Growth duration.....	99
4.3.3	Methane partial pressure.....	105
4.3.4	Discussion .....	108
4.4	Graphene formation on a bilayer Ni-Cu catalyst.....	113
4.4.1	Temperature.....	115
4.4.2	Growth duration.....	119
4.4.3	Methane partial pressure.....	123
4.4.4	Discussion .....	125
4.5	Reuse and recycle of catalyst.....	130
4.5.1	Nitric acid.....	132
4.5.2	Iron nitrate solution.....	134
4.5.3	Discussion.....	138
<b>CHAPTER 5- CONCLUSION AND RECOMMENDATIONS</b>		
5.1	Conclusions.....	149
5.2	Recommendations.....	151
	<b>REFERENCES.....</b>	<b>153</b>

**LIST OF TABLES**

	Page	
Table 1.1	Composition of raw natural gas (Gas Malaysia, 2011).	6
Table 2.1	General properties of transition metals mainly used to catalyse graphene growth.	45
Table 3.1	List of chemicals and regents.	64
Table 3.2	Major component of the experiment rig and their function.	70
Table 3.3	Parameters list for CCVD study.	77
Table 3.4	Characteristic of different types of graphene in Raman spectra.	81
Table 4.1	Methane conversion recorded in the blank test.	86

## LIST OF FIGURE

		Page
Figure 1.1	Diagram showing the nanotechnology region (Freie Universität Berlin, 2015)	2
Figure 1.2	Structures of selected allotropes of carbon. (Oganov <i>et al.</i> , 2013)	4
Figure 2.1	Graphene, the fundamental block of all dimensional carbon materials, such as fullerene (green), CNT (magenta) and graphite (cyan). (Geim and Novoselov, 2007)	14
Figure 2.2	Sketch of graphene formation steps on (a) Ni and (b) Cu (Losurdo <i>et al.</i> , 2011).	20
Figure 2.3	Summary of the interaction between graphene and transition metals. Yellow-labelled elements indicate weak interactions, and red and blue can be attributed to strong interactions and graphene grown from bulk carbide, respectively. “d” is the distance between graphene and metal (in scale of Angstrom), “c” indicates the buckling and corrugation of graphene (in scale of Angstrom), and “ $\pi$ ” refers to the amount of downward shift of the Dirac point of graphene mounted on respective transition metals. ‘S’ or ‘M’ in the upper right corner of each element-box indicates if graphene forms single or multiple rotational domains (Batzill, 2012).	27
Figure 2.4	Graphene formation on (a) a single-crystal Ni(111) surface and (b) a polycrystalline Ni surface (Zhang <i>et al.</i> , 2010).	35
Figure 2.5	Illustration of the surface growth mechanism on Cu. Black particles indicate $^{13}\text{C}$ isotope, red particles indicate $^{12}\text{C}$ isotope and white particle indicates hydrogen (Li <i>et al.</i> , 2009b).	37
Figure 2.6	SEM images of graphene with (a) a hexagonal shape (Robertson and Warner, 2011), (b) a four-lobed flower shape (Li <i>et al.</i> , 2010), and (c) a dendrite shape (Fan <i>et al.</i> , 2011).	38
Figure 2.7	(a) Flow diagrams of the transfer process with heat treatment for (a) perforated substrate and (b) flat substrate (Suk <i>et al.</i> , 2011).	53

Figure 2.8	Schematic of the direct transfer of graphene onto a TEM grid (Regan <i>et al.</i> , 2010).	55
Figure 2.9	Schematic of the roll-based production of graphene films grown on a copper foil (Bae <i>et al.</i> , 2010).	61
Figure 2.10	Schematic of an electrolysis cell used for the electrochemical exfoliation of graphene from metal foil (Wang <i>et al.</i> , 2011c).	62
Figure 3.1	Photograph of the experimental rig set-up (Descriptions of parts according to numbers listed in Table 3.2).	68
Figure 3.2	Schematic diagram of the experimental rig set-up.	69
Figure 3.3	Flowchart of overall research activities of this study.	74
Figure 3.4	Cross-section view of the Cu-wrapped Ni catalyst that used for study.	75
Figure 3.5	Setup of the reaction zone of the reactor for the implication of fast cooling.	76
Figure 3.6	The built-up of the (a) Cu- SiO <sub>2</sub> -Ni and (b) Cu-Ni- SiO <sub>2</sub> catalysts used for the control experiment.	77
Figure 3.7	The steps for the sample preparation for obtaining EDS spectrum at the middle of Ni.	83
Figure 4.1	TEM images of the black powder collected on the wall of the quartz tube that underwent CVD of 1150 °C. (a) Low magnification image and (b) High magnification image.	86
Figure 4.2	Raman spectra of graphitic materials grown on Ni and Cu with operating parameters of 950 °C, 10 min, 80 sccm of H <sub>2</sub> and 80 sccm of CH <sub>4</sub> .	87
Figure 4.3	Photographs of the graphene separation process by nitric acid with various concentrations (a) 21.67 %, (b) 6.7 % and (c) 3.35 %. The boxed area indicated the location of graphene.	88
Figure 4.4	Raman spectra of the graphitic materials grown on Cu foil with various temperatures. The growth duration was fixed at 5 min and 20 sccm of CH <sub>4</sub> was diluted into 80 sccm of H <sub>2</sub> .	90
Figure 4.5	Raman spectra of graphitic materials grown on Cu foil with various CVD durations at 950 °C and under 20 sccm of CH <sub>4</sub> diluted into 80 sccm of H <sub>2</sub> .	92
Figure 4.6	Raman spectra of graphitic materials grown on Cu foil with various partial pressure of CH <sub>4</sub> . The growth duration was fixed at 5 min, and temperature was 950 °C.	93

Figure 4.7	Raman spectra of graphitic materials grown on Ni foil with various CVD temperatures at 5 min and under 20 sccm of CH <sub>4</sub> diluted into 80 sccm H <sub>2</sub> .	96
Figure 4.8	Raman maps showing I <sub>2D</sub> /I <sub>G</sub> for graphene grown on Ni at (a) 800 °C, (c) 850 °C and (e) 900 °C and fwhm <sub>2D</sub> of graphene grown at (b) 800 °C, (d) 850 °C and (f) 900 °C. The growth duration was fixed at 5 min under the flow of 20 sccm of CH <sub>4</sub> diluted into 80 sccm of H <sub>2</sub> . Scale of maps 50µm x 50 µm.	97
Figure 4.9	HRTEM images of graphene grown on Ni at (a) 800 °C, (b) 850 °C and (c) 900 °C for 5 min under 20 sccm of CH <sub>4</sub> diluted into 80 sccm of H <sub>2</sub> .	98
Figure 4.10	Photograph of graphene sheet separated and deposited on a silicon wafer grown at 850 °C with 20 sccm of methane diluted into 80 sccm of hydrogen for (left) 4 min and (left) 5 min.	99
Figure 4.11	Raman spectra of graphitic materials grown on Ni foil with various CVD durations at 850 °C under the flow of 20 sccm of CH <sub>4</sub> diluted into 80 sccm of H <sub>2</sub> .	100
Figure 4.12	Images from optical microscopy of graphene sheets separated and deposited onto a silicon wafer. Growth conditions: 850 °C, 20 sccm of methane diluted into 80 sccm of hydrogen for (a) 4 min and (b) 5 min.	101
Figure 4.13	Raman maps of (a) I <sub>2D</sub> /I <sub>G</sub> and (b) fwhm <sub>2D</sub> for graphene grown on Ni at 850 °C for 4 min under 20 sccm of CH <sub>4</sub> diluted into 80 sccm of H <sub>2</sub> .	101
Figure 4.14	HRTEM image of graphene grown on Ni foil at 850 °C for 4 min under 20 sccm of CH <sub>4</sub> and 80 sccm of H <sub>2</sub> .	101
Figure 4.15	Photograph of graphene sheets separated and deposited onto a silicon wafer. Growth conditions: 800 °C, 20 sccm of methane diluted into 80 sccm hydrogen for (left) 5 min (center), 6 min and (left) 7 min.	103
Figure 4.16	Raman spectra of graphitic materials grown on Ni foil with various CVD durations at 800 °C under 20 sccm of CH <sub>4</sub> diluted into 80 sccm of H <sub>2</sub> .	103
Figure 4.17	Micrographs of the graphene sheets separated and deposited onto a silicon wafer. Growth conditions: 800 °C, 20 sccm of methane diluted into 80 sccm hydrogen for (a) 5 min (b) 6 min and (c) 7 min.	104

Figure 4.18	Typical HRTEM image of graphene grown on Ni foil at 800 °C for 6 min under 20 sccm of CH <sub>4</sub> diluted into 80 sccm of H <sub>2</sub> .	104
Figure 4.19	Raman maps of I <sub>2D</sub> /I <sub>G</sub> for graphene grown on Ni at (a) 6 min and (c) 7 min of reaction and fwhm <sub>2D</sub> map of graphene grown for (b) 6 min and (d) 7 min at 800 °C under of 20 sccm of CH <sub>4</sub> diluted into 80 sccm of H <sub>2</sub> .	105
Figure 4.20	Raman spectra of graphitic materials grown on Ni foil with various partial pressure of CH <sub>4</sub> at 850 °C and for 5 min.	106
Figure 4.21	Photograph of graphene sheets separated and deposited onto a silicon wafer. Growth conditions: 850 °C for 5 min with various methane partial pressure of (left) 0.1 atm, (center) 0.2 atm and (right ) 0.3 atm.	107
Figure 4.22	Micrographs of the graphene sheets grown at 850 °C for 5 min and under methane partial pressure of (a) 0.1 atm, (b) 0.2 atm, (c ) 0.3 atm and (d) 0.4 atm after separation and deposition onto silicon wafer.	107
Figure 4.23	Phase diagram of nickel-carbon (left) and copper-carbon (right) bulk system.	108
Figure 4.24	Cross-section view of the used bimetallic catalyst consisting of a Cu foil wrapping a Ni foil.	115
Figure 4.25	Average and standard deviation of I <sub>2D</sub> /I <sub>G</sub> of graphene film obtained from graphene films grown on the 4 different surfaces of the CVD device in the temperature range 850 °C - 1000 °C for 5 min.	116
Figure 4.26	Micrographs of graphene grown at 950 °C for 5 min at the inner surfaces of (a) Ni and (b) Cu after transfer on silicon wafer.	117
Figure 4.27	Raman maps of I <sub>2D</sub> /I <sub>G</sub> for graphene grown on (a) Ni and (b) Cu, and fwhm <sub>2D</sub> for (c) Ni and (d) Cu at 950 °C for 5 min. The color gradient bar is given on the right of each map.	118
Figure 4.28	HRTEM images of monolayer graphene grown on inner surface of (a) Ni and (b) Cu at the edges, after CVD reaction at 950 °C for 5 min.	118
Figure 4.29	Average and standard deviation of I <sub>2D</sub> /I <sub>G</sub> of graphene film obtained from graphene film grown on the 4 different surfaces of the CVD device at 950 °C and for durations in the 4-8 min range.	119



Figure 4.30	Micrographs of the graphene materials transferred to silicon wafer after CVD growth for 4 min on (a) Ni and on (b) Cu; for 6 min on (c) Ni and (d) Cu; and for 7 min on (e) Ni and (f) Cu.	121
Figure 4.31	Raman maps of $I_{2D}/I_G$ for graphene grown on (a) Ni and (b) Cu, and $fwhm_{2D}$ for (c) Ni and (d) Cu at 950 °C for 4 min. The color gradient bar is given on the right of each map.	122
Figure 4.32	HRTEM images of monolayer graphene grown on inner surface of (a) Ni and (b) Cu at the edges. Growth conditions: 950 °C and 4 min.	122
Figure 4.33	Average and standard deviation of $I_{2D}/I_G$ of graphene films obtained at the 4 different surfaces of the CVD device at 950 °C for 5 min, the range of methane partial pressures being 0.2-0.6 atm.	123
Figure 4.34	Micrographs of graphene grown at the inner surface of (a) Ni and (b) Cu under methane partial pressure of 0.3 atm, respectively after transfer to silicon wafer (temperature growth 950 °C and duration 5 min).	123
Figure 4.35	Raman maps of $I_{2D}/I_G$ for graphene grown on (a) Ni and (b) Cu, and $fwhm_{2D}$ for (c) Ni and (d) Cu at 950°C for 5 min, and methane partial pressure of 0.3. The color gradient bar is given on the right of each map.	124
Figure 4.36	HRTEM images of monolayer graphene grown on inner surface of (a) Ni and (b) Cu at the edges after CVD reaction at 950 °C for 5 min with a methane partial pressure of 0.3 atm.	124
Figure 4.37	TEM images of a Ni slice after the CVD reaction at 950 °C and 5 min with (a) low magnification image of the Ni strip; (b) Bright field TEM image in the area marked by the circle on the image (a); (c) Schematic showing the distribution on carbon adatoms at the middle of the Ni foil after the CVD reaction; grey areas indicating the grains of Ni and black dots illustrating the carbon adatoms.	127
Figure 4.38	EDS spectra of the cross-section area at the middle of the Ni foil as shown in Figure 4.37 at the middle of the grain in red at the grain boundary in black; magnified range from 0-1 keV is inserted at left top corner.	127
Figure 4.39	Pathways of carbon diffusion through the polycrystalline Ni foil at (a) 950 °C and (b) 1030 °C through the grain boundary of Ni (black arrows) and through the Ni grain (red arrows).	129

Figure 4.40	Optical micrograph of the web-like graphitic carbon grown at the inner surface of Ni at 1030 °C for 3 min.	129
Figure 4.41	Separation of bilayer graphene from Ni foil by nitric acid. (a) Beginning of the process. (b) Completely separated bilayer graphene, Ni foil is submerged into nitric acid and the white box helps to locate the separated graphene floating at the solution surface.	133
Figure 4.42	Photograph of the Ni foil covered with monolayer graphene in a solution of iron nitrate of a concentration of 0.2 mol/L after 2 days.	135
Figure 4.43	(a) Progress for bilayer graphene separation from Ni foil in iron nitrate solution (0.50 mol/L) from left to right; the white box indicating the separated graphene. (b) Photograph of the six bilayer graphenes after transfer on silicon wafer (with 1000 Å silicon oxide) obtained from their respective cycle, white boxes indicating the locations of graphene. (c) HRTEM image of the bilayer graphene separated under the sixth cycle.	136
Figure 4.44	(a) Raman spectra for six bilayer graphene samples after separation from Ni foil and transfer onto a silicon/silicon oxide wafer. Raman maps of (b) $\text{fwhm}_{2\text{D}}$ and (c) $\text{I}_{2\text{D}}/\text{I}_{\text{G}}$ of the bilayer graphene grown under the sixth cycle.	137
Figure 4.45	XRD patterns of the nickel foil after CVD growth of (black) monolayer graphene, (blue) bilayer graphene and (red) multilayer graphene.	139
Figure 4.46	AFM images for (a) the nickel foil before the CVD reaction, (b) the nickel foil after CVD reaction and separation with iron nitrate, (c) nickel foil after the CVD reaction and separation with nitric acid and (d) the nickel foil obtained after the separation process by the iron nitrate solution and polished with sand paper (800 mesh). The dimensions for all the images are 15 $\mu\text{m}$ x 15 $\mu\text{m}$ .	141
Figure 4.47	Optical images of graphene transferred from Ni foil for (a) graphene grown on a fresh new Ni foil, (b) graphene grown on unpolished Ni foil after separation with iron nitrate for the preceding graphene growth (c) graphene grown on unpolished Ni foil after separation with nitric acid for the preceding graphene growth. Areas with gold color are contaminations by nickel.	142
Figure 4.48	XRD patterns of the nickel foil after the CVD reaction (red), after the CVD reaction and graphene separation using iron nitrate (blue) and nitric acid (black).	143

- Figure 4.49 Schematic illustrating interactions and etching mechanism during the separation of graphene with (a) a smooth surface and (b) a corrugated surface. The particles indicating the Ni grains, black line represents the graphene layer and the arrows show interacting paths. (c) HRTEM image for encapsulated Ni particles in graphene that grown from Ni with rough surface. 144
- Figure 4.50 Schematic diagram of graphene and Ni<sub>3</sub>C formation. (a) At elevated temperature, methane decomposes at the surface and carbon adatoms dissolve into Ni foil. (b) Graphene formation by segregation of carbon from Ni above a threshold during the cooling process. (c) Very rapid cooling: inhibition of carbon diffusion to the surface of Ni. Red circles indicating hydrogen, meanwhile black circle represent carbon atoms. 148

## LIST OF SYMBOLS

%	Percent
$\pi$	pi
$^{\circ}\text{C}$	Degree Celcius
$\text{\AA}$	Angstrom

## LIST OF ABBREVIATIONS

$\mu\text{m}$	Micron
AFM	Atomic force microscopy
Ar	Argon
at%	Atomic percentage
atm	Atmospheric pressure
Au	Gold
C	Carbon
CH <sub>4</sub>	Methane
C <sub>2</sub> H <sub>6</sub>	Ethane
C <sub>3</sub> H <sub>8</sub>	Propane
C <sub>4</sub> H <sub>10</sub>	Butane
Co	Cobalt
Cu	Copper
cm	Centimeter
CVD	Chemical vapor deposition
C60	Buckminsterfullerene
CO <sub>2</sub>	Carbon dioxide
CNT	Carbon nanotube
D	Diameter
DFT	Density functional theory
EDS	Energy dispersive spectrometer
EVA	Poly(ethylene co-vinyl acetate)
Fe	Iron
fwhm <sub>2D</sub>	Full width half maximum of 2D-band
GC	Gas Chromatography
GO	Graphene oxide
H <sub>2</sub>	Hydrogen gas
H <sub>2</sub> S	Hydrogen Sulfide

He	Helium
HNO <sub>3</sub>	Acid nitrate
HOPG	Highly ordered pyrolytic graphite
HRTEM	High resolution transmission electron microscope
ICT	Information and communication technology
I <sub>2D</sub> /I <sub>G</sub>	Intensity ratio of 2D-band over G-band
IPA	Isopropyl alcohol
Ir	Iridium
J	Joule
K	Kelvin
keV	Kilo electron Volt
KOH	Potassium hydroxide
kV	KiloVolt
L	Length
m	meter
MD	Molecular dynamics
min	Minute
MIT	Massachusetts Institute of Technology
MET	Mechano-electro-thermal
ML	Monolayer
mm	Milimeter
Mg	Magnesium
MOHE	Ministry of Higher Education
mol/L	Mol per liter
MOSTI	Ministry on Science, Technology & Innovation
MR	Member ring
mW	MegaWatt
N <sub>2</sub>	Nitrogen
NaOH	Sodium hydroxide
Ne	Neon

Ni	Nickel
Ni <sub>3</sub> C	Nickel carbide
Ni TFB	Transene Thin Film Nickel Etchants
nm	Nanometer
O	Oxygen
O <sub>2</sub>	Oxygen gas
OD	Outer diameter
Pa	Pascal
PBU	Polybutadiene
PC	Poly(bisphenol-A-carbonate)
PDMS	Polydimethylsiloxane
PECVD	Plasma enhanced chemical vapor deposition
PET	Polyethylene terephthalate
PI	Polyimide
PMMA	Poly(methyl methacrylate),
Pt	Platinum
R2R	Roll-to-roll
R&D	Research and Development
Ru	Ruthenium
s	Second
sccm	Standard cubic centimeter
SiC	Silicon carbide
SiO <sub>2</sub>	Silicon oxide
SSPO1	2-(diphenylphosphoryl) spirofluorene
SW	Stone–Wales
TCD	Thermal conductivity detector
TEM	Transmission electron microscopy
Tpa	Terapascal
TRT	Thermal release tape
UHV	Ultra high vacuum
USA	United State of America
V	Volt

Xe

Xenon

XRD

X-ray Di fraction

**PENUMBUHAN GRAFENA BERLAPIS TUNGGAL PADA NIKEL  
POLIHABLURAN DAN PEMANGKIN DWILOGAM NIKEL-KUPRUM DAN  
KAJIAN UNTUK PENGGUNAAN SEMULA PEMANGKIN NIKEL**

**ABSTRAK**

Grafena merupakan struktur karbon dengan ketebalan satu atom. Grafena terdedah semua atomnya ke medium sekitar. Selepas penemuan grafena pada 2004, ia menjadi subjek utama penyelidikan di seluruh dunia. Grafena mempunyai sifat-sifat yang luar biasa dari segi mekanikal, optik, haba dan elektrik. Sifat-sifat tersebut menjadikan grafena berpotensi digunakan dalam pelbagai aplikasi. Pemendapan wap kimia bermangkin (CVD) adalah saluran yang paling baik untuk menghasilkan grafena berskala wafer, kerana teknik ini mempunyai kelebihan dalam proses pemisahan grafena daripada pemangkin selepas CVD. Dengan bantuan penyejukan pantas, grafena berlapis tunggal berjaya dibentuk pada foil nikel polihabluran dibawah CVD tekanan atmosfera, dengan suhu 850 °C, tekanan separa metana 0.2 atm and 5 min tempoh reaksi. Tetapi grafena berlapis tunggal gagal dibentuk dengan menggunakan foil kuprum sahaja. Penyejukan pantas selepas CVD mendorong pelindapkejutan aktiviti pemangkin dan menghadkan kadar difusi karbon dalam nikel ke permukaan nikel. Proses ini memudahkan pembentukan grafena berlapis tunggal berskala wafer. Untuk meningkatkan keseragaman grafena berlapis tunggal, satu teknik mudah digunakan untuk menumbuh grafena berlapis tunggal secara serentak pada kedua-dua foil nikel polihabluran dan foil kuprum polihabluran, pada suhu 950 °C, tekanan separa metana 0.2 atm and 5 min tempoh reaksi. Stuktur grafena yang



seragam dan berkualiti tinggi dapat dibukti dengan spektroskopi Raman dan mikroskop transmisi electron resolusi tinggi. Sistem pemangkin dwilogam yang dicadangkan membolehkan pengawalan difusi karbon ke permukaan dalam foil Ni dan Cu. Khususnya, kebolehcapaian karbon dapat dikurangkan pada permukaan Ni dalaman, manakala Cu memainkan peranan sebagai penghalang karbon. Mekanisme pertumbuhan grafena berlapis tunggal dapat dibantu dengan difusi karbon melalui bijian Ni dan sempadan bijian Ni. Daya penggerak untuk difusi karbon datang daripada kepekatan kecerunan karbon antara permukaan yang kaya dengan karbon dan permukaan kurang karbon. Sempadan bijian Ni telah terbukti memainkan peranan yang penting dalam kawalan difusi karbon semasa peringkat pertumbuhan. Dengan bantuan penyejukan pantas, proses pelindapkejut mengurangkan jumlah atom karbon diasing dari Ni, hanya atom karbon yang terletak berhampiran permukaan Ni mempunyai masa yang cukup untuk mengasing dan membentuk grafena. Sementara itu difusi atom karbon dalam tengah foil Ni telah dihalang dan lepas itu membentuk  $\text{Ni}_3\text{C}$ .  $\text{Ni}_3\text{C}$  dikenali sebagai perlindungan yang baik terhadap kakisan. Kehadiran  $\text{Ni}_3\text{C}$  digabungkan dengan penggunaan ferum nitrat (0.5mol/L) sebagai bahan punar lemah semasa pemisahan grafena, foil Ni boleh digunakan semula sehingga 6 kali tanpa menyebabkan sisihan yang besar terhadap kualiti dan keseragaman grafena berlapis dua.  $\text{Ni}_3\text{C}$  ternyata mampu untuk menghadkan kesan punaran foil Ni. Kerja-kerja ini telah berjaya mempamerkan cara yang mudah dan novel untuk mensintesis grafena berlapis tunggal dengan kualiti yang tinggi

**SYNTHESIS OF MONOLAYER GRAPHENE ON POLYCRYSTALLINE  
NICKEL AND NICKEL-COPPER BIMETALLIC CATALYST AND STUDY  
TOWARD THE REUSE OF NICKEL CATALYST**

**ABSTRACT**

Graphene is a layer of  $sp^2$  hybridized carbon atoms with a thickness of only one atom, which exposed most of its atoms to the surrounding medium. Since the discovery of graphene in 2004, it has become the main subject of research around the world. The attractiveness of graphene is mainly attributed to its remarkable mechanical, optical, thermal and electrical properties, enabling graphene to be potentially used in various applications. To date, CVD is the promising method to produce wafer-scale graphene, because it allows an easier separation of graphene from the catalytic substrate. With the assist of fast cooling, monolayer graphene was grown directly on polycrystalline Ni foil under atmospheric pressure CVD with temperature of 850 °C, methane partial pressure of 0.2 atm and reaction duration of 5 min. However, monolayer graphene could not be formed on Cu under the chosen CVD conditions. Fast cooling after CVD allowed the quenching of the activity of the catalyst and limiting diffusion of dissolved carbon to the surface of Ni, which later facilitate the formation of predominantly wafer scale monolayer graphene. To further improve the uniformity of monolayer graphene, a facile technique was applied to grow monolayer graphene simultaneously on both polycrystalline Ni and Cu foils using a Ni-Cu bilayer catalyst at temperature of 950 °C, methane partial pressure of 0.2 atm and reaction duration of 5 min. High uniformity and quality of the crystalline structure of the grown graphene was evidenced by Raman spectroscopy mapping and High Resolution Transmission Electron Microscope. The straightforward bimetallic

catalytic system allows the control of carbon diffusion to the interface of Ni and Cu. In particular, carbon accessibility is reduced at the inner Ni surface, and Cu behaves as a carbon barrier. The growth mechanism of monolayer graphene was facilitated by carbon diffusion through the bulk and Ni grain boundary, the driving force coming from concentration gradient between carbon-rich surface to carbon-lacked surface. The grain boundaries were shown to play a crucial role in carbon control during the growth stage. Facilitated by the applied fast cooling, the quenching process reduced the amount of carbon atoms segregated, only the carbon atoms situated near the surface had enough time to segregate and form graphene. Meanwhile, diffusion of carbon atoms at the middle of the Ni foil was highly inhibited; forming  $\text{Ni}_3\text{C}$ .  $\text{Ni}_3\text{C}$  is known to offer good protection against corrosion. The presence of  $\text{Ni}_3\text{C}$  combined with the use of iron nitrate (0.5mol/L) as soft etchant for graphene separation, the Ni foil could be reused again up to 6 cycles without causing a huge deviation on the quality and the uniformity of bilayer graphene.  $\text{Ni}_3\text{C}$  is indeed able to limit the etching effect of the Ni foil. This work has successfully demonstrated a simple and novel route to synthesize monolayer graphene with high quality.

**SYNTHÈSE DE GRAPHÈNE MONOCOUCHE SUR LE Ni  
POLYCRISTALLIN ET SUR UN CATALYSEUR BIMÉTALLIQUE  
Ni-Cu ET RÉUTILISATION DU CATALYSEUR**

**RÉSUMÉ**

Le graphène est une couche de carbone d'une épaisseur atomique pour laquelle les atomes de carbone sont hybridés  $sp^2$ . Depuis sa découverte en 2004, le graphène devient l'un des sujets les plus importants de la recherche dans le monde. L'attractivité du graphène est principalement attribuable à ses propriétés remarquables : mécaniques, optiques, thermiques et électriques, permettant au graphène d'être potentiellement utilisé pour diverses applications. Maintenant, le dépôt chimique en phase vapeur (CVD) est la méthode prometteuse pour produire du graphène à grande échelle, car il permet une séparation facile de graphène après CVD. Avec l'aide d'un refroidissement rapide, monocouche graphène a été cultivé directement sur polycristallin Ni feuille sous CVD sous pression atmosphérique, durée de 5 min à 850 °C de la température, de la pression partielle du méthane de 0,2 atm. Toutefois, nous n'avons pas réussi à faire croître du graphène monocouche sur le Cu dans les conditions choisies. Refroidissement rapide après CVD a permis à la trempe de l'activité du catalyseur et limitant la diffusion de carbone dissous à la surface de nickel, ce qui facilite ultérieurement la formation essentiellement échelle graphène monocouche. Pour améliorer l'uniformité de la monocouche graphène, nous proposons une technique simple pour préparer du graphène monocouche homogène dont la croissance est réalisée simultanément sur deux feuilles de Cu et de Ni assemblés en bicouche métallique, à température de 950 °C, le méthane pression partielle de 0,2 atm et la réaction durée de 5 min. La haute uniformité et qualité

cristalline du graphène obtenu ont été mises en évidence par les caractérisations réalisées par spectroscopie Raman et microscopie électronique à transmission haute résolution. Le système catalytique bimétallique développé permet de contrôler et de limiter la diffusion du carbone aux surfaces internes du Ni et du Cu ; le Cu se comportant comme une barrière vis-à-vis du carbone. La croissance de graphène monocouche est facilitée par la diffusion des atomes de carbone à travers l'épaisseur de la feuille de Ni et les joints de grains de Ni ; la force motrice ayant pour origine le gradient de concentration en carbone entre les deux surfaces de la feuille de nickel. Les joints de grains jouent en particulier un rôle crucial dans le contrôle de l'apport en carbone durant la phase de croissance. La trempe réalisée à la fin de la croissance réduit fortement et subitement la quantité d'atomes de carbone réactifs et seulement les atomes de carbone situés au plus près de la surface ont assez de temps pour se séparer et former le graphène. Pendant ce temps, la diffusion des atomes de carbone dans l'épaisseur de la feuille de Ni est fortement inhibée. Ils forment ainsi du  $\text{Ni}_3\text{C}$ . Le  $\text{Ni}_3\text{C}$  est connu pour offrir une bonne protection contre la corrosion. La présence de  $\text{Ni}_3\text{C}$  combinée à l'utilisation du nitrate de fer (0.5 mol/L) facilite la séparation du graphène. Ce qui permet à la feuille de Ni d'être réutilisée jusqu'à 6 fois sans causer un écart significatif de la qualité et l'uniformité du graphène bicouche formé. Le  $\text{Ni}_3\text{C}$  est en effet capable de limiter l'effet de gravure de la feuille de Ni. Ce travail a donc démontré avec succès que le coût moyen pour synthétiser une monocouche de graphène de haute qualité pouvait être réduit avec des procédés simples à mettre en œuvre.

# CHAPTER 1

## INTRODUCTION

This chapter provides an overall introduction to the research project. A brief definition of nanotechnology and graphene is outlined at the beginning of the chapter, followed a section devoted to methane which is the carbon feedstock in this study. Finally, this chapter concludes the problem statement, the objectives and scope of the work and the thesis organization.

### 1.1 Nanotechnology

Nanotechnology, also known as nanotech was first inspired by the American physicist Richard Feynman in the talk "*There's Plenty of Room at the Bottom*" at an American Physical Society meeting at Caltech on December 29, 1959 (Feynman, 1960). The term of nanotech was evaluated by Taniguchi (1974), where "Nanotechnology mainly consists of the processing, separation, consolidation, and deformation of materials by one atom or one molecule." In 1986 the book entitled *Engines of Creation: The Coming Era of Nanotechnology* was written by the American engineer Eric Drexler who proposed the idea of a nanoscale "assembler" and popularized the concept of nanotechnology (Drexler, 1986).

Nanotechnology might be specifically defined as the design, characterization, production and application of structures, devices and systems by controlling shape and size at nanometer scale. The term of "nano", is a prefix that means "dwarf" in Greek, it denotes as a billionth, while nanometer means  $10^{-9}$  of a meter. For comparison, a single human hair is about 80,000 nm wide, a red blood cell is approximately 5,000 nm wide and a water molecule is almost 0.3 nm across. Figure 1.1 presents the nanotechnology region.

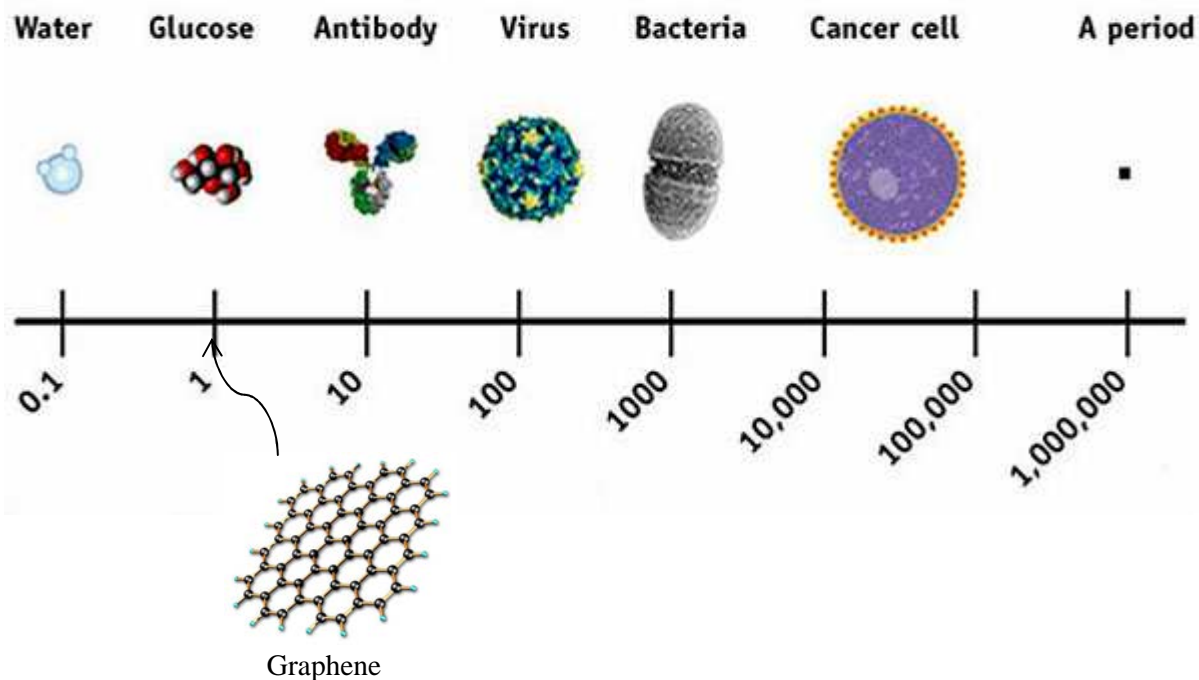


**Figure 1.1** Diagram showing the nanotechnology region (Freie Universität Berlin, 2015)

The implications of nanotechnology are now extended from medical (artificial muscle, nanomedicine), ethical (novel weaponry and defense technologies, pervasive surveillance), mental (drug carrier for nerve system), legal (fast and accurate sensor of dangerous drug or explosive) and environmental applications, to engineering, biology, chemistry, computing, materials science, military applications, and communications. Without any doubt, nanotechnology will be the renaissance of the 21<sup>st</sup> century.

Nanomaterial possesses various advantages. The tininess of nanomaterials holds a larger surface area per unit volume which makes it suitable for surface catalytic purposes. Besides, the smaller catalyst particles always possess higher catalytic activity (Hu *et al.*, 2011). Nanotechnology also brings the transistor devices into atomic scale and conducts the bloom of information and communication technology (ICT) in the early of 21<sup>st</sup> century with miniaturized internet and multimedia-enabled devices (Bonsor and Strickland, 2011). Bioavailability was

significantly improved with the implication of nanotech with a more effective drug delivery to the targeted area (Lavan *et al.*, 2003).

Nanotechnology is an expected future manufacturing technology and recognized to have the potential to revolutionize a host of industries that will make most products lighter, stronger, cleaner, less expensive and more precise. It has been forecasted that the global nanotechnology industry will grow to reach USD 75.8 billion by 2020 (Report linker, 2015).

Through MOSTI (Ministry on Science, Technology & Innovation) and MOHE (Ministry of Higher Education), the Malaysian government has funded up to RM 124.3 millions in nanotechnology area under the 9<sup>th</sup> Malaysia Plan (Economy Planning Unit, 2006). In addition, the government will set up a National Innovation Centre and a network of Center of Innovation Excellence for allowing faster commercialization and for the industry to provide fast feedback to the research work. Nanotechnology has been included as one of the growth engines for the new economic policy, as announced by the Prime Minister of Malaysia, Datuk Seri Najib Tun Razak, on a separate occasion (Jiang, 2009).

## **1.2 Carbon element**

Carbon can be found in many different compounds, it is the sixth most abundant element in the universe and the name "carbon" comes from Latin, carbo, with the same meaning. Inside the carbon atom, 2 electrons are found in the 1s orbital close to the nucleus. The next two will go into the 2s orbital. The remaining will be in two separate 2p orbitals which have the same energy level. This configuration can be further hybridized to the  $sp^3$  configuration ( $2s^1 2p_x^1 2p_y^1 2p_z^1$ ) to form tetrahedral coordinated carbon such as methane and diamond. Meanwhile, certain carbon allotropes such as graphite, graphene and carbon nanotubes, the



carbon atom undergoes  $sp^2$  hybridization. In  $sp^2$  hybridization, one s-orbital and two p-orbitals undergo hybridization, leaving another p-orbital unaffected. The remaining p-orbital is forming the distributed pi-bonds that reside above and below each graphite sheet. This delocalized pi system is responsible for the electrical conductivity of graphite. In the meantime, the other electrons in  $sp^2$  hybrid orbital form a strong covalent bond with each other and provide a magnificent mechanical strength for those materials. Figure 1.2 shows the allotropes of carbon.

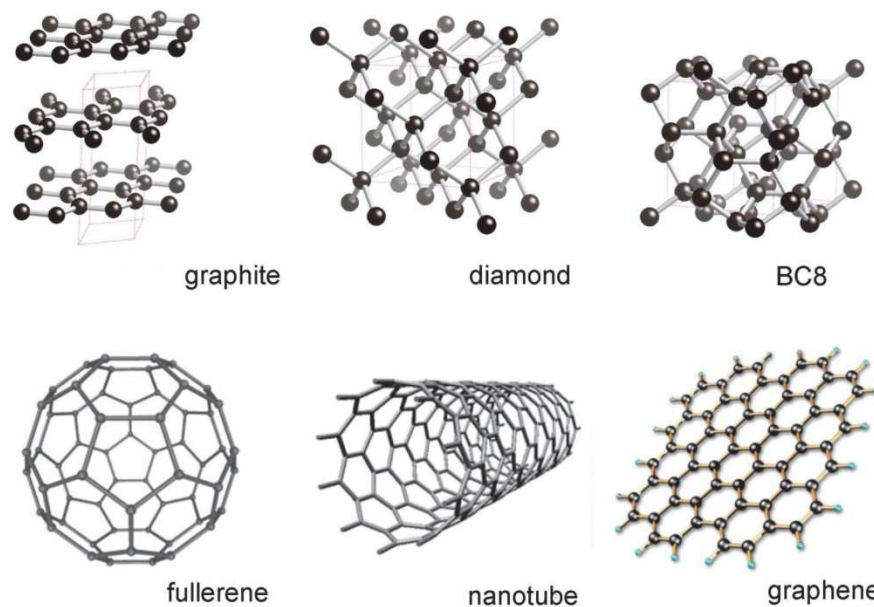


**Figure 1.2** Structures of selected allotropes of carbon. (Oganov *et al.*, 2013)

### 1.3 Graphene

The discovery of buckminsterfullerene ( $C_{60}$ ) (Figure 1.2) in 1985 had led to an entirely new branch of carbon chemistry (Kroto *et al.*, 1985). Carbon Nanotube (CNT) (Figure 1.2) was first observed by Iijima in 1991, from direct current arching of graphite for preparation of fullerenes using transmission electron microscopy (TEM) (Iijima, 1991).

Graphene is a thin film of carbon, purely carbon that is arranged in a honeycomb lattice with just one single atom in thickness. It is a new allotrope of

carbon that is widely acknowledged by the researchers in year 2004 and the discoverers of graphene won the Nobel Prize of Physics in 2010 by Professor Geim and Professor Novoselov from Manchester University. The discovery of graphene has materialized it from theory that has been discussed for decades. Since then, enormous effort and resources were poured in to carry out various tests and experiments on this material. Graphene possesses numerous magnificent properties that are not shared by other materials and which could be applied in various applications. The discovery of graphene had opened up a new chapter of nanocarbon materials after CNTs. The graphene market will reach nearly USD 200 million in 2026 (Khasha, 2015).

#### **1.4 Methane**

Methane is a colorless, odorless gas with a wide distribution in nature with chemical formula  $\text{CH}_4$ . It has a high global warming potential of 72 as compared with carbon dioxide with 25 (IPCC, 2007). The major source of methane comes from natural gas reservoir underground. Alternative sources of methane including biogas are generated by the fermentation of organic matter such manure, wastewater sludge, municipal solid waste or biodegradable feedstock under anaerobic conditions. The world reserve of natural gas was estimated at 6,609 trillion cubic feet in 2010 (EIA, 2010). Malaysia is a net exporter for natural gas having 2.3 trillion cubic meter of proven natural gas reserves and ranks 16<sup>th</sup> in the world (CIA, 2010). Raw natural gas in Malaysia shows a relatively high composition of methane and relatively clean, due to low hydrogen sulfide composition, a source for contaminant, sulphur oxides (Table 1.1).

**Table 1.1** Composition of raw natural gas (Gas Malaysia, 2011).

Hydrocarbon	Formula	Composition	
		Typical natural gas	Malaysian natural gas
Methane	CH <sub>4</sub>	70-90%	92.73%
Ethane	C <sub>2</sub> H <sub>6</sub>	} 0-20%	4.07%
Propane	C <sub>3</sub> H <sub>8</sub>		0.77%
Butane	C <sub>4</sub> H <sub>10</sub>		0.14%
Carbon dioxide	CO <sub>2</sub>	0-8%	1.83%
Oxygen	O <sub>2</sub>	0-0.2%	Trace
Nitrogen	N <sub>2</sub>	0-5%	0.45%
Hydrogen Sulfide	H <sub>2</sub> S	0-5%	Trace
Rare gas	Ar, Ne, He, Xe	Trace	Trace
Other hydrocarbon		Trace	Trace

In the industrial sector, methane is often used as a raw material for products such as hydrogen, fertilizer and etc. It is also commonly used as an energy source. Now, the utilization of methane can be extended to CNTs and graphene which are more valuable products. Methane decomposes to carbon radical and hydrogen by using a catalyst and high temperature. The carbon decomposed from methane could dissolve into the catalyst. During the cooling process, the threshold of carbon solubility gets lowered, and later segregate the excess carbon to form graphene. Meanwhile, hydrogen is a side product for the reaction. Since the reaction takes place in inert conditions, the hydrogen produced is CO<sub>x</sub>-free, which is a suitable fuel for fuel cells and methanol production.

## 1.5 Problem statement

Already more than ten years, a physical graphene was first reported experimentally by mechanical exfoliation (Novoselov *et al.* 2004). Since then, various methods were proposed in order to produce graphene with larger area and higher uniformity, including reduction of graphene oxide (Zhu *et al.*, 2010), sublimation of SiC (Silicon Carbide) (Berger *et al.*, 2004) and Chemical Vapor Deposition (CVD). Among these techniques, sublimation of SiC and CVD are two promising methods to produce wafer-scale graphene; and CVD especially because it allows an easier separation of graphene from the catalyst (Allen *et al.* 2009b).

Ni and Cu are two most promising catalysts due to moderate and low carbon solubility into Ni (Jacobson *et al.*, 2012b) and Cu (Hwang *et al.*, 2011), respectively. The growth mechanism of graphene on Cu is known to be surface mediated, and Cu possesses self-limiting surface deposition which enhances the formation of predominantly monolayer graphene. However, Cu requires strict process conditions to grow monolayer graphene, including high vacuum conditions, a low carbon concentration environment and a synthesis temperature near to the melting point of Cu (Seah *et al.*, 2014). Ni rather follows a bulk-mediated graphene formation mechanism, which unfortunately favors the formation of multilayer graphene. The formation of monolayer graphene on Ni requires high-speed cooling after CVD or the use a very thin Ni film as catalyst.

The two transition metals mentioned above possess their own advantages and shortcomings respectively. In order to combine the stronghold of each transition metal, bi- or multi-metallic catalytic systems have been designed and used for graphene synthesis research. The combination of Ni and Cu as alloy is the most common and most broadly reported catalyst. Cu and Ni have a very distinct

solubility of carbon under various recipes for Cu-Ni preparation, which allows a fine control of carbon solubility properties for optimization of graphene growth. There are 2 types of commonly used Ni-Cu combination. The first one is the direct using of the Ni-Cu alloy. The second one consists the coating a Ni-Cu bimetallic film which thickness is of several nm. To date, Ni-Cu bimetallic research remains at its initial stage and the role of each metal in the growth mechanism is yet to be well understood.

Meanwhile, graphene grown from CVD is normally firmly attached to its original metallic foil. The properties of graphene are therefore severely degraded, due to the strong interactions with the metallic sublayer catalyst. The monolayer thickness of graphene is the main source of its unique properties but also the cause of many issues. Graphene exposes the majority of its charge carriers to the surrounding environment. It easily interacts with the supporting substrate, resulting in inhomogeneity in charge and altering the conduction path of electrons. Furthermore, graphene adheres firmly and adopts the surface morphology of the substrate. This feature creates undesired strain and further scattering of electrons (Castro Neto *et al.*, 2009, Ishigami *et al.*, 2007, Geringer *et al.*, 2009). Wet chemical etching and mechanical exfoliation are the 2 major branches of graphene transfer processes that have been intensively studied. Among them, wet chemical etching is the dominant technique that is widely applied. Damages from the catalyst and contamination are the most important disadvantages of the wet chemical etching approaches. The wet chemical etching method is not an ideal transfer process because the loss of the metal catalyst is unavoidable as a large scale transfer process is required. Hence a new method is urgently required to preserve the catalyst foil during separation

In the present study, after summarizing the problems faced in monolayer graphene synthesis, a conventional CVD followed by very rapid cooling is studied to find the possibility to produce monolayer graphene with high uniformity in term of thickness and crystalline. To further improve the quality and uniformity of graphene, we demonstrate a facile technique to grow uniform monolayer graphene simultaneously on both polycrystalline Ni and Cu foils using a Ni-Cu bilayer catalyst, that both Ni and Cu could be separated easily after CVD process, rather than single sheet of graphene in single CVD reported in literature. The CVD reaction was carried out under atmospheric pressure. Lastly, a simple method is first to enable the recycle of the Ni foil for repeated growths of graphene has been studied extensively.

## **1.6 Objectives**

The present study has the following objectives

1. To study the suitability of polycrystalline nickel, copper foil and bilayers Ni-Cu catalyst on methane decomposition into graphene, that uniform in number of layers under wide range of operating parameters (reaction duration, temperature and methane partial pressure).
2. To define the graphene formation mechanism by atmospheric pressure CVD under different kind of catalysts studied.
3. To study the effect of graphene morphology, the type of catalyst, and concentration of etchant toward the reuse and recycle of Ni catalyst foils under conventional graphene separation method.

## **1.7 Scope of study**

The present study mainly focuses on the production of graphene, particularly monolayer graphene with the self-designed atmospheric pressure CVD reactor. The conventionally available Ni and Cu foil with polycrystalline structure utilized in the

first stage of graphene formation study. The aim of current stage is to identify the most suitable condition to produce monolayer graphene with highest selectivity, and with the aid of very fast cooling. The operating parameters studied are the CVD temperature, CVD duration and methane/hydrogen ratio for the reaction.

The grown graphene would be separated from the Ni and Cu foil with wet chemical etching approach, and deposited onto silicon wafer for characterization. Point-based Raman spectroscopy is employed as the preliminary characterization technique to identify the morphology and crystal structure perfectness of the as-grown graphene. Later on, Raman mapping and optical microscope applied to further identify uniformity of graphene. High Resolution Transmission Electron Microscope (HRTEM) used to give a most direct observation on the carbon atoms arrangement at the graphene. The effect of studied parameters for the graphene formation could be determined through cross-checking of the data given by aforementioned characterization techniques.

Second stage, a novel-designed bimetallic catalyst is investigated for the improvement on the quality and uniformity of grown monolayer graphene. One of the Ni surface is wrapped with Cu foil to create a carbon-lacked environment at the interface of Ni and Cu. Same operating parameters, CVD temperature, CVD duration and methane/hydrogen ratio for the reaction in CVD are varied for graphene formation. The grown graphene separated with the same method and also gone through same characterization technique to examine the characteristic of graphene. Ion slicer used to thin the catalyst foil and monitor the carbon distribution in the middle of catalyst foil. X-ray Diffraction (XRD) also performed to survey the crystal structure changing on catalyst and reaction. A mechanism of the graphene formation by studied catalyst system derived through the data collected.

Milder etchant, iron nitrate solution and low concentration nitric acid used to graphene separation with aim for the reuse of catalyst foil. Graphene with different characteristic grown from previous study, either by Cu or Ni utilized in current stage to identify the best condition for graphene separation from respective catalyst foil with minimum catalyst consumption. Lastly, the factor that the catalyst reuse is identified.

## **1.8 Thesis organization**

This thesis consists of five chapters. Chapter One (Introduction) gives an outline of the present research, including a brief introduction of nanotechnology and graphene, followed by a part devoted to methane. Problem statement is then defined after reviewing the existing limitations faced in the synthesis of monolayer graphene. Hence, a relatively new approach is designed to overcome these limitations. The objectives of the present work are carefully set and the scope of study is given. Finally, the organization of the thesis and the arrangement of each chapter are described.

Chapter Two (Literature Review) summarizes the past research work related to the area of interest for the present study and their findings. It starts with a brief introduction of monolayer graphene, followed by the existing methods for graphene synthesis, process variables and catalysts of CVD and their influence on the produced graphene. Next, the transfer methods of graphene from its original substrate to arbitrary substrate are reviewed to investigate the advantages and the disadvantages of each method. It is followed by the current strategy to enable the reuse and recycle of the catalyst. The chapter ended up with a summary.

Chapter Three (Materials and Methods) describes in details the experimental materials and research methodologies for the present work. Information of all



materials and chemicals used are listed as well. After their principle, the conditions used for the characterization techniques used are given.

Chapter Four (Results and Discussions) relates the results and the discussion of the research work. Two commonly used catalysts, namely Cu and Ni, were studied to grow graphene by atmospheric pressure. They were used separately and the operating conditions (temperature, duration and methane partial pressure, cooling rate) were optimized. A new approach proposing a bimetallic Ni/Cu catalytic system is further studied. And efforts devoted to the separation process that allow to realize the reuse and recycle of catalyst are described at the end of the chapter.

Chapter Five (Conclusions and Recommendations) summarizes the results obtained in the present research. It includes the overall research findings and some concluding remarks. Later on, suggestions are given to improve the present study and future study to be conducted is proposed. These recommendations and suggestions are given considering the significant findings, the conclusions as well as the limitations and difficulties encountered in the present work.

## CHAPTER 2

### LITERATURE REVIEW

In this chapter, the current knowledge, substantive findings, theoretical and methodological contribution on the synthesis of wafer-scale graphene were summarized in 6 sections. Section 2.1 briefly introduces the graphene followed by the properties of graphene in Section 2.2. In Section 2.3, the available methods to synthesis graphene were reviewed; particularly CVD is further discussed in more details. The conventional catalysts used in CVD are revised in Section 2.4. Meanwhile, Section 2.5 reports on the approaches for graphene separation from catalyst. Finally, a summary wraps up the whole chapter in Section 2.6.

#### 2.1 Introduction

Graphene is an allotrope of carbon which acts as the fundamental block for zero-dimensional fullerene, one-dimensional CNT and three-dimensional graphite. The editors of the journal “Carbon” come out with a very clear definition as below to avoid wrong usage of the word “graphene” (Bianco *et al.*, 2013).

*“a single-atom-thick sheet of hexagonally arranged,  $sp^2$  -bonded carbon atoms that is not an integral part of a carbon material, but is freely suspended or adhered on a foreign substrate. The lateral dimensions of graphene can vary from several nanometers to the macroscale.”*

Graphene only appears under spotlight after the ground breaking discovery by Manchester University. Geim and Novoselov first reported the “scotch tape” method for exfoliating graphene from highly ordered pyrolytic graphite (HOPG) in 2004 (Novoselov *et al.*, 2004). They produced graphene with a perfect crystal structure, as predefined in HOPG. This discovery had won them the Nobel Prize of Physics in 2010. Basically, graphene is a two-dimensional graphitic material. It is the

fundamental block of zero-dimensional fullerene, one-dimensional carbon nanotube (CNT) and three-dimensional graphite (Figure 2.1). The discovery of the exfoliation method ignited additional interest in research on carbon nanomaterials after 1991, when carbon nanotubes were reported by Professor Sumio Iijima (Iijima, 1991).

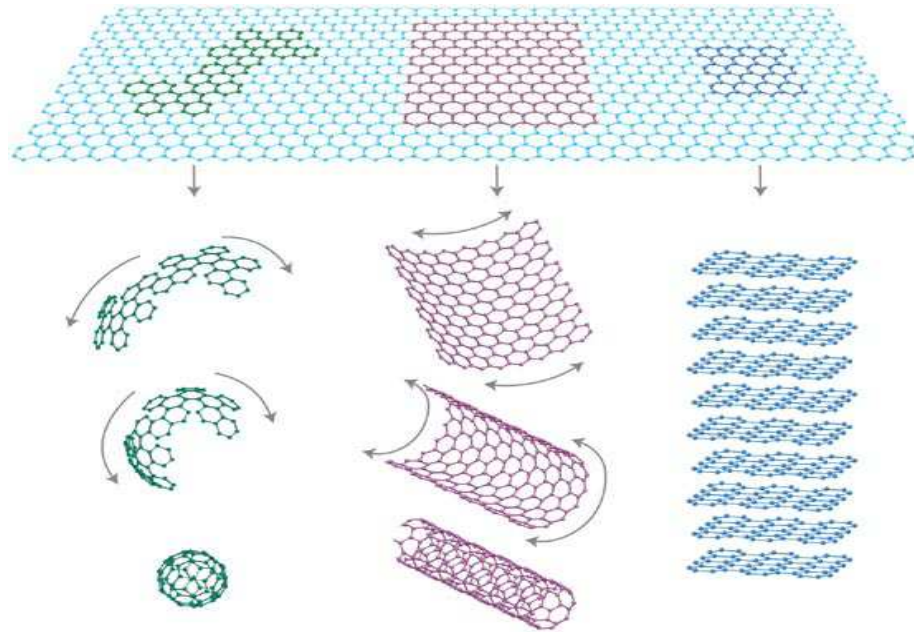


**Figure 2.1** Graphene, the fundamental block of all dimensional carbon materials, such as fullerene (green), CNT (magenta) and graphite (cyan). (Geim and Novoselov, 2007)

## 2.2 Properties of graphene

Graphene is an attractive material from the point of view of both science and engineering. The rise of graphene is basically attributed to its astounding electronic properties (Novoselov *et al.*, 2004, Geim and Novoselov, 2007), such as the occurrence of massless Dirac fermions due to the linearity of electron dispersion around the Fermi level under the smallest binding energy. The electrons behave massless; electron travel a long distance without scattering and have been clocked at speeds about 300 times below the speed of light in vacuum, much higher than the typical speed of electrons in semiconductors (Novoselov *et al.*, 2005, Castro Neto *et al.*, 2009, Power and Ferreira, 2011). The electron has chirality, which is dependent

on the direction of the electron propagation and the amplitude of the wave function (Pirchler, 2011). Graphene also shows an anomalous integer quantum hall effect that is seldom found in other materials; it is a special phenomenon that is only exhibited by certain semiconductor devices at low temperature and high magnetic field (Zhang *et al.*, 2005). The electrons and holes can be transferred to the graphene surface and also its underlying materials (Morozov *et al.*, 2005). The electron mobility for a free-standing monolayer of graphene exceeds  $200,000 \text{ cm}^2\text{V}^{-1}\text{s}^{-1}$  with the maximum value recorded at  $230,000 \text{ cm}^2\text{V}^{-1}\text{s}^{-1}$  (Bolotin *et al.*, 2008). Graphene owns ambipolar electric field effects, where electrons and holes can be continuously tuned as the charge carrier (Novoselov *et al.*, 2004), and its electronic properties are more similar to a zero band gap semiconductor (Novoselov *et al.*, 2007). The low resistivity of graphene is recorded at  $10^{-6} \Omega\cdot\text{cm}$  at room temperature (Chen *et al.*, 2008). Graphene is known to be one of the strongest materials on earth with a Young's modulus of 1 Tpa (Lee *et al.*, 2008), which is  $\sim 200$  times stronger than steel. With a visible light transmittance up to 97% possessed by monolayer graphene, it is also known as one of the best transparent conductive materials (Li *et al.*, 2009c). The unique properties of graphene provide potential applications as gas sensor (Schedin *et al.*, 2007), transistor (Lin *et al.*, 2008), solar cell (Wang *et al.*, 2007), transparent electrode (Kim *et al.*, 2009) and etc.

### **2.3 Methods of graphene synthesis**

Graphene that grown through CVD is firmly attached to the catalyst foil. The separation of graphene from the catalyst is required so that it could be applied in various applications. In this section, the commonly utilized techniques for graphene separation are discussed in detail.

### **2.3.1 Mechanical exfoliation**

The aforementioned Manchester group first reported the “scotch tape” method for exfoliating graphene from HOPG in 2004 (Novoselov *et al.*, 2004). Their work produced graphene with a perfect crystal structure, as predefined in HOPG. It is a simple and straightforward approach to obtain graphene flake. It is widely utilized in numerous reports that mainly study the intrinsic physical and chemical properties of graphene, which highly depend on the perfectness of its crystallinity. However, the mechanical exfoliation of HOPG is not suitable for mass production. Furthermore, the size of the graphene produced by this method is usually on the order of micrometres. But the quality of its structure is the best among all the known graphene synthesis approaches (Geim and Novoselov, 2007).

Mechanical exfoliation is a slow and time consuming process to synthesize graphene. A lot of repeated exfoliating steps required in order to obtain thin graphene from graphite. The low production rate is the crucial weakness of mechanical exfoliation. This is the reason why efforts are required to find alternative simpler approaches to produce graphene of high quality and relatively large domain (Geim and Novoselov, 2007).

### **2.3.2 Wet chemical exfoliation**

Wet chemical exfoliation of graphene involves a modification of graphite, nanographite or multilayer graphene in a liquid medium to weaken the interlayer interactions and to induce the separation of the layers individually. Wet chemical exfoliation can be simply performed through an ultrasonication treatment of graphite using polymer-organic solvents (Liang and Hersam, 2010) or organic solvents (Zhu *et al.*, 2010) with a surface energy that matches that of graphene. This approach produces graphene with a smaller size. Moreover, prolonged exposure to ultrasounds

may cause structural damage to the basal plane of graphene. Graphene is often obtained from a strong oxidation of graphite, the obtained graphene or graphene oxide (GO) is prepared by the Hummers' method (Hummers and Offeman, 1958) or the Brodie, and Staudenmaier's method (Staudenmaier, 1898). High amount of oxygen-containing groups introduced at the graphene surface makes it hydrophilic and consequently dispersible in water as individualized graphene sheets under mild sonication (Allen *et al.*, 2009b). GO can be reduced in order to partly recover the C=C double bond conjugated system (Pei and Cheng, 2012). GO can be also exfoliated thermally. Under high temperature and inert conditions, the oxygen partially oxidises the carbon basal plane of GO to form CO<sub>2</sub> and water. The provoked sudden expansion due to the formation of CO<sub>2</sub> in between 2 graphene planes would weekend the coupling of both graphene sheets, lead to exfoliate graphite into graphene (McAllister *et al.*, 2007). Other volatile substances, such as ClF<sub>3</sub> (Lee *et al.*, 2009), are also employed to insert foreign molecules in between the graphene sheets of graphite. A thermal shock is afterwards applied to induce the exfoliation. The wet chemical approaches have the advantage to produce graphene in large quantity (Hernandez *et al.*, 2008, Zhang *et al.*, 2009b, Levchenko *et al.*, 2010). However, they produce contaminated and defected graphene for which the physical properties (electronic for example) are undoubtedly nevertheless lessened.

### **2.3.3 Sublimation of SiC**

There are two main methods that have been widely used to grow wafer-scale graphene, namely: (i) the epitaxial growth of graphene from SiC and (ii) the catalytic chemical vapour deposition (CVD) of carbon precursors. The epitaxial growth of graphene on SiC consists of heating a SiC thin film under Ultra High Vacuum (UHV). The hexagonal  $\alpha$ -SiC (6H-SiC and 4H-SiC) decomposes and sublimates

from the surface while the remaining carbon atoms order themselves into graphitic carbon (Tetlow *et al.*, 2014). The advantage of epitaxial growth is the ability to produce monolayer graphene in a controllable manner. The produced graphene is cleaned because the mechanism avoids the use of any metal catalyst with a carbon solubilisation stage (Rümmeli *et al.*, 2011). However, this method requires advances in SiC substrate preparation and high knowledge of graphene nucleation and growth (Robinson *et al.*, 2009). Since, prevention of excessive sublimation from SiC for graphene formation is hard to control. In addition, the transfer of graphene to another substrate is complicated. The grown graphene is indeed considered as covalently bonded to the SiC substrate and the first layer of graphene is referred as a buffer layer without graphene characteristics (Varchon *et al.*, 2007). The distance between the graphene and SiC was recorded to be as low as 2 Å on the Si-terminated surface (Varchon *et al.*, 2007). The distance is much smaller than the interlayer spacing of graphite (~3.3 Å). When the graphene is firmly mounted on the SiC, the Fermi is distorted to above the Dirac point, causing the graphene to behave like a weak n-type semiconductor with a narrow band gap. Since graphene exposed all its atoms. This behavior is a result of the upward shift in the Fermi level from the Dirac point due to the dangling bonds on the SiC surface (Ohta *et al.*, 2006). The intrinsic doping effect may persistently influence more than one layer of graphene (Riedl *et al.*, 2010). The band gap is approximately of 0.26 eV for monolayer graphene, and it decreases as the number of graphene layers increases (Zhou *et al.*, 2007). However, it was also found that the electronic properties of 10 layers graphene on SiC was similar of that of free standing single layer graphene (Hass *et al.*, 2008).

The strong coupling effect between graphene and SiC leads to a temperature dependence of the conductance of graphene (Jobst *et al.*, 2010). The highest electron

mobility of graphene on SiC ever recorded is  $150,000 \text{ cm}^2\text{V}^{-1}\text{s}^{-1}$  (Tedesco *et al.*, 2009) on a C-terminated surface, but the majority of the articles reports a mobility in the range of  $500\text{-}5000 \text{ cm}^2\text{V}^{-1}\text{s}^{-1}$  under various conditions (Panchal *et al.*, 2012, Shishir and Ferry, 2009, Weingart *et al.*, 2010, Jobst *et al.*, 2010, Tzalenchuk *et al.*, 2010), which is lower than the mobility recorded for free standing graphene, i.e.  $200,000 \text{ cm}^2\text{V}^{-1}\text{s}^{-1}$  (Bolotin *et al.*, 2008). The charge carrier density is in the range of  $10^{11}\text{-}10^{14} \text{ cm}^{-2}$ . The high charge density is suspected to be due to the strong interaction of graphene with SiC, which limits its application in devices due to gating difficulties (Chen *et al.*, 2007). These changes in properties were only found in graphene directly grown on SiC and not in graphene physically deposited on SiC (Sonde *et al.*, 2012).

#### **2.3.4 Chemical vapour deposition**

CVD is widely known to involve decomposition and reconstruction of a carbon feedstock, either hydrocarbons or polymers, with the aid of heat and metal catalysts. Various metals, such as Cu, Ni, Pt, Ru, and Ir, have been proven to have the ability to catalyse the growth of graphene. The formation of graphene on majority of transition metals through CVD follows 2 stages. The first stage is about dilution or incorporation of carbon atoms into the metal, which is better known as dissolution. The second stage is the subsequent formation of graphene through cooling called segregation, the mechanism of the second stage may divert depending on the transition metal utilized. Figure 2.2 shows the typical graphene formation by the process using CVD. According to Blakely's group from Cornell University (Shelton *et al.*, 1974), segregation of graphene from a Ni surface involves an heterogeneity of composition that corresponds to one single phase in the phase diagram. Precipitation on the contrary indicates a composition inhomogeneity due to a phase separation (Li



*et al.*, 2009b). In a later study by the same authors, they found that monolayer graphene grew with segregation in the initial stage, followed by precipitation for graphite formation (Eizenberg and Blakely, 1979). As shown in Figure 2.2 (a), the hydrocarbon that chemisorbs on the metal surface (step 1) dissociates through dehydrogenation (step 2), and the carbon adatoms dissolve and diffuse into the metal (step 3). The chemisorption is facilitated by the empty d-shell of the transition metals, which is ready to serve as an electron acceptor. While under stage 2, the segregation process starts as the concentration of carbon adatoms in the bulk metal has achieved the threshold for nucleation or during the cooling process. The cooling induces a decrease of carbon solubility lowering the threshold. The excess of diluted carbon adatoms diffuses to the surface (step 4), and the segregation process for graphene formation occurs (step 5). The segregation continues until the concentration of carbon within the metal has decreased below a threshold. Both the nucleation and equilibrium concentrations are different under different operating conditions.

The solubility of carbon in Cu is very low. Thus, the chemisorption/deposition or surface growth mechanism better explains the graphene formation. The growth of graphene starts right after the hydrocarbon dissociation and stops immediately when the supply of hydrocarbons is cut off (step 1-2 in Figure 2.2 (b)). The detailed growth mechanism for graphene will be further discussed in Section 2.5.5.

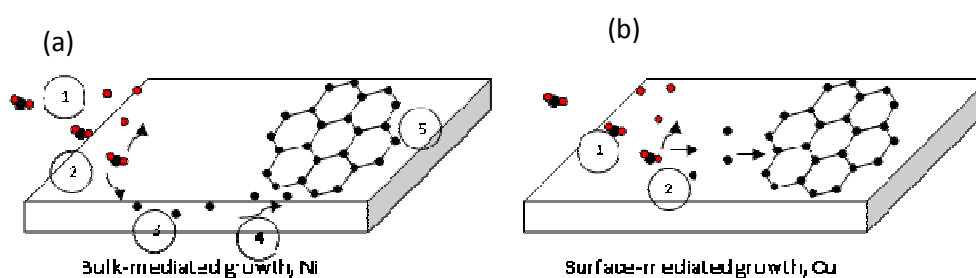


**Figure 2.2** Sketch of graphene formation steps on (a) Ni and (b) Cu (Losurdo *et al.*, 2011).

CVD has been extensively modified to improve its performance for graphene formation. Plasma-enhanced CVD (PECVD) is a feasible approach for large-area graphene synthesis with enhanced growth rates at lower temperature. The lowest temperature ever recorded for growing graphene was 240 °C (Kalita *et al.*, 2012). In this method, a plasma is generated through radio frequencies (Qi *et al.*, 2011, Terasawa and Saiki, 2012), magnetically enhanced arc discharges (Levchenko *et al.*, 2010, Volotskova *et al.*, 2010) or microwaves (Yamada *et al.*, 2012, Kalita *et al.*, 2012). The plasma and metal coupling causes localised rapid heating of the metal catalyst, which reduces the heating time. Moreover, plasma has the ability to remove the native oxide layer and to ensure the uniform nucleation of graphene on the metal substrate (Kumar *et al.*, 2012). However, PECVD has several drawbacks including the fact that a continuous plasma bombardment causes defects in the graphene. Moreover, the resulting graphene has a grain size that is inversely correlated to the intensity of the radicals, which causes a discontinuous graphene sheet with more defects, mainly contributed by the strong destroying properties of plasma. Woo *et al.* (2013) had reviewed that the quality of graphene is much better under high temperature PECVD rather than low temperature PECVD.

#### **2.3.4(a) Hydrogen**

Hydrogen gas (H<sub>2</sub>) is a key ingredient to produce graphene. Some researchers believe that the presence of H<sub>2</sub> in CVD degrades the crystallinity of graphene and slows down the growth rate on the Cu catalyst (Gao *et al.*, 2010b). H<sub>2</sub> dissociative chemisorption is competing with the dehydrogenation of hydrocarbon by occupying the surface active sites, inhibiting the growth of graphene, and creating defects on the graphene (Losurdo *et al.*, 2011). It is believed to be responsible for the formation of hydrocarbon radicals from graphene during the growth stage (Zhang *et al.*, 2012c).

However, other works suggest that  $H_2$  plays the vital double role of enhancing the bonding of carbon to the surface and etching the surface inhibiting that way unorganised or defective graphene edges; these edges being non favourable for graphene growth. Vlasiouk *et al.* (2011a) found that graphene could not be grown in the absence of  $H_2$ . The role of  $H_2$  seems to be not fully elucidated and it depends also on the operating conditions. Under high  $H_2$  partial pressure,  $H_2$  assists the formation of  $CH_3$  radicals, which are required to grow graphene. Meanwhile, under moderate  $H_2$  partial pressure, the graphene grains formed were irregular in shape. The effect of  $H_2$  is different according to the used catalyst. The diffusivity of hydrogen atoms in Ni is much lower than that in Cu. The fast recombination and desorption of hydrogen allows the surface of Ni to be continuously available for hydrocarbons and radicals, facilitating a fast in-diffusion of carbon into Ni (Losurdo *et al.*, 2011). For other transition metals such as Pt,  $H_2$  has been reported to suppress the extension of minority domains, leaving one millimetre-scale single-crystalline graphene as the dominant domain, which is more difficult to etch with  $H_2$  (Gao *et al.*, 2012). Other than that, the working parameter such as temperature, carbon source and pressure are also playing a decisive role in determining the overall outcome of as-grown graphene.

#### **2.3.4(b) Temperature**

Temperature is the main source of energy for the decomposition of carbon precursors and for the activation of the catalyst. For a typical CVD, temperature ranging from 800 to 1000 °C is usually employed for most of the catalysts, such as Cu, Ni, Ru and Pt, to grow graphene sheets (Memon *et al.* 2013b, Regmi *et al.*, 2012, Li *et al.*, 2010, Liu *et al.*, 2011b). The activity of Cu is one of the lowest among the aforementioned catalysts. Cu has a filled 3d shell which leads to both low carbon solubility and low adsorption of hydrocarbons (Memon *et al.*, 2013b). As a

consequence, higher temperature is required to form graphene on Cu. Regmi *et al.* (2012) reported graphene synthesis below 850 °C using Cu but the graphene sheet contained a large amount of defects. The quality of graphene and the ability to form monolayer graphene increase with temperature (Li *et al.*, 2010). Higher adsorption of hydrocarbon onto the Cu surface is responsible for denser nucleation at relatively low temperature (Vlassiuk *et al.*, 2011b). In fact, methane could be decomposed to form graphene at a temperature of as low as 400 °C (Li *et al.*, 2011b). Carbon supersaturation is less likely to occur at this temperature and low diffusion energy of carbon atoms onto the Cu surface causing the expansion of graphene is less significant (Rasool *et al.*, 2011a).

According to Liu *et al.* (2011a), the high diffusion rate of carbon in Ni catalyst at a temperature of 1000 °C forms multilayer graphene sheets. At 1100 °C, the equilibrium shifts to condensed monolayer state which leads to the formation of monolayer graphene on the Ni surface. Meanwhile, above 1150 °C, the solubility of carbon increases exponentially, and lower coverage of graphene can be obtained. Odahara *et al.* (2011) observed a similar trend but the condensed monolayer state is obtained in that case at ~800 °C. On the other hand, at lower temperature, the characteristics of Ni are different from those of other transition metals. Ni<sub>2</sub>C with a single atom thickness was evidenced to be formed on Ni and this carbide inhibits the growth of graphene. However, disagreement still exists about how the carbide layer may affect the graphene formation and regarding its interaction with the grown graphene. According to Lahiri *et al.* (2011a, 2011b), under ultra-high vacuum condition, three different scenarios can happen. (i) At low temperature (< 460 °C), a single layer of Ni<sub>2</sub>C preferentially grows on Ni(111) after exposure to hydrocarbons. It is believed that the carbide slowly transforms into graphene. (ii) For intermediate

temperature range (460 – 650 °C), the graphene formation follows the segregation/precipitation mechanism. (iii) At temperature of higher than 650 °C, the solubility of carbon increases with temperature, but still barely below 0.1 wt% at 650 °C and carbon segregates to graphene during the cooling stage (Xu *et al.*, 2011). However, this theory was opposed by Jacobson *et al.* (2012b) who failed to observe Ni<sub>2</sub>C. Grüneis *et al.* (2009) also showed that carbide is unable to transform into graphene.

Various temperatures have been reported for graphene nucleation on Pt catalyst (Peng *et al.*, 2012a). Most of the studies showed that ~1000 °C is the most suitable temperature for growing continuous graphene (Gao *et al.*, 2012, Sutter *et al.*, 2009c, Yong and Hahn, 2011). The temperature to form high quality graphene over Ru catalyst was found around 1000 °C (Sutter *et al.*, 2009b, Yi *et al.*, 2007). The studies of Zhang *et al.* (2009a) showed that high density and small graphene islands were seen all over the Ru surface at low temperature (500 °C).

#### **2.3.4(c) Carbon precursor**

Hydrocarbon is the major carbon source of graphene formation. Among, gaseous short chain hydrocarbons, such as methane and ethane are the most common carbon precursors for the growth of graphene. In the latest studies, some researchers found that unsaturated hydrocarbons, such as ethylene and acetylene, could also be used as carbon precursors for the formation of graphene. It was reported that the growth temperature is significantly reduced to ~650 °C as acetylene is used as the carbon precursor (Nandamuri *et al.*, 2011). Furthermore, it was noted that the decomposition temperature of ethylene is relatively low as compared to that of methane (Yao *et al.*, 2011). Acetylene or ethylene is easier to attach on the transition metals due to the planar geometry. The easier hybridization of the  $\sigma$ -bond with the

empty d-shell facilitates the dissociation of the hydrocarbon for the formation of graphene sheets (Hwang *et al.*, 2011). On the other hand, aliphatic alcohols are easier to be handled and stored (Guermoune *et al.*, 2011). Monolayer and poor-defected graphene sheets were obtained with alcohol on Ni catalyst (Kishi *et al.*, 2012). For both Ni and Cu catalysts, short chain alcohols were found to form monolayer graphene of high crystallinity (Guermoune *et al.*, 2011, Kishi *et al.*, 2012). A significant breakthrough in the liquid-carbon CVD was reported, where graphene flake was found on Cu catalyst at the growth temperature of 300 °C using benzene as the carbon precursor (Li *et al.*, 2011b, Choi *et al.*, 2013). Other aromatic hydrocarbons such as pyridine (Xue *et al.*, 2012), hexachlorobenzene (Gan *et al.*, 2012) and bianthryl (Cai *et al.*, 2012), as well as the polycyclic aromatic hydrocarbons such as hexabenzocoronene (Eom *et al.*, 2009) and corroenene (Cui *et al.*, 2011) required lower temperature to grow graphene. On the other hand, solid carbon precursors such as amorphous carbon (Seo *et al.*, 2012), HOPG (Xu *et al.*, 2011) and polymers such as poly(methyl methacrylate) (PMMA), high-impact polystyrene and acrylonitrile-butadiene-styrene can form graphene in the presence of the suitable catalyst (Ji *et al.*, 2011, Sun *et al.*, 2010b, Peng *et al.*, 2012b). Recent results showed that food, solid waste and insect parts can also be used as the source of carbon to grow pure graphene (Ruan *et al.*, 2011, Ray *et al.*, 2012).

#### **2.3.4(d) Pressure**

Graphene growth pressure is an important parameter that is widely debated by researchers. Atmospheric pressure CVD would allow a faster saturation of carbon on metal catalyst, but the carbon precipitation process at the later stage is hard to control (Lahiri *et al.*, 2011a). The variation of pressure is giving more significant effect when Cu serves as catalyst. The sputtered Cu film could be dewetted under low

pressure CVD (Su *et al.*, 2011). Besides that, hydrocarbon is difficult to be decomposed under high vacuum condition (Nie *et al.*, 2011b). The shape of the graphene flake formed also varies depending on the applied pressure during the graphene synthesis. The self-limiting monolayer graphene formation over Cu is only achieved at very low pressure. Under ambient pressure, non-uniform multilayer graphene is obtained, caused by the low mass transport rate of carbon (Yan *et al.*, 2011a). It is known that the coverage of graphene on the catalyst and the number of graphene sheets increase with the growth pressure. It has been reported that the rate-limiting-step for graphene formation in an atmospheric pressure CVD is the mass transport of hydrocarbon from bulk to the surface of the catalyst. On the contrary, the surface reaction is the rate-limiting-step in a low pressure or UHV CVD (Bhaviripudi *et al.*, 2010). Besides that, the activation energy of graphene nucleation is significantly lower for atmospheric pressure as compared to the low pressure conditions. It is moderately caused by the partial sublimation of Cu under high temperature and low pressure, removal the carbon species adsorbed on the Cu surface thus leading to lower nucleation density (Vlassiuk *et al.*, 2013).

## **2.4 Catalysts**

Fe, Ni and Co are known to be active metal catalysts for the synthesis of CNTs through CVD. These transition metals have non-filled d-shells that enable them to adsorb and interact with the hydrocarbons used as carbon sources (Seah *et al.*, 2011a). Similarly, graphene synthesis requires the same transition metal group as for CNT synthesis. But, there is a main difference between formation graphene and CNTs. Large amount of dissolved carbon adatoms is needed to increase conversion yield in the case of CNTs. Meanwhile, for graphene synthesis, optimum amount of dissolved carbon needs to be controlled precisely to grow graphene with a minimum thickness.

The ideal transition metals are different for both graphene and CNTs formation. Batzill (2012) had gathered interaction properties of 11 different transition metals with graphene (Figure 2.3) Each metal has its own mechanism for growing graphene. The quality of the graphene grown is dependent on the ability of the transition metal to facilitate hydrocarbon dehydrogenation and carbon segregation. The as-grown graphene would show interaction strength and growth mechanism depending on the used substrate. In this section, the roles of each transition metal competent for graphene formation are reviewed in detail.

Ti carbide	V	Cr	Mn	Fe	Co <sup>S</sup> d=2.1 <sup>ns</sup> c=0 π=?	Ni <sup>S</sup> d=2.1 <sup>n</sup> c=0 π=2 eV <sup>o</sup>	Cu <sup>M</sup> d=3 (3.3) <sup>i</sup> c=? π=intact <sup>u</sup>
Zr	Nb	Mo	Tc	Ru <sup>S</sup> d=2.1-3.6 <sup>ns,c</sup> c=1.5 <sup>ns</sup> (0.82) <sup>n</sup> π=2.6 eV <sup>d</sup>	Rh <sup>S</sup> d=2.2-3.8 <sup>i</sup> c=1.6 <sup>ns</sup> π=?	Pd <sup>M</sup> d=2.6 <sup>ns</sup> c=? π=?	Ag d=3.3 <sup>v</sup> c=? π=intact <sup>w</sup>
Hf carbide	Ta carbide	W carbide	Re <sup>S</sup> d=2.1-3.8 <sup>ns</sup> c=1.6 <sup>ns</sup> π=?	Os	Ir <sup>S/M</sup> d=3.4-4 <sup>ns</sup> c=0.3 <sup>i</sup> π=intact <sup>m</sup>	Pt <sup>M</sup> d=3.3 <sup>ns</sup> c=? π=intact <sup>s</sup>	Au <sup>M</sup> d=3.3 <sup>z</sup> c=? π=intact <sup>y</sup>

**Figure 2.3** Summary of the interaction between graphene and transition metals. Yellow-labelled elements indicate weak interactions, and red and blue can be attributed to strong interactions and graphene grown from bulk carbide, respectively. “d” is the distance between graphene and metal (in scale of Angstrom), “c” indicates the buckling and corrugation of graphene (in scale of Angstrom), and “π” refers to the amount of downward shift of the Dirac point of graphene mounted on respective transition metals. ‘S’ or ‘M’ in the upper right corner of each element-box indicates if graphene forms single or multiple rotational domains (Batzill, 2012).

#### 2.4.1 Ruthenium (Ru)

Ru, which has a hexagonal closest-packed (hcp) structure, is one of the foremost transition metals that were found to be capable to grow graphene, and the Ru(0001) surface is the most stable because of the hcp crystal structure. Ru has a carbon solubility of approximately 0.34 at.% at 1000 °C. Moreover, Ru always appears in single-crystalline form after heating, and this ensures a relative flatness and a lack of grain boundaries for growing uniform graphene (Arnoult and McLellan,



1972). These properties make Ru one of the most widely studied transition metals for graphene synthesis.

The well-recognised growth mechanism of graphene on a Ru(0001) surface involves the “carpet growth mode”, which is also shared by most of the transition metals. Hydrocarbons are dissociated and adsorbed on the Ru surface, producing a layer of adsorbed hydrocarbon intermediates at room temperature. During the heating stage, the hydrocarbon intermediates dehydrogenate and decompose to form carbon clusters. These carbon clusters coalesce due to surface tension and form graphene after reaching saturation and during cooling (Zhang *et al.*, 2009a).

The interaction between graphene and Ru is strong, which causes alterations in the topography of the lattice steps on the Ru surface. The first layer of graphene is believed to be covalently bonded to the Ru atoms by hybridisation of carbon  $2p_z$  orbitals with Ru d-states near the Fermi level (Sutter *et al.*, 2008).

Ru is one of the best catalysts for the epitaxial growth of graphene. It is easy to obtain a single-crystal surface with an orientation of (0001), and the interstitial carbon solubility can be reduced by a factor of six upon cooling. Moreover, the segregation of carbon can form graphene with a monocrystalline domain with perfect rotation alignment, a low defect density, and thickness control (Arnoult and McLellan, 1972, Sutter *et al.*, 2009a). Furthermore, the graphene grown from Ru is mostly free of wrinkles. The number of the graphene layers can be controlled by the growth temperature to limit the carbon solubility in Ru (Cui *et al.*, 2010). However, the downhill carpet growth mechanism of graphene on Ru that nucleates at the step edge introduces defects in the graphene as the islands meet, especially from islands of two different terraces (Loginova *et al.*, 2008). The strong interaction between the graphene and the Ru surface metal is likely to distort the high density of electron

states around the Fermi level of graphene. It causes strong hybridisation of graphene and Ru states, which severely affects the electronic structure of graphene (Brugger *et al.*, 2009). To date, there is no effective method to separate graphene that has been grown on Ru.

#### 2.4.2 Iridium (Ir)

Ir(111) with face-centred cubic (fcc) crystal structure is capable of nucleating graphene. Ir has a low carbon solubility, and the interaction between the Ir surface and graphene is weaker than that between Ru surface and graphene. The growth path of graphene on Ir is slightly different compared with the growth on Ru. Graphene may grow in both the uphill and downhill directions across the lattice step. The main reason for Ir to overcome the lattice step is the large distance between the graphene plane and the Ir surface. The smallest distances between carbon atoms are 3.77 Å and 3.80 Å for hcp and fcc regions, respectively. Meanwhile, the largest distance between graphene and Ir surface is 4.04 Å for a top-type region, whereas the step height is 2.2 Å (N'Diaye *et al.*, 2006). This phenomenon is attributed to the weak interaction between graphene and Ir (Gong *et al.*, 2010). The interactions between the two surfaces mainly involve physisorption with chemical modulation (Busse *et al.*, 2011).

The nucleation mechanism of graphene on Ir(111) is quite similar to that of Ru(001). The growth of graphene follows the nonlinear kinetic model. The carbon has to first be dissolved into the Ir metal until it reaches supersaturation. According to the simulation reported by Wu *et al.* (2012a), compared with the terrace, the most stable site for carbon adatom adsorption is the step edge. It is unstable for carbon monomers to escape from the step edge to form graphene islands, and the dimers that would escape from the step edge are C<sub>5</sub>, C<sub>8</sub>, and C<sub>11</sub> or larger, and these dimers are

shown to serve as the nucleus for further growth. The subsequent expansion of the graphene island requires a dimer of C<sub>5</sub>, which is a relatively stable form (Loginova *et al.*, 2009a). The nucleation preferentially occurs at the step edge because of the rapid cluster growth at high temperature and the occupation of the preferred configuration (Lacovig *et al.*, 2009)

Ir is a unique transition metal that slightly distorts the electronic Dirac cone of pristine graphene (Pletikosić *et al.*, 2009). As mentioned earlier, Ir has a low carbon solubility, which is useful for self-limiting the growth of graphene to a monolayer (Coraux *et al.*, 2008, N'Diaye *et al.*, 2008), although bilayer graphene is often obtained (Nie *et al.*, 2011a). Graphene grown with Ir is highly defected. Large-scale wrinkles are formed on the graphene during cooling. Some of the wrinkles recorded are up to 0.55 nm from the adjacent surface. The main cause is the difference in the thermal contraction between Ir and graphene: Ir contraction is of 0.8% during cooling from 1000°C to room temperature, whereas the thermal contraction of graphene is insignificant (Loginova *et al.*, 2009b).

### **2.4.3 Platinum (Pt)**

The use of Pt for hydrocarbon transformation can be traced back to the last few decades. Initially, the formation of carbon crystals on Pt was unwelcomed due to the poisoning of the catalytic converters in automobiles and the formation of coke in alkane transformation. Pt(111) has a weak interaction with graphene (Gao *et al.*, 2011c, Politano *et al.*, 2012). The reason for this weak interaction is similar to the case of Ir, which was mentioned in an earlier section; the exposed outer electron 5d shell can only weakly interact with the  $\pi$  electrons from graphene (Preobrajenski *et al.*, 2008). However, the interaction becomes stronger if a vacancy is introduced to graphene (Ugeda *et al.*, 2011). The fact that binding between graphene and the Pt

surface is weak allows graphene with random orientations to be present on the Pt surface (Sutter *et al.*, 2009c), and 22 different Moiré superstructures have been reported (Merino *et al.*, 2011). Some researchers have categorised Pt into the same group as Cu in terms of the chemisorption/deposition growth mechanism due to the self-limiting growth mechanism and the epitaxial growth mechanism observed for bilayer graphene, which are similar to those seen for Cu (Nilsson *et al.*, 2012, Kang *et al.*, 2009).

Graphene can be fairly easily nucleated on Pt with various crystal facets, and the results vary under different operating conditions. The common Pt(111), Pt(110), Pt(100), and Pt(311) are able to grow graphene at ambient pressure CVD. Among these, Pt(111) is the most suitable for growing high-quality graphene, followed by Pt(110) and Pt(100) (Gao *et al.*, 2011d). A large and continuous graphene has also been reported on Pt(100) (Nilsson *et al.*, 2012). Pt(311) only produces low-continuity graphene, which is attributed to the large lattice mismatch (Gao *et al.*, 2011d). The work of Gao *et al.* showed that a millimetre-scale graphene could be formed even though a polycrystalline Pt surface was used (Gao *et al.*, 2012). Moreover, multi-crystalline graphene was reported to form on single-crystal Pt(111), and this occurred on the preferential decomposition of the grain boundaries with surface contamination.

Graphene shows both uphill and downhill directions of growth on Pt; the downhill growth is much faster, and the growth mechanism is the carpet mode like Ru and Ir (Sutter *et al.*, 2009c). Graphene has been observed to follow a step-mediated growth with surface restructuring, in which graphene preferably nucleates from the steps of the lattice (Peng *et al.*, 2012a). Carbon atoms are mostly adsorbed at the fcc hollow sites of Pt films (Viñes *et al.*, 2009). From the calculation by Viñes *et al.*, adsorbed carbon atoms above 0.3 ML would induce aggregates of C<sub>3</sub> and C<sub>2</sub>

species (Viñes *et al.*, 2009). These carbon species will form graphene later. Meanwhile, the effect of graphene activity on the Pt surface remains uncertain. The observation of Fujita *et al.* showed that the graphene islands were hexagonal in shape and that they could induce Pt atom rearrangement of the lower terrace (Fujita *et al.*, 2005). Meanwhile, Land *et al.* reported a different finding in which irregular-shaped graphene islands were obtained and the upper lattice terrace was etched by the island during the graphene growth (Land *et al.*, 1992).

Large area graphene grown on Pt also possesses wrinkles. The wrinkles can be attributed to the thermal contraction of Pt after cooling and the decrease in carbon density inside the metal after the depletion of the reservoir to form graphene (Sutter *et al.*, 2009c). However, the low solubility of carbon is the main reason for the high selectivity of Pt towards monolayer graphene formation. The growth of a large-scale bilayer graphene film can be realised using a thicker Pt film with a single-crystal grain structure (Yong and Hahn, 2011).

#### **2.4.4 Nickel (Ni)**

Ni is one of the most widely studied catalysts for the synthesis of graphene. The theory of nucleation on the Ni surface and the atomistic mechanism are still highly debated. The high solubility of carbon enables single-crystalline Ni(111) and polycrystalline Ni to form graphene. Polycrystalline Ni is composed with many crystallites that not uniform in size and shape. The solubility of carbon in Ni was recorded at 0.9 at.% at 900 °C (Li *et al.*, 2009b). There is a significant hybridisation between the  $\pi$  orbitals and Ni  $d_{z^2}$ , which provides strong chemisorption between them, but at the same time, weak physisorption also exists at the hollow-site carbon  $p_z$  orbitals, where the hybridisation is lacking (Mittendorfer *et al.*, 2011). The lattice mismatch for Ni(111) is small, and no Moiré pattern can be observed (Lahiri *et al.*,

2011a). However, there are other observations showing that a Moiré superstructure could be observed on both Ni(111) and Ni(110) (Murata *et al.*, 2010, Fedorov *et al.*, 2011). The spacing between Ni atoms in the bulk phase is 2.49 Å, whereas the in-plane lattice parameter of graphite is 2.46 Å; the lattice mismatch is approximately 1% (Cheng *et al.*, 2011a). This would lead to epitactic growth with minimum additional strain induced in the graphene and would facilitate the growth of graphene on the Ni(111) surface (Mittendorfer *et al.*, 2011).

The high performance of Ni has caused researchers to use Ni(111) as a substrate for calculation of the atomistic mechanism involved in carbon adatoms forming graphene using different types of software. By using Density Functional Theory (DFT), it was proposed that the carbon adatoms are the first to form the chain cluster. It was found that the terminal atoms have a stronger interaction with the surface due to the local minima of the adsorption energy possessed by the chain cluster of carbons. Meanwhile, carbons in a single ring cluster cannot adhere to the Ni surface while maintaining their optimal gas-phase configurations and fulfil the constraints due to the epitaxial relationships (Cheng *et al.*, 2011a). Moreover, a single, small, six-member ring (MR) cluster is always found to be not stable on transition metal terraces (Gao *et al.*, 2011b, Gao *et al.*, 2011a, Cheng *et al.*, 2011a). The carbon chain cluster diffuses in the <110> direction of Ni(111). At the step edge, the ring cluster is more stable due to the enhanced activity of the metal step edge, and the aromatisation would occur there (Gao *et al.*, 2011a). The transformation of the carbon chain into a hexagon ring would dissipate chemical potential energy, and this process is utilised for nucleation. The nucleation occurs mainly on the step edge, whereas nucleation at the terrace becomes significant at relatively high temperatures (>1000 °C) and on a flat surface, which is caused by the lower barrier energy (Gao *et*

*et al.*, 2011a). The finding is different when molecular dynamics (MD) or quantum chemical MD is carried out. The nucleation of graphene can be started with the aggregation of carbon on a plain transition metal surface under a high concentration of carbon. The initial nucleated graphitic structure is in a multi-MR, and the defect healing that occurs under high-temperature annealing increases the portion of six-MR carbon. Further healing and extension of the graphene island is completed by adding carbon adatoms rather than carbon clusters (Meng *et al.*, 2012), as simulated by DFT. Wang *et al.* (2011a) claimed that Haeckelite structures are preferentially nucleated first and later healed by the Ni(111) surface to form graphene. During healing, the role of Ni is to provide rapid stabilisation for the system. The Ni atoms partially move out of the surface to stabilise the dangling  $\sigma$ -bonds during healing (Wang *et al.*, 2011a, Jacobson *et al.*, 2012a). The Ni-C bonds keep breaking and reforming at the defect area for healing (Karoui *et al.*, 2010). All the simulation results show that the pentagon and heptagon ring or Stone–Wales (SW) defects are rarely healed due to their energetic stability. The healing effect and mechanism have been verified by experimental investigations (Jacobson *et al.*, 2012a).

Readily available polycrystalline Ni foil is always used to grow large-area graphene films. However, the graphene grown from polycrystalline Ni is found to have various thicknesses and numbers of layers (Zhang *et al.*, 2010, Reina *et al.*, 2008a, Takahashi *et al.*, 2012) (Figure 2.4). Polycrystalline Ni with a large number of grain boundaries contains a high density of lattice steps. Most of the multilayer graphene nucleates at these lattice steps (Reina *et al.*, 2008a). This is because the curvature of the grain edge allows the accumulation of carbon at these sites for multilayer graphene nucleation, as shown in Figure 2.4(b). Meanwhile, the smooth surface of single-crystal Ni(111) enhances the monolayer graphene nucleation

(Zhang *et al.*, 2010) (Figure 2.4(a)). The graphene formation temperature is different on different surfaces, and the lowest is found on (001). The grown graphene was observed to dissolve back into Ni at 850 °C, whereas this is the ideal temperature for other surfaces to nucleate graphene (Takahashi *et al.*, 2012). Ni(001) has a strong binding energy with graphene because each carbon atom is in contact with four Ni atoms. The strong Ni-C interaction would cause a repulsive interaction within the C-C interaction and also dissolution at the edge of graphene (Takahashi *et al.*, 2012).

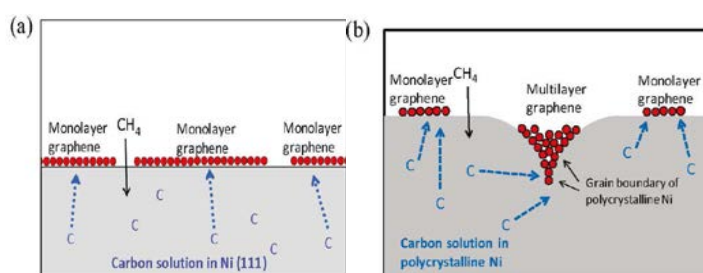


**Figure 2.4** Graphene formation on (a) a single-crystal Ni(111) surface and (b) a polycrystalline Ni surface (Zhang *et al.*, 2010).

Multilayer graphene is always formed on polycrystalline Ni, which is attributable to its high solubility of carbon. Various methods are investigated to limit the graphene to monolayers and bilayers. These methods include controlling the carbon concentration in CVD and increasing the cooling rate after CVD. A high cooling rate is known to restrict excess of carbon precipitation because carbon atoms have insufficient time to diffuse (Odahara *et al.*, 2012). However, when the carbon feedstock is low, a fast cooling rate causes little graphene coverage on the Ni surface (Reina *et al.*, 2009). The solubility of carbon in Ni can be reduced by lowering the growth temperature to approximately 550 °C to self-limit graphene segregation, but a too low temperature induces competing formation of nickel carbide (Addou *et al.*, 2012). The surface of polycrystalline Ni can be polished by using a longer annealing time before the CVD reaction to induce the surface transformation that favours the formation of Ni(111) with fewer grain boundaries, thus inhibiting the multilayer



graphene nucleation in the later CVD step (Zhang *et al.*, 2010). The flatness of terraces can also be improved by using a better buffer layer, such as MgO deposited at low temperatures. A smooth Ni(111) surface can be formed by subsequent Ni deposition (Iwasaki *et al.*, 2011). The high carbon solubility and high carbon diffusion rate in Ni can also be utilised to control the number of graphene layers formed. The dissolved carbon may diffuse through the Ni film, ultimately forming bilayer graphene in the middle of the Si substrate and the Ni film (Peng *et al.*, 2012b). Xu *et al.* (2011) directly deposited a Ni film on HOPG to synthesise monolayer graphene by carbon diffusion through the Ni film.

Graphene that grows on Ni is bounded matchless on Ni; fewer grain boundary defects can be observed on graphene when two islands coalesce due to the strong healing ability of Ni. The in-plane lattice constant for graphene expands by 1.2% from bulk graphite to match that of the Ni(111) substrate at room temperature. In contrast, Ni contracts 1% from 827 °C to room temperature, the thermal stress is reduced, and graphene free of wrinkles is obtained (Odahara *et al.*, 2011). As-grown graphene on Ni always consists of small individual graphene domains with different thicknesses, regardless of whether single-crystal or polycrystalline Ni is used, which is mainly caused by the large solubility of carbon in Ni (Sutter *et al.*, 2010). Research involving Ni catalysts still remains in the preliminary stage, and precise control over graphene formation has yet to be achieved.

#### **2.4.5 Copper (Cu)**

The discovery of the ability of Cu to be used for graphene synthesis came later compared with other catalysts. As discussed in section 2.3, the nucleation and extension mechanism of graphene catalysed by Cu is quite different; a surface growth approach has been proposed. The solubility of carbon in Cu bulk is very low,

it can be concluded to be a purely surface-based process (Shu *et al.*, 2012). In addition, the diffusion barrier of carbon atoms on Cu is also low (Yazyev and Pasquarello, 2008), which gives to Cu a different catalytic role compared with other transition metals. The Ruoff research group published several articles about alternating the exposure of  $^{12}\text{CH}_4$  and  $^{13}\text{CH}_4$  isotopes to copper foil (Li *et al.*, 2010, Li *et al.*, 2011a, Li *et al.*, 2009b). The authors clearly showed that the growth front of graphene could be delineated by the boundaries between the domains of  $^{12}\text{C}$ - and  $^{13}\text{C}$ -based graphene (Figure 2.5). The observation made by Ruoff indicates that the growth of graphene on Cu is surface mediated and diffusion of carbon into the Cu bulk is highly limited. Generally, the formation of graphene is initiated by nucleation at the initial instant of carbon precursor exposure, and the number of islands increases with exposure time to the carbon precursor. The carbon adatoms are found to interact mainly with free-electron-like surface states in Cu, leading to a weak surface diffusion barrier on the Cu surface (Chen *et al.*, 2010). The islands grow with time, whereas some of the islands may coalesce with other islands if the temperature is high (Kim *et al.*, 2012b, Hwang *et al.*, 2011). The unique growth mechanism of graphene on Cu has enabled it to be self-limiting during graphene formation on Cu, thus yielding predominantly to monolayer graphene with excellent quality (Li *et al.*, 2009a).

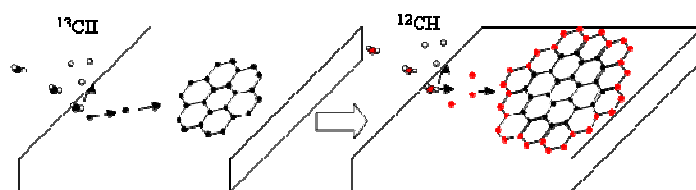


**Figure 2.5** Illustration of the surface growth mechanism on Cu. Black particles indicate  $^{13}\text{C}$  isotope, red particles indicate  $^{12}\text{C}$  isotope and white particle indicates hydrogen (Li *et al.*, 2009b).

The graphene islands tend to have an ordered shape, such as a hexagonal shape with  $120^\circ$  corners (Yu *et al.*, 2011, Luo *et al.*, 2011, Fan *et al.*, 2011, Shu *et al.*,

2012, Robertson and Warner, 2011, Wu *et al.*, 2011a) (Figure 2.6 (a)), a flower-like shape with four or six lobes (Figure 2.6(b)), or a dendrite shape (Figure 2.6(c)). The hexagonal shape of graphene islands formed by the zigzag edge is preferred in graphene grown on polycrystalline Cu (Yu *et al.*, 2011). The low diffusion barrier of carbon on the Cu surface enables the carbon monomer to attach to the graphene islands on its own, which is different from the carbon cluster attachment on graphene for Ru and Ir. The DFT calculation by Luo *et al.* (2011) showed that the carbon monomer attachment to the armchair edges is energetically favourable. The graphene grows following the mechanism converting armchair edges to zigzag edges and maintain the growth of zigzag edges afterwards. In addition, the armchair-like edges are intended to be passivated by Cu atoms, and the passivation lowers the barrier for carbon atoms attaching to the graphene edge. This behaviour leads to the very fast growth of the armchair edge, and it gradually disappears, whereas the more inert zigzag edge grows slowly but dominates the growing graphene islands (Shu *et al.*, 2012). These mechanisms are only feasible under low-carbon-source conditions. The temperature must be high enough to support the molecular activity, or a dendritic domain will be obtained. If the growth duration is increased, the six corners of the hexagonal graphene islands protrude to become six-petal flower-like shapes (Fan *et al.*, 2011).

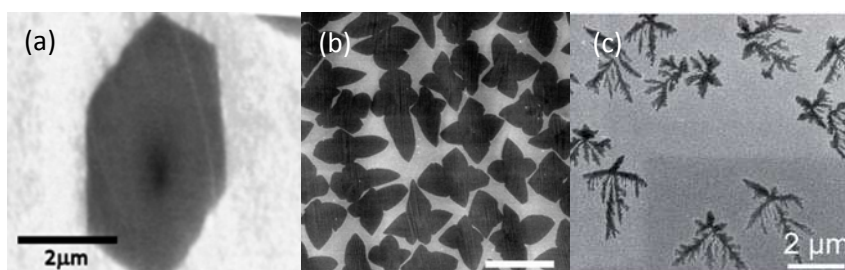


**Figure 2.6** SEM images of graphene with (a) a hexagonal shape (Robertson and Warner, 2011), (b) a four-lobed flower shape (Li *et al.*, 2010), and (c) a dendrite shape (Fan *et al.*, 2011).

The CVD mechanism regarding Cu under low-pressure conditions would also start with the nucleation of a large number of domains but with four-lobed flower-like (Hwang *et al.*, 2011, Li *et al.*, 2010, Wofford *et al.*, 2010, Rasool *et al.*, 2011b) (Figure 2.6(b)) or six-lobed flower-like (Li *et al.*, 2011a, Zhang *et al.*, 2012d) structures across the Cu surface. The understanding of the actual formation mechanism of those structures remains weak. There are several explanations proposed. First, the behaviour is attributed to the underlying Cu substrate: either mobile carbon atoms on the surface or those carried by Cu atoms may diffuse along one of the four equivalent lattice axes of the substrate and extend the growth along one of the directions (Rasool *et al.*, 2011b). Wofford *et al.* believe the graphene islands undergo complex nucleation and simultaneously seed a graphene island with multiple orientations. The growth is faster at the four corners, which forms the four-lobed shape (Wofford *et al.*, 2010). Full coverage of Cu surface with monolayer graphene can be obtained through proper control of the operating parameters, such as carbon precursor feed rate, temperature, pressure, and hydrogen ratio (Zhang *et al.*, 2012d, Li *et al.*, 2010).

Graphene can be nucleated on various crystal facets of Cu, including Cu(310), Cu(410), Cu(411), Cu(433), Cu(632), Cu(100), and Cu(111) (Wood *et al.*, 2011). However, only Cu(100) and Cu(111) can outclass other facets. The graphene formed on Cu(001) is polycrystalline (Rasool *et al.*, 2011b). Carbon diffusion is slower on Cu(100) and may cause carbon stacking to form multilayer graphene (Wood *et al.*, 2011). However, a continuous graphene can be obtained through proper manipulation of the process parameters (Ogawa *et al.*, 2012). Tao *et al.* pre-annealed a Cu(111) film to form a continuous graphene with the help of a co-catalyst, hydrogen (Tao *et al.*, 2012). The performance of Cu(111) is better than that of

Cu(001) in the formation of monolayer graphene with a single domain (Ogawa *et al.*, 2012, Wood *et al.*, 2011, Ishihara *et al.*, 2011). The higher binding energy of graphene on Cu(111) ensures the graphene to be in the most energetically stable state on Cu(111) to prevent other orientations and grain defects (Shi *et al.*, 2012). The presence of different graphene orientations on Cu(100) would cause defects at the graphene grain boundaries when graphene islands meet and grow (Zhao *et al.*, 2011). Zhao *et al.* also found that the graphene on Cu(111) has a hexagonal superstructure, whereas the superstructure is linear on Cu(100) and it is not uniform (Zhao *et al.*, 2011). In contrast, four different graphene variations can be found on a single graphene island nucleated at the same site on Cu(100) due to surface imperfections that induce complex heterogeneous nucleation events (Wofford *et al.*, 2010). Meanwhile, the triangular Cu(111) crystal has a greater similarity with the hexagonal graphene lattice in terms of crystallographic geometry and a lower energy barrier for nucleation that results from a smaller lattice mismatch (Hu *et al.*, 2012b). Wu *et al.* (2011b) made a different observation, in which the graphene formed equally on the Cu surfaces with any crystal lattice; Cu(111) forming rectangle graphene islands instead of the hexagonal graphene islands normally found. The small and different graphene orientation on Cu(111) was also found by Gao *et al.* (2010a). The formation of a different graphene orientation on Cu(111) is generated by misalignment during the growth across the step edges. However, the problem of multiple orientations can be reduced by using higher growth temperature and smoother Cu surfaces either in high-vacuum or atmospheric-pressure CVD (Nie *et al.*, 2011b, Hu *et al.*, 2012a). As reported by Walter *et al.* (2011), the multiple orientation of domains could be found on both Cu(111) and Cu(100) surfaces when relatively low temperature (850-900°C) was used for graphene growth.

Polycrystalline Cu foil is the preferred catalyst because it is easy to obtain at lower cost compared with single-crystal Cu surfaces. In addition, Cu substrate would end up with scarification from graphene separation. Furthermore, the single-crystal Cu requires a longer exposure to harsh chemicals to fully etch it away, which damages the graphene sheet (Reddy *et al.*, 2011). Various observations have been reported on graphene grown from polycrystalline Cu substrates. Both single-crystal graphene (Wu *et al.*, 2011a, Radhakrishnan *et al.*, 2011) and polycrystalline graphene (Liu *et al.*, 2011c, Wofford *et al.*, 2010, Nie *et al.*, 2011b) have been reported to be formed on polycrystalline Cu. Polycrystalline Cu contains the largest number of atomic steps and grain boundaries, and these sites always have higher chemical activation energy for hydrocarbon decomposition and serve as the sites for graphene nucleation (Liu *et al.*, 2011c, Wofford *et al.*, 2010, Li *et al.*, 2010). It has also been reported that the nucleation of graphene is a random event (Regmi *et al.*, 2012). Although low-pressure CVD and similar operating conditions were used, many articles reported that the grain size of Cu has no effect on the grain size of the graphene formed (Terasawa and Saiki, 2012, Hwang *et al.*, 2011). Wood *et al.* (2011) reported that graphene can be nucleated on any crystal facet of polycrystalline Cu, but only the Cu(111) surface promotes fast monolayer graphene growth with fewer defects. The graphene grown from Cu(111) will spill over to other facets and may cover the existing graphene island on the other facets, thus forming graphene with non-uniform layers. Under prolonged growth with the assistance of plasma, the graphene would be lifted up to form graphene nanowalls (Kumar *et al.*, 2012). The defects at the grain boundary have also been reported to serve as a channel for diffusion of carbon adatoms to the non-exposed bottom surface of Cu, thus forming graphene at both surfaces (Su *et al.*, 2011).

Although it has been believed that Cu possesses the ability to form predominantly monolayer graphene, some researchers have started to question this ability of Cu, especially under atmospheric-pressure CVD. Bhaviripudi *et al.* (2010) found that monolayer graphene could only be grown under atmospheric pressure with methane on the ppm scale, and the general crystallinity of graphene is also poor due to the low mass transport rate of the carbon source. The formation of multilayer graphene is induced by the high level of precursor saturation due to excess supply of the carbon source (Robertson and Warner, 2011). It is believed that the projected density of states (PDOS) of the underlying Cu may penetrate through the graphene. The PDOS would dissociate the carbon precursor above the graphene sheet which causes formation of subsequent graphene layers (Jeon *et al.*, 2011). Moreover, the boundaries of grains and the impurities that lie on graphene can provide nucleation sites for additional layers of graphene (Yan *et al.*, 2011a), and it is believed that the subsequent graphene layer grows on top of the first layer (Kalbac *et al.*, 2012). Zhang *et al.* (2012a) demonstrated a different view in which a C-Cu alloy exists during the whole graphene formation process. The authors proposed a new mechanism in which the carbon atoms adsorb on the Cu surface first and form a C-Cu alloy. This alloy provides the carbon source for graphene extension. The carbon rich C-Cu alloy may also provide a carbon source for the subsequent layer.

The study of the synthesis of graphene on Cu has flourished since the first report by Li *et al.* (2009a). However, the understanding of the kinetics and the mechanisms of graphene formation is still lacking. There are many mysteries yet to discover and many theories waiting to be verified. Cu has been proven to outperform other metals, such as Ru, Ir, and Pt, in terms of cost-effective graphene growth. However, there are also drawbacks to the use of Cu, such as the appearance of

wrinkles on the graphene and structural defects at the joints of graphene islands due to different crystallinities. Pentagon or heptagon carbon rings do always appear which may limit the application of graphene in the field of electronics.

#### **2.4.6 Nickel-Copper Bicatalyst (Ni-Cu)**

The combination of Ni and Cu is the most common and most broadly reported bimetallic catalyst in graphene synthesis. Cu and Ni have a very distinct solubility of carbon under various recipes of Cu-Ni, which allows the management of carbon solubility for optimization of graphene growth.

There are 2 types of common Ni-Cu combination, first, the direct using of a Ni-Cu alloy or bilayer bimetallic film with thickness in nanoscale. The nanoscale metal is expected to be partially molten under high temperature annealing. Both Ni and Cu atoms could diffuse into each other due the high miscibility between these two metals. The control of graphene to monolayer becomes much easier by using lower growth temperature, faster cooling rate and Ni-Cu catalyst with smaller content of Ni (Chen *et al.*, 2011, Liu *et al.*, 2011d, Liao *et al.*, 2013). Meanwhile, if the growth temperature is not high enough, presence of nickel carbide would break up the Ni with surrounding metal, forming nanoparticles and subsequently induces nucleation of CNTs (Memon *et al.*, 2013a). But for full coverage, higher temperature and slower cooling rate are required. The purely surface mediated growth mechanism of Cu is broken with addition of Ni, even with 5.5% of Ni (Wu *et al.*, 2012b, Liu *et al.*, 2011d). A small amount of Ni can be used to enhance the self-limiting ability of Cu to precisely control the graphene layer formation (Chen *et al.*, 2011). However, an alloy with a large amount of Ni is not different than pure Ni. Besides that, the different lattice structure shows a very distinct variation on the energy barrier on the dehydrogenation. Cu/Ni(111) shows a much higher dehydrogenation energy barrier,



while that of the Cu/Ni(100) is about 40-60% lower (Yuan *et al.*, 2013). Another type is the separated bilayer Ni-Cu alloy. This bilayer catalyst is more likely operating separately to grow graphene. It composes a composite substrate with C-dissolving (Ni) layer and a C-rejecting (Cu) layer; Cu playing the role of inhibiting the amount of diluted carbon atoms (Wan *et al.*, 2012).

The role of each element in the alloy of Ni-Cu is yet to be well understood. In conclusion, each catalyst has its own advantages and disadvantages. Table 2.1 summarizes the properties of 5 major known catalysts to wrap-up this section.

## **2.5 Transfer of graphene**

Graphene grown using the CVD method is normally bounded firmly on the substrate, such as transition metals, due to the strong graphene-substrate interaction. The removal of graphene from its substrate is always difficult. Currently, monolayer graphene produced in laboratories contains a certain amount of defects. These defects make the graphene brittle and can be easily torn or broken under physical stress. To unnecessary defects such as surface folding or breaking during the transfer process and impurities (Sun *et al.*, 2011), various graphene transfer techniques have been developed. This section reviews the up-to-date techniques for graphene transfer, including mechanical exfoliation and wet chemical etching.

### **2.5.1 Mechanical exfoliation**

The famous mechanical exfoliation method was first reported by Novoselov *et al.* using a scotch tape to exfoliate HOPG (Novoselov *et al.*, 2004). Mechanical exfoliation is a straightforward transfer process and a popular approach for wafer-scale graphene separation from its initial substrate. This method was more practical to be applied for the transfer of graphene that was grown using SiC sublimation.

**Table 2.1** General properties of transition metals mainly used to catalyse graphene growth.

Transition Metals	Growth Mechanism	Carbon solubility at ~1000 °C	Active crystal facet	Spacing between graphene to transition metals
Ru	Bulk-mediated growth, carpet growth mode	0.34 at.% (Arnoult and McLellan, 1972)	Ru(0001)	1.45-2.20 Å (Sutter <i>et al.</i> , 2008)
Ir	Bulk-mediated growth, carpet growth mode	0.041 at.% (Arnoult and McLellan, 1972)	Ir(111)	3.77-4.04 Å (N'Diaye <i>et al.</i> , 2006)
Pt	Still in debate either bulk-mediated growth or surface-mediated growth	$\sim 3.1 \times 10^{-4}$ – 0.0043 at.% (Kang <i>et al.</i> , 2009, Siller <i>et al.</i> , 1968, Selman <i>et al.</i> , 1970)	Pt(111) ( the best performance), Pt(110), Pt(100), Pt(311),	3.23-3.67 Å (Vanin <i>et al.</i> , 2010)
Ni	Bulk-mediated growth	$\sim 0.6$ -0.9 at.% (2002, Li <i>et al.</i> , 2009b)	All facets are active. Ni(111) with the best performance	2.46-2.49 Å (Cheng <i>et al.</i> , 2011a)
Cu	surface-mediated growth	$\sim 7.4 \times 10^{-4}$ - 0.008 at.% (Mattevi <i>et al.</i> , 2011, 2002, Bhaviripudi <i>et al.</i> , 2010, López and Mittemeijer, 2004)	All facets are active , Cu(100) and Cu(111) with the best performance	3.26-3.70 Å (Adamska <i>et al.</i> , 2012, Giovannetti <i>et al.</i> , 2008)

Mechanical exfoliation requires the use of an adhesive agent, such as a polymer or tape to provide an adhesion force that is stronger than the interaction force between the graphene and the metal catalyst or SiC. Early mechanical exfoliation of graphene from SiC involved the coating of the supporting metal. Au with thickness of ~100 nm was first coated onto graphene using physical vapor deposition, followed by coating another layer of liquid polyimide (PI) through spin coating, where PI serves as the mechanical support for the Au/graphene film during the transfer process. The PI film is next cured through annealing for drying. The PI film forms a better contact with Au. The PI/Au/graphene is ready for peeling (Unarunotai *et al.*, 2009). However, due to the lower adhesion force of Au, holes and wrinkles are normally found in the transferred graphene. The authors replaced Au by Pd in a later report, and the number of defects in graphene was significantly reduced (Unarunotai *et al.*, 2010). The advantage of this approach is the effectiveness of the transfer. Separation of monolayer graphene from few-layer graphene sample can be also realized. However, removal of metal and PI film involves some tedious processes. For example, reactive ion etching is required for PI removal. Additionally, wet chemical etching is required to remove the metallic film (Unarunotai *et al.*, 2009).

The adhesive force between graphene and Cu is weaker than that of graphene on SiC. Polydimethylsiloxane (PDMS) is a common polymer used for stamp printing, and now it has been developed for physical exfoliation of graphene. A simple PDMS film can be used as adhesive tape to peel off the graphene (Kim *et al.*, 2012a). In this method, liquid PDMS is directly coated onto the graphene/catalyst sample. After the polymer is dried and hardened, the PDMS/catalyst film is ready for peeling to separate the graphene from the metal substrate. The number of graphene layers to be peeled off can be

controlled by adjusting the ratio of PDMS to the curing agent. PDMS has been utilized by researchers to exfoliate graphene from HOPG or in the transfer printing of patterned graphene (Allen *et al.*, 2009a). However, the PDMS stamp transfer method works only if the adhesion energy between graphene and the desired substrate is strong enough. The PDMS stamp transfer is only useful for transferring graphene to flat and hydrophilic substrates, and cracks easily form during the transfer process (Choi *et al.*, 2013).

To simplify the entire transfer process, thermal release tape (TRT) has been applied as support for graphene during peeling. TRT is a special type of adhesive tape that loses its tackiness and fully releases the adhered object when it is heated to a certain temperature. The adhesion energy between graphene and Cu was measured experimentally to be around  $0.51 \text{ J.m}^{-2}$  -  $0.72 \text{ J.m}^{-2}$ , the TRT should have adhesion energy high enough for graphene peeling from Cu (Yoon *et al.*, 2012, Lahiri *et al.*, 2011b). The TRT is first attached directly onto the graphene grown on the transition metal. The graphene and TRT are pressed under vacuum to remove any air trapped between the TRT and the graphene and later peeled off directly to separate the graphene from the SiC or metal catalyst (Caldwell *et al.*, 2010). Meanwhile, for the release of graphene, the TRT/graphene film is simply pressed to the desired substrate, such as silicon or glass, followed by a heating treatment at  $\sim 120 \text{ }^\circ\text{C}$  to eliminate the adhesion strength of the TRT. The adhesion energy between graphene and silicon was reported to be  $0.45 \text{ J.m}^{-2}$  (Yoon *et al.*, 2012), thus heating is required to reduce the adhesion between TRT and graphene. Roll-to-roll hot pressing and direct hot pressing methods have been demonstrated to improve the strain distribution between the TRT/graphene film and the arbitrary substrate to increase the contact (Kang *et al.*, 2012). This is leading to less deformation of the graphene structure and shape. The residue of the tape, such as glue,

can be cleaned using acetone or other common organic solvents (Lee *et al.*, 2010a). Subsequent wet chemical etching is necessary for the removal of the metal film if the graphene is grown on nanoscale catalyst film on silicon. The catalyst is normally peels off together along with graphene (Lee *et al.*, 2010b).

Additional adhesion metals, such as gold, have been coated on graphene before exfoliation using TRT, and this method avoids exposing graphene to glue (Song *et al.*, 2009). Meanwhile, the combination of TRT with thin metal films was reported to be able to predominantly exfoliate monolayer graphene through a 2-steps exfoliation. Graphene grown on SiC is coated with a thin layer of Ni and peeled off from SiC using TRT (Kim *et al.*, 2013a). Ni is calculated to have an adhesion energy about  $3.47 \text{ J.m}^{-2}$  (Lahiri *et al.*, 2011b). It is strong enough for the peeling of graphene from SiC. However, the strong adhesion energy between Ni and graphene has made it almost impossible with a direct peel off without introducing excessive defects on graphene. The work of Chen *et al.* (2014) using a commercial laminating film that was made by laying a thin poly(ethylene co-vinyl acetate) (EVA) film onto a flexible polyethylene terephthalate (PET) substrate for separation. The separated graphene from Ni foil was broken into pieces and failed to be maintained as a whole piece of wafer scale graphene.

Recently, the utilization of bubbles generated through electrolysis process to delaminate graphene from catalyst has been demonstrated. The PMMA/graphene/catalyst/support can be immersed into an electrolyte. Electric current was then conducted into the catalyst to generate hydrogen bubbles between the catalyst surface and the support through the electrolysis process. It peels the PMMA/graphene/catalyst from support much more gentle to maintain the perfectness of graphene (Lee *et al.*, 2014). Meanwhile, in another report using similar method, the

hydrogen bubbles are generated in between catalyst and graphene for direct separation. However, there is still no reliable strategy to control the side where the bubbles are formed (Fan *et al.*, 2014), They are formed between either graphene and PMMA or between graphene and catalyst. The spacing between graphene and Cu or Pt is larger compared with other catalyst, due to the weaker interaction between graphene and Cu or Pt (Seah *et al.*, 2014). These properties can be utilized for a much simpler transfer method. Water molecules were proved to be able to penetrate in between graphene and Cu or Pt under long period of soaking inside hot water. However, large scale tears have also been observed on graphene (Gupta *et al.*, 2014).

Mechanical exfoliation can be as simple as a direct peeling off graphene from its substrate. It is easy and time-saving. The transition metal substrate can normally be preserved, and it is readily recycled for subsequent syntheses. However, the mechanical force can cause damages to graphene. To maintain the quality of graphene, researchers have attempted to apply additional transfer steps such as intercalation of foreign element in between graphene and metal, to weaken the interaction force between the graphene sample and the metal catalyst. Mechanical exfoliation still remains a reliable method, allowing recycling of metal catalyst and the simplicity of the transfer process will be important in the mass production of graphene at low cost.

### **2.5.2 Wet chemical etching**

Wet chemical etching is a method to separate the graphene sheet from its catalytic metal surface by removing this latter through an etching process. This approach involves chemicals that are able to dissolve the transition metal catalyst (Ni or Cu). It avoids the use of excessive mechanical force that may cause severe mechanical defects

to graphene. Initially, the purpose of metal etching was to transfer graphene sheets to a copper grid for TEM characterization. The graphene detachment from one substrate can be performed with simple acid etching. Because graphene is highly hydrophobic, it spontaneously floats on an aqueous solution and can then be separated and transferred to the TEM grid.

The direct etching of metal is not an ideal method for graphene transfer; introduction of folds and tears to the graphene sheet being the main drawback (Regan *et al.*, 2010). Isolated graphene could roll into a ball-like structure inside the aqueous etching solution due to the hydrophobic nature of graphene. Thus, the surface tension of the etching solution is utilized to prevent the graphene from rolled up (Cai *et al.*, 2009). Sometimes, isopropyl alcohol is added to reduce the surface tension of water and minimizes the external force around graphene for an easier deposition of graphene onto later substrate (Lin *et al.*, 2014). Normally, the process of graphene transfer involves spin coating of a suitable polymer onto the graphene/metal film before it is subjected to the metal etching process. The polymer/graphene is placed onto the desired substrates, followed by the polymer removal. Silicon rubber was first used as a support polymer (Yu *et al.*, 2008). The main drawback of using silicon rubber is the difficulty in its removing due to its inertness.

A research group from MIT had successfully modified the transfer process of graphene to other substrates by using polymers (Reina *et al.*, 2008a, Reina *et al.*, 2008b). Two supporting polymers, PMMA and PDMS were experimentally verified to be competent for graphene transfer, and these polymers can also be removed thereafter using organic solvents, such as ethanol and acetone. This method is commonly used for the transfer of aligned carbon nanotube arrays and has now been modified for graphene

transfer (Seah *et al.*, 2011a, Seah *et al.*, 2012). The polymer film is normally coated on the graphene/metal foil through spin coating, and a few reports use drop coating (Li *et al.*, 2009c). The typical route for graphene transfer via wet chemical etching and a supporting polymer layer is shown in chart 2.1.

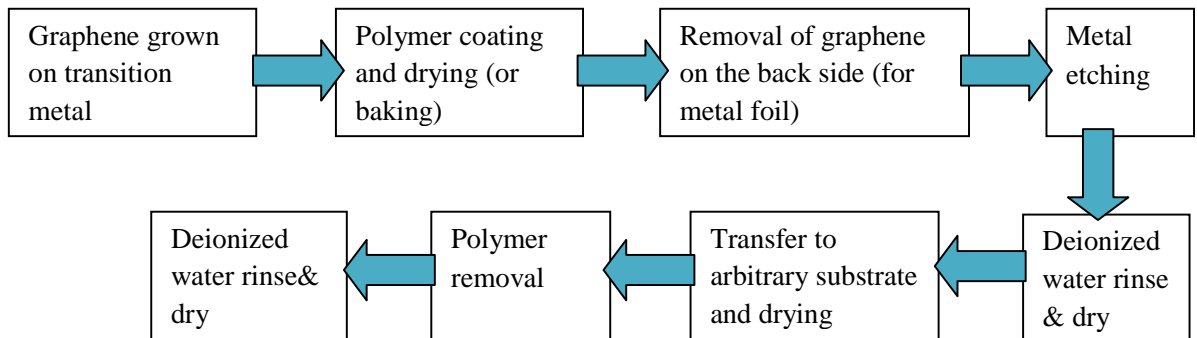


**Chart 2.1** Typical route for graphene transfer by polymer supported wet etching method.

The customary transfer method is a multiple step process which possesses several shortcomings, such as the difficulty to remove the polymer completely, graphene deterioration due to the chemical attack, contamination of metal particles and etc. Each of the steps listed in chart 2.1 will cause some damage to the graphene sample. To date, various improvements have been suggested to minimize the introduction of defects and contaminants during the transfer process.

Physical degradation, such as tears, folds and wrinkles are easily formed on the transferred graphene. A crack or tear can be formed under various causes, including direct contact with graphene and improper handling of graphene during transfer. Meanwhile, wrinkle formation is related to the difference in thermal expansion between the metal catalyst and the graphene during the CVD process (Obraztsov *et al.*, 2007). The presence of wrinkles later result in gaps between the graphene and the substrate, subsequently inducing cracks (Li *et al.*, 2009c). The surface morphology of CVD-grown



graphene has high tendency of copying the surface of the metal surface. The graphene grown on a rough metal catalyst surface will be curvy in structure. The graphene surface maintains its curvature after removal of the catalyst because PMMA forms a rigid coating in firm contact with graphene. Flattening of the PMMA/graphene film is crucial to place the graphene onto the desired surface perfectly. Liu *et al.* (2011b) reported the use of a simple method by prolonging the soaking period of PMMA/graphene sheet in water. The surface tension of water has been shown to contribute to flatten the wrinkles. Li *et al.* (2009c) proposed a second PMMA coating layer. The second layer of PMMA is able to re-dissolve the first layer of PMMA, inducing the flattening of graphene/PMMA sheet and increasing the contact area between the graphene and the substrate, which provides a protective layer for graphene after PMMA removal. An additional layer of PDMS can be added as a flexible frame for the PMMA/graphene film after transfer to the desired substrate. Heat can then be applied to soften the PDMS/PMMA/graphene film so that full contact of graphene with its substrate is achieved (Suk *et al.*, 2011). The whole process is summarized in Figure 2.7 (a) and (b).

Combination of PDMS and other polymers can also be used in the transfer of graphene onto soft and non-flat substrates. The PMMA/graphene film is relatively rigid, thus wrinkles or voids can be easily formed when it is transferred to soft or non-flat substrates. By adding PDMS onto the graphene/polymer film, transfer of monolayer graphene can be performed onto almost all surfaces and with higher contact areas between graphene and its substrate (Song *et al.*, 2013, Choi, 2013), preventing voids between the graphene and the substrate surface that would be crucial to minimize tearing of graphene. A screen protector for portable display devices has also been utilized for graphene transfer. The screen protector contains two layers of materials, namely PET

and silicon, which has a low adhesion force to graphene on the silicon side. Graphene can attach on the PET/silicon film after etching away the catalyst foil. The PET/silicon film can be separated easily after the graphene is placed onto the desired substrate. The weak adhesion force between the graphene and the PET/silicon film facilitates the separation (Chen *et al.*, 2013a). The entire process adopts almost the same mechanism as contact printing than that using for PDMS stamps. Under certain conditions, the graphene can be glued directly onto the substrate before the catalyst being etched using epoxy to enhance the contact of graphene with the substrate, which minimizes the physical damage during the transfer process (Kim *et al.*, 2013b).

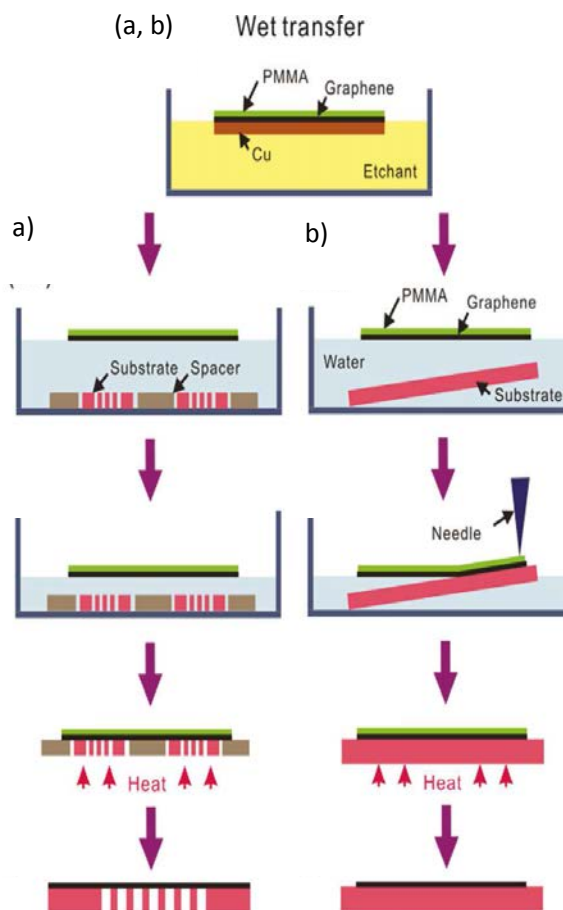


**Figure 2.7** (a) Flow diagrams of the transfer process with heat treatment for (a) perforated substrate and (b) flat substrate (Suk *et al.*, 2011).

Meanwhile, another type of defect may form during the graphene transfer through wet chemical etching method is the trapping of moisture or solvent between graphene and the substrate. The graphene is unable to deposit flatly onto a desired substrate, such as a copper TEM grid or silicon wafer (Liang *et al.*, 2011). This gap can be eliminated by simple baking of the PMMA/graphene (Liang *et al.*, 2011) or by vacuum annealing at low temperature. However, long annealing time would also create defects onto the graphene sheet (Wang *et al.*, 2011b). The existence of trapped moisture may cause serious problems during TEM characterization. Under high vacuum, the trapped moisture evaporates and damages the graphene or dislodges it from the grid. An adhesive layer is proposed as a method to improve the contact between the graphene and the electron microscope grid to obtain more accurate data. Regan *et al.* (2010) directly placed the grid onto a graphene/Cu film, and isopropanol was dropped onto the grid (Figure 2.8). As isopropanol is evaporated (along with the water), the vacuum formed during evaporation was able to induce adhesion of graphene to the grid before Cu etching. Baking can also be added to enhance the evaporation and strengthen the contact between the graphene/Cu film and the TEM grid. Addition of isopropanol also can be applied to graphene flakes as well. In that case, the TEM grid can be placed onto a pile of graphene flakes, and a small drop of isopropanol is dropped onto the grid. The flakes will adhere firmly onto the TEM grid after evaporation of isopropanol. Heating can be added to obtain a firmer attachment (Meyer *et al.*, 2008). Chloroform, an adhesion promoter, is also proposed for deposition of graphene films onto a TEM grid. Chloroform is first applied between the TEM grid and graphene/Cu film. The adhesion force formed after evaporation could induce attachment of the film, and the moisture is simultaneously evaporated through baking. Formvar plastic was coated across the grid to

further stabilize graphene on the copper grid to promote the gradual etching of Cu during the metal etching process (Pantelic *et al.*, 2011).

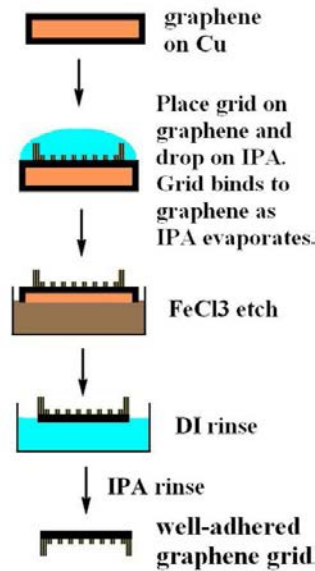


**Figure 2.8** Schematic of the direct transfer of graphene onto a TEM grid (Regan *et al.*, 2010).

### 2.5.2(a) Etchants

The common metal etchants are iron nitrate (Li *et al.*, 2009a), iron chloride (Kim *et al.*, 2009), ammonium persulfate (Bae *et al.*, 2010, Petrone *et al.*), hydrochloric acid (Zheng *et al.*, 2010), marble solution (Yan *et al.*, 2011b), Transene Thin Film Nickel Etchants (Ni TFB) (Shi *et al.*, 2010), etc. Aqueous iron salts are preferred compared to acid as etching agent. Iron salt solutions are odorless, harmless to human skin, and do not produce dangerous fumes in contrast to concentrated acid. It has been reported that the etching power of iron chloride is stronger than that of hydrochloric acid for etching nanoscale Ni film (Delamoreanu *et al.*, 2014). Although iron salt solutions are more efficient, but the ferromagnetism property of iron would alter the electromagnetic

transport of graphene (Lee and Lee, 2010). The presence of 3d-transition metal (Fe, Ni, Co and etc) on graphene would severely degrade the charge transfer through the graphene plane. Transition metals within the 3d group containing empty d-orbital would form a strong hybridization with the  $\pi$ -electrons of graphene and distort the electron diffusion path. This effect is known to downgrade the electronic property of graphene (Liu *et al.*, 2011e). The presence of very small amount of metal doping, even though after the repeated cleaning of graphene with distilled water, would severely affect graphene transport properties and conductivity (Blake *et al.*, 2009, Ambrosi and Pumera, 2014). Etching by acid could avoid contamination of the organic material, but it introduces hydroxyl and carboxylic groups on the graphene which causes point defects in graphene. Additionally, fuming during etching results in trapping bubbles that might cause mechanical defects in the graphene sheet (Srivastava *et al.*, 2010). Conversely, the use of ammonia persulfate as etching agent would introduce heavy p-doping to graphene (Bae *et al.*, 2010).

Strong bases, such as KOH (Wang *et al.*, 2011b) and NaOH (Reina *et al.*, 2008b) are better for etching of SiO<sub>2</sub>. For some reasons, such as for the transfer of patterned graphene, etching of SiO<sub>2</sub> is necessary for a second time transfer. PMMA can be used for the transfer of chemically derived graphene, such as graphene oxide or graphene flakes to arbitrary substrate (Yamaguchi *et al.*, 2010). In case of re-transfer of graphene to another substrate, an easier method was demonstrated by seeping a small amount of water into the gap between graphene and the support to displace the graphene from its support. The graphene/support was first coated with PMMA and covered with another PDMS film, water was then dropped at one edge of the polymer-coated substrate. Water can penetrate into the hydrophobic-hydrophilic interface between graphene and substrate,

thus the separation can be done easily (Li *et al.*, 2014). A method based on the use of bubbles also can be carried out by direct immersion of the PMMA/graphene/substrate into a mixture of ammonia solution and hydrogen peroxide. The aqueous solution intercalates in between graphene and substrate. The oxygen bubbles formed in between graphene and substrate, thus displace graphene from substrate (Gorantla *et al.*, 2014).

### **2.5.2(b) Protective layers**

Another source of contamination that is often found on graphene is the polymer residue. The presence of polymer residues could severely suppress the phonon transport and lower the thermal conductivity of graphene (Pettes *et al.*, 2011). Such contamination also makes the characterization of graphene inaccurate, especially under Raman spectroscopy, by amplifying the D-band (Zhang *et al.*, 2012d). Moreover, the experimental data showed that graphene was significantly n-doped up to  $3.8 \times 10^{12} \text{ cm}^{-2}$  (Geringer *et al.*, 2010), and the carrier mobility was significantly lowered after PMMA contamination (Cheng *et al.*, 2011b). Graphene, PMMA and PDMS are organic compounds in the form of macromolecules. The strong van der Waals force between graphene and PMMA prevents the acetone from removing PMMA completely (Cheng *et al.*, 2011b). Graphene with hydrophobic property easily balls-up it is in contact with organic solvents. The PMMA removal must be completed carefully to prevent the unnecessary folding of graphene. The effect of polymer contamination becomes significant as multilayer stacking of graphene is required. The carrier mobility and graphene sheet resistance would be brutally blocked with polymer contamination in between the graphene sheets (Güneş *et al.*, 2010). A few strategies have been proposed to overcome this problem, such as alternately washing the PMMA with acetone and

isopropyl alcohol (IPA) (Zheng *et al.*, 2010, Chen *et al.*, 2013b). Chloroform is found to be effective to remove PMMA or the photoresist materials that are required for graphene patterning. The properties of graphene are not altered under prolonged exposure to chloroform (Cheng *et al.*, 2011b). Acetic acid has also been reported to possess better performance than acetone for PMMA removal from graphene surface (Her *et al.*, 2013).

Recently, polystyrene and poly(isobutylene) were used to replace PMMA to prevent residue contamination on graphene (Song *et al.*, 2013). Other kind of removable polymers, such as poly(bisphenol-A-carbonate) (PC), are reported to be good supporting polymers for graphene transfer (Park *et al.*, 2010). PC can be removed using chloroform (Lin *et al.*, 2011). However, by using only chloroform, the dissolution of PC is too rapid. The graphene was found to be deteriorated more easily and it experiences mechanical damage during the vigorous dissolution process. Acetone-buffered chloroform is a better choice that could prevent unnecessary damaging of graphene (Lin *et al.*, 2011). Fluoropolymer cannot be easily removed after coating on graphene. However, fluoropolymer has the ability to rearrange the fluorine atoms on the graphene basal plane (Lee *et al.*, 2012), which provides a single step for graphene transfer with fluoride-doping on graphene (Shi *et al.*, 2010). Another strategy has been demonstrated by adding a buffer layer that is easier to remove in between PMMA and graphene, such as 2-(diphenylphosphory) spirofluorene (SPPO1) (Han *et al.*, 2014) or gold (Lee *et al.*, 2013). They were sandwiched between PMMA and graphene to form a matrix. This method enables the utilization of PMMA as a physical support material but without direct contact with graphene to prevent contamination. Meanwhile, if polybutadiene (PBU) is used as interface material between PMMA and graphene, PBU could prevent

the Fermi level change on graphene and it reduces the charged-impurity scattering from a polar adjacent layer (Kim *et al.*, 2014).

High temperature (>250 °C) evaporation of PMMA under an inert atmosphere is another route for PMMA removal, which has been used for CNT transfer (Jiao *et al.*, 2008). It has been reported to be more effective for PMMA removal than acetone dilution (Park *et al.*, 2013). Time and temperature are crucial factors in the prevention of oxidation of the graphene sheets. Moreover, the thermal stress would also induce cracks of graphene. During annealing, the radicals formed during the thermal decomposition of PMMA may lead to rehybridization of the carbon atoms from  $sp^2$  to  $sp^3$  in graphene. Meanwhile, the partially decomposed PMMA with radical sites can easily attach to neighboring PMMA residues, resulting in more difficult PMMA removal (Lin *et al.*, 2012). Additionally, the metal residue, either from the catalyst (Ni, Cu) or from the etching solution (Fe) would play the role of graphene structural reconstruction under elevated temperature (Boukhvalov and Katsnelson, 2009).  $CO_2$ , a weaker oxidizer was utilized to oxidize PMMA under elevated temperature, but the complete removal of PMMA was still far from realized (Gong *et al.*, 2013). Additionally, moisture or oxygen remaining between the graphene sheet and the substrate would act as an oxidizing agent and creates structural defects on the basal plane of graphene during heat treatment (Suzuki *et al.*, 2013). UV irradiation was used by Jeong *et al.* (2014) to degrade the polymer by destroying the side chain of ester group in PMMA in advance and reduce the interaction between the PMMA film and the graphene, which enables a much more effective PMMA removal to aid in the recovery of clean graphene.

The polymer assisted transfer possesses a critical weakness, i.e., difficulty in transferring large area graphene, due to the difficulty in handling the PMMA film (De



Arco *et al.*, 2009). To avoid the use of PMMA or PDMS, some strategies have been proposed, Martins *et al.* (2013.) laminated the graphene-copper onto the desired substrate before copper etching. However, this method is only applicable for hydrophobic substrate and with the utilizing of van der Waals force to hold the graphene while etching. This method introduces significant mechanical defects onto the graphene. Another special process has been proposed, i.e., “roll-to-roll” (R2R), which can be used to transfer 30-inch graphene films (Bae *et al.*, 2010). The process is illustrated in Figure 2.9. The process contains 3 main steps: (i) attach thermal-released tape as a polymer support onto a graphene/metal film, (ii) etch the metal and (iii) release the graphene from the tape and place onto an arbitrary substrate. The discovery of the R2R process has opened a new chapter in the study of graphene synthesis and transfer. This R2R method has been adapted by researchers to continuously synthesize graphene using CVD (Yamada *et al.*, 2012, Hesjedal, 2011). However, the critical drawback of the R2R method is the large amount of mechanical damages done to the graphene. Line-shaped cracks propagate perpendicularly to the roll direction, and holes on the micron scale can be easily formed in the graphene (Kang *et al.*, 2012). In the later publication of the authors, they utilized EVA as the binder between polymer substrate and graphene to reduce the mechanical defects (Han *et al.*, 2011) .

The wet chemical transfer of graphene is a multi-step approach and the deterioration is amplifying from one step to the next in the transfer process. To minimize the number of steps for graphene transfer, the CVD process has been modified so that the synthesis of transfer-free graphene can be obtained. The metal catalyst is directly deposited onto the desired substrate for CVD. After growth, the metal between the substrate and the graphene is etched away using an etchant, leaving

only the graphene on the substrate (Kim *et al.*, 2012c). However, this method is more suitable for small area graphene due to the small exposed area between the metal and the etchant. The majority of the metal is well protected by the graphene, as reported in (Levendorf *et al.*, 2009).

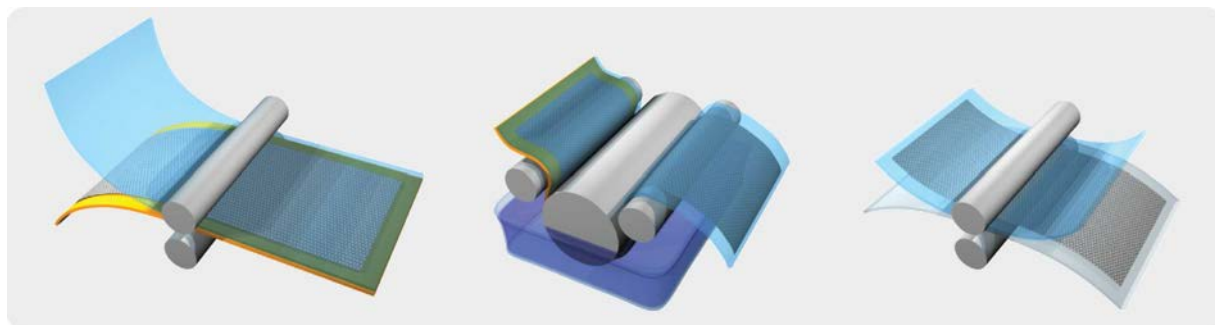


**Figure 2.9** Schematic of the roll-based production of graphene films grown on a copper foil (Bae *et al.*, 2010).

## 2.6 Reuse of catalyst

Researchers are working aggressively on other approaches to further find the better graphene transfer method. Some complicated routes have been designed to overcome the shortcomings possessed by both the wet chemical etching approach and the mechanical exfoliation methods. For example, a simple electrolysis cell with a constant current supply can be applied for graphene exfoliation. Metal etching has been performed using an electrochemical process (Yang *et al.*, 2012). A small voltage is applied to enhance oxidation of the metal. The authors claimed that the electrochemical etching could effectively remove the majority of the metal leaving clean graphene behind. A better electrochemical cell is shown in Figure 2.10 for a better control of the graphene transfer without causing damage to the catalyst foil as reported in (Yang *et al.*, 2012). Reduction of water at the surface of the anode (graphene/metal foil) produces hydrogen bubbles, which would detach the graphene sheet from the metal foil (Wang *et*

*al.*, 2011c, Gao *et al.*, 2012). The electrochemical exfoliation is a “wet” process; a layer of polymer is always required for the prevention of graphene folding. Moreover, the polymer layer could serve as a protective layer for graphene from the mechanical damage caused by the hydrogen bubbles. The main advantages of this approach are that the expensive single crystal structure of metal foil can be preserved and the topographical features that were transferred to the graphene, such as ripples on a copper foil, can be preserved (Wang *et al.*, 2011c).

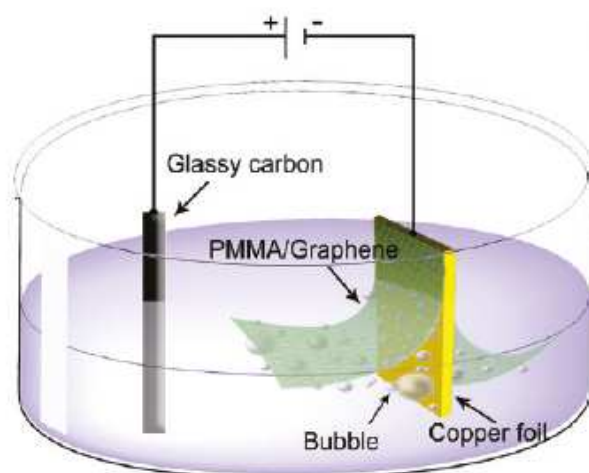


**Figure 2.10** Schematic of an electrolysis cell used for the electrochemical exfoliation of graphene from metal foil (Wang *et al.*, 2011c).

Potential differences have been employed for the electrostatic transfer of graphene from SiC or a metal foil catalyst. This approach takes advantage of the anionic bonding between the metal and a semiconductor or glass. A glass substrate with a negative charge produces an electric field and pulls the graphene/SiC substrate. The anionic bonding facilitates a firm bond between the 2 interfaces and enables the graphene transfer (Biedermann *et al.*, 2010). The firm bond minimizes the void or trapped air or moisture between the graphene and the substrate (Wang *et al.*, 2013).

Meanwhile, electrostatic deposition is also occasionally used for the exfoliation of HOPG to graphene platelets (Liang *et al.*, 2009).

Mechano-electro-thermal (MET) process is a new proposed chemical free process (Jung *et al.*, 2014). An electric field was used to exfoliate the graphene from Cu, the high physical pressure allows the graphene to have maximum contact with the later substrate. Meanwhile, high temperature was used to increase the visco-elasticity of the targeted substrate which enhances adhesion force to graphene. Combination of these 3 forces, strong and ultraconformal contact between the graphene and the targeted substrate can be achieved. It makes the graphene to be able to exfoliate with minimum physical damage and chemical contamination free.

## **2.7 Summary**

This comprehensive review of the literature has outlined the definition of monolayer graphene, current strategies for graphene synthesis and separation methods to obtained free standing graphene film. It also summaries the trend of graphene research, particularly wafer scale graphene for the past decade, CVD is the most promising and economical approach to synthesis wafer scale monolayer graphene. On the other hand, wet chemical etching would be the most gentle graphene separation approach that could highly preserve the perfectness of wafer scale graphene. However, there is still a lot of debate, especially on the fundamental mechanism of graphene formation and separation. Graphene is an innovative material that possesses various desirable properties. The rapid pace of graphene research ensures that a more practical graphene synthesis and transfer method will be discovered. However, there are many challenges and opportunities for applications in daily life.

## CHAPTER 3

### MATERIALS AND METHODS

This chapter describes the details of the experimental work done in the current study. In the first part, the specification of all materials and chemicals used is listed, followed by the experimental equipment and the rig set-up which were used in the decomposition of methane for the production of graphene. Later on, the details of the experimental procedures are presented. The analysis of the products by various means of characterization instruments used in this study is shown in the last part of this chapter.

#### 3.1 Materials and Chemicals

All the chemicals and reagents involved in this research are listed in Table 3.1 with the corresponding assay, name of supplier and purpose of use.

**Table 3.1** List of chemicals and reagents

Chemical/Reagent	Assay	Supplier (Grade)	Purpose of use
Copper foil	Thickness: 0.125mm >99.900%	Aldrich	Catalyst
Nickel Foil	Thickness: 0.025mm >99.900%	Aldrich	Catalyst
Nitric Acid	>65.000%	Merck (EMSURE® ISO) (Malaysia) Sigma-Aldrich (ISO. Reg. Ph.Eur.) (France)	Etchant for Ni
Iron (III) nitrate nonahydrate, Fe(NO <sub>3</sub> ) <sub>3</sub> .9H <sub>2</sub> O	99.900% (Malaysia)	Sigma-Alrich (Malaysia)	Etchant for Ni and Cu

**Table 3.1.** Continue

Chemical/Reagent	Assay	Supplier (Grade)	Purpose of use
Iron (III) nitrate nonahydrate, Fe(NO <sub>3</sub> ) <sub>3</sub> ·9H <sub>2</sub> O	99.000% (France)	Merck ((EMSURE® ACS Reg. Ph. Eur.) (France)	
Methane	99.999%	Air product	Carbon source
Nitrogen	99.999%	Air product	Inert gas used after reaction
Hydrogen	99.999%	MOX	Reduction agent for metal catalyst
Deionized water	-	-	Diluting reagent and for cleaning purposes
Standard gas	1.000% C <sub>3</sub> H <sub>6</sub> 1.000% H <sub>2</sub> 1.000% CO 1.250% O <sub>2</sub> 2.000% C <sub>2</sub> H <sub>4</sub> 2.000% C <sub>2</sub> H <sub>6</sub> 2.000% CO <sub>2</sub> 20.000% CH <sub>4</sub> 69.750% N <sub>2</sub>	MOX	Gas chromatography calibration
Silicon wafer (1000Å thermal oxide)	Orientation <100> Type/ Dopant: N/Ph Diameter: 100mm Thickness 525 ± 25 μm Resistivity 0~30 Ohm-cm Surface : One side polished	Medina	Substrate for transferred graphene

## **3.2 Experimental equipment and rig set-up**

### **3.2.1 Graphene growth rig**

The CVD reaction of methane for the production of graphene was carried out in a horizontal quartz tube reactor system. The schematic diagram of the experimental rig set-up and brief description of the major components of the rig are shown in Figures 3.1 and 3.2 and Table 3.2, respectively. Generally, the experimental rig comprises 3 main parts: gas mixing section, reaction section and gas analysis section. The gas mixing section and reaction section were connected with 1/4" stainless steel 316 tubing, meanwhile the effluent gas was connected to gas analysis section by 1/8" Teflon tubing.

#### **3.2.1(a) Gas mixing section**

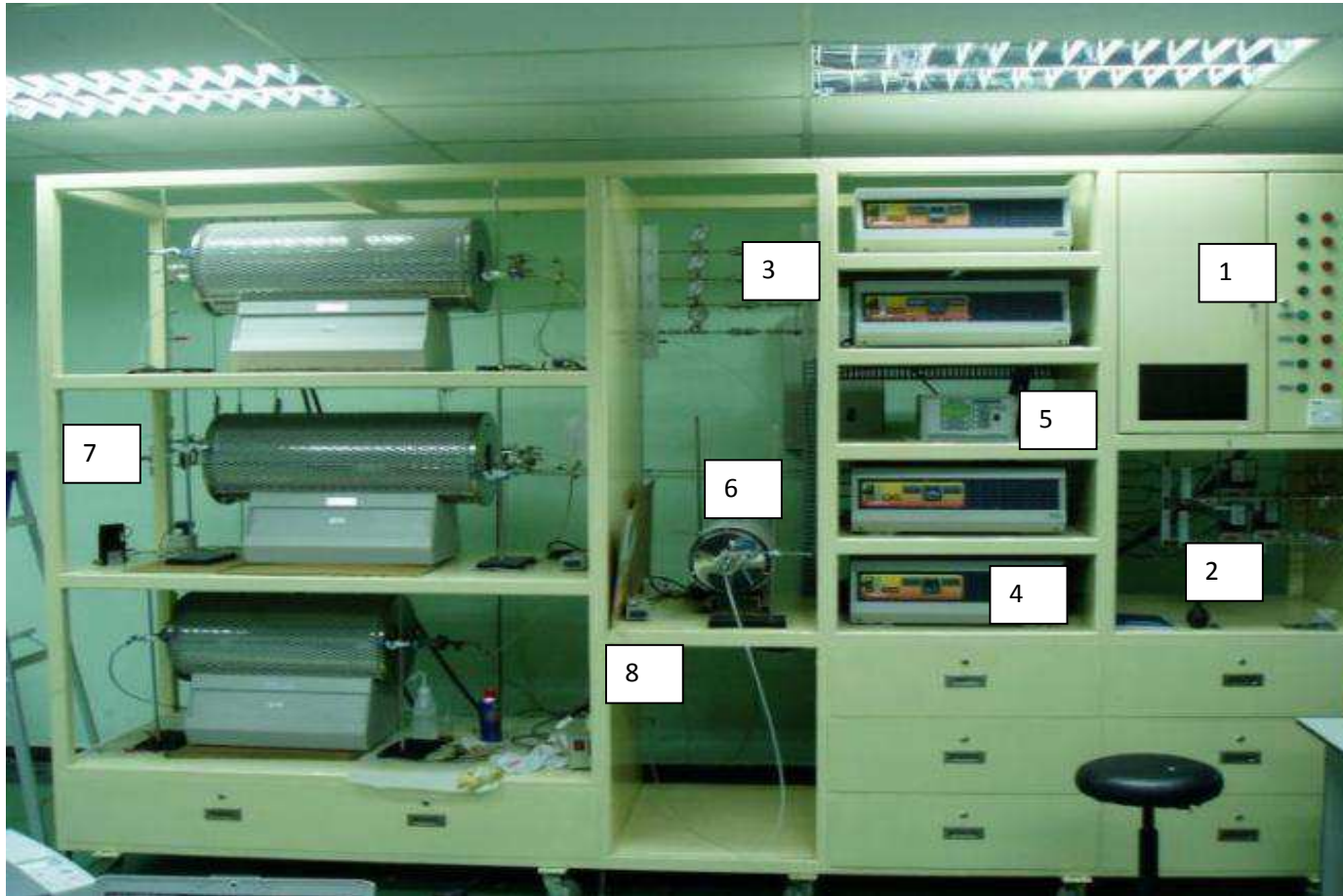
The gas mixing section consisted with 5 major parts: three gas cylinders (nitrogen, hydrogen and methane), two mass flow controllers (No.2 in Table 3.2), a static mixer, a pressure gauge (No. 3) and 4-channel power supply and a readout system (No.5). Hydrogen was used as a reduction agent to reduce the metal catalyst. Purified methane was selected as the carbon source of the reaction due to its less toxic compared with other hydrocarbons. Meanwhile, nitrogen gas was used as protective inert gas to purge the reactor after reaction. The flows of all 3 gases mentioned were controlled by 3 mass flow controllers and 4-channel power supply and readout. Hydrogen and nitrogen shared the same pipeline and controller. Methane gas has its own controller and pipeline. Both pipelines were connected and the gases flowed through a static mixer to create turbulence to obtain well-mixed gases before being charged into the reactor for the growth of graphene. A pressure gauge was installed after the mixer to

monitor the pressure inside the reactor throughout the process to prevent pressure built up inside the reactor. All the piping used in this section were 1/4" stainless steel 316.

### **3.2.1(b) Reaction section**

After the mixer, the gas mixing section was connected to the reaction section with a Teflon 1/8" pipe. The reaction section mainly consists of a furnace, a quartz tube reactor (internal diameter: 30 mm, outer diameter: 34mm, length: 1500mm), a thermocouple (No. 6), a temperature controller (No. 4), a mass flow meter (No.7) and a temperature indicator (No. 8). The furnace used was a three zone furnace with a temperature controller. Quartz with high thermal stability was selected as the tube reactor material. The catalyst nanoparticles deposited on silicon wafer was placed in the center of the reactor during the reaction. A type K thermocouple was also placed in the middle of the tube to measure the actual temperature during the reaction and the temperature was displayed through a temperature indicator. To further confirm the flow rate of the reactant gas and to prevent the leakage, the effluent before reaction was measured with a portable mass flow meter that was placed near the reactor. Meanwhile, the pressure of the reactor was monitored through the pressure gauge in the gas mixing section.

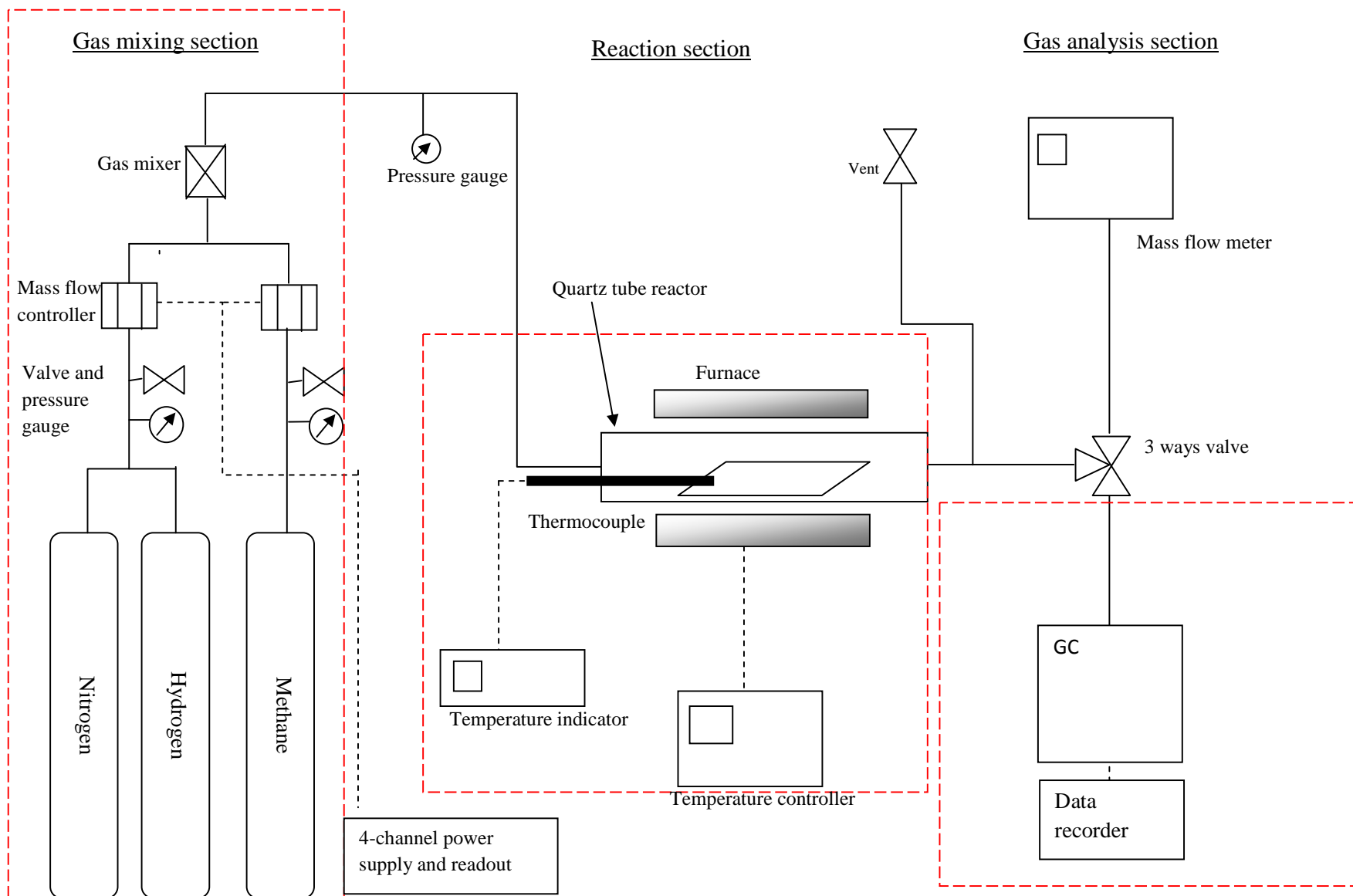




**Legend**



1. Switch
2. Mass flow controller
3. Static mixer and pressure gauges
4. Temperature controller
5. 4-channel power supply and readout
6. Three zone horizontal furnace & Quartz tube reactor and thermocouples
7. Portable Mass flow meter

**Figure 3.1** Photograph of the experimental rig set-up (Descriptions of parts according to numbers listed in Table 3.2)






**Figure 3.2** Schematic diagram of the experimental rig set-up

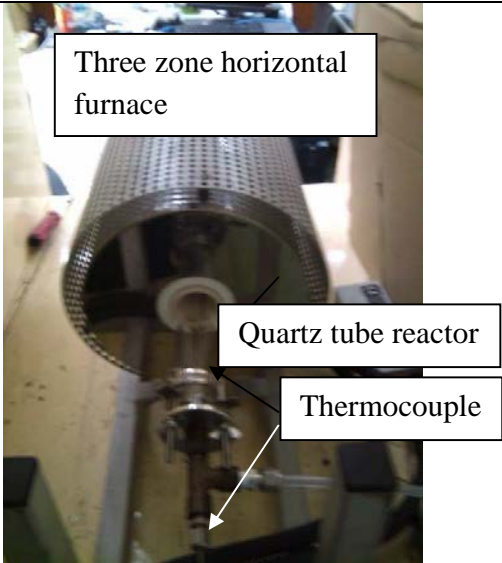

**Table 3.2** Major components of the experiment rig and their function

No (Refer to Figure 3.3)	Component	Image	Specification/ model	functions
1	Switch		-	To cut off the power supply during the emergency case
2	Mass flow controller		Model: Brooks® 5850E (Range of accuracy: 10sccm-150sccm)	To regulate and control the flow rate of nitrogen, hydrogen and methane



**Table 3.2** Continue

No	Component	Images	Specification/ model	functions
3	Static mixer and pressure gauges		Static mixer: OD 1/2"  Pressure gauge: Model: Ashcroft	To create turbulence flow for the mixing of gases before discharged into reactor.  To measure the pressure in the reactor.
4	Temperature controller		Eurotherm 3216P1	To precisely control the temperature for every parts in three zone horizontal furnace
5	4-channel power supply, readout and control panel		Model: Brooks 0152E (Range of accuracy: 10sccm-150sccm)	To regulate and control the flow rate of nitrogen, hydrogen and methane

**Table 3.2** Continue

No	Component	Images	Specification/ model	functions
6	Three zone horizontal furnace & Quartz tube reactor and thermocouples		<p>Horizontal tubular furnace: Carbolite, GHC 12</p> <p>Quartz reactor (Length: 1500mm, internal diameter: 30mm)</p> <p>Thermocouples: Type K D=3mm L= 600mm</p>	<p>To heat up the reactor to the desired operating temperature</p> <p>To provide chamber for the reaction to take place</p> <p>To measure the actual reaction temperature inside the quartz reactor</p>
7	Portable Mass flow meter		<p>Model: Aalborg GFM-17A</p>	<p>To verify the actual flow in the reactor and to monitor the possibility of leak.</p>

**Table 3.2** Continue

Component	Images	Specification/ model	Specification/Model	Functions
8	Temperature indicator			To indicate the actual temperature inside the quartz reactor as comparison with the temperature controller.
-	Gas tanks		Nitrogen: 99.999% Hydrogen: 99.999% Methane : 99.999%	To store reaction gases
-	Gas Chromatography (GC)		Agilent Series 7890A	To analyze the effluent gas of the reaction in blank tests.

### 3.3 Experimental steps

Figure 3.3 shows the flowchart of the research overview of this study.

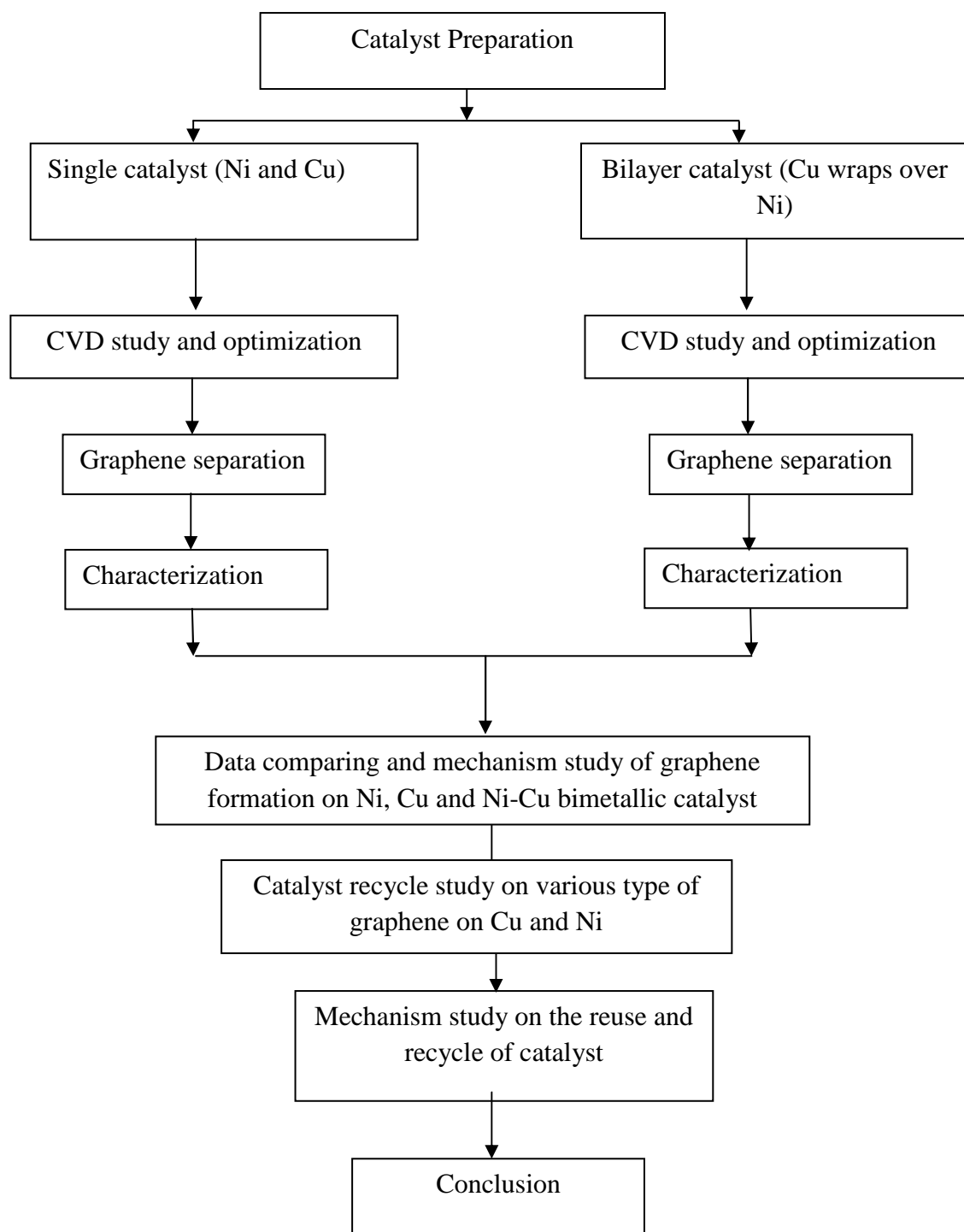


**Figure 3.3** Flowchart of overall research activities of this study.

### 3.3.1 Catalyst preparation

In the present study, the active metal catalysts used were Ni and Cu foils. The commercially available polycrystalline Ni and Cu foils with purity of 99.9% was first cut with the desired dimensions. For the study of individual graphene formation, both foils were cut into square of 5mm x 5mm. Meanwhile, for bimetallic catalyst study, Cu was cut into 7mm x 7mm, as Ni cut into 5mm x 5mm. Both Cu and Ni foils were repeatedly rinsed with ethanol and DI water alternatively for 5 times to remove any organic and inorganic contaminations. Subsequently, the Cu foil was used to wrap the Ni foil as shown in Figure 3.4. The bimetallic catalyst was later pressed with a hydraulic press with a force of 20N to displace the air trapped inside the bimetallic catalyst and also to maximize the contact between Ni and Cu. The bimetallic catalyst was sandwiched with 2 clean Teflon boards to prevent unnecessary contamination during pressing; it was then ready to place in the furnace for the CVD reaction.



**Figure 3.4.** Cross-section view of the Cu-wrapped Ni catalyst used for the study.

### 3.3.2 Production of graphene by CVD and process study

Before the study carried out into full throttle, preliminary test was carried out in advance to test the ability of the quartz tube reactor to grow graphene. A more extreme condition was selected to grow graphene with operating parameters of 950 °C, 10 min, 80 sccm of H<sub>2</sub> and 80 sccm CH<sub>4</sub> to grow graphene on both Ni and Cu foil in the preliminary study. If graphene could be found on Ni and Cu foil, milder condition would be further utilized for optimization to grow predominantly monolayer graphene. Generally, the CVD reaction was carried out in a horizontal quartz tube reactor (Figure 3.2). The catalyst was placed directly in the middle of the



quartz tube and located at the middle of the furnace. The reactor was heated from room temperature to desired temperature with a ramping rate of 10 °C/min under a flow of 80 sccm/min H<sub>2</sub> gas. The purpose is to reduce the native oxide that may present on Ni or Cu foils. When the desired temperature was achieved, high purity CH<sub>4</sub> was mixed with H<sub>2</sub> gas under desired flowrates and duration of reaction. After the reaction was completed, CH<sub>4</sub> and H<sub>2</sub> were switched off and replaced with N<sub>2</sub> gas of 100 sccm/min. The reactor was allowed to cool down to the ambient temperature naturally, normally it took several hours to get the furnace cooled to room temperature. For the application of fast cooling, a steel wire was attached at the end of the quartz boat containing the catalyst foil placed in the heating of the reactor. After reaction, the stainless steel wire was pulled to bring the quartz boat out from the heating zone to room temperature zone experiencing a rapid cooling. It reduces the activity of catalyst and carbon rapidly under low temperature. The general strategy was illustrated in Figure 3.5. A thermal couple was bind at the outer surface of quartz tube, at the area where the sample placed after displaced from the furnace, to estimate the temperature of sample.

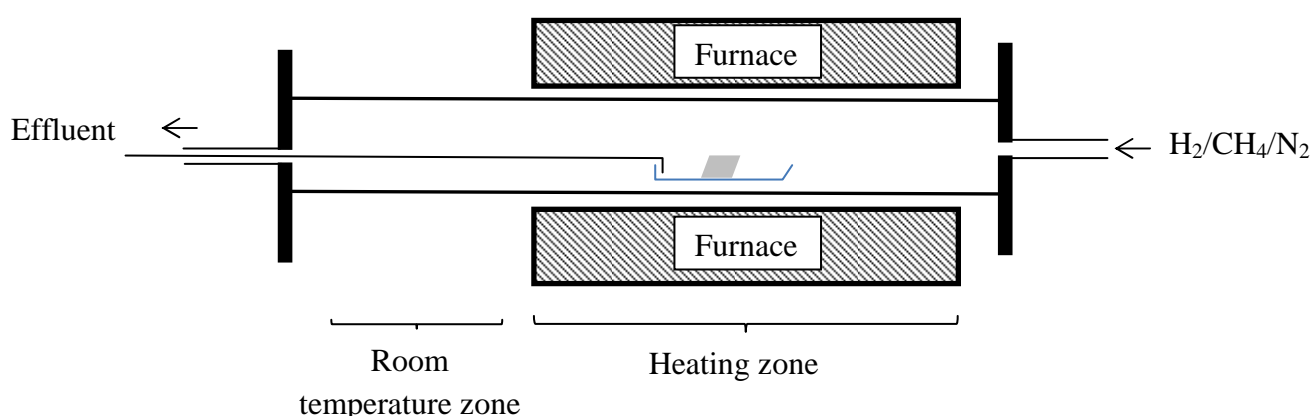


**Figure 3.5** Setup of the reaction zone of the reactor for the implication of fast cooling.

After the reactor was found to have the ability to grow graphene, catalyst foils i.e. Ni, Cu and Ni-Cu bilayer catalysts were studied extensively. The process

parameters studied were reaction temperature, reaction period and partial pressure of methane. The range of the parameters is listed in Table 3.3

**Table 3.3** Parameters list for CVD study

Parameter	Range
Temperature	800-1000 °C
Reaction period	1-8 minutes
Partial pressure of methane	0.10-0.70 atm

### 3.3.3 Controlled experiment for bilayer catalyst

The purpose of this controlled experiment is to verify that there was no leak of carbon precursor into the middle of the “sandwiched” catalyst and the carbon obtained mainly came from the diffusion through the Ni foil. The Cu-SiO<sub>2</sub>-Ni trilayer catalysts (Figure 3.6(a)) and Cu-Ni-SiO<sub>2</sub> trilayer catalysts (Figure 3.6(b)) was prepared and firmly pressed with hydraulic press to displace the air between and maximize the contact between each couple of foils respectively. The CVD reaction was carried out with 80 sccm H<sub>2</sub>, 20 sccm CH<sub>4</sub>, and temperature of 1000 °C and last for 10 min. Longer period and higher temperature were also used to confirm that the leak is still insignificant even though under harsher conditions.

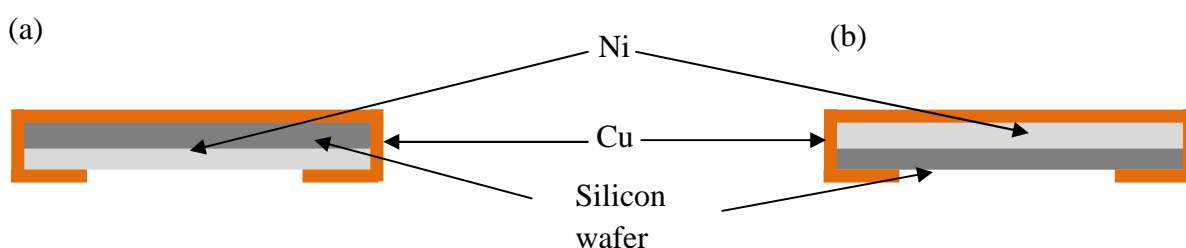


**Figure 3.6** Scheme of the tri-layer catalytic systems: (a) Cu- SiO<sub>2</sub>-Ni and (b) Cu-Ni-SiO<sub>2</sub> used for control experiments.

### 3.3.4 Graphene separation

After the CVD reaction, graphene, graphite or maybe other graphitic materials would form on both surfaces of the metal foil. The properties of graphene are severely hindered, especially for the graphene that grow on Ni foil. In order to obtain a trustworthy data, graphene needs to be separated from the original metal foils and transferred to the appropriate substrate. In preliminary study, iron nitrate solution and nitric acid were tested in their effectiveness for separating graphene from both Ni and Cu. Graphene itself is highly corrosion resistance to weak and mild chemical attack. Thus, the unwanted surfaces need to be scrubbed with sand paper (mesh 800) to destroy and remove the graphene formed at that area. It provides direct contact of metal foil with etchant to provide more effective chemical attack on the metal foil.

Graphene/metal foil was directly floated onto the etchant during the separation process. Any protective layer that was normally used to prevent the mechanical defect was avoided. Most of the graphene produced in the current study are strong enough to resist to the mild mechanical force experienced by our separation process. After the metal foil was totally etched, the etchant was diluted 150-200 times. The free-standing graphene that is highly hydrophobic remained floated on the solution, and the surface tension of water ensures the graphene floated flatly and prevent the ball-up effect. It was then hooked onto a TEM grid for HRTEM observations. Meanwhile for other characterization, it was gently applied onto silicon wafer, and dried at 60 °C overnight. After the suitable etchant with suitable conditions (concentration, exposure time) was determined in the blank tests, it would be applied throughout the whole study unless stated.

### **3.3.5 Study on the reuse and recycle of catalyst**

Monolayer, bilayer and few-layered graphene that were directly synthesized on Ni foil through CVD under particular operating condition were utilized in the current study. 2 different etchants namely aqueous iron(III) nitrate and nitric acid with different concentrations, by diluting nitric acid (65%, Merck) and iron(III) nitrate nonahydrate (>99.95%, Sigma-Aldrich) were used. Only the 4 edges of graphene/Ni foil were scrubbed with sand paper (800 mesh) to provide the opening for direct contact between Ni and the etchant. Meanwhile, graphene grown on unwanted Ni surfaces was preserved to minimize the chemical attack on Ni. It was then floated on nitric acid or aqueous iron nitrate solution for separation. After graphene and Ni were separated, iron nitrate and nitric acid were diluted with huge amount of DI water to minimize the contamination on the graphene sheet. It was then transferred onto silicon/silicon oxide (1000 Å) wafer for characterization. Meanwhile, the remaining Ni foil can be easily removed from iron nitrate solution or nitric acid and rinsed with DI water. The surface of Ni was polished with sand paper (800 mesh) to obtain a smooth surface and later placed into the reactor for the subsequent reaction. These steps were repeated until the Ni foil was too thin to be handled by hands or holes were observed. Since the dimension of graphene fully copy the topography of catalyst, a catalyst with hole would not give a continuous graphene film.

## **3.4 Characterization**

### **3.4.1 Raman spectroscopy**

Raman spectroscopy is the most direct and efficient method to determine the quality of the graphene. All the separated graphene and deposited onto silicon substrate before characterized with Reinashaw *inVia* Raman spectroscopy (USM)

(unless for sample grown on Cu foil with temperature of 900 °C and below, since the samples appear in tiny flakes and very hard to deposit onto any substrate. Hence it was characterized directly on the Cu foil). The incident light from a 632.8 nm argon laser was focused on the samples with a 50x microscope objective and no filter was used. The range Raman shift with 1100  $\text{cm}^{-1}$  to 3000  $\text{cm}^{-1}$  was scanned. The laser power of 50 mW was directly focused onto the graphene sample. Meanwhile for the Raman mapping, a Horiba LabRAM HR 800 (Université de Lorraine) micro-Raman spectrometer was utilized. The area of 50  $\mu\text{m}$  x 50  $\mu\text{m}$  was scanned under the same laser with incident light (632.8 nm argon laser) was focused on the samples with a 50x microscope objective without filter. As for Raman mapping, the range of Raman shift narrowed to 1500-1700  $\text{cm}^{-1}$  (to scan only the G-band) and 2550-2750  $\text{cm}^{-1}$  (for the 2D-band). Each spot was exposed to laser for 30 seconds and 2 cycles.

The optical light microscopes with both Raman spectroscopies (Reinshaw and Horiba) were used to take magnified micrographs of the graphene samples with magnification of 50x.

Three major bands in the Raman spectrum of graphitic materials are typically used to infer structural information: (1) D-("disorder") band at  $\sim 1350 \text{ cm}^{-1}$ ; the relative intensity of this peak imitates the degree of disorder, dangling bonds or relative  $\text{sp}^3$  carbon content, in the carbon structure; (2) G-band at  $\sim 1580 \text{ cm}^{-1}$  is the peak that reflects the  $\text{sp}^2$  graphitic bond; (3) 2D -band at  $\sim 2680 \text{ cm}^{-1}$ , which is the second harmonic of the D-band. The main Raman features used to evidence a graphitic material with one single sheet are: (1) relative intensity of the 2D- and G-bands,  $I_{2D}/I_G$ , higher than 1.4; (Reina *et al.*, 2008a, Wu *et al.*, 2012c, Liu *et al.*, 2011d) (2) full width half maximum (fwhm) of the 2D-band below 40  $\text{cm}^{-1}$  (Ferrari *et al.*, 2006, Chen *et al.*, 2011, Liu *et al.*, 2011d). To provide a better view on the overall

pattern of the Raman spectra, all the spectra shown in the Chapter 4 are normalized based on the maximum value of respective spectrum.

**Table 3.4** Characteristic of different types of graphene in Raman spectra.

Graphene	$I_{2D}/I_G$	Fwhm <sub>2D</sub>
Monolayer graphene	>1.4	< 40 cm <sup>-1</sup>
Bilayer graphene	1-1.3	40-50 cm <sup>-1</sup>
Multilayer graphene	<1	>50 cm <sup>-1</sup>

### 3.4.2 Atomic force microscopy

Atomic force microscopy (AFM) (USM) is one of the foremost tools for imaging, measuring, and manipulating matter at the nanoscale. It was used to study the surface topography of the catalyst foil. The model of AFM used in this study is a Park System XE-100 equipped with program XEI. No sample preparation was required for AFM and a non-contact mode was utilized for the scan area of 15 μm x 15 μm.

### 3.4.3 X-ray Diffraction

XRD was performed using an INEL CPS120 Diffractometer (Université de Lorraine) equipped with a spatial location detector in a semiconductor focusing geometry. An anticathode of Cobalt Co K $\alpha$  served as the source of X-rays. The diffracted X-rays was characterized with an INEL multichannel detector (4096 channels), the angular opening of 120° coinciding with the goniometer circle. The diffraction angles are corrected for meter linearity errors (due to recording) by prior calibration with standard Y<sub>2</sub>O<sub>3</sub>.

The sample, catalyst foil was placed at the center of the goniometer circle, by prior adjustment of the height of this one, bringing the sample ( $\theta = 6^\circ$ ) has a height such that the intensity of the direct beam is reduced of half. The sample is driven with a rotary movement in order to minimize the problem of preferential orientation of the crystallites. The angle of incidence of the variable beam is adjusted so as to explore more or less deeply in the sample.

#### **3.4.4 High Resolution Transmission Electron Microscopy (HRTEM), electron diffraction and Energy Dispersive Spectrometer (EDS)**

High Resolution Transmission Electron (HRTEM) images were taken by utilizing Jeol ARM 200F (Université de Lorraine).or Fei *Tecnai* 20 (Osaka University) operating at 80 kV. The graphene sample separated from metal foils was directly placed on the TEM holey grids (300 mesh). The grid was treated under 100 °C in air to remove the moisture before TEM observation. Electron diffraction pattern for the graphene sample was taken on the bulk of the graphene sheet during HRTEM characterization.

To characterize the elementary composition inside the bulk of Ni catalyst, Jeol JEM-09100IS (Osaka University) Ion Slicer was utilized for the thinning of the Ni foil to observe the element composition at the middle of the bulk Ni foil. First, a Ni strip with a thickness of 250  $\mu\text{m}$  was cut with motorized diamond cutter from the center of the Ni foil after the CVD reaction (Figure 3.7(a)). It was further polished with sand paper (micro-Mesh 4000) to obtain a Ni strip with a thickness of 100  $\mu\text{m}$  (Figure 3.7(b)). The Ni strip was placed into an ion slicer and a shield belt with a thickness of 10  $\mu\text{m}$  was placed atop of the strip. The Ni strip oscillated with a low-angle ( $3^\circ$ ), while an Ar ion beam (4kV) continuously irradiates the Ni strip from the top, as the thin shield belt allows low-angle irradiation of the Ar ion beam at both

sides of the Ni strip, until an etched hole appeared (Figure 3.7(c)). The hole appeared at roughly 90 $\mu\text{m}$  from the top. The Ni strip was adhered onto a copper ring with epoxide. It was then transferred to the HRTEM *Tecnai 20* apparatus for imaging and also Energy Dispersive Spectroscopy (EDS) spectra were acquired to study the elementary composition of the Ni grains and grain boundaries.

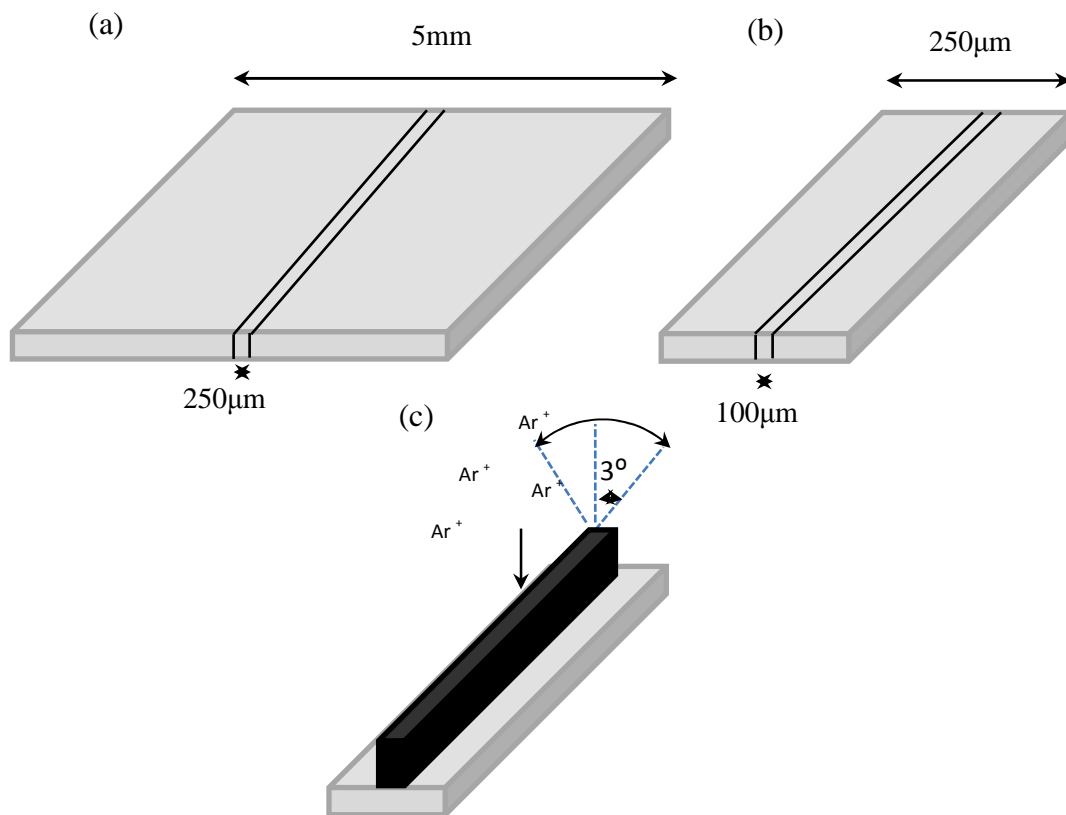


**Figure 3.7** The steps for the sample preparation for obtaining EDS spectrum at the middle of Ni.



## CHAPTER 4

### RESULTS AND DISCUSSION

This chapter reports the results and discussion of the whole study. It is divided into 6 main sections. Section 4.1 presents the results of preliminary studies on the proficiency of a horizontal quartz CVD reactor to grow graphene on Ni and Cu. It is followed by the CVD process study for Cu and Ni for graphene formation in sections 4.2 & 4.3, respectively. Section 4.4 is devoted to the process study and the related chemical growth mechanism using Ni-Cu bilayer as catalyst to form graphene. Section 4.5 describes the strategy utilized and the theory behind graphene separation toward the reuse of Ni to grow graphene.

#### 4.1 Preliminary studies

In this section, the main purpose is to verify that our CVD system is suitable to synthesize graphene and that it has the ability for subsequent graphene separation from the respective metal catalyst. In preliminary studies, two blank tests were performed. A first test was intended to study the appropriateness of the self-designed horizontal quartz tube reactor for methane decomposition and the effectiveness of the metal foils (Cu and Ni) to produce graphene. The second test was carried out to ensure the effectiveness of two chosen etchants for the graphene separation from its metal foil substrate.

##### 4.1.1 Blank test on methane decomposition and preliminary studies of Ni and Cu foil for graphene formation

In the blank test, methane decomposition was performed with only the presence of a quartz boat that was placed in the middle of the quartz tube reactor. The atmosphere of 80 sccm of CH<sub>4</sub> with 80 sccm of N<sub>2</sub> was tested. Different temperatures

(700 °C-1150°C) were studied and the effluent gases were analyzed by an online GC to determine the average conversion of methane. The calculated methane conversion after stabilization of the system for are listed in Table 4.1. The results show that the methane conversion was very low at 700 and 850 °C, and it highly increases at 1000 °C. Quartz is an inert material, and as expected the quartz tube and the quartz boat do not contribute to decomposition of methane.

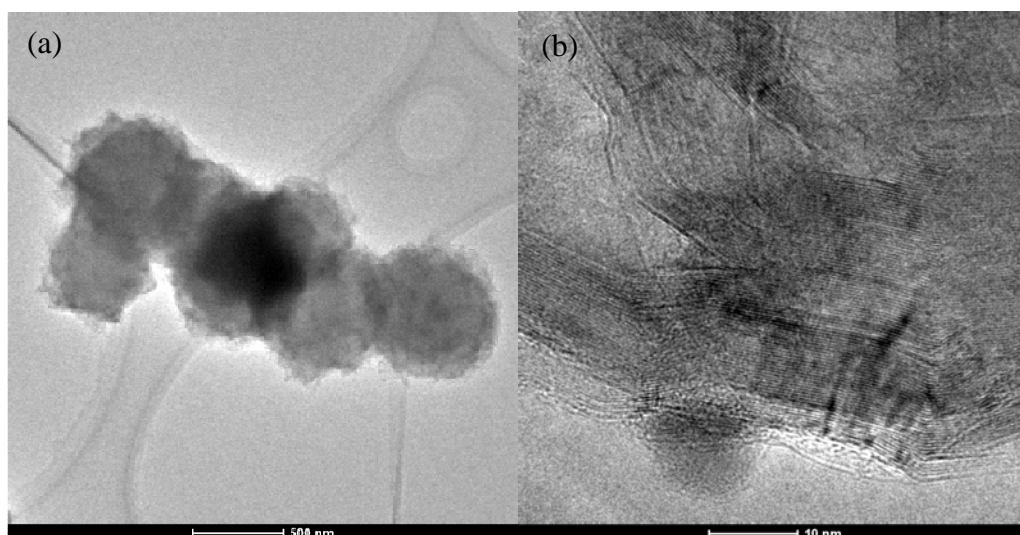
Sackett (1995) had investigated the thermal stability of methane under inert atmosphere. He found that the half-time for the thermal decomposition of methane at temperature of 800, 900 and 1000 °C were 108, 34, and 4 hours, respectively. Since the CVD reaction involves a continuous flow of methane, with a total flow of 160 sccm/min and the tube diameter was 30 mm and the furnace length 45 cm, the residence time for methane was 1.98 min and around 0.6 % of methane was thermally decomposed. This value is in agreement with that obtained with GC: 0.8 % of methane conversion at 1000 °C (Table 4.1). Meanwhile, at 1150 °C, the thermal decomposition becomes very significant; a “black smoke” could be visualized with naked eyes. The “black smoke” was mainly composed with carbon soot resulted by thermal decomposition of methane (Seah *et al.*, 2013). It was not suitable to be characterized with GC because of an irreversible contamination to the column. As a quartz boat was put in the reactor for 10 min under such operating conditions and cooled down to room temperature naturally, a thick black powdered film was coated on the quartz boat.

Figure 4.1 shows the TEM images of the blackish powder. Observation at low magnification reveals large carbon species (Figure 4.1a). High magnification TEM images at the edges of the particles show a highly packed graphitic structure which suggests that, the material formed was pyrolytic carbon materials (Figure 4.1b).

Hence, at 1150 °C, the thermal decomposition becomes very significant and that seems not suitable for graphene production because of an unavoidable poisoning phenomenon of the catalyst foils.

**Table 4.1** Methane conversion recorded in the blank test.

Reaction temperature (°C)	Methane conversion (%)
700	~ 0.2
850	~ 0.2
1000	~ 0.8



**Figure 4.1** TEM images of the black powder collected on the wall of the quartz tube that underwent CVD of 1150 °C. (a) Low magnification image and (b) High magnification image.

After verifying that the poisoning effect did not occur at 1000 °C and below, the suitability of both Cu and Ni to grow graphene under proposed system was tested. Cu and Ni foils with a size of 5 mm x 5 mm were used for the CVD reaction with the following operating parameters: 950 °C, 10 min, 80 sccm of H<sub>2</sub> and 80 sccm of CH<sub>4</sub>. The sample was allowed to cool down to room temperature naturally under N<sub>2</sub> used as protecting gas.

The Ni and Cu foils after the CVD reaction were characterized with Raman spectroscopy and the spectra obtained are shown in Figure 4.2. The peaks for all D-, G- and 2D-band were very obvious. For both Ni and Cu, the height of the G-band is much higher compared with that of the 2D-band indicating the presence of either multilayer graphene or perhaps graphite.

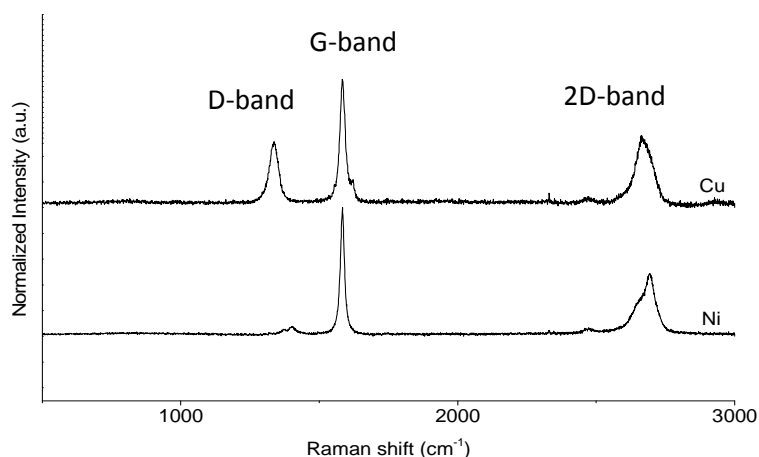


**Figure 4.2** Raman spectra of graphitic materials grown on Ni and Cu with operating parameters of 950 °C, 10 min, 80 sccm of H<sub>2</sub> and 80 sccm of CH<sub>4</sub>.

#### 4.1.2 Preliminary test of graphene separation from Ni and Cu

The CVD as-grown graphene, irrespective to any transition metal utilized, is attached to its original metal substrate. Graphene has limited value if it remains attached firmly onto the catalyst foil. Furthermore, most of the characterization technique, such as HRTEM, Raman spectroscopy, electrical properties measurement and etc. need a free-standing graphene to be deposited onto a suitable grid or substrate (silicon wafer for example). As a result, the separation process of graphene is a vital step to acquire accurate and trustworthy characterization.

Normally, the whole surface of the metal foil is covered with graphene after the CVD process. Graphene is inert and highly resistant to corrosion. To allow the etching of metal foils and facilitate the graphene separation, direct contact between the etchant solution and the metal foil has to occur. First, it was proceeded by rubbing

the unwanted surface of graphene/metal foil with sand paper (800 mesh) to completely destroy the grown graphene. The foil was next directly floated onto the etchant, namely aqueous iron(III) nitrate (0.5 mol/L). The Cu foils could be completely etched away in 1-2 hours. However, as iron(III) nitrate was utilized to separate graphene from the Ni foil, graphene was not able to be separated from Ni. To enable to whole research work more efficiently in time, nitric acid was tested for graphene separation from Ni. Nitric acid with a concentration of 4.80 mol/L (21.67 %) was too strong, the etching was too vigorous and numerous hydrogen bubbles were deliberated. The prepared graphene was broken into small pieces (Figure 4.3(a)). When the concentration of acid was reduced to 1.44 mol/L (6.7 %), graphene could be separated within a wide range of 2-24 hours (Figure 4.3(b)). Interestingly, an adequate amount of Ni foil remained after the separation process, but at the same time, the graphene sheet suffered some deterioration. In order to preserve the perfectness of graphene sheet, the concentration of acid was further reduced to 0.73 mol/L (3.35 %). It took around 1-2 days to completely etch away the Ni foil for separation (Figure 4.3(c)). Furthermore, the perfectness of the graphene was highly preserved. Hence, nitric acid with a concentration of 0.73 mol/L was utilized throughout the whole research for graphene separation from Ni. The separation of graphene from Cu was done by aqueous iron(III) nitrate of 0.5 mol/L.

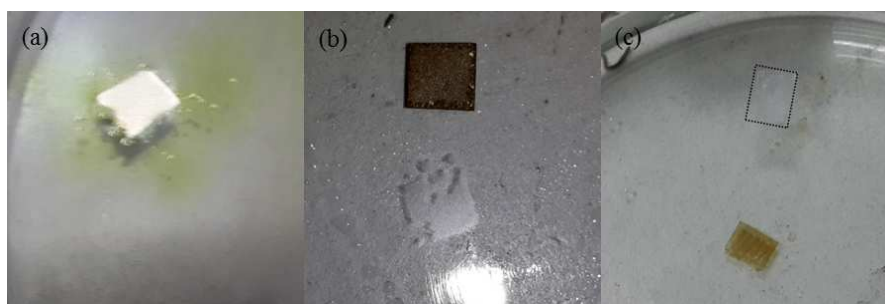


**Figure 4.3** Photographs of the graphene separation process by nitric acid with various concentrations (a) 21.67 %, (b) 6.7 % and (c) 3.35 %. The boxed area indicates the location of graphene.

The separated graphene being hydrophobic was visible with naked eyes floating at the surface of the etchant solution (Figure 4.3(c)). The etchants were then diluted with a huge amount of DI water (100-150 times) to prevent contamination of graphene. This latter was finally transferred gently onto silicon wafer for characterization with Raman spectroscopy.

## **4.2 Graphene formation on polycrystalline Cu foil**

The main purpose of this section is to find the possibility of utilizing conventional polycrystalline Cu foil with a thickness of 25  $\mu\text{m}$  to grow monolayer graphene by using our self-build quartz tube reactor under various operating parameters. In this section, Cu foils of 5 mm x 5 mm were used for the CVD process to grow graphene by varying the growth temperature, the growth duration and the partial pressure of methane. Fast cooling was applied to the sample after the growth stage. The post-CVD Cu foils underwent the etching process by an iron nitrate solution, as described in Section 4.1.2 to obtain free standing graphene which is subsequently deposited onto a silicon wafer. The main objective of the current research is to obtain uniform monolayer graphene. At least 5 Raman spectra from random and discrete locations were taken on each sample for reliable analysis of the characteristics of the obtained graphene. Only the samples with Raman characteristics of monolayer or bilayer graphene (as described in Section 3.4.1) was selected for further characterization with HRTEM and for Raman spectroscopy mapping.

### **4.2.1 Temperature**

In this section, the effect of temperature on the formation of graphene on Cu foil was studied. The growth duration was fixed at 5 min and 20 sccm of  $\text{CH}_4$  diluted into 80 sccm of  $\text{H}_2$  was used to maintain the partial pressure of methane at 0.2 atm.

The temperatures studied were 800, 850, 900, 950 and 1000 °C. Figure 4.4 shows the Raman spectroscopy spectra obtained from the corresponding samples grown.

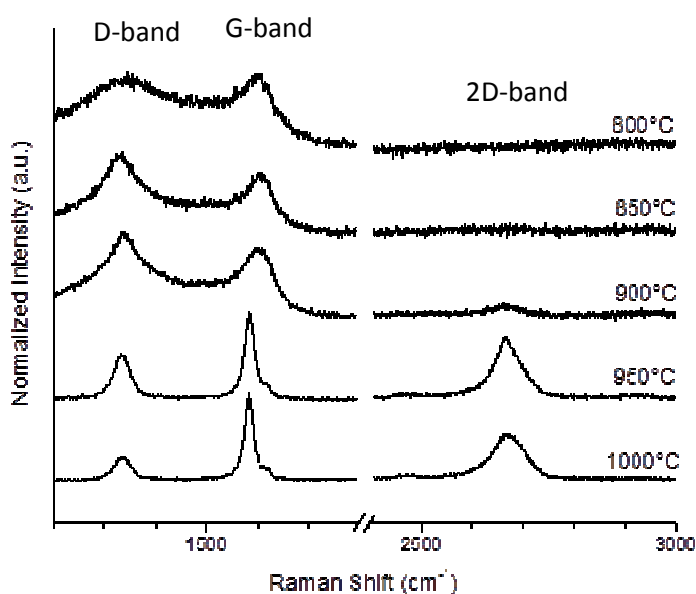


**Figure 4.4** Raman spectra of the graphitic materials grown on Cu foil with various temperatures. The growth duration was fixed at 5 min and 20 sccm of CH<sub>4</sub> was diluted into 80 sccm of H<sub>2</sub>.

The Raman spectra of the carbon materials grown at 800-900 °C were taken directly from the Cu foil while for the films grown at 950 °C and 1000 °C were recorded after separation and transfer on a silicon wafer. The materials obtained at 800-900 °C show similar features of broad and joined D- and G-band. The wide and high intensity of D-band indicates that the carbon materials are full of various types of defects. Meanwhile, G-band is the signal for graphitic carbon. The broad and joined D-band and G-band come from a mixture of highly disordered graphene flakes with a large amount of amorphous carbon. Based on the data from Raman, it is very obvious, neither monolayer nor multilayer graphene could be formed under these conditions. Furthermore, the carbon films formed on Cu in that temperature range were not continuous. Regarding the separation process, the films were totally dispersed at the surface of the iron nitrate solution and hard to collect and deposit on

silicon. Even though a protective layer of PMMA was coated onto the Cu foil to hold them together, the carbon film broke into pieces and dissolved into chlorobenzene during the PMMA removing stage. This is the reason why Raman spectra were directly taken from the Cu foil. Cu is a transition metal with a weak ability for graphitic carbon formation. Under the used conditions, 900 °C and below is a low temperature range for Cu activation of catalytic decomposition of methane and carbon restructuration for graphene formation.

Graphene films grew at 950 °C and 1000 °C were continuous and could be easily separated and deposited onto silicon wafer. The Raman spectra from the 2 corresponding graphene films show a very low ratio of  $I_{2D}/I_G$ , suggesting that the films were multilayer graphene. The pronounced D-bands could be due to the presence of defects in the film. As the temperature is further raised to 1050 °C (just below the melting point of the Cu, 1085 °C), the Cu foil was partially melted and balled-up; the surface of the Cu foil being uneven. At the meantime, the thermal decomposition of methane becoming significant, the quartz tube was covered with a thick layer of carbon materials meaning that the environment was not suitable for CVD. Hence, 950 °C-1000 °C is the best range for our study. The blank test and the calculations carried out in Section 4.1.1 have already showed that the thermal decomposition of methane is much more favorable around 1000 °C; 950 °C being the preferred temperature to grow graphene with better quality. 950 °C was thus selected for the subsequent studies and the effect of growth duration and methane partial pressure was investigated.

#### **4.2.2 Growth duration**

The durations tested were in the range of 1-8 min. The ratio of methane/hydrogen was fixed at 0.2 with a total flowrate of 100 sccm; the partial



pressure of methane being of 0.2 atm. Figure 4.5 shows the Raman spectra obtained from the graphene grown with different durations of CVD reaction. No sample was obtained for 1-2 min of reaction. The graphene grew with 3 min of reaction was a small flake (sub-millimeter) but it could be transferred onto silicon wafer. After 4 min of reaction, a continuous film of graphene could be monitored but its size smaller than that of the Cu foil. A square film of 5 mm x 5 mm was formed as the growth duration was increased to 5 min and above. Unfortunately, Raman spectroscopy does not give evidence of monolayer or bilayer graphene (Figure 4.5); all the spectra obtained showing very low ratio of  $I_{2D}/I_G (<0.5)$ . Furthermore, there is no correlation between the ratio of  $I_{2D}/I_G$  and the duration of the reaction. However,  $I_G/I_D$  is getting higher with longer growth duration, indicating that the crystallinity of graphene is improving with longer CVD duration.

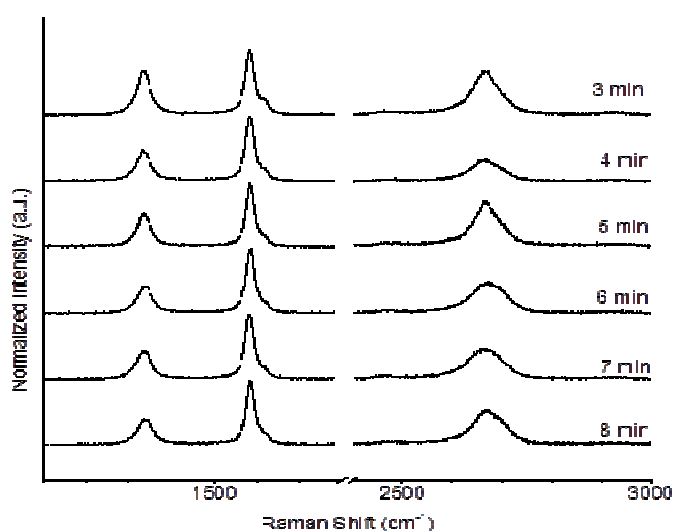


**Figure 4.5** Raman spectra of graphitic materials grown on Cu with various CVD durations at 950 °C and under 20 sccm of CH<sub>4</sub> diluted into 80 sccm of H<sub>2</sub>.

#### 4.2.3 Methane partial pressure.

In current section, based on the results of Sections 4.2.1 and 4.2.2, the temperature for the CVD was fixed at 950 °C and the duration was kept at 5 min. The flowrates of methane were 10, 20, 30, 40, 50, 60 and 70 sccm, diluted in the adequate

amount of hydrogen to maintain a flowrate of 100 sccm; the partial pressure of methane being thus in the range of 0.1-0.7 atm. The Raman spectra of the samples formed under these conditions are shown in Figure 4.6. Again, the Raman spectroscopy does not give any sign of monolayer or bilayer graphene (Figure 4.6). All the spectra obtained show very low  $I_{2D}/I_G$  ( $<0.5$ ). Still, there is no correlation between  $I_{2D}/I_G$  and the duration of reaction. Meanwhile,  $I_G/I_D$  is decreasing as the methane partial pressure applied was 0.6 atm and above. That effect is most probably due to an enhanced thermal decomposition of methane. The atmosphere inside the CVD reactor containing more carbon soot which may deposit onto the graphene film as amorphous carbon. At a methane partial pressure of 0.7 atm or higher, a clear contamination of black powder-like materials was observed on the wall of the quartz tube. Furthermore, the D-band is well pronounced. The ratio of methane gas to hydrogen seems not to be a relevant parameter to control methane decomposition leading to the formation of monolayer graphene. Since it is not playing a significant role to form monolayer graphene ( $I_{2D}/I_G$  always lower than 0.5).

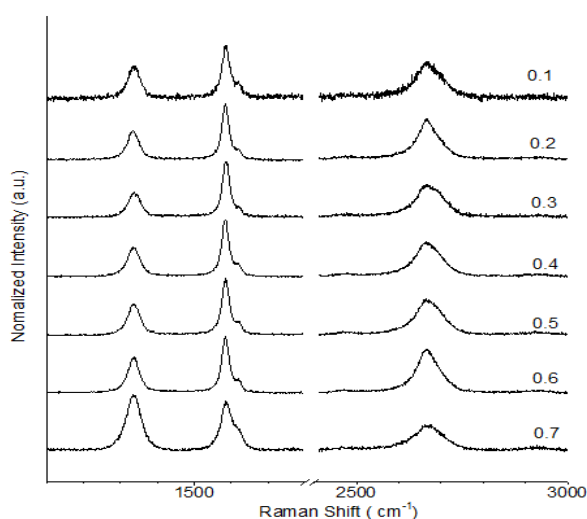


**Figure 4.6** Raman spectra of graphitic materials grown on Cu with various partial pressure of  $\text{CH}_4$ . The growth duration was fixed at 5 min, and temperature was 950  $^\circ\text{C}$ .

#### **4.2.4 Summary**

No sample prepared under the wide range of the operating parameters used on Cu has showed the sign of the presence of monolayer graphene or bilayer graphene. Even with wider operating conditions tested by interchanging the operating parameters, monolayer and bilayer graphene could not be formed. Natural (slow) cooling was as well tested but without giving any improvement to reduce the number of layers to monolayer or bilayer graphene. A rapid cooling was applied in an aforementioned study without any fruitful success. The results are in well agreement with literature as discussed in Section 2.4.5, since Cu is always described as an ideal catalyst with a self-limiting mechanism to form graphene predominantly monolayer under high vacuum (<1 Pa); very low carbon precursor ratio (part per thousand or ppm) and higher temperature (~1050 °C) being the favorable conditions to grow monolayer graphene. The objective of the present work being to grow mono- or bilayer graphene under atmospheric pressure, it was in current study.

Cu is known to induce a surface mediated growth mechanism; methane dissociating at the surface of Cu is directly utilized for the graphene formation. Under atmospheric pressure CVD, the relatively high feedstock of carbon precursor provokes an oversupply of carbon and multilayer graphene are grown. However, the present study is important for the following work involving the use of Ni-Cu bimetallic catalyst.

#### **4.3 Graphene formation on polycrystalline Ni foil**

It has been shown that Cu is not able to grow monolayer graphene under atmospheric pressure in our simple quartz tube reactor. In this section, we have investigated the ability to grow graphene from Ni used as catalyst under atmospheric pressure using the same reactor. Conventional polycrystalline Ni foil with a thickness

of 125  $\mu\text{m}$  and dimension of 5 mm x 5 mm was used under various operating parameters: temperature, duration and partial pressure of methane. Subsequent to the CVD reaction, the grown graphene samples were easily separated from the Ni foil using nitric acid with concentration of 0.72 mol/L (3.25 %), and deposited on a silicon wafer (as described in Section 4.1.2) for preliminary characterization with Raman spectroscopy.

### 4.3.1 Temperature

This section mainly reports the effect of temperature on the characteristics of graphene grown on Ni, the growth duration was fixed at 5 min and the CVD atmosphere was created by a flow of 20 sccm of methane diluted into 80 sccm of hydrogen. The temperatures studied were 800, 850, 900, 950 and 1000  $^{\circ}\text{C}$ . A rapid cooling was applied as for the previous experiments using Cu. Figure 4.7 shows the Raman spectra of the graphene samples grown on Ni at different temperatures.

At 800  $^{\circ}\text{C}$ , only small flakes of graphene could be found after the Ni foil was etched away in nitric acid. As temperature was raised to 850  $^{\circ}\text{C}$ , a thin film of graphene that completely covered the Ni foil used was formed. From the Raman spectroscopy features, interestingly the intensity of the 2D-band is significantly much higher than that of the G-band for both graphene obtained at 800  $^{\circ}\text{C}$  and 850  $^{\circ}\text{C}$ ; which is the characteristic of monolayer graphene. For highest temperature,  $I_{2D}/I_G$  ratio is severely reduced to around 1 which could evidence the presence of bilayer graphene. For 950  $^{\circ}\text{C}$  or above,  $I_{2D}/I_G$  ratio is reduced to well below 1, indicating that the number of graphene layers is above 3, in other words, the graphene obtained was mainly multilayer graphene.

Uniformity of the number of layers across the graphene sheet was further investigated by Raman mapping over areas as large as 50  $\mu\text{m}$  x 50  $\mu\text{m}$ . From the

Raman maps, we extracted the ratio of  $I_{2D}/I_G$  and the  $\text{fwhm}_{2D}$  (Figure 4.8). For both graphene grown at 800 °C and 850 °C,  $I_{2D}/I_G$  is in the range of 1.4 -2.1 (Figure 4.8 (a) & (c)) and  $\text{fwhm}_{2D}$  is well below  $37 \text{ cm}^{-1}$  (Figure 4.8 (b) & (d)) over the quite large areas scanned; that means that the formed samples are uniform monolayer graphene. For the graphene sheet obtained at 900 °C,  $I_{2D}/I_G$  are in the range of 1-1.3 (Figure 4.8 (e)) and  $\text{fwhm}_{2D}$  in the range of 41-45  $\text{cm}^{-1}$  (Figure 4.8 (f)) which are both typical range for bilayer graphene. HRTEM images are in agreement with Raman spectroscopy showing a very clear single line which strongly indicates that both graphene sheets obtained at 800 °C (Figure 4.9(a)) and 850 °C (Figure 4.9(b)) are monolayer in thickness. Bilayer graphene with a double line characteristic was observed on graphene grown at 900 °C (Figure 4.9 (c)).

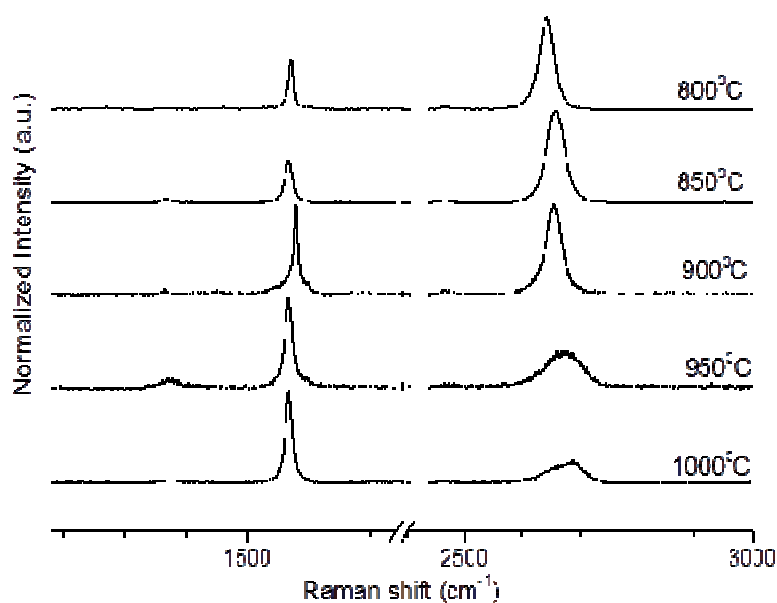


**Figure 4.7** Raman spectra of graphitic materials grown on Ni foil with various CVD temperatures at 5 min and under 20 sccm of  $\text{CH}_4$  diluted into 80 sccm of  $\text{H}_2$ .

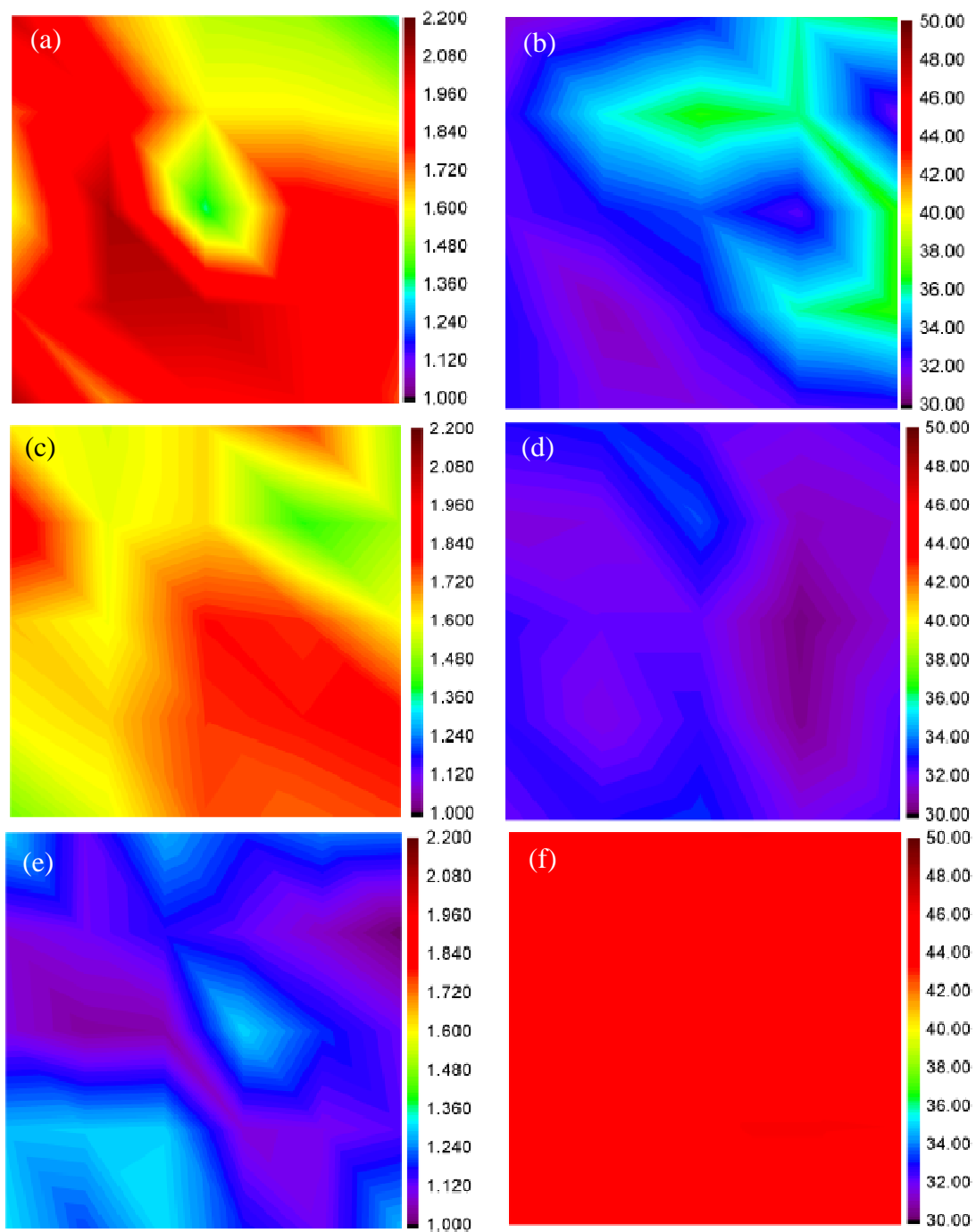


**Figure 4.8** Raman maps showing  $I_{2D}/I_G$  for graphene grown on Ni at (a) 800 °C, (c) 850 °C and (e) 900 °C and  $fwhm_{2D}$  of graphene grown at (b) 800 °C, (d) 850 °C and (f) 900 °C. The growth duration was fixed at 5 min under the flow of 20 sccm of  $CH_4$  diluted into 80 sccm of  $H_2$ . Scale of maps  $50\mu m \times 50\mu m$ .

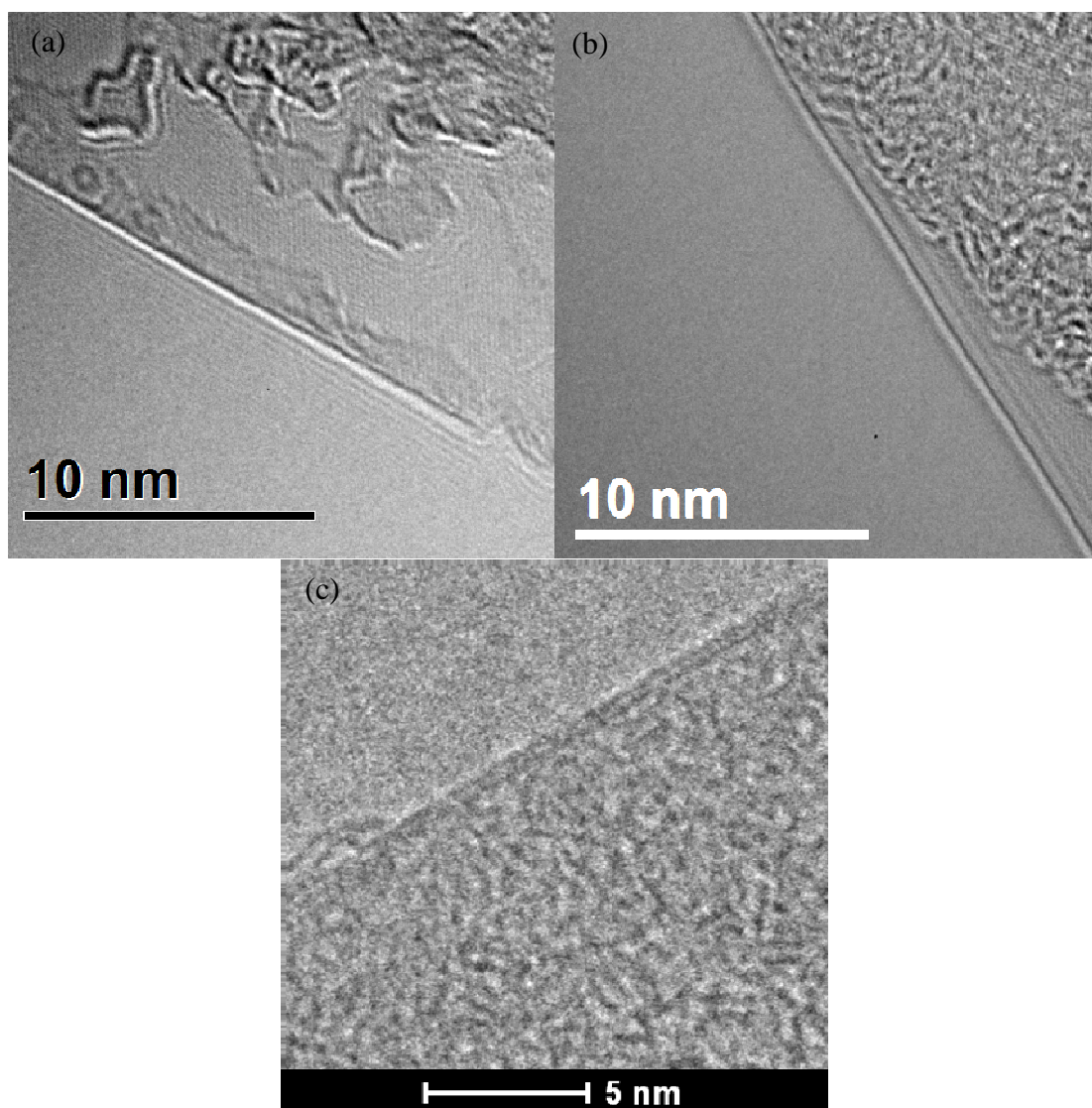


**Figure 4.9** HRTEM images of graphene grown on Ni at (a) 800 °C, (b) 850 °C and (c) 900 °C for 5 min under 20 sccm of CH<sub>4</sub> diluted into 80 sccm of H<sub>2</sub>.

In summary, 850 °C would be the optimum temperature to form a uniform and complete sheet of monolayer graphene on Ni under our CVD conditions. Monolayer graphene could also be formed at 800 °C, but the domain size of graphene was not as large as that of graphene grown at 850 °C, for which almost the whole surface of Ni is covered with graphene. At 900 °C, the graphene sheet increases in thickness to bilayer graphene; some areas are also composed of monolayer and trilayer graphene. As a result, 850 °C which gives a much more uniform monolayer graphene after CVD

was selected for the subsequent study on the effect of the CVD duration and the methane partial pressure.

#### 4.3.2 Growth duration

The durations tested for the CVD reaction were ranging in the 1-8 min. Temperature was fixed at 850 °C and the methane partial pressure was fixed at 0.2 atm with a total flowrate of 100 sccm. No sample was obtained for 1 or 2 min of reaction. Under 3 min, very small domains of graphene could be observed floated on the nitric acid solution. However, the domains were too small for characterization. Graphene that was strong enough to be handled by hands was obtained with CVD duration of at least 4 min (Figure 4.10 (left)). The graphene sheet fully covered the Ni foil used for 5 min of reaction (Figure 4.10 (right)) and with longer durations.

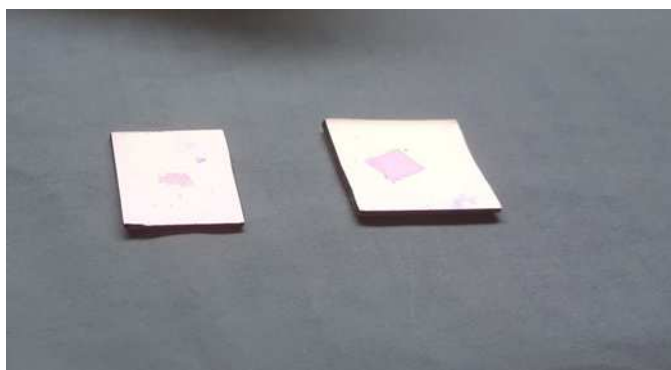


**Figure 4.10** Photograph of graphene sheet separated and deposited on a silicon wafer. Growth conditions: 850 °C, 20 sccm of methane diluted into 80 sccm of hydrogen for CVD duration of (left) 4 min and (left) 5 min.



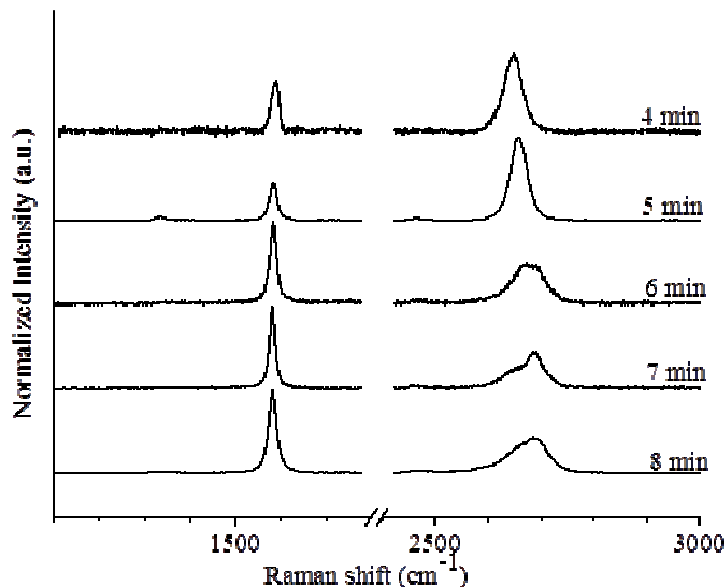


**Figure 4.11** Raman spectra of graphitic materials grown on Ni foil with various CVD durations at 850 °C under 20 sccm of CH<sub>4</sub> diluted into 80 sccm of H<sub>2</sub>.

Figure 4.11 shows the Raman spectra of graphene formed at 850 °C with different durations in the 4-8 min range. Graphene grown under durations of 4 and 5 min at 850 °C show Raman characteristics of monolayer graphene ( $I_{2D}/I_G > 1.6$ ). Full coverage of the Ni foil surface could be achieved only from 5 min of reaction. Optical micrographs of the graphene grown with 4 and 5 min of CVD duration at 850 °C are shown in Figures 4.12(a) and 4.12(b), respectively. Even if some domains of multilayer graphene are noticeable as marks localized on the grain boundary and on few other areas, the sample grown for 4 min (Figure 4.12(a)) is more uniform than that grown for 5 min (Figure 4.12 (b)). Both graphene sheets are quite uniform in color contrast, meaning that one type of graphene is mainly formed from the two experiments. Raman spectroscopy mapping shows that both graphene sheets grown show the characteristics of monolayer graphene since  $I_{2D}/I_G$  is greater than 1.4 and  $fwhm_{2D}$  is less than  $36 \text{ cm}^{-1}$  (Figure 4.13 (a) & (b) for 4 min of reaction and Figure 4.8 (c) & (d) for 5 min of reaction). HRTEM images, showing one line, are in agreement with Raman mapping for both samples (Figure 4.14 and Figure 4.9 (b)).

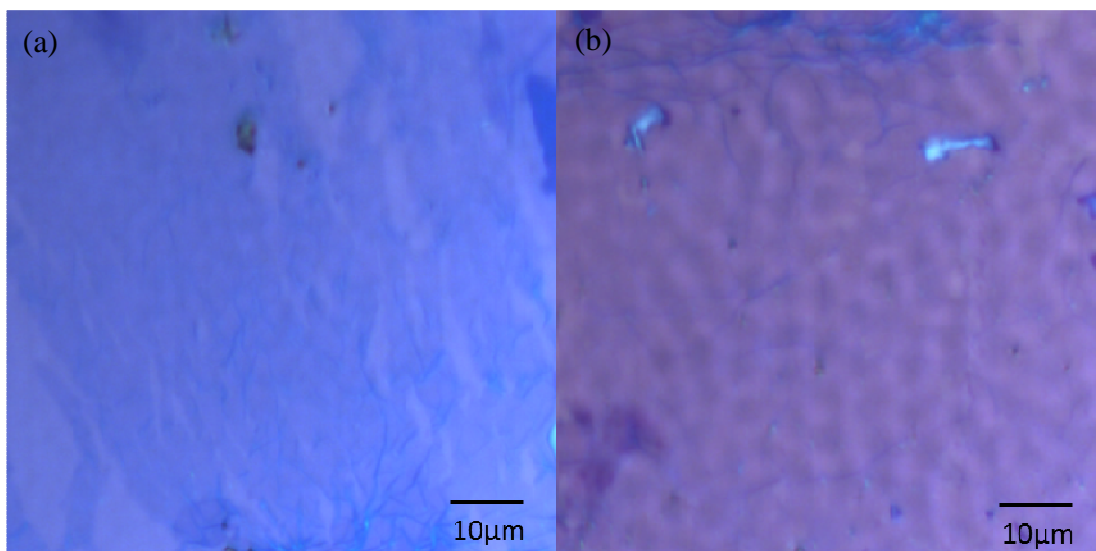


**Figure 4.12** Images of optical microscopy of graphene sheets separated and deposited onto a silicon wafer. Growth conditions: 850 °C, 20 sccm of methane diluted into 80 sccm of hydrogen for (a) 4 min and (b) 5 min.

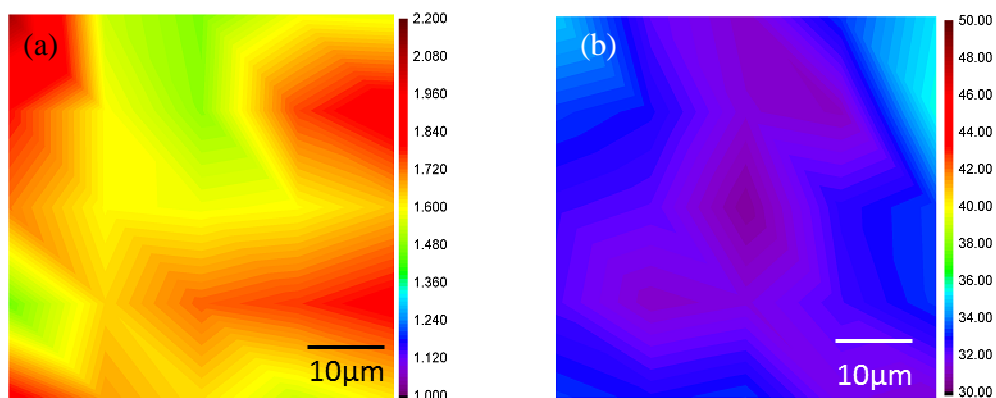


**Figure 4.13** Raman maps of (a)  $I_{2D}/I_{1G}$  and (b)  $fwhm_{2D}$  for graphene grown on Ni at 850 °C for 4 min under 20 sccm of  $CH_4$  diluted into 80 sccm of  $H_2$ .

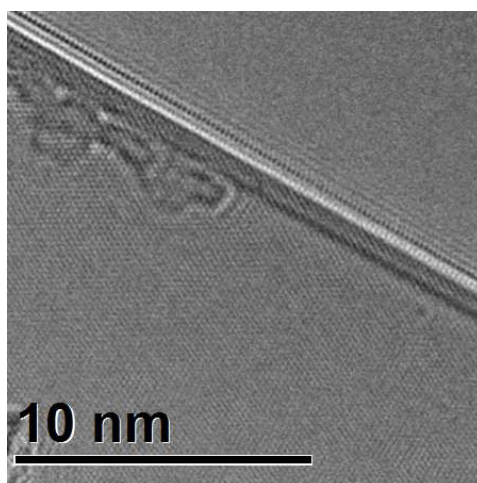


**Figure 4.14** HRTEM image of graphene grown on Ni foil at 850 °C for 4 min under 20 sccm of  $CH_4$  and 80 sccm of  $H_2$ .

The study was extended to temperature of 800 °C to investigate the experimental range for monolayer graphene formation. Under these experimental conditions, graphene is found to cover the foil only partly for 5 and 6 min of reaction and completely after 7 min of reaction (Figure 4.15). The corresponding Raman spectra seem to show that all the graphene sheets grown at 800 °C for 5-7 min have the characteristics of monolayer graphene (Figure 4.16), but these results are not consistent with the optical microscopy observations. For 5 and 6 min of reaction, a uniform contrast of color is observable (Figure 4.17 (a) & (b)), indicating the good uniformity of the grown graphene. Raman mapping shows uniform monolayer graphene for both samples (Figure 4.8 (a) & (b) & 4.19 (a) & (b)); which was also confirmed by HRTEM with a very clear characteristic single line (Figure 4.9 (a) & Figure 4.18). As the growth duration is extended to 7 min optical microscopy image is less uniform due to the presence of multilayer graphene (Figure 4.17 (c)). Higher duration of CVD leads to larger domain of graphene, but the uniformity of graphene was deteriorated. Raman mapping investigation shows that the graphene grown for 6 min has a uniform feature of monolayer graphene, i.e.  $I_{2D}/I_G$  greater than 1.5 and  $fwhm_{2D}$  less than  $35\text{ cm}^{-1}$  (Figure 4.19 (a) & (b)). In the case of the growth for 7 min, the range of  $I_{2D}/I_G$  and  $fwhm_{2D}$  are getting wider,  $0.7 < I_{2D}/I_G < 2.1$  and  $32\text{ cm}^{-1} < fwhm_{2D} < 60\text{ cm}^{-1}$  (Figure 4.19 (c) & (d)) in agreement with the non-uniformity in layer distribution suspected from optical micrographs (Figure 4.17 (c)). Hence, 800 °C of CVD reaction was not suitable to form large area of graphene without compromising the uniformity of graphene. 850 °C with duration of 5 min was selected as optimized operating conditions to study the effect of methane partial pressure.

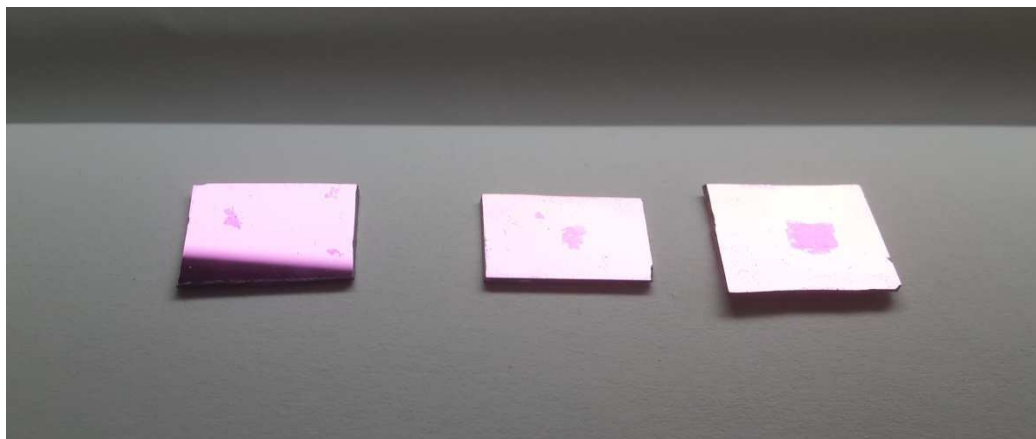


**Figure 4.15** Photograph of graphene sheets separated and deposited onto a silicon wafer. Growth conditions: 800 °C, 20 sccm of methane diluted into 80 sccm of hydrogen for (left) 5 min (center), 6 min and (left) 7 min.

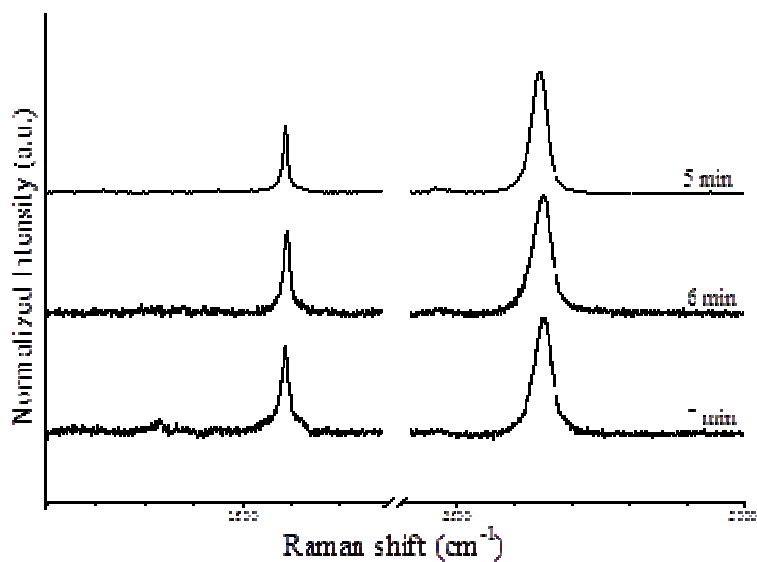


**Figure 4.16** Raman spectra of graphitic materials grown on Ni foil with various CVD durations at 800 °C under 20 sccm of CH<sub>4</sub> diluted into 80 sccm of H<sub>2</sub>.

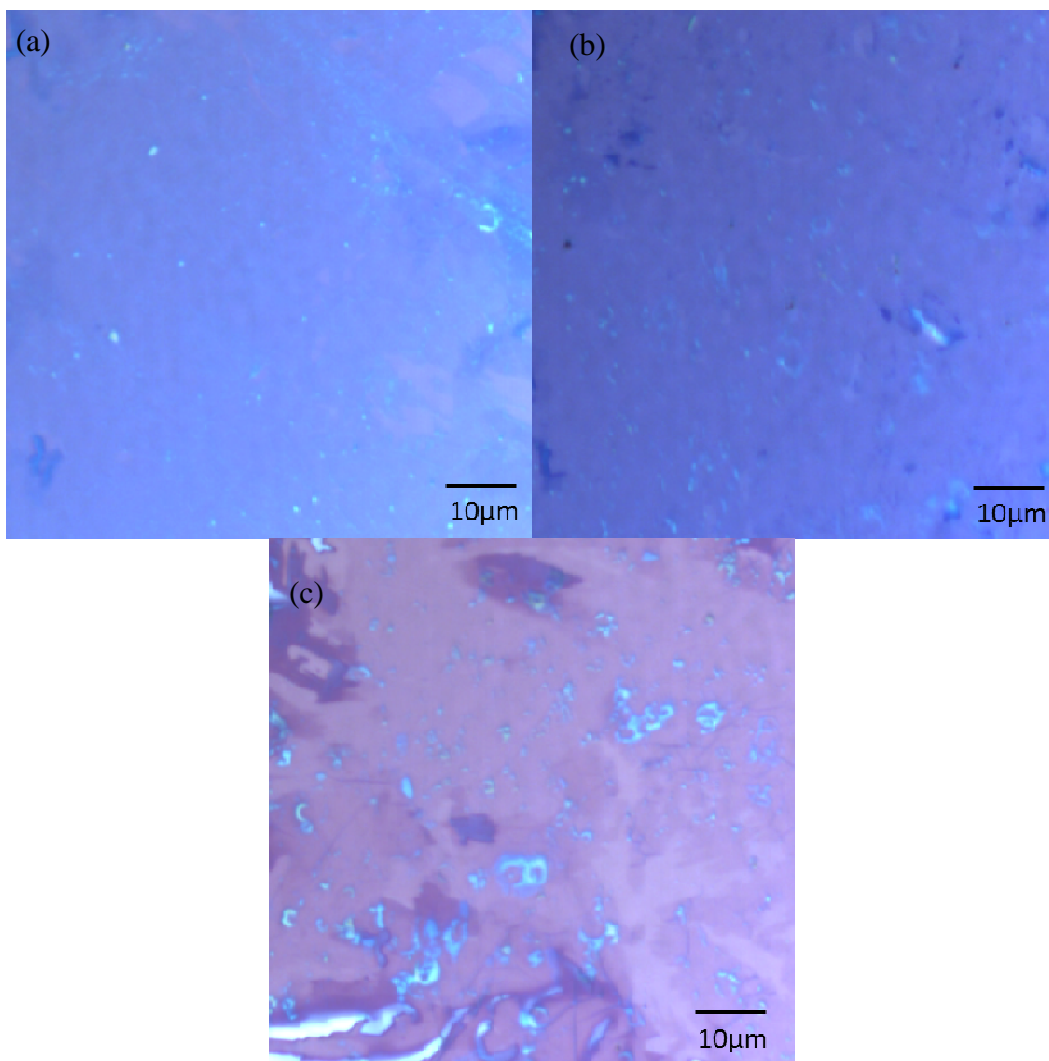


**Figure 4.17** Micrographs of the graphene sheets separated and deposited onto a silicon wafer. Growth conditions: 800 °C, 20 sccm of methane diluted into 80 sccm of hydrogen for (a) 5 min (b) 6 min and (c) 7 min.

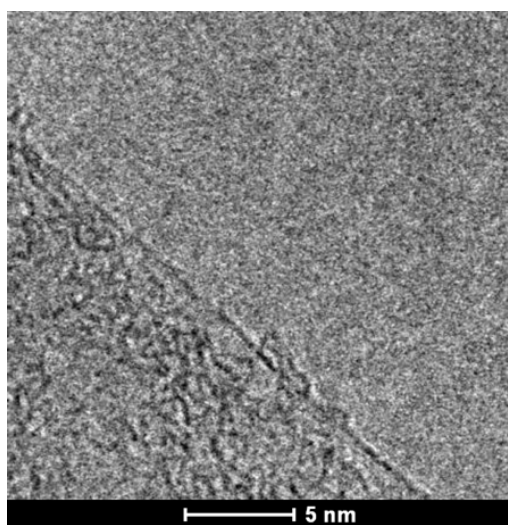


**Figure 4.18** Typical HRTEM image of graphene grown on Ni foil at 800 °C for 6 min under 20 sccm of CH<sub>4</sub> diluted into 80 sccm of H<sub>2</sub>.

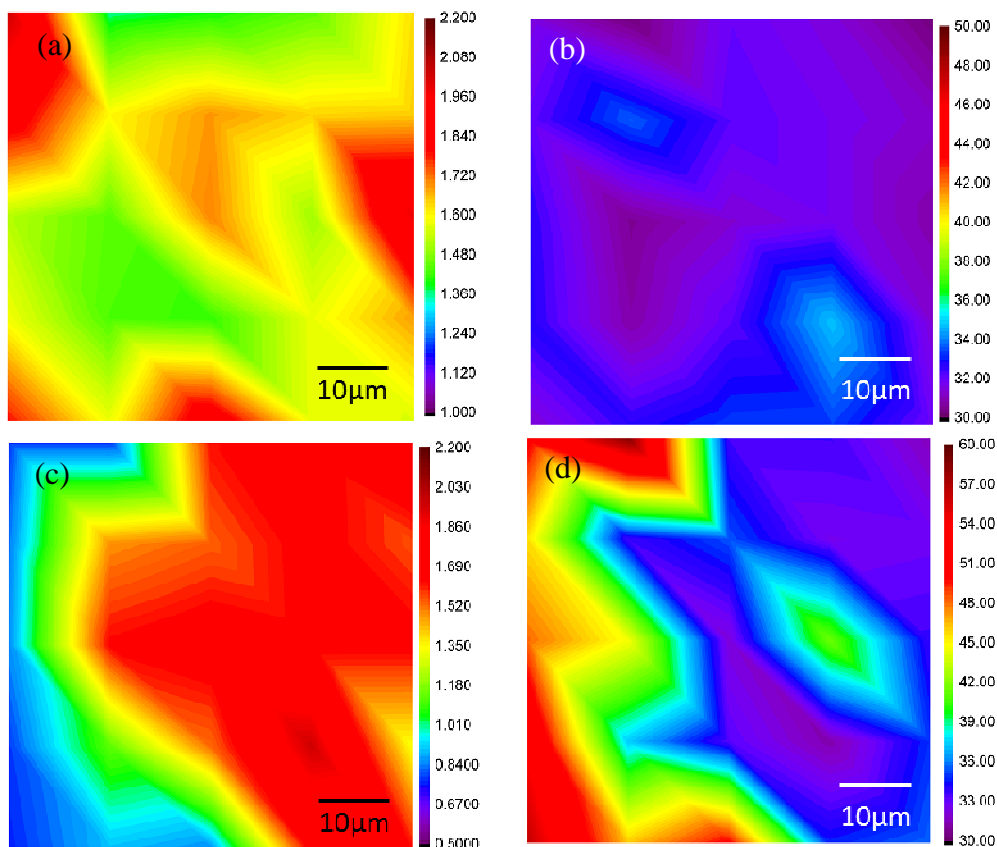


**Figure 4.19** Raman maps of  $I_{2D}/I_G$  for graphene grown on Ni at (a) 6 min and (c) 7 min of reaction and  $fwhm_{2D}$  map of graphene grown for (b) 6 min and (d) 7 min at 800 °C under of 20 sccm of  $\text{CH}_4$  diluted into 80 sccm of  $\text{H}_2$ .

### 4.3.3 Methane partial pressure

In current section, methane partial pressure was varied and temperature for the CVD reaction was fixed at 850 °C and duration at 5 min. The total flow of the mixture methane/hydrogen was fixed at 100 sccm. The flowrate of methane studies were 10, 20, 30, 40, 50 and 60 sccm, diluted in the adequate amount of hydrogen; methane partial pressure ranges in 0.1-0.6 atm. The Raman spectra of the samples prepared by varying the methane partial pressure are shown in Figure 4.20.

Raman spectroscopy spectra of the grown graphene for the methane partial pressure in the 0.1-0.3 atm show the characteristics usually attributed to monolayer graphene. The Intensity of 2D-bands are higher than G-bands, furthermore, the D-bands are very weak in intensity. However, only the graphene samples grown under

methane partial pressure of 0.2 and 0.3 atm (Figure 4.21 (center) & (right)) were large enough to cover the whole surface of the Ni foil. Graphene formed with 0.1 atm of methane partial pressure was composed with several flakes (Figure 4.21 (left)). Referring to optical microscopy, a very obvious trend observed: uniformity of the samples is decreasing as the gas mixture is enriched in methane (Figure 4.22) and the grain boundaries become noticeable. However, the area of monolayer graphene remains quite large and this is the major graphene type in the samples. Generally, the higher the methane partial pressure; the thicker the graphene formed. Methane partial pressure of 0.4 atm and above giving  $I_{2D}/I_G$  lower than 1 signals graphene with more than 2 layers.

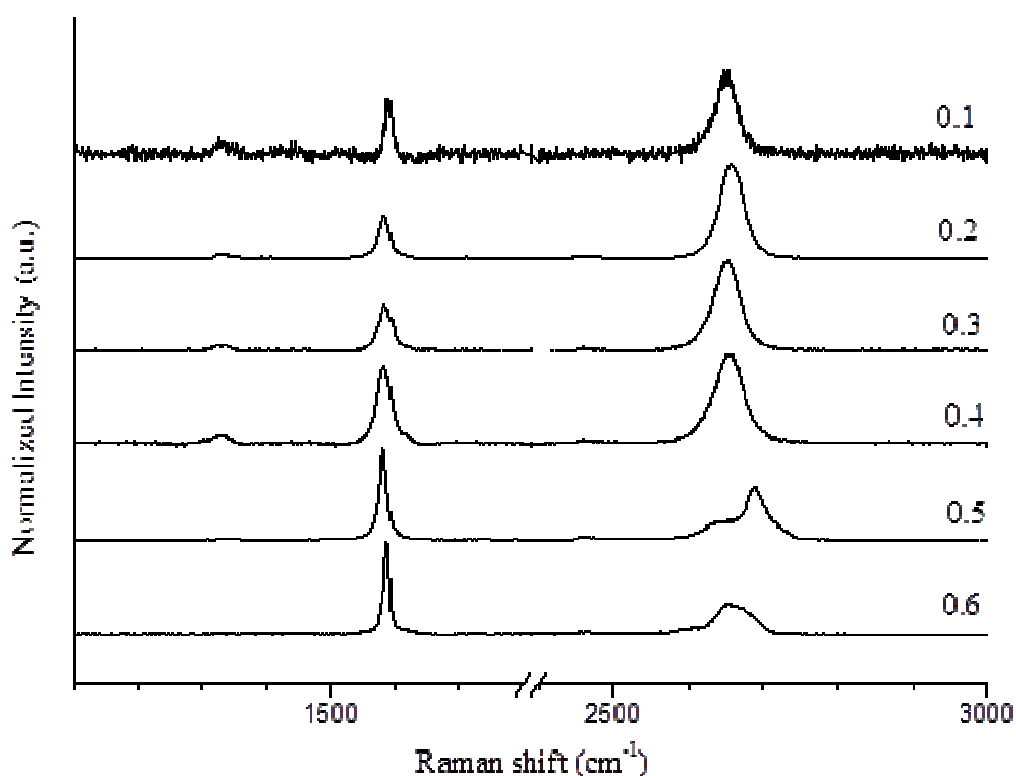


**Figure 4.20** Raman spectra of graphitic materials grown on Ni foil with various partial pressure of CH<sub>4</sub> at 850 °C and for 5 min.

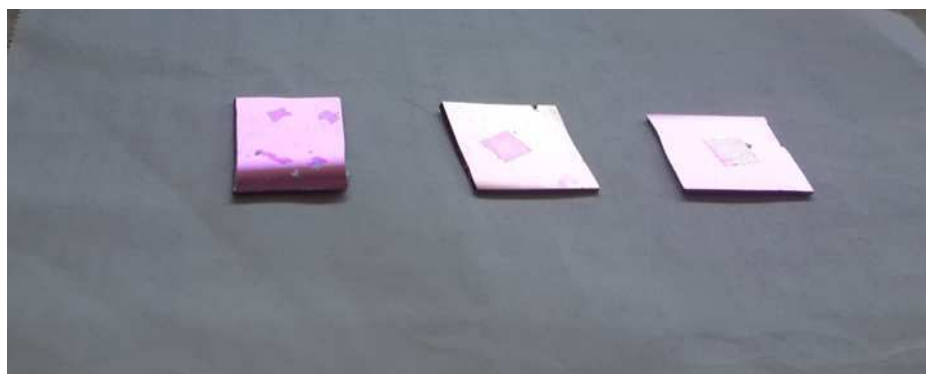


**Figure 4.21** Photograph of graphene sheets separated and deposited onto a silicon wafer. Growth conditions: 850 °C for 5 min with various methane partial pressure of (left) 0.1 atm, (center) 0.2 atm and (right) 0.3 atm.

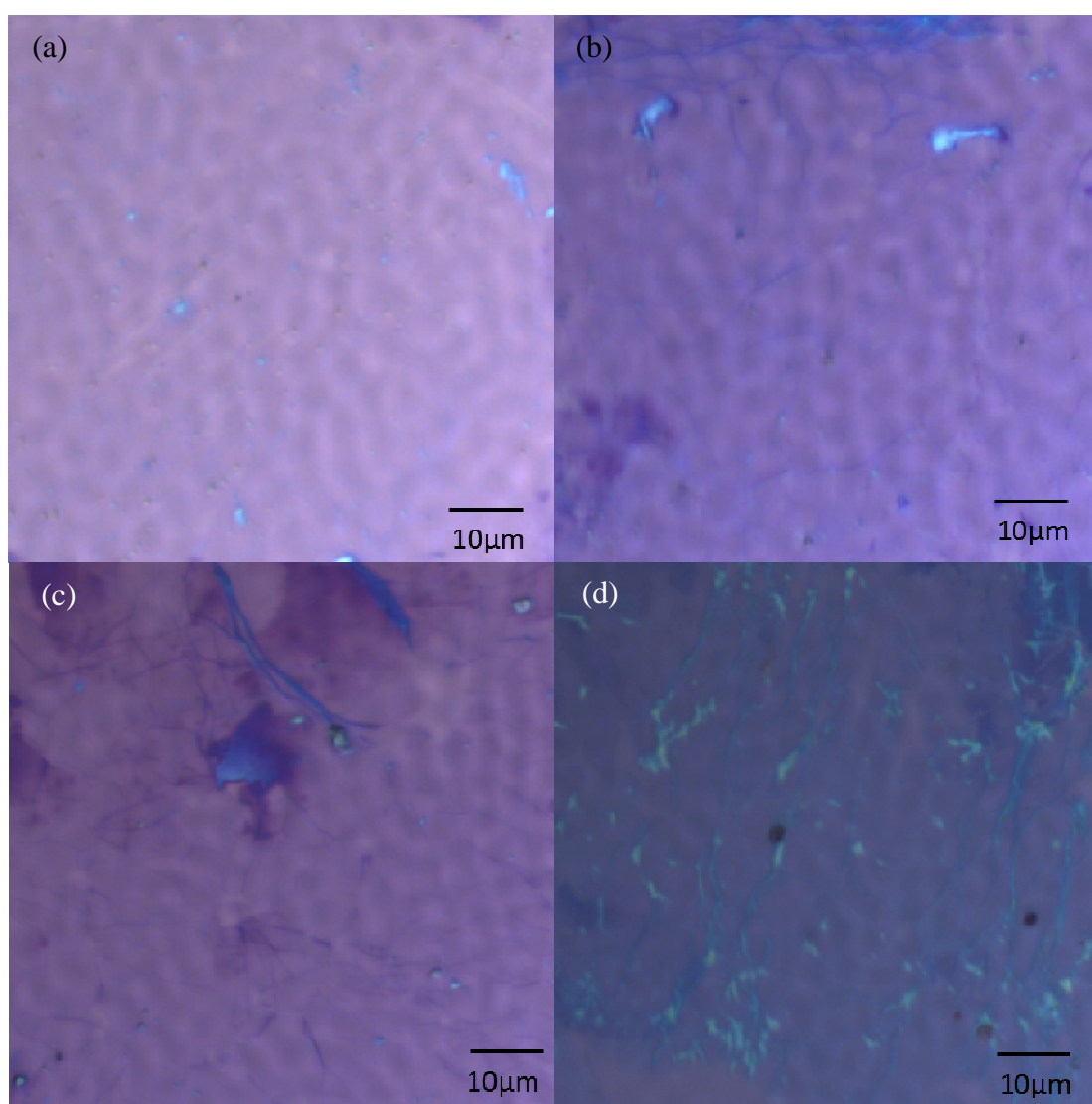


**Figure 4.22** Micrographs of the graphene sheets grown at 850 °C for 5 min and under methane partial pressure of (a) 0.1 atm, (b) 0.2 atm, (c) 0.3 atm and (d) 0.4 atm after separation and deposition onto silicon wafer.



#### 4.3.4 Discussion

Ni is losing its attractiveness as the catalyst for monolayer graphene formation. Ni has relatively higher carbon solubility as compared to that of Cu (Shu et al., 2012). During the cooling process after the growth stage, relatively large amount of carbon segregates out from Ni which leads to form multilayer graphene. For this reason, Cu is often preferred in the field of graphene CVD research due to the favored formation of monolayer graphene with the utilization of high vacuum and low carbon precursor feeding. In current research, monolayer graphene formation could be evidenced as Ni was used as catalyst with the assist of fast cooling, meanwhile Cu was no able to grow monolayer graphene under wide range of operating parameters tested.

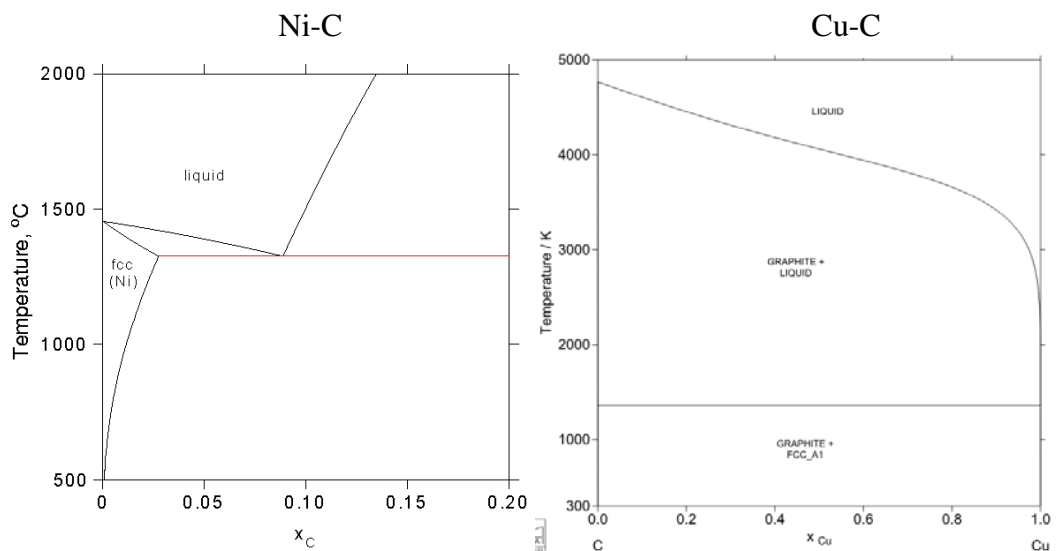


**Figure 4.23** Phase diagram of nickel-carbon (left) and copper-carbon (right) bulk system.

According to the reported growth mechanism on Ni, methane gas adsorbed decomposes at the surface on Ni, while the carbon atoms from methane dilute into the Ni foil. Referring to the Ni-C phase diagram (Figure 4.23 (left)), carbon solubility in bulk Ni increases with increasing temperature. The excess diluted carbon allows the formation of solid graphitic materials, such as graphene or graphite. In another

circumstance, the cooling process after the CVD reaction also involves the process of discarding the excess of diluted carbon atoms, namely segregation. Referring to Figure 4.23, as temperature decreased, the excess of diluted carbon dissipates out from the bulk onto the Ni surface to achieve equilibrium. Segregation is hence much easier to control to obtain graphene with minimum number of layers. Comparing with Cu, the carbon solubility is much lower compared with that of Ni (Figure 4.23), most of carbon activity is only restricted on the surface of Cu. Under atmospheric pressure CVD, the excess supply of carbon to Cu surface is expected to produce graphene with higher number of layers.

In order to grow monolayer graphene on Ni foil, 2 criteria need to be satisfied. (1) saturation of diluted carbon atoms in Ni need to be avoided and (2) the amount of segregated carbon at the surface of Ni during the cooling process needs to be limited to grow graphene with a minimum number of layers. The dissolved carbon is commonly lowered either through vacuum CVD, (Tan *et al.*, 2012) by utilizing low ratio of carbon precursors under excess of dilution gas, with very thin nickel film as catalyst (Xu *et al.*, 2011) or by introducing an inhibitor, that could limit the diffusion rate and solubility of carbon into the system (Weatherup *et al.*, 2013). Under these conditions, carbon atoms can segregate and precipitate at the surface of Ni with the optimum level and lead to formation of monolayer or bilayer graphene. However, sophisticated equipment, such as vacuum reactor and high sensitive mass flow controller are used to create the ideal operating conditions that are commonly used for Ni-catalysed CVD in order to grow monolayer graphene. In current research, as already mentioned, the aim is to prepare monolayer graphene using a simple CVD process that does not require any sophisticated deposition technique: (1) our self-

designed CVD reactor, (2) atmospheric pressure, (3) polycrystalline thick catalyst foil of low prize.

Fast cooling is known to assist formation of monolayer graphene under ambient pressure CVD. As discussed in Section 3.3.2, the actual strategy to quench the CVD reaction was to apply a fast displacement of the Ni foil from the heating zone to room temperature zone. Under calibration, cooling of the Ni foil to 100 °C was reached in around 1 min. That means that the applied cooling rate was greater than 700 °C/min: higher than those reported in literature in the range of 10-600 °C.min<sup>-1</sup> (Zhang *et al.*, 2010, Jacobson *et al.*, 2012b, Xu *et al.*, 2011, Kim *et al.*, 2009).

The results obtained with high-speed cooling step were compared to those of the syntheses that were carried out with slow natural cooling that requires 6-7 hours. Characterization by Raman spectroscopy shows that only multilayer graphene (not shown here) could be grown under various operating conditions, which confirms that fast cooling facilitates the quenching process and reduces the amount of carbon atoms segregated, a key parameter for the Ni-catalysed reaction. Under fast cooling, only the carbon atoms situated near the surface have enough time to segregate and form graphene. Meanwhile, diffusion of carbon atoms in the middle of the Ni foil is highly inhibited and majority of the carbon atoms remains trapped inside the Ni foil.

Carbon solubility in Ni highly depends on temperature. It is multiplied by more than 6 (from 0.4 to 2.7 at.%) for temperature increasing from 700 to 1300 °C, a temperature range that is widely reported to favor various kinds of graphene (Figure 4.23). Our study is focused in the 800-1000 °C range for which the carbon solubility varies between 0.8 and 1.0 at.%. Since graphene itself is of just one single atomic thickness (0.34 nm in thickness), this small variation of carbon solubility in bulk Ni could be responsible in high variation of the number of layers of graphene.

Another factor correlated to temperature is the carbon diffusion rate within Ni. From the data shown in Section 4.3.2, the most uniform graphene obtained was found to be grown at 800 °C and for 5-6 minutes of CVD duration, but the domain was small and these conditions did not lead to segregate a perfect graphene with the desired sizes. A graphene sheet with larger size could be obtained as the CVD reaction duration was further increased to 7 min. However, a significant amount of multilayer graphene could be also observed in that case. Under relatively low temperature, the carbon diffusion rate is low. The supply of carbon adatoms was continuous from the atmosphere inside the reactor whereas the adsorption of methane is probably more favorable to happen at the Ni boundaries. The boundary of grains composed with unorganized lattice steps that offer higher affinity of methane; which induces also a higher carbon concentration located at the grain boundary. Diffusion of dissolved carbon adatoms later to the center of the Ni foil is driven by the concentration gradient. 800 °C is relatively low to permit an effective diffusion of carbon which induces an excessive accumulation of carbon at the Ni surface especially enhanced near the grain boundary (7 minutes of CVD). Carbon atoms surplus accumulated near the grain boundary start the precipitation process rather than the segregation process. A higher temperature (850 °C) provides more energy for the carbon diffusion and reduces the effect of localized saturation of carbon. For temperature higher than 850 °C, the carbon solubility seems to become the dominant parameter and it is difficult to limit the segregation phenomenon to one atomic layer of carbon throughout the whole surface of Ni.

The carbon concentration is also increased with increasing the period of exposition of carbon precursor. It was indeed observed that the number of graphene layers was increased for longer duration of CVD reaction. In literature, the effect of

methane/hydrogen ratio is also reported to play a significant role in graphene layer control. As discussed in Section 2.3.4.1, the role of hydrogen is believed to create methyl radicals or induce amorphous carbon cleaning, but the actual role is still highly arguable. From the results, the methane/hydrogen ratio does not seem to be a sensitive parameter to finely control the graphene layer number. Methane partial pressure in range of 0.1-0.3 atm leads to monolayer graphene and for 0.5 atm of methane partial, multilayer graphene starts to appear in large area. The methane ratio utilized in the current study is very high (0.1-0.7) as compared with the reported operating conditions (for example 0.02 (Tan *et al.*, 2012) or 0.04 (Zhang *et al.*, 2010)). It shows that the most vital step to achieve monolayer graphene formation under atmospheric CVD reaction is the cooling step.

In summary, monolayer graphene could be obtained if a high-speed cooling step is applied to quench the reaction. In order to get a uniform monolayer graphene, the saturation of carbon in the bulk of Ni foil is also needed to be prevented. Last but not least, the diffusion of carbon also requires to be optimized to achieve uniform of carbon concentration distribution at the surface of the Ni foil. Hence, after the fast cooling of Ni foil, limited carbon amount could segregate which favours to form uniform monolayer graphene. However, the main drawback of this simple Ni-catalysed CVD is the problem of numerous grain boundaries on the surface of polycrystalline CVD. The graphene segregated near to the grain boundary is favourably multilayer graphene, even though under optimized conditions. High selectivity of monolayer graphene could be achieved under single-crystalline Ni surface. With the purpose to get a much more uniform monolayer graphene by using polycrystalline catalysts, a new bimetallic catalyst system was designed; it will be described and discussed in detail in the next section.

#### 4.4 Graphene formation on a bilayer Ni-Cu catalyst

In Section 4.2, it was found that Cu alone was not suitable for monolayer graphene formation under our experimental conditions. Monolayer graphene could be grown as polycrystalline Ni foil was used under optimized operating parameters, especially very fast cooling. However, carbon concentration is probably too high at the boundary of the Ni foil which limits the size and the uniformity of monolayer graphene areas. This is the reason why a new method needed to be utilized to break the bottleneck of current study.

Cu and Ni could form binary isomorphous alloys for which both metals are mutually miscible (Wan *et al.*, 2012). Some researchers had searched the possibility of using Cu-Ni alloys to grow graphene with the hope to combine the benefits of Cu and Ni. Two strategies have been reported to grow graphene from bimetallic catalyst, either by using layer-by-layer bimetallic catalyst foil (Liao *et al.*, 2013, Tyagi *et al.*, 2015) or by using alloy foils (Chen *et al.*, 2011, Robinson *et al.*, 2012). Just 10 wt.% of Ni in the Ni-Cu alloy is enough to change the surface mediated growth mechanism of Cu to a bulk mediated growth (Wu *et al.*, 2012b). By increasing the composition of Ni to roughly 30 wt.%, larger domains of monolayer graphene could be obtained under narrow operating parameters (Chen *et al.*, 2011). Monolayer graphene could be grown on bilayered nanoscaled thin film of Ni/Cu obtained by sputtering under elevated temperature (Liu *et al.*, 2011d, Wan *et al.*, 2012, Woo *et al.*, 2013). However, the synthesis process is complicated to control because high vacuum and low carbon precursor/diluting gas is required to grow monolayer graphene.

In the present study, an alternative approach to grow monolayer graphene on a Ni-Cu bimetallic catalyst was investigated under a simple CVD process. The thick Ni foil used is here essential to control the carbon diffusion rate during the growth step.

The proposed mechanism involves a reduced solubility of carbon in Ni induced by carbon diffusion from a carbon-rich surface to a carbon-lacked surface through bulk Ni and grain boundary. Monolayer graphene was formed on both surfaces of Ni and Cu. The robustness of proposed catalytic device allows a further facile separation of the grown graphene that can be transferred without damaging.

As already mentioned, Ni is known to offer a relatively high carbon solubility and high carbon diffusion rate in a bulk state. The formation of monolayer graphene on Ni catalyst is rather difficult under conventional CVD; and multilayer graphene is more often obtained. It was then proposed an alternative process that involves the diffusion of carbon adatoms across the Ni film, formation of graphene occurring at the opposite surface of graphene (Yan *et al.*, 2011b, Peng *et al.*, 2012b, Xu *et al.*, 2011). A carbon-lacked environment is created to reduce the carbon-concentration and leads to a successful synthesis of graphene with a minimum number of layers. Moreover, the uniformity of graphene layer was found to be much higher under such strategy compared with conventional Ni-catalyzed CVD. However, the graphene grown with this method is normally attached firmly onto the silicon that served as substrate, which makes it difficult to obtain as free-standing graphene.

To overcome this problem, an alternative technique able to solve the aforementioned problems by simply wrapping a Cu foil over a Ni foil was tested. The bicatalyst system is schematized in Figure 3.4. Its 4 main surfaces of interest are named according to Figure 4.24. The suitability of this developed bilayer catalyst to form monolayer graphene was investigated with our quartz tube reactor. A wide range of the operating parameters was tested to find the optimum conditions to form monolayer graphene and their respective role in graphene formation was studied.

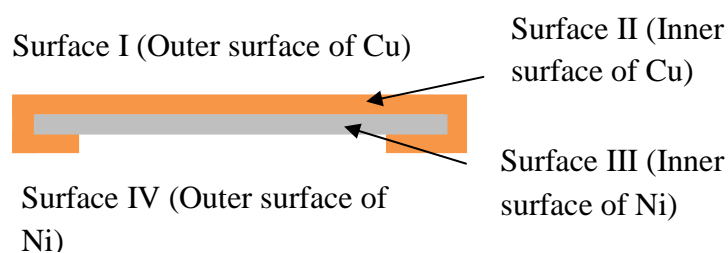


**Figure 4.24** Cross-section view of the used bimetallic catalyst consisting of a Cu foil wrapping a Ni foil.

#### 4.4.1 Temperature

This section mainly studies the effect of temperature on the characteristics of the graphene samples grown using our Ni-Cu bilayer catalyst, the growth duration was fixed at 5 min and 20 sccm of methane diluted into 80 sccm of hydrogen (0.2 atm partial pressure of methane) were used. The temperatures studied were 850, 900, 950 and 1000 °C. The bilayer catalyst also underwent the fast cooling process as described in previous experiments (Section 4.2 and 4.3).

After CVD, the 4 surfaces of the catalyst were covered with carbon materials. Raman spectroscopy results are given in a single plot to give a clear view of the characteristics of the samples obtained (Figure 4.25). On Cu (both sides), 900 °C and below did not allow to synthesize graphene; no signal of 2D-band were obtained. At 1050 °C, just below the melting point of Cu (1085 °C), disordered thick graphitic layers instead of graphenic materials were obtained. At high temperature, uncontrolled decomposition of methane occurred and the walls of the CVD reactor were covered with a thick layer of disorder graphitic materials (Seah *et al.*, 2013). At 900 °C,  $I_{2D}/I_G$  were found to be above 1.4 for the graphene grown at the inner surface of Ni, but the size of the samples was small. Interestingly, at 950 °C, much larger domains of graphene that fully covered the catalyst surface were grown on both inner



surfaces of Ni and Cu, and the corresponding  $I_{2D}/I_G$  for the both samples are well above 1.4. Uniformity of the grown graphene samples was further analyzed using Raman mapping.

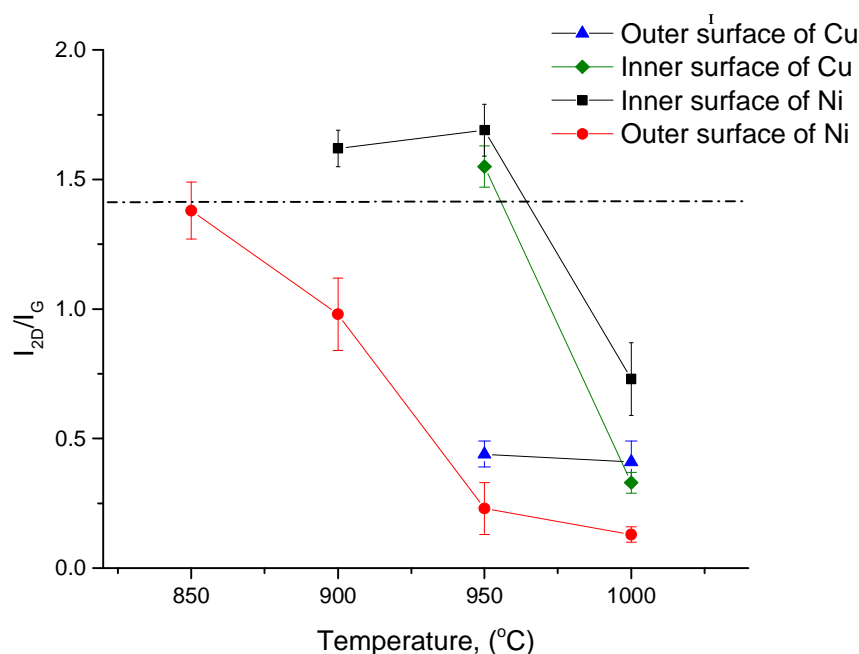


**Figure 4.25** Average and standard deviation of  $I_{2D}/I_G$  of graphene film obtained from graphene films grown on the 4 different surfaces of the CVD device in the temperature range 850 °C -1000 °C for 5 min.

Figure 4.26 shows the optical micrographs of the graphene grown at 950 °C for 5 min and separated from both inner surfaces of Ni and Cu. Even if some voids or wrinkles are visible after transfer, the optical images show a quite uniform color over all the imaged areas (Figure 4.26 (a) & (b)). For Ni, marks at the grain boundary are hardly visible. Raman mapping of  $I_{2D}/I_G$  and  $fw_{2D}$  corresponding to the two graphene samples after separation is shown in Figure 4.27. For all of the regions of graphene,  $I_{2D}/I_G$  is higher than 1.4 (Figure 4.27 (a) & (c)) and the  $fw_{2D}$  of the 2D-band is below  $36\text{ cm}^{-1}$  (Figure 4.27 (b)) and  $37\text{ cm}^{-1}$  (Figure 4.27 (d)) for graphene grown on Ni and Cu, respectively. HRTEM observations were randomly carried out at the edges of the graphene sheet. A clear single straight line is visibly monitored for

both graphene samples grown at the inner surfaces of Ni (Figure 4.28 (a)) and Cu (Figure 4.28 (b)).

To conclude, results from Raman mapping and HRTEM show that monolayer graphene with high uniformity and good crystallinity could be formed using the proposed bi-metallic system at the inner surfaces of Cu and Ni. For the subsequent experiments, 950 °C was thus selected and the effect of the growth duration and the methane partial pressure were investigated.

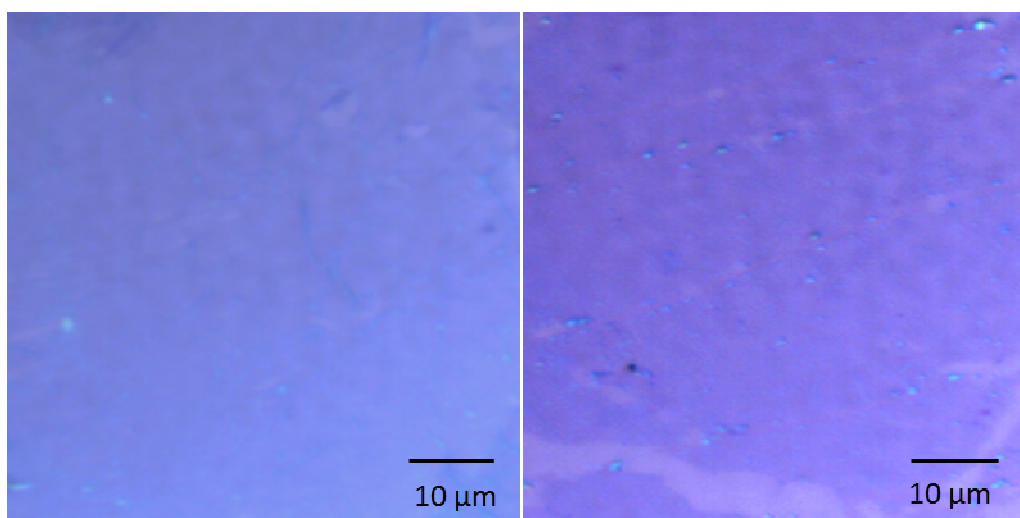


**Figure 4.26** Micrographs of graphene grown at 950 °C for 5 min at the inner surfaces of (a) Ni and (b) Cu after transfer on silicon wafer (methane partial pressure 0.2 atm).

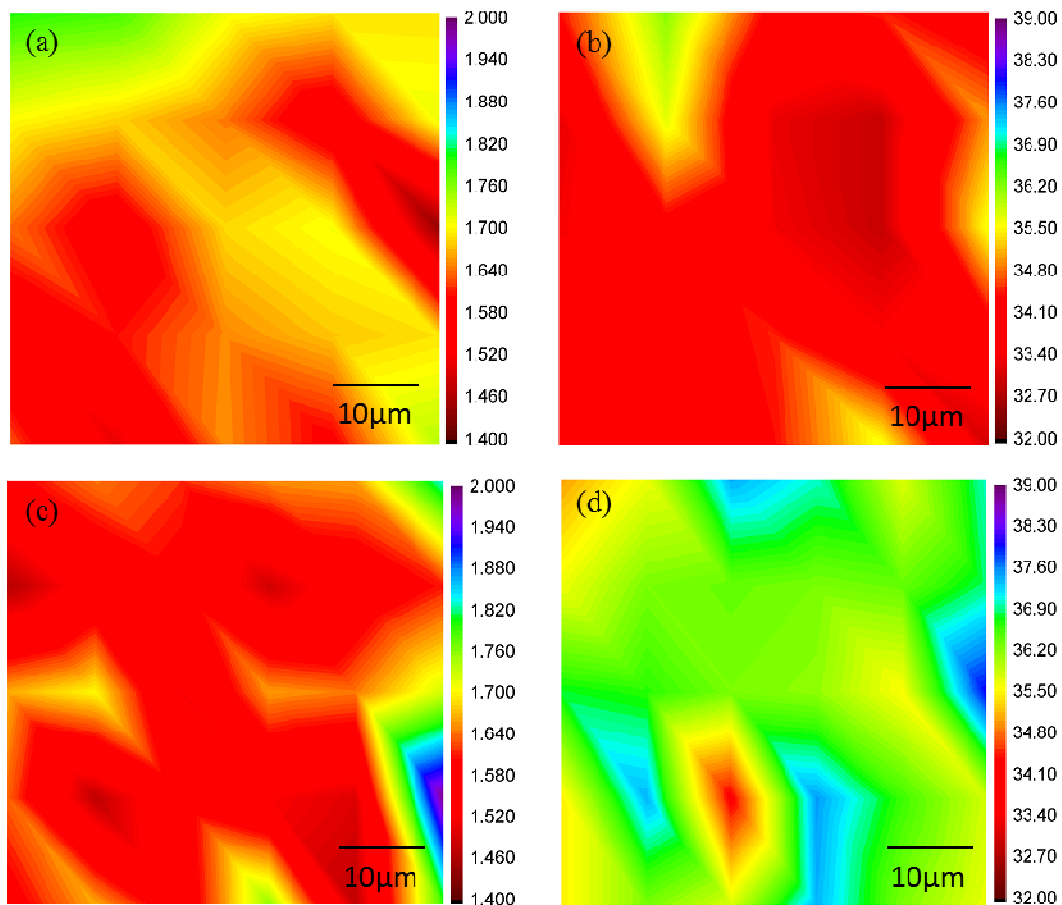


**Figure 4.27** Raman maps of  $I_{2D}/I_G$  for graphene grown on (a) Ni and (b) Cu, and  $fwhm_{2D}$  for (c) Ni and (d) Cu at 950 °C for 5 min. The color gradient bar is given on the right of each map.

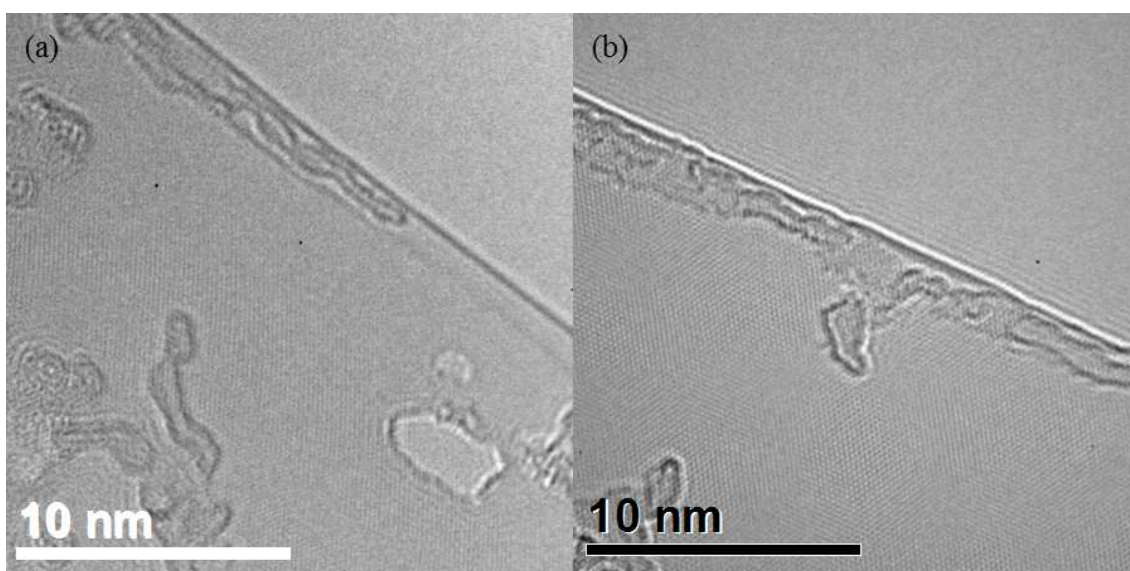


**Figure 4.28** HRTEM images of monolayer graphene grown on inner surface of (a) Ni and (b) Cu at the edges, after CVD reaction at 950 °C for 5 min.

#### 4.4.2 Growth Duration

The temperature of reaction was fixed at 950 °C and 20 sccm of methane diluted into 80 sccm of hydrogen (methane partial pressure of 0.2 atm) were used as the duration was varied in the 2-8 min range; fast cooling as aforementioned was used subsequent to the chosen reaction time. Figure 4.29 summarizes  $I_{2D}/I_G$  of the Raman spectra obtained for graphene materials grown at the 4 surfaces of the Ni/Cu bimetallic catalyst system.

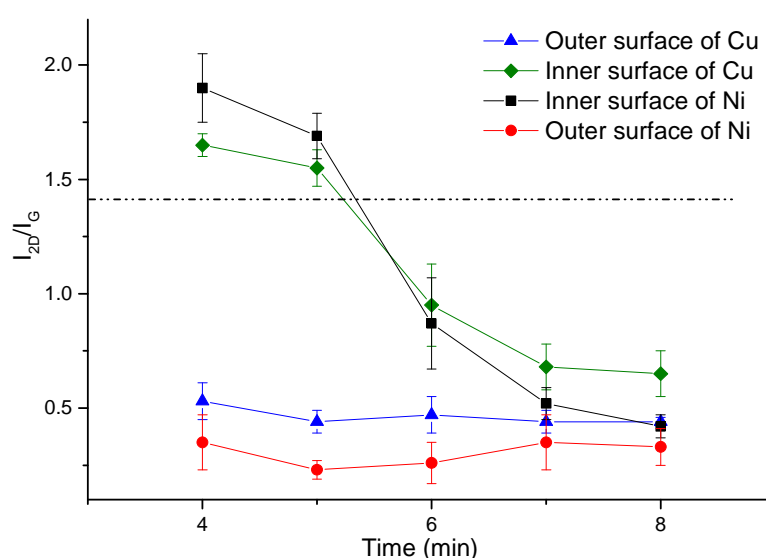


**Figure 4.29** Average and standard deviation of  $I_{2D}/I_G$  of the graphene films obtained on the 4 different surfaces of the CVD device at 950 °C and for durations in the 4-8 min range.

For duration of 3 min and below, no graphene formed. The increase of the duration to 4 min of CVD reaction, graphene could be separated from all 4 surfaces for Raman spectra obtaining (presence of D-, G- and 2D-band) at both outer and inner surfaces of Ni and Cu; but only small domains of graphene sheets were formed. The 4 surfaces were fully covered by graphene after 5 min of reaction, and Raman spectroscopy evidences monolayer graphene at both inner surfaces of Ni and Cu. For 6 and 7 min of reaction, Raman characteristics of multilayer graphene were obtained. These results are in agreement with optical microscopy observations showing that the

color contrast becomes very apparent as the CVD duration is extended to 6 or 7 min, for both graphene samples obtained at the inner surfaces of Ni and Cu (Figure 4.30 (c-f)). The sign of grain boundaries for graphene on Ni are getting larger and more obvious with longer period of reaction (Figure 4.30 (c) & (e)). One can notice that as multilayer graphene is obtained on Ni surface (Figure 4.30 (c) & (e)), similar areas of multilayer graphene were also found on the Cu surface (Figure 4.30 (d) & (f)). It seems that the graphene that was obtained on the inner surface of Cu has copied the topography of the graphene grown on the Ni surface, regarding both its uniformity and its number of layers. For the graphene grown on the inner surface of Cu, voids were appearing on the graphene film; they are probably caused by some imperfect contacts between Ni and Cu surface during the pressing for the catalyst preparation. Graphene that grew on the inner surfaces of Ni and Cu gives the best uniformity under 4 min of reaction observed by color contrast in optical micrographs (Figure 4.30 (a) & (b)). Raman mapping shows that the whole corresponding graphene sheet is mainly monolayer graphene (Figure 4.31 (a-d)) with  $I_{2D}/I_G > 1.4$  and  $fwhm_{2D} < 36 \text{ cm}^{-1}$ ). The presence of monolayer graphene is also verified by HRTEM (Figure 4.32). Even if some marks at grain boundaries tends to appear for 5 min of reaction, the overall uniformity of the grown monolayer graphene remains good; both graphene from the inner surfaces of Ni and Cu were continuous large films. 950 °C and 5 min lead to graphene with largest domain and high selectivity of monolayer graphene; and these conditions were selected for the subsequent studies.

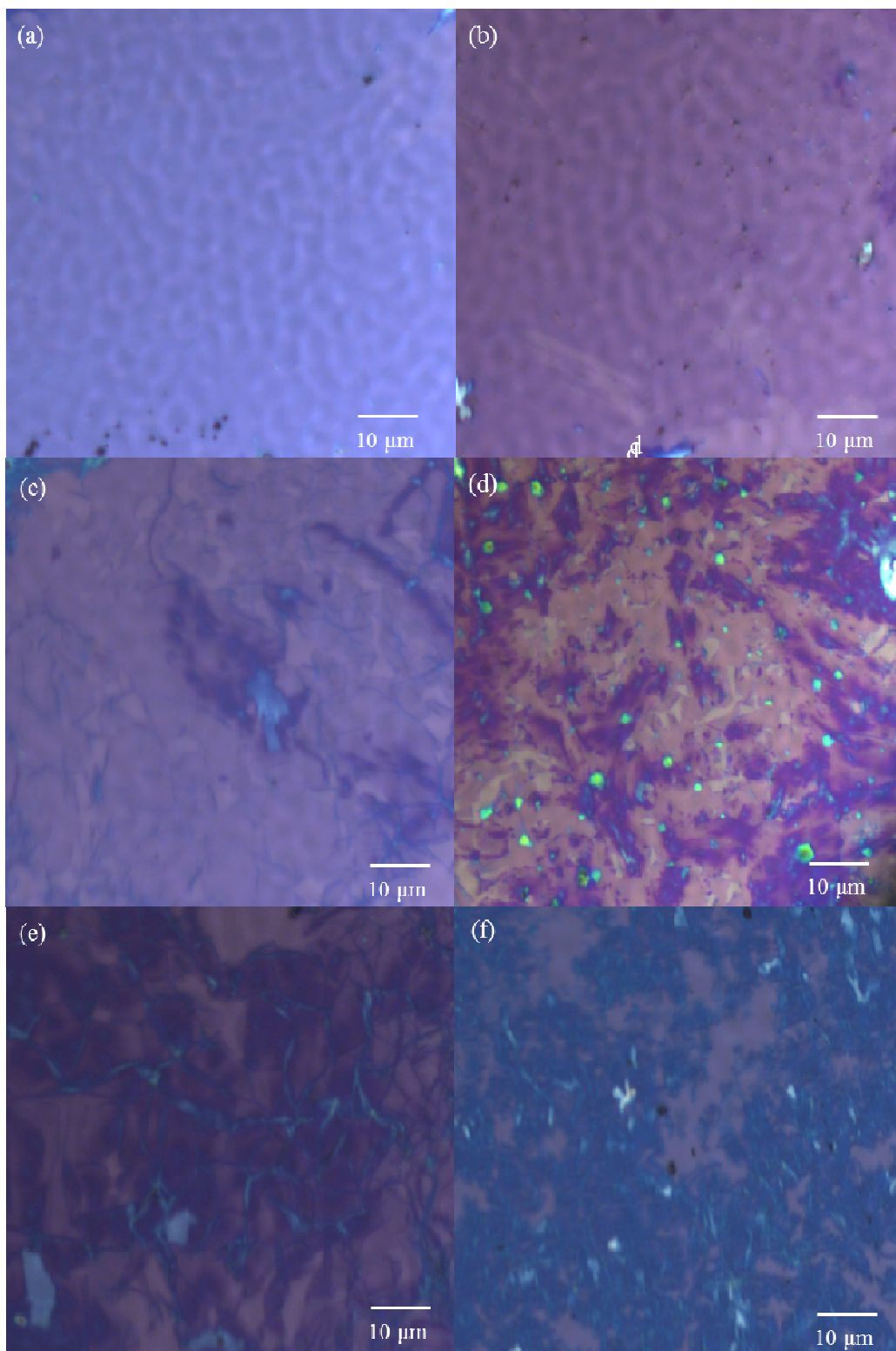


**Figure 4.30** Micrographs of the graphene materials transferred to silicon wafer after CVD growth for 4 min on (a) Ni and on (b) Cu; for 6 min on (c) Ni and (d) Cu; and for 7 min on (e) Ni and (f) Cu.

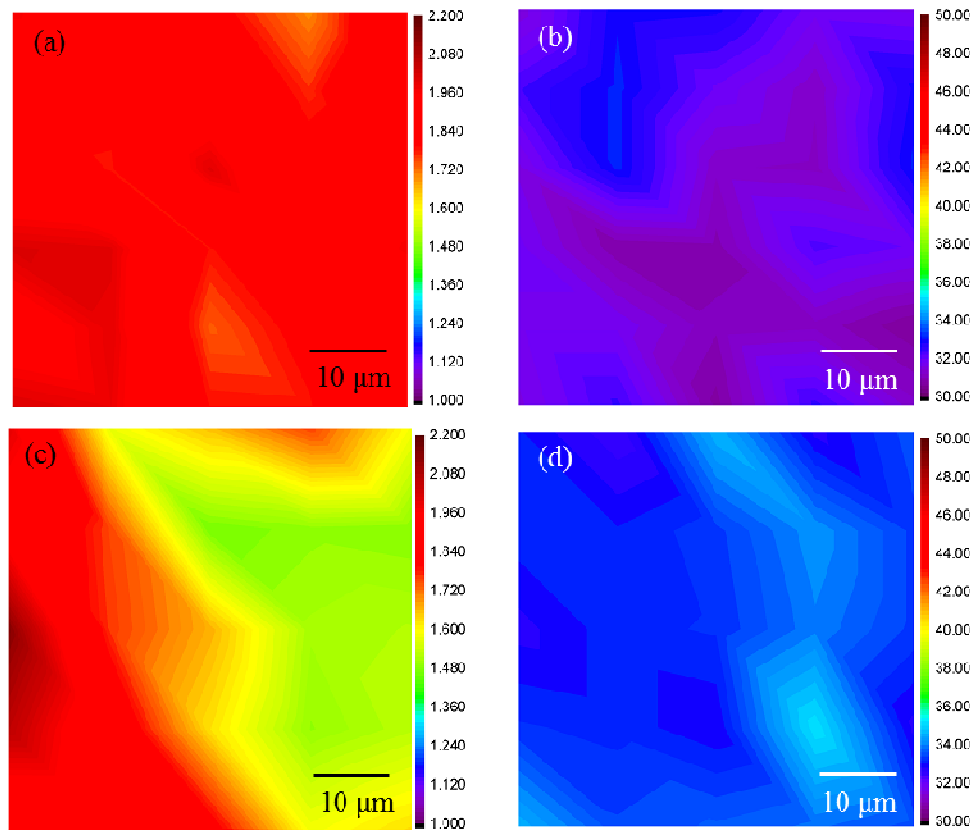


**Figure 4.31** Raman maps of  $I_{2D}/I_G$  for graphene grown on (a) Ni and (b) Cu, and  $fwhm_{2D}$  for (c) Ni and (d) Cu at 950 °C for 4 min. The color gradient bar is given on the right of each map.

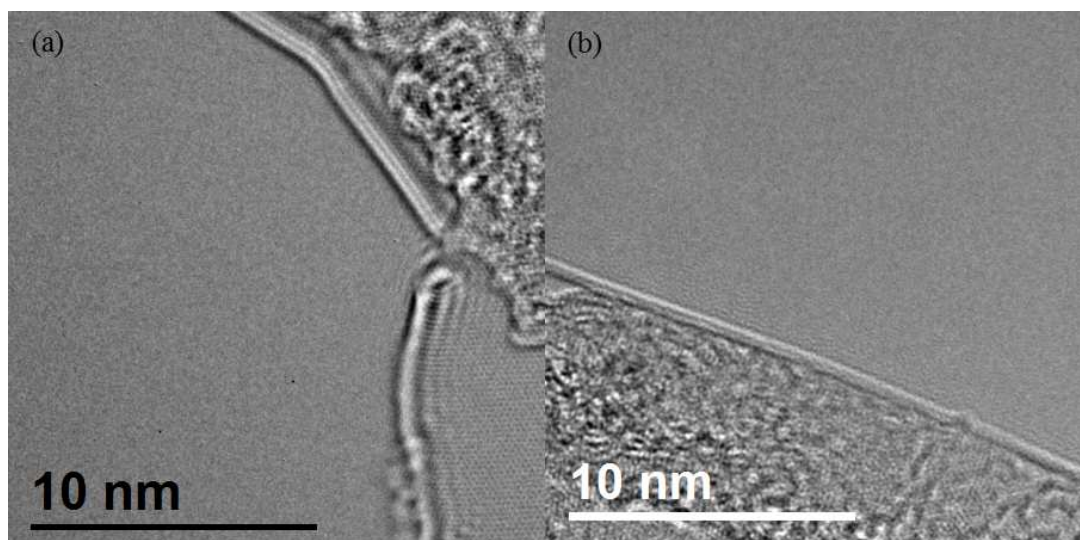


**Figure 4.32** HRTEM images of monolayer graphene grown on inner surface of (a) Ni and (b) Cu at the edges. Growth conditions: 950 °C and 4 min.

### 4.4.3 Methane partial pressure

In current section, the temperature for the CVD was fixed at 950 °C and the duration at 5 min; the total flow of the mixture of methane and hydrogen remaining at 100 sccm, the flowrate of methane was modified and 10, 20, 30, 40, 50 or 60 sccm of methane was diluted in the adequate amount of hydrogen. The Raman spectra of the samples prepared are shown in Figure 4.33.

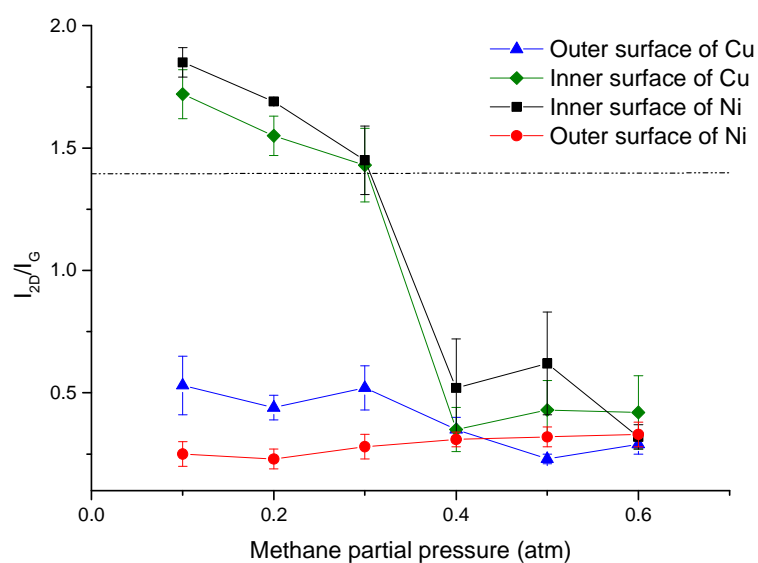


**Figure 4.33** Average and standard deviation of  $I_{2D}/I_G$  of the graphene films obtained at the 4 different surfaces of the CVD device at 950 °C for 5 min, the range of methane partial pressures being 0.2-0.6 atm.

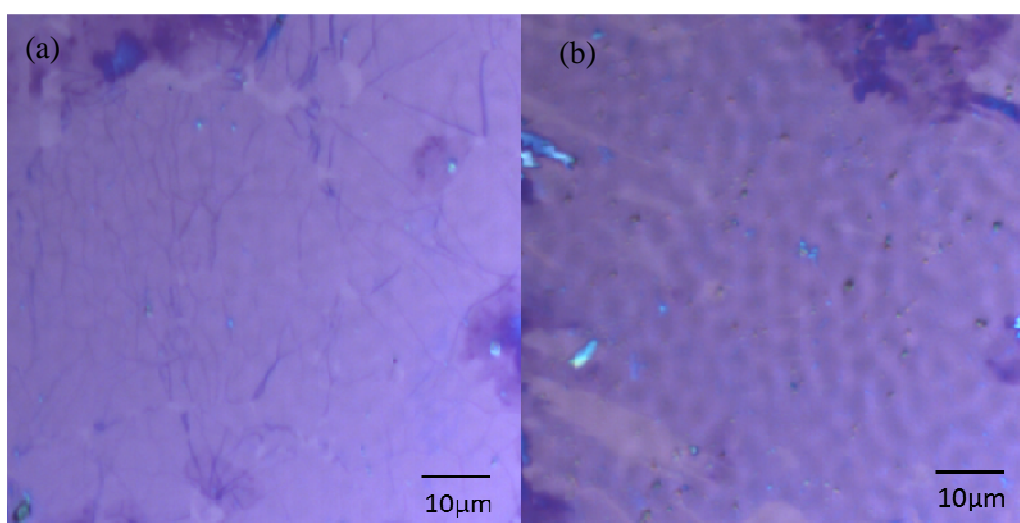


**Figure 4.34** Micrographs of graphene grown at the inner surface of (a) Ni and (b) Cu under methane partial pressure of 0.3 atm, respectively after transfer to silicon wafer (temperature growth 950 °C and duration 5 min).



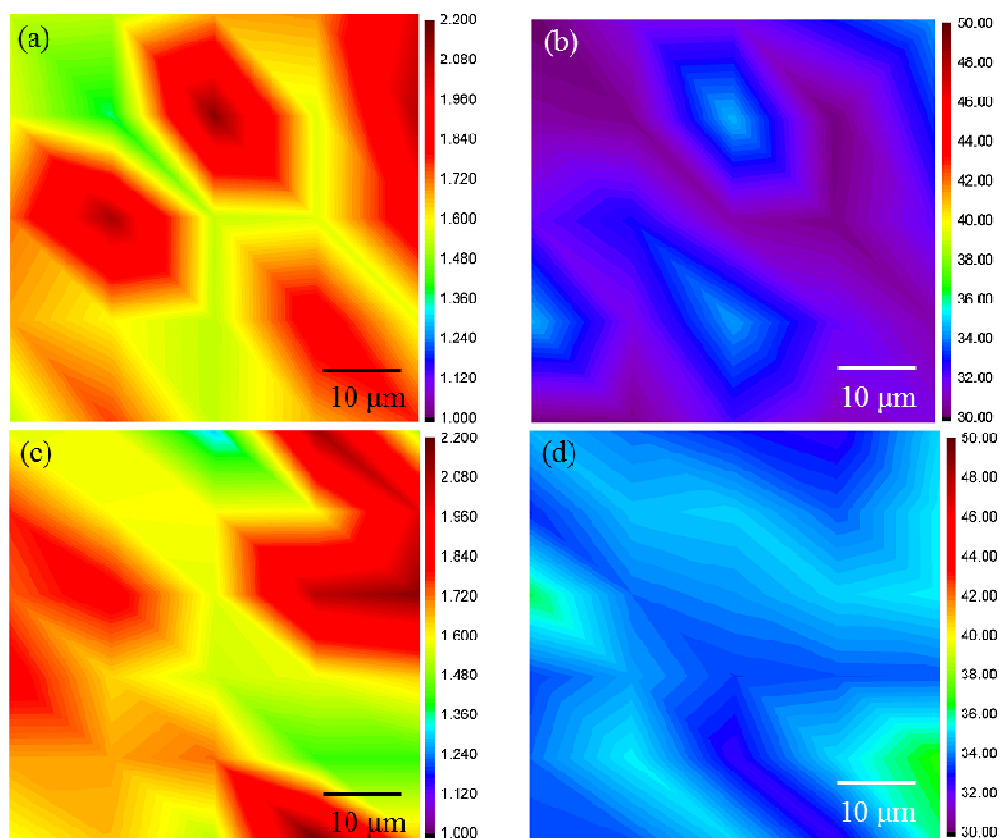


**Figure 4.35** Raman maps of  $I_{2D}/I_G$  for graphene grown on (a) Ni and (c) Cu, and  $fwhm_{2D}$  for (b) Ni and (d) Cu at 950°C for 5 min, and methane partial pressure of 0.3 atm. The color gradient bar is given on the right of each map.

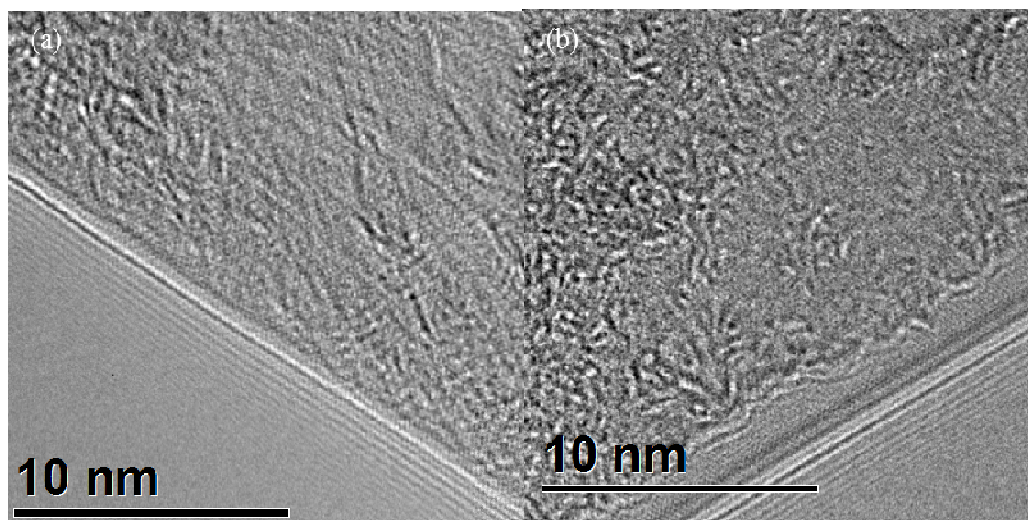


**Figure 4.36** HRTEM images of monolayer graphene grown on inner surface of (a) Ni and (b) Cu at the edges after the CVD reaction done at 950 °C for 5 min with a methane partial pressure of 0.3 atm.

For the graphene samples grown on both inner surfaces of Ni and Cu, the presence of monolayer graphene was evidenced from Raman spectroscopy ( $I_{2D}/I_G$

>1.4) under a methane partial pressure of 0.1 and 0.2 atm (Figure 4.33). Only the graphene formed at 0.2 atm appears as a continuous film at both inner surfaces of Ni and Cu. If the methane partial pressure is further increased to 0.3 atm,  $I_{2D}/I_G$  varied within the 0.5-2.0 range, for both inner surfaces of Ni and Cu, meaning that the graphene grown is composed of areas of monolayer and multilayer graphene. Multilayer graphene were mainly found as the methane partial pressure applied was 0.4 atm or higher. On the other hand, both outer surfaces of Ni and Cu were covered with multilayer graphene in the whole range of the methane partial pressure studied.

Relatively uniform graphene materials could be grown on both inner surfaces of Ni and Cu as the methane partial pressure is of 0.2 atm (Figure 4.26 (a-b)). As the methane partial pressure was increased to 0.3, the marks of grain boundaries from the polycrystalline Ni foil become more and more visible (Figure 4.34 (a)). For Cu, the type of graphene similar to that grown on Ni (Figure 4.34 (b)) was observed again, confirming the copying effect previously mentioned. Even if some marks at boundary are visible, large areas of monolayer graphene were grown at 0.3 atm of methane partial pressure evidenced in Raman maps ( $I_{2D}/I_G > 1.4$  and  $fwhm_{2D} < 36 \text{ cm}^{-1}$ ) (Figure 4.35 (a-d)). HRTEM images further confirm the presence of monolayer graphene grown at 0.3 atm at both inner surfaces of Ni and Cu (Figure 4.36).

#### 4.4.4 Discussion

The results show that the proposed simple approach that mainly involves the use of a Ni/Cu catalyst facilitates the formation of monolayer graphene. Cu is known to have a weak carbon solubility and it is indeed a good candidate to insulate carbon atoms. (Shu *et al.*, 2012) The system uses the properties of Cu in order to dramatically reduce the carbon content at the inner Ni surface. In order to verify that the source of carbon near the inner surface of Ni and Cu was not caused by a direct

leak from the CVD atmosphere, additional control experiment involving silicon, described in Section 3.3.3, was carried out. Silicon has no carbon solubility and is catalytically inactive to form graphitic carbon. This is the reason why silicon wafer was used as a carbon shield for our control experiment. A silicon wafer was first placed between Cu and Ni (Figure 3.6 (a)) and the sandwiched catalyst was used for the CVD reaction. No graphene formation could occur on the inner surface of Cu (no Raman signal) and on both surfaces of Ni, well visible peaks of D-, G- and 2D-bands indicate the presence of graphene. For the second experiment, the silicon wafer was placed on the Ni surface so Ni was sandwiched in between Cu and silicon (Figure 3.6 (b)). After the CVD reaction, no carbon materials were grown on Ni. That means that carbon atoms involving in graphene formation mainly comes through diffusion over the bulk Ni foil and neither from a leak of gas nor over the Cu foil. Carbon diffusion was evidenced through the grain boundaries of a Cu foil of 100 nm-thick; (Su *et al.*, 2011) our Cu foil being much thicker (25  $\mu\text{m}$ ) is probably able to efficiently inhibit carbon diffusion and access to the inner surface of nickel is completely reduced through the copper foil.

To further identify the path of carbon diffusion through Ni, characterization of the Ni foil after the synthesis process was investigated. Since the reaction was quenched by the use of high-speed cooling, this analysis provides a snapshot of the state during the reaction. A cross section of the Ni foil was thinned down to around 20 nm (for the position around 90  $\mu\text{m}$  from the surface) (Figure 4.37 (a)). Bright field TEM image (Figure 4.37 (b)) reveals grain boundaries enriched by carbon atoms. EDS analysis confirms that carbon concentration is higher at the Ni grain boundaries; C/Ni atomic ratio is higher at the grain boundary compared to that recorded within the Ni grains (Figure 4.38). Figure 4.37 (c) shows the schematic of the distribution of

carbon adatoms near the grain boundary at the middle of Ni foil after the CVD reaction.

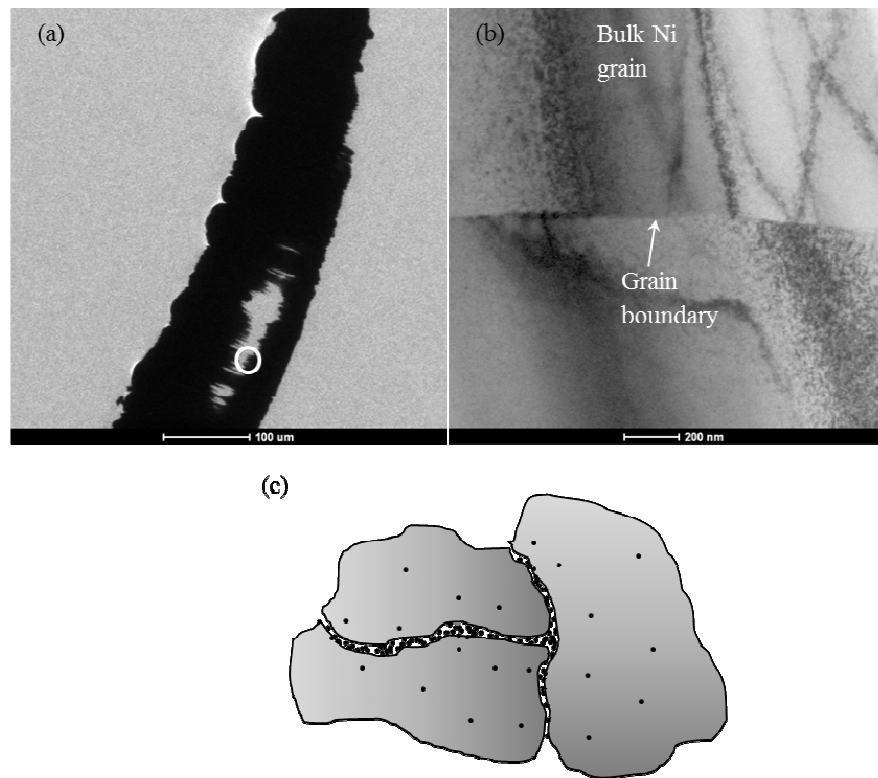


**Figure 4.37** TEM images of a Ni slice after the CVD reaction at 950 °C and 5 min with (a) low magnification image of the Ni strip; (b) bright field TEM image in the area marked by the circle on the image (a); (c) Schematic showing the distribution on carbon adatoms at the middle of the Ni foil after the CVD reaction; grey areas indicating the grains of Ni and black dots illustrating the carbon adatoms.

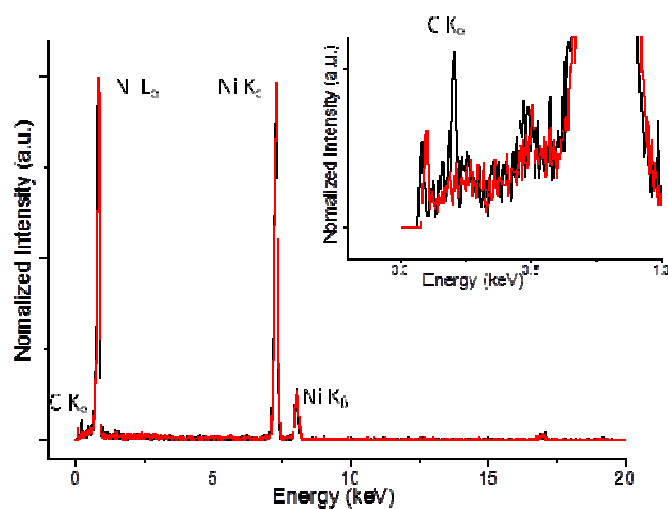


**Figure 4.38** EDS spectra of the cross-section area at the middle of the Ni foil as shown in Figure 4.37 at the middle of the grain in red at the grain boundary in black; magnified range from 0-1 keV is inserted at the top left-hand corner.

The Ni foil selected is a conventional polycrystalline Ni foil. Contrary to monocrystalline Ni, it is made of grains with irregular sizes and shapes. Diffusion of carbon adatoms is consequently not uniform towards the Ni foil and it could take place either through the bulk of the grain and also through the gap in between the grains, known as grain boundary. The solubility of carbon into bulk Ni at 950 °C is around 1.0 at.%. (Singleton and Nash, 1989) Diffusion rate of carbon atoms is thus lower within the Ni grains but it is certainly favored at the grain boundaries.

The carbon concentration gradient between the Ni surface facing carbon-rich CVD atmosphere (outer surface of Ni) and the carbon lacked region of Ni (inner surface of Ni) would be the main driving force for carbon diffusion. The carbon diffusion mechanism is illustrated in Figure 4.39. Carbon adatoms diffuse faster through the grain boundary, but at the same time, some carbon adatoms are diluted into the grain due to the concentration gradient (red arrows in Figure 4.39 (a)). The process allows a good control of the carbon concentration within Ni grains leading to a uniform carbon distribution over the whole Ni surface. Combined with a post CVD fast cooling, uniform graphene in term of number of layers is favorably obtained. Under higher temperature (1030 °C), the diffusion of carbon through the gap between the grains being increased, the CVD reaction duration applied was intentionally reduced down to 3 min (Figure 4.39 (b)). No graphene was obtained but instead web-like carbon material could be observed (Figure 4.40). The period allowed for the carbon to dilute within Ni grains was too short and carbon distribution was obviously non-uniform throughout of the Ni surface. After fast cooling, graphitic material were segregated at the locations enriched by carbon (grain boundaries) while no carbon material was formed on the surface far from grain boundary. It was here as well

confirmed that the grain boundary was the major channel for the carbon supply to the interface between Ni and Cu.

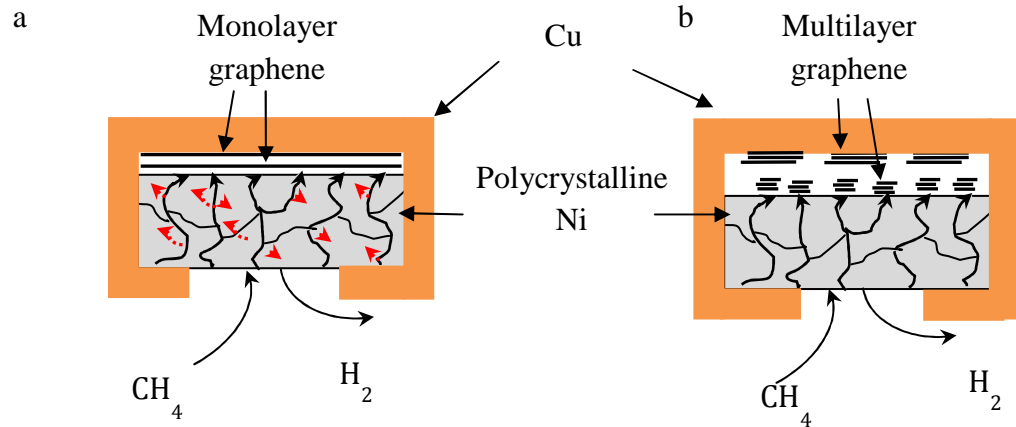


**Figure 4.39.** Pathways of carbon diffusion through the polycrystalline Ni foil at (a) 950 °C and (b) 1030 °C through the grain boundaries of Ni (black arrows) and through the Ni grains (red arrows).

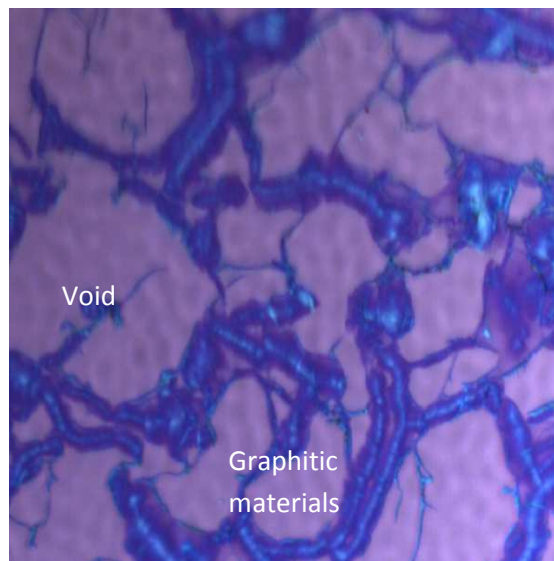


**Figure 4.40** Optical micrograph of the web-like graphitic carbon grown at the inner surface of Ni at 1030 °C for 3 min.

Formation of multilayer graphene is usually observed from polycrystalline Ni in atmospheric pressure CVD. (Reina *et al.*, 2008a, Reina *et al.*, 2009) The misalignment of the distance of the Ni grains is reported to provide abundant nucleation sites for graphene to segregate into multilayer graphene. (Zhang *et al.*,

2010) This is the main reason why Ni is normally forsaken to grow graphene. With our bilayer catalyst system, accumulation of the carbon at grain boundaries is reduced, inhibiting the excessive carbon segregation and thus enhancing the formation of monolayer graphene. Multilayer graphene would be more likely to form on Cu due to the excessive supply of carbon. But, through our strategy, a carbon-lacked atmosphere is created at the interface of Ni-Cu, and at both outer surfaces of Ni and Cu have the same behavior than that found in the case of the use of single Ni or Cu foil is observed. The main carbon supply comes from the contact with Ni. This is the reason why voids appear on the graphene film formed on the inner surface of Cu coming from areas where the Ni and Cu were not perfectly pressed.

In summary, by utilizing bilayer bimetallic catalyst through wrapping a Cu foil over a Ni foil, the supply of carbon adatoms at the interface between Ni and Cu was managed to be well controlled. Under optimum operating conditions and with the aid of fast cooling, high quality monolayer graphene could be grown on both inner surfaces of Ni and Cu under single atmospheric pressure CVD. The graphene that was grown at the outer surface for both Ni and Cu has the same characteristics that those of graphene grown on single Ni or Cu under the same operating conditions. The growth mechanism proposes that the gap between the grains of Ni foil is the main channel to supply carbon adatoms at the inner surface of Ni. Meanwhile, the contact between Ni and Cu was the pathway for the carbon supply to the Cu surface.

#### **4.5 Reuse and recycle of catalyst**

In the Section 4.1.2, the preliminary study showed that after the separation of graphene from the Ni foil by using nitric acid (Figure 4.3 (b)), the whole Ni foil remained after separation. Thus, a series of studies were carried out to investigate the

possibility of reusing the catalyst to grow graphene in a subsequent CVD reaction under the same conditions.

Cu is weak in corrosion resistance; it was completely etched away even at very low concentration of iron nitrate or nitric acid to achieve the graphene separation. This is the reason why, for the following study devoted to the recycle of catalyst for graphene CVD growth, Ni instead of Cu was used.

In the preliminary study, the main objective was to minimize the deterioration imposed to the graphene sheet during the separation, and the catalyst lost was not the concern. The etching mechanism involves a redox reaction: oxidation of Ni by  $\text{HNO}_3$ ; oxidized  $\text{Ni}^{2+}$  produced being able to solubilize in the solution and reduction of hydrogen ions forms hydrogen bubbles that could be clearly seen for high  $\text{HNO}_3$  concentration. Such reaction could be quite aggressive towards graphene which needs cautious manipulation. Iron nitrate could provide milder conditions that can be interesting as an alternative process for graphene separation.

Regarding the graphene separation process, our work was focused on 2 main objectives: (1) limitation of Ni consumption in order to investigate proficiency of catalyst recycling and (2) avoiding degradation of separated graphene. The Ni foil applied in current study was 1 cm x 1cm (instead 0.5 cm x 0.5 cm) in dimension to further prove that the proposed method could be up-scaled to larger area graphene. 3 types of graphene, namely with high selectivity of monolayer graphene, bilayer graphene and multilayer graphene were prepared by the Ni-catalyzed CVD reaction for 5 min, under 80 sccm of hydrogen and 20 sccm of methane at 850, 900 and 950 °C, respectively.



### 4.5.1 Nitric acid

Nitric acid is known as a strong oxidative acid. Significant amount of bubbles (as shown in Figure 4.3 (a)) were observed in HNO<sub>3</sub> concentration ranging from 14.4 mol/L (65 %) to 4.80 mol/L (21.6 %) for all the investigated graphene samples. During the separation process, the greenish solution was enriched with Ni<sup>2+</sup> produced from high amount of Ni oxidized and solubilized. The case of multilayer graphene was especially complex. As the acid concentration was further reduced to 2.88 mol/L (13.00 %), the separated graphene was severely damaged. As lower concentrations of acid were used, the duration until the separation process was complete was very long (several days) and the Ni foil was also etched (same observation as shown in Figure 4.3 (c)).

For monolayer and bilayer graphene, the separation conditions could be optimized. For acid concentrations of 1.80 mol/L (8.13 %), 1.44 mol/L (6.50 %) and 1.20 mol/L (5.42 %), large amount of Ni could be preserved after separation. The direct observation of the separation process with naked eyes indicates that the process started from the edges and seems to follow kind of intercalation mechanism. Nitric acid solution is able to gradually and gently detach the graphene sheet from the edges to the center of the sample (Figure 4.41 (a)). At the meantime, graphene being very light and highly hydrophobic preferentially floats at the solution surface. The sinking of the Ni foil at the bottom of the solution certainly helps the separation by providing a gentle force in tearing the graphene from the Ni foil. Bilayer graphene could be totally separated according to this process (Figure 4.41 (b)), but the edges were slightly deteriorated.

The concentration of nitric acid plays a very important role to limit both consumption of the Ni foil and damaging of graphene. Too low acid concentrations

have to be avoided because the separation process becomes very slow and a long period of acid exposure induces high damages to the Ni foil that is unable to be reused as catalyst. The surface of Ni became rough especially at the edges due to the formation of an oxidized layer. Nitric acid with of concentration of 1.44 mol/L (6.5 %) was found to be a good compromise for graphene separation and preservation of Ni substrate and the Ni foil could be used a second time for graphene synthesis. After the second reaction, the Ni foil was too thin to be able to be handled by hands. The thickness of the nickel foil after the first separation was of 75  $\mu\text{m}$  (more than 40 % of Ni loss), and after the polishing process, only 52  $\mu\text{m}$  left. The nickel foil was completely etched away during the second cycle. Furthermore, the overall uniformity of the grown bilayer graphene at the second cycle was not comparable with that obtained at the first cycle. The graphene obtained at the second synthesis stage was full of holes and composed with a lot amount of areas of multilayer graphene.

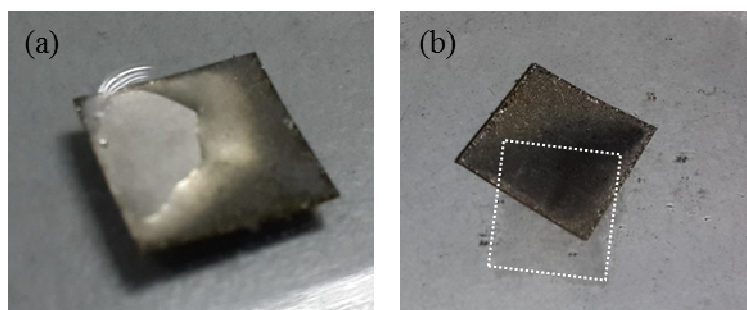


**Figure 4.41** Separation of bilayer graphene from the Ni foil by nitric acid. (a) Beginning of the process. (b) Completely separated bilayer graphene, the Ni foil is submerged into nitric acid and the white box helps to locate the separated graphene floating at the solution surface.

In summary, by using nitric acid, none of the condition suitable for an efficient route leading to the recycle of Ni. Nitric acid is probably too strong as the oxidation agent for Ni, which forbids an optimization of the experimental conditions. However, from the observations using nitric acid, it becomes clear that the preservation of the metallic Ni is a key parameter leading to the formation of

graphene of good quality over the subsequent cycles. Considering that the etching capability of iron nitrate solution is relatively weak compared with that of nitric acid; possibility of recycling Ni if iron nitrate solution was applied for graphene separation was further explored.

#### **4.5.2 Iron nitrate solution**

Iron nitrate is the most widely used etchant for the separation of graphene from Cu, but less on Ni. By referring to the standard potential chart, the redox reaction of oxidizing Cu by  $\text{Fe}^{3+}$  has a standard potential as high as +1.11 V, this is reason why etching Cu by iron nitrate is quite aggressive and Cu could not be preserved. For oxidation of Ni by  $\text{Fe}^{3+}$ , the standard potential is of +0.52 V. The oxidation reaction by  $\text{Fe}^{3+}$  being less favorable for Ni than for Cu, we focused our study on the potential reuse of Ni using iron nitrate as separation agent.

3 different types of graphene grown on Ni, namely monolayer, bilayer and multilayer graphene (for the synthesis conditions see Section 4.5.1) were selected. The concentration of iron nitrate was varied from 0.1 to 2.0 mol/L.

For the monolayer graphene, optimizing the concentration of iron nitrate was not successful. The outcome was inconsistent. Sometimes, Ni was totally etched away, but in certain occasions, the etching process was less rapid but the graphene film could not be properly detached from Ni. Figure 4.42 shows the nickel foil thinned by the etchant partially transparent. A large amount of Ni residue remains trapped between both sheets of monolayer graphene, since only 4 edges of Ni foil been rubbed with sand paper to remove graphene. Both surfaces were covered with films of graphene. On the other hand, multilayer graphene was also very difficult to be separated from Ni whatever the iron nitrate concentration, no obvious detachment

of graphene could be visually observed, and iron nitrate has no real effect for the separation.

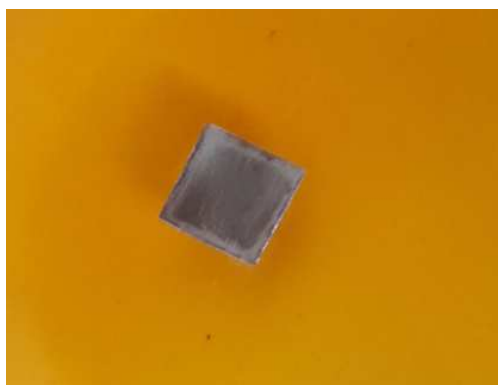


**Figure 4.42** Photograph of the Ni foil covered with monolayer graphene in a solution of iron nitrate of a concentration of 0.2 mol/L after 2 days.

Separation of bilayer graphene was dissimilar to the behavior observed for monolayer and multilayer graphene. Iron nitrate with a concentration of 0.50 mol/L was the most efficient condition for separation. Further increase of the concentration of iron nitrate solution did not give any significant enhancement for the process and lower concentration (0.25 mol/L) did not favor the separation process; after several days, no progress in graphene separation could be observed. Figure 4.43 (a) shows the process of graphene separation from the Ni foil by iron nitrate (0.50 mol/L). A “white zone” started to appear at the edges of the foil. Adding to the commonly observed etching phenomenon by Ni oxidation, the observed white zones seem to result from intercalation of iron nitrate that could occur in between the Ni surface and the graphene sheet. The interaction between the bilayer graphene and the Ni surface was obviously broken as the “white zones” were enlarged with time and eventually the whole Ni foil became whitish. Meanwhile, the Ni foil sinking applied an additional driving force to tear the graphene from the Ni foil. The same phenomenon was observed regardless of how many cycles the Ni foil was used for the CVD stage and the subsequent bilayer graphene separation. From the study, recycle the Ni foil up

to 6 times and the graphene samples that were synthesized were shown in Figure 4.43 (b). The size of the graphene sheets obtained was shrinking as the number of cycles the Ni was increased. Scrubbing the edges of the Ni foil indeed favors the etching process which becomes more and more aggressive reducing the quality of Ni for the subsequent CVD reaction. The graphene material synthesized under the 6<sup>th</sup> cycle was mostly bilayered as shown in the HRTEM image (Figure 4.43 (c)).

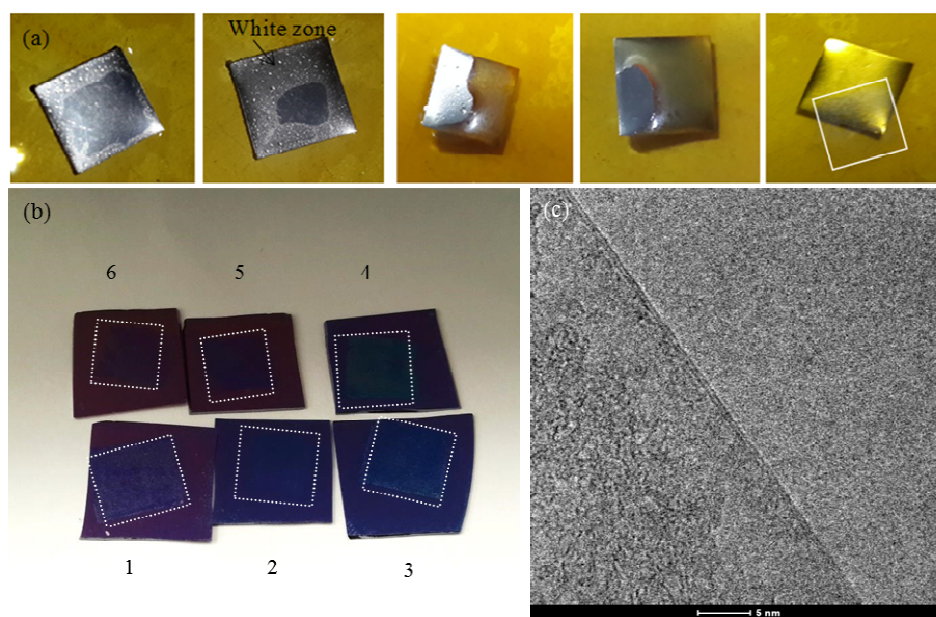


**Figure 4.43** (a) Progress for bilayer graphene separation from Ni in iron nitrate solution (0.50 mol/L) from left to right; the white box indicating the separated graphene. (b) Photograph of the six bilayer graphenes after transfer on silicon wafer (with 1000 Å silicon oxide) obtained from their respective cycle, white boxes indicating the locations of graphene. (c) HRTEM image of the bilayer graphene separated under the sixth cycle.

Figure 4.44 (a) shows the 6 Raman spectra of graphene from the 6 cycles processed on Ni under the same CVD reaction conditions and separation using iron nitrate. From Raman spectroscopy analysis, the intensity of the D-band is very weak as compared that of the G-band, indicating the high quality of the formed graphene (Ferrari *et al.*, 2006) even after the separation process. For all 6 spectra, the  $I_{2D}/I_G$  ratio is in the range of 0.979-1.352 and the  $fwhm_{2D}$  in the 40-50  $cm^{-1}$  range, in agreement with what it is reported for bilayer graphene (Sun *et al.*, 2010b, Peng *et al.*,

2012b, Yan *et al.*, 2011b). Uniformity of the grown graphene was further investigated by Raman mapping that was carried out for the graphene prepared under the sixth cycle (Figure 4.44 (b) & (c)). Over the 50  $\mu\text{m}$  x 50  $\mu\text{m}$  scanned,  $I_{2D}/I_G$  ranges between 1.03 and 1.35 and  $\text{fwhm}_{2D}$  between 43 and 46  $\text{cm}^{-1}$ , suggesting a good uniformity of the graphene type (bilayer), which is almost identical for the graphene obtained at the first cycle (Figure 4.8 (e-f)). The graphene sheets obtained after different cycles of reaction and separation are of bilayer type of good crystallinity and uniformity meaning that the characteristics of the synthesized graphene do not depend on the cycle. The quality of Ni especially its surface could be well preserved by the used conditions of the separation process. The following discussion part could give some comments regarding this particular aspect.

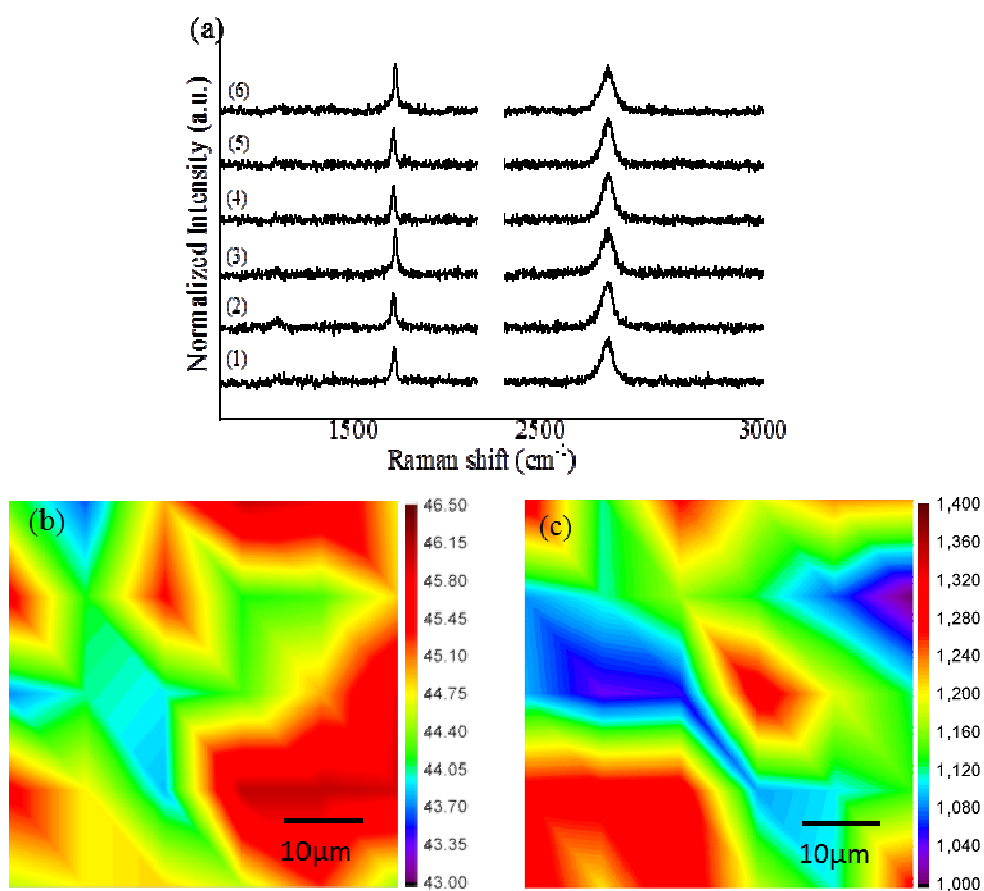


**Figure 4.44** (a) Raman spectra for six bilayer graphene samples after separation from Ni foil and transfer onto a silicon/silicon oxide wafer. Raman maps of (b)  $\text{fwhm}_{2D}$  and (c)  $I_{2D}/I_G$  of the bilayer graphene grown under the sixth cycle.

### 4.5.3 Discussion

To go further in the understanding of the mechanisms involved in the graphene separation using iron nitrate that allows an efficient way for Ni recycling, characterization was carried out on the Ni foil that was used for the CVD reactions. XRD patterns of the Ni foil after the first cycle of the CVD growth for the 3 graphene types are shown in Figure 4.45. As expected, the Ni(200) peak around  $51.5^\circ$  was highly pronounced. The range of  $40^\circ$ - $52^\circ$  was intentionally magnified to visualize the less pronounced peaks around  $46.3^\circ$  and  $49.1^\circ$ , they can be well assigned to the (110) and (006) peaks of rhombohedral  $\text{Ni}_3\text{C}$ . Even if a quantitative analysis is not possible, under the same XRD recording conditions, the peak of  $\text{Ni}_3\text{C}$  becomes less and less pronounced as the nickel foil was used for the growth of multilayer graphene (Figure 4.45 (red)), bilayer (Figure 4.45 (blue)) and monolayer graphene (Figure 4.45 (black)). As expected,  $\text{Ni}_3\text{C}$  formation is favored as higher temperature was applied for CVD to grow graphene with higher number of layers.  $\text{Ni}_3\text{C}$  is usually known to offer a good protection against corrosion.  $\text{Ni}_3\text{C}$  is reported in several patents for its use as an insulating layer covering Ni in order to inhibit oxidation and other chemical reactions (Zhang *et al.*, 2012b, Hasz *et al.*, 2002, Armstrong, 1982).  $\text{Ni}_3\text{C}$  is here believed to be the key ingredient that allows the reuse of the Ni foil.

The reuse of the Ni foil used to grow monolayer graphene was not possible by using neither iron nitrate nor nitric acid solution. This can be explained by 2 reasons:

1. Only the four edges of the Ni foil were scrubbed with sand paper. Moreover, the graphene grown at the unwanted sides was expected to provide some protection to minimize the loss of Ni. But if the basal plane of monolayer graphene contains some voids, the iron nitrate solution could seep through them and enhance attack of Ni

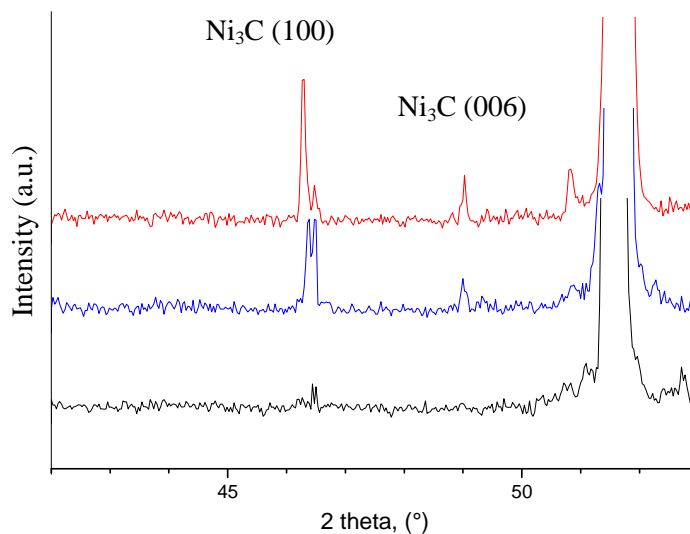


**Figure 4.45** XRD patterns of the nickel foil after CVD growth of (black) monolayer graphene, (blue) bilayer graphene and (red) multilayer graphene.

2. The amount of  $\text{Ni}_3\text{C}$  at the surface of the Ni foil could be too little and/or its coverage highly inhomogeneous to provide an effective protection. It is much easier for iron nitrate to attack Ni. Most of the Ni was etched, but the  $\text{Ni}_3\text{C}$  remained untouched and trapped between the 2 sheets of graphene.

The aim of enabling the reuse of Ni foil with multilayer graphene was also unsuccessful. Graphene is indeed known to strongly interact with Ni due to hybridization between  $\pi$  orbitals of graphene and  $d_{z^2}$  states Ni (Mittendorfer *et al.*, 2011, Dahal and Batzill, 2014). The spacing between the graphene sheet and the Ni surface is thus reduced and was calculated as low as 2.11 Å (Gamo *et al.*, 1997); the  $\pi$ -band structure of graphene could not be found in the first few layers of graphene mounted on Ni (Sun *et al.*, 2010a). Ni induces strong modifications of electronic structure of the graphene layer leading to appearance of an effective magnetic moment in the graphene layer (Dedkov and Fonin). More layers of graphene means higher degree of hybridization between the  $\pi$  orbitals of graphene and the  $d_{z^2}$  states of Ni, making the iron nitrate harder to intercalate between Ni and graphene.



Furthermore, the graphene layer grown at the other side of Ni (along with a huge amount of Ni<sub>3</sub>C) reduces the accessibility of iron nitrate to Ni. Hence the etching of Ni by iron nitrate becomes insufficient resulting in the observed failed separation for multilayer graphene.

On the contrary, the separation of bilayer graphene was successful. In fact, the graphene shows a higher selectivity of bilayer graphene even if monolayer, and multilayer graphene could also be noticed (by TEM observations and Raman mapping). The surface of the Ni foil after separation using nitric acid is obviously different from the original Ni foil and from that after separation by the iron nitrate solution. The long period exposed to acid favors the formation of an oxidized layer. On the contrary, the surface of the Ni foil seems undamaged after being exposed to iron nitrate.

Figure 4.46 shows AFM images of the Ni foil surface before and after the separation process using both nitric acid and iron nitrite. After separation using iron nitrate, the Ni surface was well preserved and no severe damages are visible (Figure 4.46 (b)), except a few small holes of around 1 μm. For the Ni foil exposed to nitric acid (Figure 4.46 (c)), the observed surface was highly uneven with a lot of protrusions. The surface flatness of the Ni foil is important for graphene transfer. If an untreated/unpolished Ni foil is directly used for the CVD reaction, graphene can grow but it is highly contaminated; especially, Ni particles deposited on the graphene surface could be observed by optical microscopy (Figure 4.47). To minimize contamination on the separated graphene and reduce the roughness of the Ni foil, its surface was systematically polished with sand paper prior to the growth stage (Figure 4.46(d)).

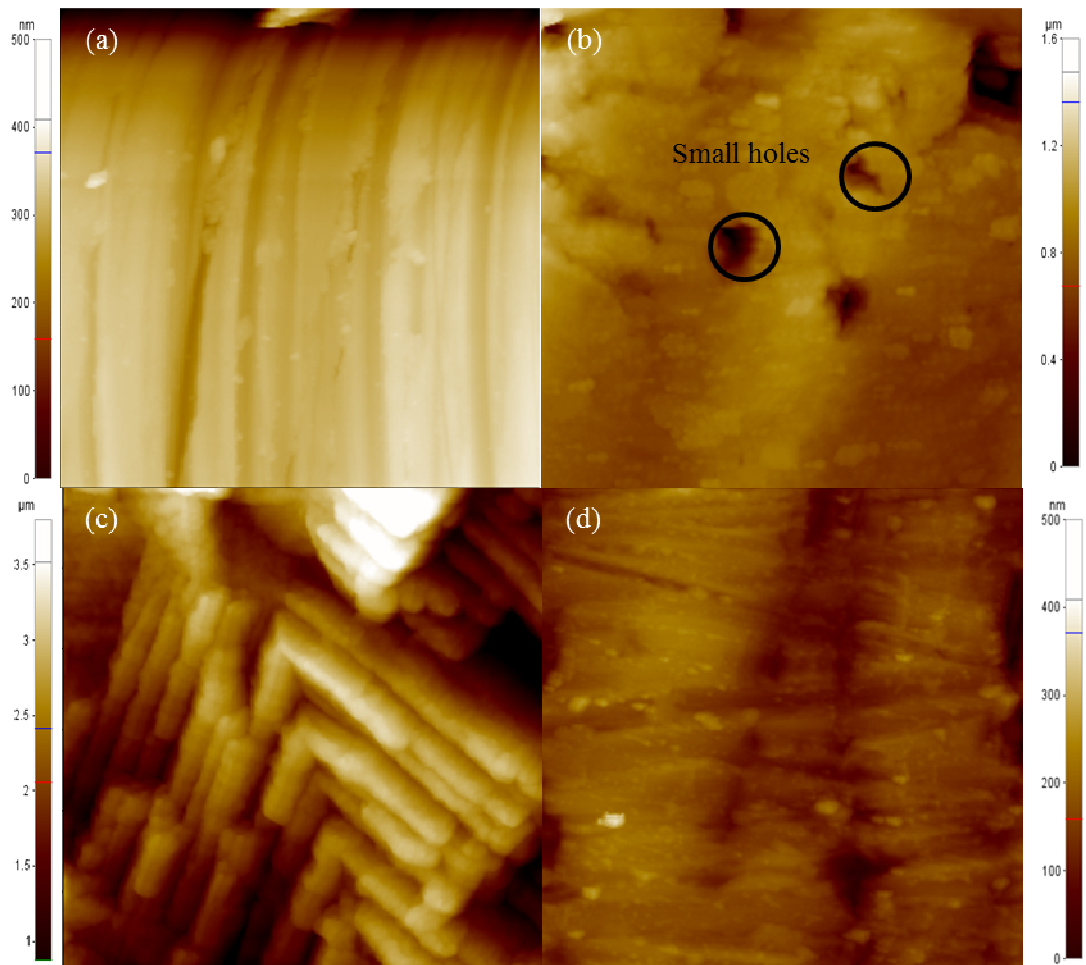


**Figure 4.46** AFM images for (a) the nickel foil before the CVD reaction, (b) the nickel foil after CVD reaction and separation with iron nitrate, (c) nickel foil after the CVD reaction and separation with nitric acid and (d) the nickel foil obtained after the separation process by the iron nitrate solution and polished with sand paper (800 mesh). The dimensions for all the images are  $15\ \mu\text{m} \times 15\ \mu\text{m}$ .

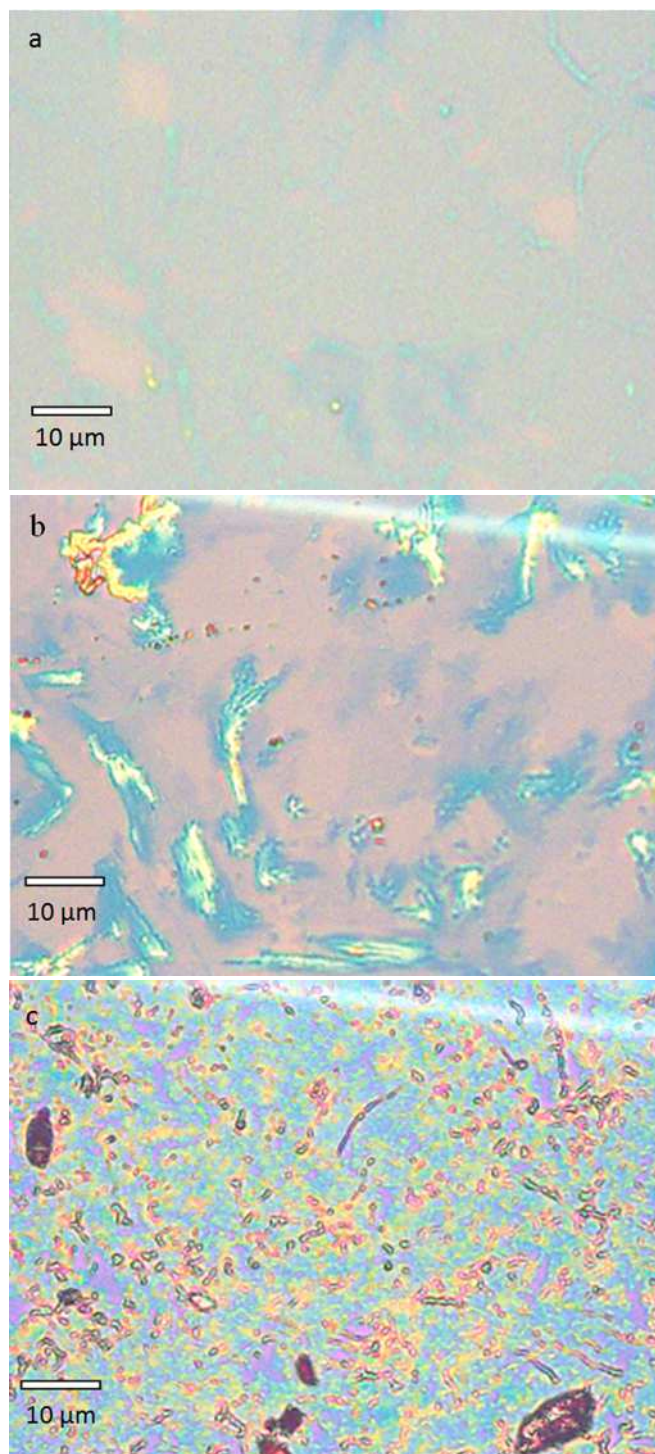


**Figure 4.47** Optical images of graphene transferred from Ni foil for (a) graphene grown on a fresh new Ni foil, (b) graphene grown on unpolished Ni foil after separation with iron nitrate for the preceding graphene growth (c) graphene grown on unpolished Ni foil after separation with nitric acid for the preceding graphene growth. Areas with gold color are contaminations by nickel.

Figure 4.48 shows XRD patterns taken from the Ni foil after bilayer graphene catalysis and, before and after separation with iron nitrate and nitric acid, respectively.  $\text{Ni}_3\text{C}$  that is doubtless assigned remains almost untouched after the treatment process

with iron nitrate.  $\text{Ni}_3\text{C}$  becomes however hardly visible as the nitric acid-based separation process is applied, showing that  $\text{Ni}_3\text{C}$  was unable to resist to nitric acid etching.

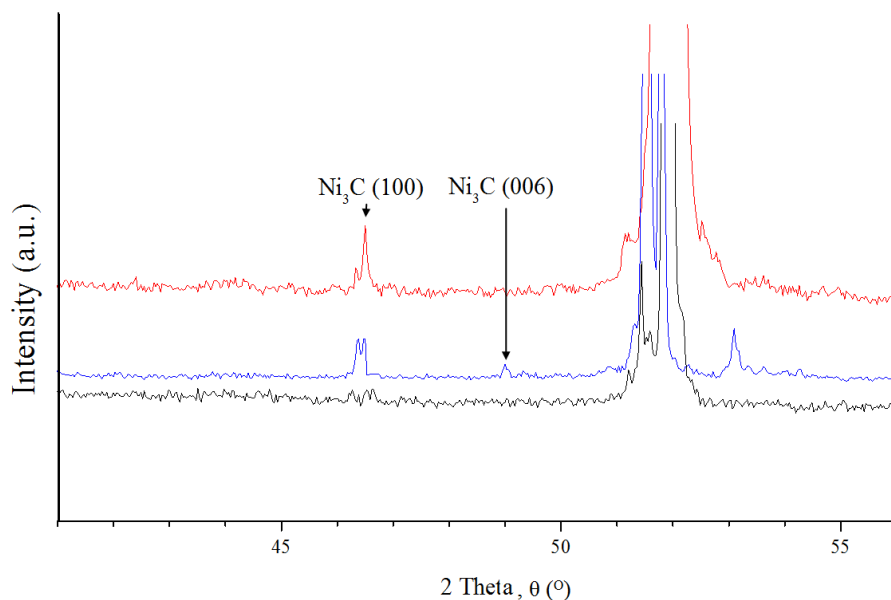


**Figure 4.48** XRD patterns of the nickel foil after the CVD reaction (red), after the CVD reaction and graphene separation using iron nitrate (blue) and nitric acid (black).

It has been shown that as the surface of the Ni foil is relatively smooth, intercalation and mild etching by iron nitrate solution is favoured between graphene and Ni foil surface. This soft separation process is partly responsible for the graphene cleanliness. As the Ni surface was exposed to nitric acid, the surface became highly uneven and full of protrusions resulted from the edges of grains of Ni were visible (Figure 4.46 (c)). The conventional polycrystalline Ni foil is composed of numerous grains that are closely bounded. As reported by Zhang *et al.* (2010), graphitic carbon could be accumulated in between the grains during the graphene growth stage. The presence of graphitic carbon probably weakens the interactions between the Ni grains and changes the way for the etchant to intercalate between the grains. This phenomenon is emphasized as nitric acid was utilized as etchant. The strong etching property of nitric acid attacks the surface of the Ni foil vigorously. Besides that,

graphene usually mitigates the surface morphology of the catalyst. If an individual grain is over exposed, the interaction with neighbouring grains is weakened leading to encapsulation of Ni particles by graphitic layers. Graphene is indeed known to strongly interact with Ni. In that case, interactions between protruded grains and the foil are expected to be highly reduced. The graphitic layers prevent the encapsulated particles from being etched, which results in high Ni residue on the transferred graphene (Figure 4.49 (b)). Encapsulated Ni particles were widely observed under HRTEM for graphene grown from Ni foil with rough surface (Figure 4.49 (c)). Ni residue on graphene could be minimized by a simple polishing process applied to the Ni foil using sand paper. The cleanliness of the transferred graphene could be preserved as the Ni surface was smoothed under mild polishing conditions. Graphene separation is hence favoured as illustrated in Figure 4.49 (a) and uniformity of bilayer graphene could be preserved under various cycles.

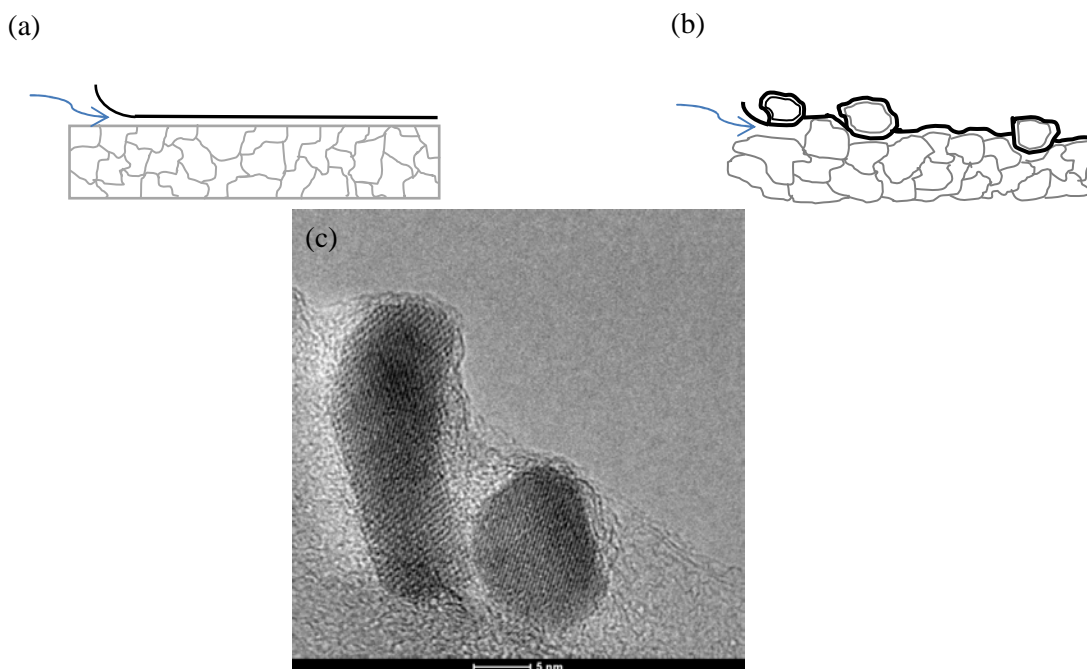


**Figure 4.49** Schematic illustrating interactions and etching mechanism during the separation of graphene with (a) a smooth surface and (b) a corrugated surface. The particles indicating the Ni grains, the black line represents the graphene layer and the arrows show interacting paths. (c) HRTEM image for encapsulated Ni particles in graphene grown from Ni with rough surface.

As already mentioned, acid and aqueous iron solutions are widely used for the separation of graphene from both Ni and Cu substrates. Normally, the substrates are etched away completely (*Seo et al.*, 2012, *Qi et al.*, 2011, *Reina et al.*, 2008a). Indeed, if pure metal foil is placed into the etchant solution, it is rapidly solubilized even with weak concentrations. Interestingly, in our study, the etching rate of Ni was significantly reduced which has allowed the Ni foil to be reused several times. From the Ni-C phase diagram, the concentration of the diluted carbon adatoms in the bulk Ni is as low as 0.9 at.% at 900 °C. Under our CVD conditions, the amount of formed Ni<sub>3</sub>C is thereby expected to be small. The presence of a small amount of Ni<sub>3</sub>C was also reported to be formed during (*Weatherup et al.*, 2011) and after (*Son et al.*, 2014) the CVD reaction. However, in most of the studies, Ni<sub>3</sub>C was unfortunately unnoticed. It is believed that the evidenced Ni<sub>3</sub>C covering the surface of our Ni foil acts as a shield from etching by iron nitrate. Some etch pits (depth of around 1 μm) that can be however observed on the surface of Ni foil (Figure 4.46 (b)) show that the Ni<sub>3</sub>C layer is not uniform on the nickel surface. They could provide weak points for the etchant attack. Meanwhile as stronger etchant like nitric acid was used, this non-uniformed and thin Ni<sub>3</sub>C was not able to preserve the perfectness of surface of Ni foil. The presence of Ni<sub>3</sub>C is vital to inhibit the excessive etching of the Ni foil by mild etchant. Several conditions are required for the formation of sufficient Ni<sub>3</sub>C. It will be elaborated in the subsequent section.

It is widely accepted that graphene formation follows a bulk-mediated growth mechanism (*Losurdo et al.*, 2011), whereas the concentration of carbon solubilized in nickel is relatively high compared with that for the other catalysts. During the CVD process, the methane gas is catalytically decomposed at the surface of the Ni foil and the carbon adatoms dissolve within Ni (Figure 4.50 (a)). The nucleation process of

graphene starts as the carbon concentration has achieved or is above a threshold, especially during the cooling process (Figure 4.50 (b)). Referring to Ni-C phase diagram, the carbon solubility in bulk Ni decreases with descending temperature, the excess of carbon would segregate from Ni upon cooling. Fe, Co and Ni are among transition metals that are known to easily form carbides after been exposed to elevated temperature with a carbon source (Seah *et al.*, 2011b).

The presence of Ni<sub>3</sub>C is however rarely reported in the area of the Ni-catalysed CVD for the graphene synthesis. Presence of Ni<sub>3</sub>C is commonly reported at the surface of core-shell Ni-Ni<sub>3</sub>C nanoparticles in CNT samples (Singh *et al.*, 2002, Singh *et al.*, 2003, Panagiotopoulos *et al.*, 2012). The growth conditions of CNTs and graphene differ especially regarding the control of dissolved carbon adatoms into the bulk metal catalyst. Large amount of dissolved carbon adatoms is favourable to increase the yield of CNT formation. Meanwhile, for graphene synthesis, the dissolved carbon is commonly lowered either through vacuum CVD (Tan *et al.*, 2012), by utilizing low ratio of carbon precursor to dilution gas, with very thin nickel film as catalyst (Xu *et al.*, 2011) or by introducing an inhibitor in the system (Weatherup *et al.*, 2013). Under these conditions, carbon atoms could segregate and precipitate at the surface of Ni with the optimum level and lead to formation of monolayer or bilayer graphene. Conversely, in our CVD process, the ratio of carbon precursor to dilution gas is 0.25, which is much higher as compared to those usually reported for the growth of monolayer or bilayer graphene, typically 10 times lower. Under our high carbon precursor concentration, the number of graphene layers was minimized to two layers by the very fast cooling.

In comparison to other reported works with fast cooling rates in the range of 10-600 °C.min<sup>-1</sup> (Zhang *et al.*, 2010, Jacobson *et al.*, 2012b, Xu *et al.*, 2011, Kim *et*

*al.*, 2009), our average cooling rate is higher ( $\sim 700\text{ }^{\circ}\text{C}\cdot\text{min}^{-1}$ ). Fast cooling facilitates the quenching process and reduces the amount of carbon atoms segregated; only the carbon atoms situated near the surface had enough time to segregate and form graphene. Meanwhile, diffusion of the carbon situated in the middle of the Ni foil is highly inhibited. They would eventually form  $\text{Ni}_3\text{C}$ , as evidenced by XRD (Figure 4.48). Moreover, the thickness of the used Ni foil is quite thick ( $125\text{ }\mu\text{m}$  instead of standard nanometer scale catalyst); leading to increase the amount of carbon atoms dissolved in nickel. At the same time, the longer diffusion path for the carbon atoms certainly assists the trapping of carbon inside the Ni foil (Figure 4.50(c)). This is the reason why the presence of  $\text{Ni}_3\text{C}$  is more obvious for iron nitrate treated Ni foil (blue) compared with the spectra before graphene separation (red) in Figure 4.50. The etching of metallic Ni surface favours the exposure of  $\text{Ni}_3\text{C}$  to the surface.

The fast cooling of Ni is the key step to create the necessary conditions for  $\text{Ni}_3\text{C}$  formation and control the number of layers of the grown graphene. It subsequently facilitates the reuse of the catalyst if the right etchant is used for graphene separation. If the catalyst was cooled down naturally, which took around 6 hours, only multilayer graphene was obtained and we were unable to reuse the catalyst.



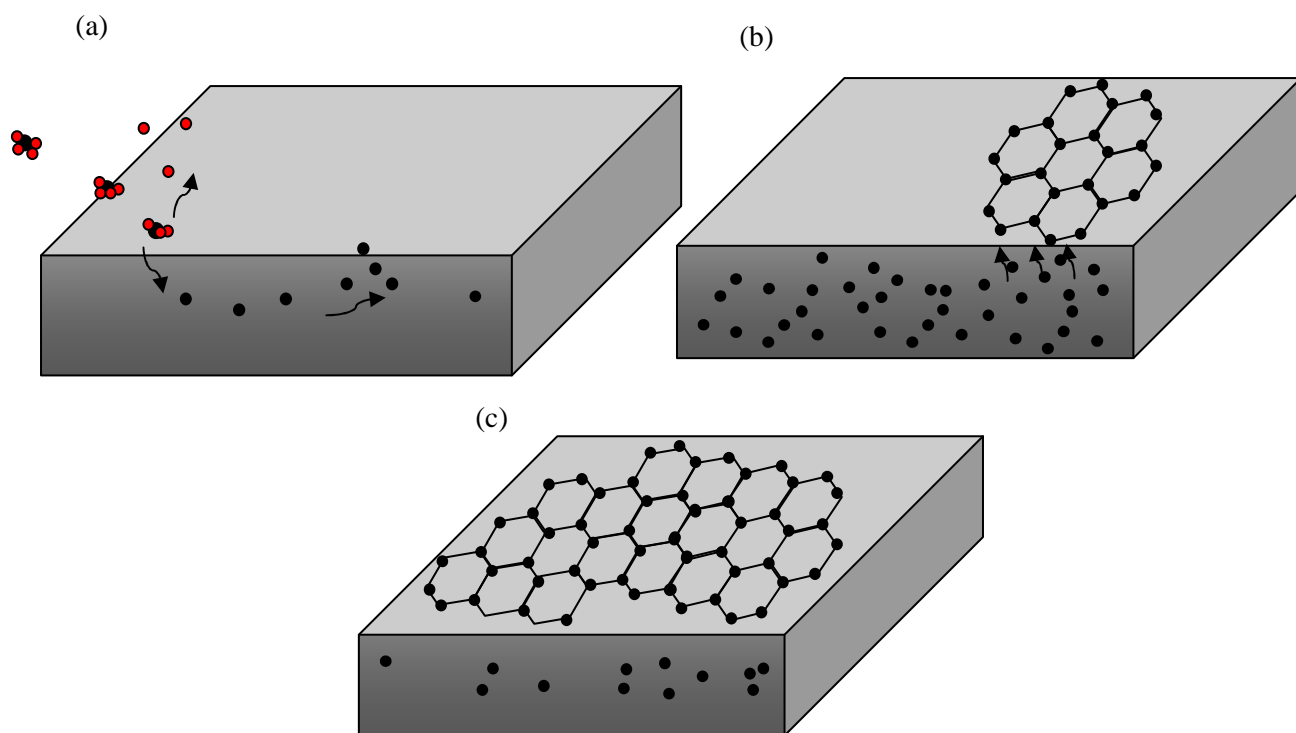


**Figure 4.50** Schematic diagram of graphene and  $\text{Ni}_3\text{C}$  formation. (a) At elevated temperature, methane decomposes at the surface and carbon adatoms dissolve into Ni foil. (b) Graphene formation by segregation of carbon from Ni above a threshold during the cooling process. (c) Very rapid cooling: inhibition of carbon diffusion to the surface of Ni. Red circles indicating hydrogen, meanwhile black circle represent carbon atoms.

## CHAPTER 5

### CONCLUSION AND RECOMMENDATIONS

#### 5.1 Conclusion

Graphene, a thin film of carbon arranged in a  $sp^2$  honeycomb lattice of monoatomic thickness, is one of the popular new materials. It possesses various magnificent properties not shared by other materials, especially for monolayer graphene. However, sophisticated equipment is required to produce monolayer graphene through the CVD process. In this work, a straightforward approach was proposed to grow monolayer graphene. Conventional Cu foil failed to produce monolayer graphene under a wide range of operating conditions either with rapid cooling or natural cooling. Catalytic decomposition of methane was successfully carried out to produce monolayer graphene on a polycrystalline Ni foil with the assist of fast post-CVD cooling. Monolayer graphene with good uniformity and selectivity was grown at 850 °C under methane partial pressure of 0.2 atm (under atmospheric total pressure) for 5 minutes; however multilayer graphene could be observed mainly located at the grain boundary.

Interestingly, by utilizing a bilayer bimetallic catalyst by simply wrapping of a Cu foil over a Ni foil, the supply of carbon adatoms at the Ni/Cu interface could be advantageously controlled. Monolayer graphene could be grown simultaneously at 950 °C under methane partial pressure of 0.2 atm for 5 minutes. Under optimized operating conditions and with the aid of a high-speed cooling, a more uniform monolayer graphene could be grown on both inner surfaces of Ni and Cu under single atmospheric pressure CVD. The graphene grown at the two outer surfaces Ni and Cu had the same characteristics than those that could be obtained either on Ni or Cu under the same operating conditions. The proposed growth mechanism shows that the

gap between the grains within the Ni foil is certainly the main channel to supply a controlled amount of carbon adatoms to the inner surface of Ni. Meanwhile, the contact between Ni and Cu was the pathway for the carbon supply to the Cu surface.

Moreover, the application of rapid cooling was shown to favor the formation of Ni<sub>3</sub>C in the Ni foil. The provoked quenching of graphene segregation process minimizes the number of layers of graphene formed. At the same time, diffusion of the carbon dissolved was inhibited and the carbon atoms remained trapped within the Ni foil which stabilized Ni<sub>3</sub>C. Ni<sub>3</sub>C is commonly known to offer a good protection against corrosion. It was indeed reported for its use as an insulating layer covering Ni in order to inhibit oxidation and other chemical reactions. Ni<sub>3</sub>C plays a major role for both graphene cleanliness and catalyst reuse. The presence of Ni<sub>3</sub>C combined with the use of iron nitrate as soft etchant for the graphene separation process enables to reuse the Ni foil again up to 6 cycles without causing any deviation on the quality and the uniformity of bilayer graphene. Ni<sub>3</sub>C is indeed able to limit the etching effect of the Ni foil. The surface smoothness of the Ni surface is crucial to ensure an efficient separation of the grown graphene. A corrugated surface results in encapsulation of Ni particles on the graphene layers and makes the separation incomplete. However, the reuse of catalyst was only achievable for bilayer graphene grown with high selectivity, attributed to the presence of high amount of Ni<sub>3</sub>C formed. The amount of Ni<sub>3</sub>C formed in Ni foil for the CVD reaction the favored the formation of monolayer graphene was too little to protect the Ni foil. On the other hand, multilayer graphene that strongly interacts with the Ni surface highly reduce the accessibility of the iron nitrate solution.

## 5.2 Recommendations

The following recommendations are proposed to further improve this research work for future studies.

1. A smaller quartz tube reactor is recommended in the future. The reactor is very large compared with the size of the metal foil used for the CVD reaction. Large quartz tube allows longer period for a homogeneous stabilization of the gas composition inside the tube. Moreover, it also requires longer time to purge away the methane after reaction for utterly reaction quenching. Such inconsistency may cause some variations of characteristic and morphology of as-grown graphene while identical operating procedures and conditions are preferred for a control CVD growth.
2. The deposition of graphene film onto silicon wafer was imperfect. During the deposition process, air and moisture are easily trapped between the graphene film and the silicon wafer. The corrugated surface of graphene provides a certain degree of stress and strain to the C-C bonds. The Raman signal mainly comes from the phonon activity of the C-C bonds which probably distort the phonon dispersion of the carbon atoms due to the stress and strain imposed onto the C-C bonds. This is the reason why  $I_{2D}/I_G$  and  $fwhm_{2D}$  obtained from monolayer graphene were distributed in huge range. In future studies, the silicon wafer could be chemically treated to provide a hydrophobic surface that favors the graphene deposition with minimizing the stress or strain of C-C bonds.
3. For reusing and recycling the catalyst, the main loss of Ni came from the polishing process, rather than from the chemical etching for the separation stage.

Both sides of the Ni foil had to be polished to give a smooth surface prior to the CVD reaction. The back side of Ni (facing the etchant during the separation process) was polished as well to remove any remaining graphenic materials. The cleaning of this surface could be replaced with a plasma treatment to prevent the encountered excessive loss. Meanwhile the front surface could be polished with a sand paper of mesh 1200 and above to reduce Ni loss.

4. The actual distribution of carbon adatoms within the Ni foil is still unknown. XRD mapping is recommended in the future in order to better know how  $\text{Ni}_3\text{C}$  is distributed on the Ni surface, especially if its distribution is related to the grain boundary and the middle of grain. Furthermore, a more precise depth profile of Ni foil after CVD could be studied to get a better view of the post-synthesis carbon adatom distribution.
5. Methane was the only carbon source used in the present study. High purity methane is costly and the supply is limited. On the other hand, low cost carbon sources such as natural gas and liquefied petroleum gas are present abundantly in Malaysia. The possibility of replacing high purity carbon source by natural gas or liquefied petroleum gas should be included in the future work.

## REFERENCES

- Adamska, L., Lin, Y., Ross, A. J., Batzill, M. & Oleynik, I. I. (2012) Atomic and electronic structure of simple metal/graphene and complex metal/graphene/metal interfaces. *Physical Review B*, 85, 195443.
- Addou, R., Dahal, A., Sutter, P. & Batzill, M. (2012) Monolayer graphene growth on Ni(111) by low temperature chemical vapor deposition. *Applied Physics Letters*, 100, 021601-3.
- Allen, M. J., Tung, V. C., Gomez, L., Xu, Z., Chen, L. M., Nelson, K. S., Zhou, C., Kaner, R. B. & Yang, Y. (2009a) Soft transfer printing of chemically converted graphene. *Advanced Materials*, 21, 2098-2102.
- Allen, M. J., Tung, V. C. & Kaner, R. B. (2009b) Honeycomb carbon: A review of graphene. *chemical reviews*, 110, 132-145.
- Ambrosi, A. & Pumera, M. (2014) The CVD graphene transfer procedure introduces metallic impurities which alter the graphene electrochemical properties. *Nanoscale*, 6, 472-476.
- Armstrong, H. W. (1982) Decomposing carbide to elemental nickel. US Patent 4,312,896,
- Arnoult, W. J. & McLellan, R. B. (1972) The solubility of carbon in rhodium ruthenium, iridium and rhenium. *Scripta Metallurgica*, 6, 1013-1018.
- Bae, S., Kim, H., Lee, Y., Xu, X., Park, J.-S., Zheng, Y., Balakrishnan, J., Lei, T., RI Kim, H., Si Y. I., Kim, Y.-J., Kim, K. S., Ozyilmaz, B., Al, J.-H., Hong, B. H. & Iijima, S. (2010) Roll-to-roll production of 30-inch graphene films for transparent electrodes. *Nat Nano*, 5, 574-578.
- Batzill, M. (2012) The surface science of graphene: Metal interfaces, CVD synthesis, nanoribbons, chemical modifications, and defects. *Surface Science Reports*, 67, 83-115.
- Berger, C., Song, Z., Li, T., LiI, X., Ogbazghi, A. Y., Feng, R., Dai, Z., Marchenkov, A. N., Conrad, E. H., First, P. N. & De Heer, W. A. (2004) Ultrathin epitaxial graphite: 2D electron gas properties and a route toward graphene-based nanoelectronics. *The Journal of Physical Chemistry B*, 108, 19912-19916.
- Bhavioripudi, S., Jia, X., Dresselhaus, M. S. & Kong, J. (2010) Role of kinetic factors in chemical vapor deposition synthesis of uniform large area graphene using copper catalyst. *Nano Letters*, 10, 4128-4133.
- Bianco, A., Cheng, H.-M., Enoki, T., Gogotsi, Y., Hurt, R. H., Koratkar, N., Kyotani, T., Monthieux, M., Park, C. R., Tascon, J. M. D. & Zhang, J. (2013) All in the graphene family: A recommended nomenclature for two-dimensional carbon materials. *Carbon*, 65, 1-6.

- Biedermann, L. B., Beechem, T. E., Ross, A. J., Ohta, T. & Howell, S. W. (2010) Electrostatic transfer of patterned epitaxial graphene from SiC(0001) to glass. *New Journal of Physics*, 12, 125016.
- Blake, P., Yang, R., Morozov, S. V., Schedin, F., Ponomarenko, L. A., Zhukov, A. A., Nair, R. R., Grigorieva, I. V., Novoselov, K. S. & Geim, A. K. (2009) Influence of metal contacts and charge inhomogeneity on transport properties of graphene near the neutrality point. *Solid State Communications*, 149, 1068-1071.
- Bolotin, K. I., Sikes, K. J., Jiang, Z., Klima, M., Fudenberg, G., Hone, J., Kim, P. & Stormer, H. L. (2008) Ultrahigh electron mobility in suspended graphene. *Solid State Communications*, 146, 351-355.
- Bonsor, K. & Strickland, J. (2011) How nanotechnology works [Online]. [Accessed July 2015]  
Available from World Wide Web  
<http://science.howstuffworks.com/nanotechnology.htm>
- Boukhvalov, D. W. & Katsnelson, M. I. (2009) Destruction of graphene by metal adatoms. *Applied Physics Letters*, 95, 023109-3.
- Brugger, T., Günther, S., Wang, B., Dil, J. H., Bocquet, M.-L., Osterwalder, J., Wintterlin, J. & Greber, T. (2009) Comparison of electronic structure and template function of single-layer graphene and a hexagonal boron nitride nanomesh on Ru(0001). *Physical Review B*, 79, 045407.
- Busse, C., Lazić, P., Djemour, R., Coraux, J., Gerber, T., Atodiresei, N., Caciuc, V., Brako, R., N'diaye, A. T., Bügel, S., Zegenhagen, J. & Michely, T. (2011) Graphene on Ir(111): physisorption with chemical modulation. *Physical Review Letters*, 107, 036101.
- Cai, J., Ruffieux, P., Jaafar, R., Bieri, M., Braun, T., Blankenburg, S., Muoth, M., Seitsonen, A. P., Saleh, M., Feng, X., Mullen, K. & Fasel, R. (2012) Atomically precise bottom-up fabrication of graphene nanoribbons. *Nature*, 466, 470-473.
- Cai, W., Zhu, Y., Li, X., Piner, R. D. & Ruoff, R. S. (2009) Large area few-layer graphene/graphite films as transparent thin conducting electrodes. *Applied Physics Letters*, 95, 123115-3.
- Caldwell, J. D., Anderson, T. J., Culbertson, J. C., Jernigan, G. G., Hobart, K. D., Kub, F. J., Tadjer, M. J., Tedesco, J. L., Hite, J. K., Mastro, M. A., Myers-Ward, R. L., Eddy, C. R., Campbell, P. M. & Gaskill, D. K. (2010) Technique for the dry transfer of epitaxial graphene onto arbitrary substrates. *ACS Nano*, 4, 1108-1114.
- Castro Neto, A. H., Guinea, F., Peres, N. M. R., Novoselov, K. S. & Geim, A. K. (2009) The electronic properties of graphene. *Reviews of Modern Physics*, 81, 109-162.
- Chen, C.-S. & Hsieh, C.-K. (2014) An easy, low-cost method to transfer large-scale graphene onto polyethylene terephthalate as a transparent conductive flexible substrate. *Thin Solid Films*. 50, 595–598

- Chen, H., Zhu, W. & Zhang, Z. (2010) Contrasting behavior of carbon nucleation in the initial stages of graphene epitaxial growth on stepped metal surfaces. *Physical Review Letters*, 104, 186101.
- Chen, J.-H., Jang, C., Xiao, S., Ishigami, M. & Fuhrer, M. S. (2008) Intrinsic and extrinsic performance limits of graphene devices on SiO<sub>2</sub>. *Nat Nano*, 3, 206-209.
- Chen, J. H., Ishigami, M., Jang, C., Hines, D. R., Fuhrer, M. S. & Williams, E. D. (2007) Printed graphene circuits. *Advanced Materials*, 19, 3623-3627.
- Chen, S., Cai, W., Piner, R. D., Suk, J. W., Wu, Y., Ren, Y., Kang, J. & Ruoff, R. S. (2011) Synthesis and characterization of large-area graphene and graphite films on commercial Cu-Ni alloy foils. *Nano Letters*, 11, 3519-3525.
- Chen, X.-D., Liu, Z.-B., Zheng, C.-Y., Xing, F., Yan, X.-Q., Chen, Y. & Tian, J.-G. (2013a) High-quality and efficient transfer of large-area graphene films onto different substrates. *Carbon*, 56, 271-278.
- Chen, Y. P., Yu, Q., Newell, D., Wu, W., Jauregui, L. A., Cao, H., Shen, T. & Chung, T. F. (2013b) Synthetic graphene grown by chemical vapor deposition on copper foils. *International Journal of Modern Physics B*, 27, 1341002.
- Cheng, D., Barcaro, G., Charlier, J.-C., Hou, M. & Fortunelli, A. (2011a) Homogeneous nucleation of graphitic nanostructures from carbon chains on Ni(111). *The Journal of Physical Chemistry C*, 115, 10537-10543.
- Cheng, Z., Zhou, Q., Wang, C., Li, Q., Wang, C. & Fang, Y. (2011b) Toward intrinsic graphene surfaces: A systematic study on thermal annealing and wet-chemical treatment of SiO<sub>2</sub>-supported graphene devices. *Nano Letters*, 11, 767-771.
- Choi, J.-H., Li, Z., Cui, P., Fan, X., Zhang, H., Zeng, C. & Zhang, Z. (2013) Drastic reduction in the growth temperature of graphene on copper via enhanced London dispersion force. *Sci. Rep.*, 3, 1925.
- Choi, J.-Y. (2013) Graphene transfer: A stamp for all substrates. *Nat Nano*, 8, 311-312.
- CIA (2014) The World factbook. [Online] [Accessed January 2016]  
Available from World Wide Web  
<https://www.cia.gov/library/publications/the-world-factbook/rankorder/2253rank.html>
- Coraux, J., N`diaye, A. T., Busse, C. & Michely, T. (2008) Structural coherency of graphene on Ir(111). *Nano Letters*, 8, 565-570.
- Cui, Y., Fu, Q. & Bao, X. (2010) Dynamic observation of layer-by-layer growth and removal of graphene on Ru(0001). *Physical Chemistry Chemical Physics*, 12, 5053-5057.
- Cui, Y., Fu, Q., Zhang, H. & Bao, X. (2011) Formation of identical-size graphene nanoclusters on Ru(0001). *Chemical Communications*, 47, 1470-1472.



- Dahal, A. & Batzill, M. (2014) Graphene-nickel interfaces: a review. *Nanoscale*, 6, 2548-2562.
- De Arco, L. G., Yi, Z., Kumar, A. & Chongwu, Z. (2009) Synthesis, transfer, and devices of single- and few-layer graphene by chemical vapor deposition. *Nanotechnology, IEEE Transactions on*, 8, 135-138.
- Dedkov, Y. S. & Fonin, M. Electronic and magnetic properties of the graphene-ferromagnet interface. *New Journal of Physics*, 12, 125004.
- Delamoreanu, A., Rabot, C., Vallee, C. & Zenasni, A. (2014) Wafer scale catalytic growth of graphene on nickel by solid carbon source. *Carbon*, 66(48-56).
- Drexler, K. A. (1986) Engines of creation: The coming era of nanotechnology New York Knopf Publishing Group
- EIA (2010) International energy outlook 2010, natural gas [Online] [Accessed July 2015] Available from World Wide Web [http://www.eia.doe.gov/oiaf/ieo/nat\\_gas.html#16](http://www.eia.doe.gov/oiaf/ieo/nat_gas.html#16)
- Eizenberg, M. & Blakely, J. M. (1979) Carbon monolayer phase condensation on Ni(111). *Surface Science*, 82, 228-236.
- Eom, D., Prezzi, D., Rim, K. T., Zhou, H., Lefenfeld, M., Xiao, S., Nuckolls, C., Hybertsen, M. S., Heinz, T. F. & Flynn, G. W. (2009) Structure and electronic properties of graphene nanoislands on Co(0001). *Nano Letters*, 9, 2844-2848.
- Fan, L., Li, Z., Li, X., Wang, K., Zhong, M., Wei, J., Wu, D. & Zhu, H. (2011) Controllable growth of shaped graphene domains by atmospheric pressure chemical vapour deposition. *Nanoscale*, 3, 4946-4950.
- Fan, Y., He, K., Tan, H., Speller, S. & Warner, J. (2014) Crack-free growth and transfer of continuous monolayer graphene grown on melted copper. *Chemistry of Materials*, 26, 4984-4991
- Fedorov, A. V., Varykhalov, A. Y., Dobrotvorskii, A. M., Chikina, A. G., Adamchuk, V. K. & Usachov, D. Y. (2011) Structure of graphene on the Ni(110) surface. *Physics of the Solid State*, 53, 1952-1956.
- Freie Universität Berlin, (2015) Focus area nanoscale functional materials (nanoscale) [Online] [Accessed July 2015] Available from World Wide Web <http://www.nanoscale.fu-berlin.de/>
- Ferrari, A. C., Meyer, J. C., Scardacì, V., Casiraghi, C., Lazzeri, M., Mauri, F., Piscanec, S., Jiang, D., Novoselov, K. S., Roth, S. & Geim, A. K. (2006) Raman Spectrum of Graphene and Graphene Layers. *Physical Review Letters*, 97, 187401.

- Feynman, R. (1960) There's plenty room at the bottom. *Engineering and Science Magazine* vol.XXIII, no. 5. California California Institute of Technology
- Forster, P., Ramaswamy, V., Artaxo, P., Berntsen, T., Betts, R., Fahey, D.W., Haywood, J., Lean, J., Lowe, D.C., Myhre, G. and Nganga, J. (2007). Changes in atmospheric constituents and in radiative forcing. Chapter 2. *In Climate Change 2007. The Physical Science Basis.*
- Fujita, T., Kobayashi, W. & Oshima, C. (2005) Novel structures of carbon layers on a Pt(111) surface. *Surface and Interface Analysis*, 37, 120-123.
- Gas Malaysia (2011) Chemical safety data sheet-natural gas [Online] [Accessed July 2015]  
Available from World Wide Web  
[http://www.gasmalaysia.com/docs/datasheet/datasheet\\_ng.pdf](http://www.gasmalaysia.com/docs/datasheet/datasheet_ng.pdf).
- Gamo, Y., Nagashima, A., Wakabayashi, M., Terai, M. & Oshima, C. (1997) Atomic structure of monolayer graphite formed on Ni(111). *Surface Science*, 374, 61-64.
- Gan, X., Zhou, H., Zhu, B., Yu, X., Jia, Y., Sun, B., Zhang, M., Huang, X., Liu, J. & Luo, T. (2012) A simple method to synthesize graphene at 633K by dechlorination of hexachlorobenzene on Cu foils. *Carbon*, 50, 306-310.
- Gao, J., Yip, J., Zhao, J., Yakobson, B. I. & Ding, F. (2011a) Graphene nucleation on transition metal surface: Structure transformation and role of the metal step edge. *Journal of the American Chemical Society*, 133, 5009-5015.
- Gao, J., Yuan, Q., Hu, H., Zhao, J. & Ding, F. (2011b) Formation of carbon clusters in the initial stage of chemical vapor deposition graphene growth on Ni(111) surface. *The Journal of Physical Chemistry C*, 115, 17695-17703.
- Gao, L., Guest, J. R. & Guisinger, N. P. (2010a) Epitaxial graphene on Cu(111). *Nano Letters*, 10, 3512-3516.
- Gao, L., Ren, W., Xu, H., Jin, L., Wang, Z., Ma, T., Ma, L.-P., Zhang, Z., Fu, Q., Peng, L.-M., Bao, X. & Cheng, H.-M. (2012) Repeated growth and bubbling transfer of graphene with millimetre-size single-crystal grains using platinum. *Nat Commun*, 3, 699.
- Gao, L., Ren, W., Zhao, J., Ma, L.-P., Chen, Z. & Cheng, H.-M. (2010b) Efficient growth of high-quality graphene films on Cu foils by ambient pressure chemical vapor deposition. *Applied Physics Letters*, 97, 183109-3.
- Gao, M., Pan, Y., Huang, L., Hu, H., Zhang, L. Z., Guo, H. M., Du, S. X. & Gao, H. J. (2011c) Epitaxial growth and structural property of graphene on Pt(111). *Applied Physics Letters*, 98, 033101-3.
- Gao, T., Xie, S., Gao, Y., Liu, M., Chen, Y., Zhang, Y. & Liu, Z. (2011d) Growth and atomic-scale characterizations of graphene on multifaceted textured Pt foils prepared by chemical vapor deposition. *ACS Nano*, 5, 9194-9201.

- Geim, A. K. & Novoselov, K. S. (2007) The rise of graphene. *Nature Materials*, 6, 183-191.
- Geringer, V., Liebmann, M., Echtermeyer, T., Runte, S., Schmidt, M., Rückamp, R., Lemme, M. C. & Morgenstern, M. (2009) Intrinsic and extrinsic corrugation of monolayer graphene deposited on SiO<sub>2</sub>. *Physical Review Letters*, 102, 076102.
- Geringer, V., Subramaniam, D., Michel, A. K., Szafranek, B., Schall, D., Georgi, A., Mashoff, T., Neumaier, D., Liebmann, M. & Morgenstern, M. (2010) Electrical transport and low-temperature scanning tunneling microscopy of microsoldered graphene. *Applied Physics Letters*, 96, 082114-3.
- Giovannetti, G., Khomyakov, P. A., Brocks, G., Karpan, V. M., Van Den Brink, J. & Kelly, P. J. (2008) Doping graphene with metal contacts. *Physical Review Letters*, 101, 026803.
- Gong, C., Floresca, H. C., Hinojos, D., McDonnell, S., Qin, X., Hao, Y., Jandhyala, S., Mordi, G., Kim, J., Colombo, L., Ruoff, R. S., Kim, M. J., Cho, K., Wallace, R. M. & Chabal, Y. J. (2013) Rapid selective etching of PMMA residues from transferred graphene by carbon dioxide. *The Journal of Physical Chemistry C*, 117, 23000-23008.
- Gong, C., Lee, G., Shan, B., Vogel, E. M., Wallace, R. M. & Cho, K. (2010) First-principles study of metal-graphene interfaces. *Journal of Applied Physics*, 108, 123711-8.
- Gorantla, S., Bachmatiuk, A., Hwang, J., Alsalman, H. A., Kwak, J. Y., Seyller, T., Eckert, J., Spencer, M. G. & Rummeli, M. H. (2014) A universal transfer route for graphene. *Nanoscale*, 6, 889-896.
- Grüneis, A., Kummer, K. & Vyalikh, D. V. (2009) Dynamics of graphene growth on a metal surface: A time-dependent photoemission study. *New Journal of Physics*, 11.
- Guermoune, A., Chari, T., Popescu, F., Sabri, S. S., Guillemette, J., Skulason, H. S., Szkopek, T. & Sijaj, M. (2011) Chemical vapor deposition synthesis of graphene on copper with methanol, ethanol, and propanol precursors. *Carbon*, 49, 4204-4210.
- Güneş, F., Shin, H.-J., Biswas, C., Han, G. H., Kim, E. S., Chae, S. J., Choi, J.-Y. & Lee, Y. H. (2010) Layer-by-layer doping of few-layer graphene film. *ACS Nano*, 4, 4595-4600.
- Gupta, P., Dongare, P., Grover, S., Dubey, S., Mamgain, H., Bhattacharya, A. & Deshmukh, M. (2014) A facile process for soak-and-peel delamination of CVD graphene from substrates using water. *Sci Rep.*4. *Scientific Reports*, 4, 3882.
- Han, G., Shin, H.-J., Kim, E., Chae, S., Choi, J.-Y. & Lee, Y. (2011) Poly(ethylene co-vinyl acetate)-assisted one-step transfer of ultra large graphene. *Nano*, 6, 59-65.

- Han, Y., Zhang, L., Zhang, X., Ruan, K., Cui, L., Wang, Y., Liao, L., Wang, Z. & Jie, J. (2014) Clean surface transfer of graphene films via an effective sandwich method for organic light-emitting diode applications. *Journal of Materials Chemistry C*, 2, 201-207.
- Hass, J., Varchon, F., Millán-Otoya, J. E., Sprinkle, M., Sharma, N., De Heer, W. A., Berger, C., First, P. N., Magaud, L. & Conrad, E. H. (2008) Why multilayer graphene on 4H-SiC(0001) behaves like a single sheet of graphene. *Physical Review Letters*, 100, 125504.
- Hasz, W. C., Thompson, A. M. & Borom, M. P. (2002) Method of providing wear-resistant coatings, and related articles. US Patent 6,302,318, 2001.
- Her, M., Beams, R. & Novotny, L. (2013) Graphene transfer with reduced residue. *Physics Letters A*, 377, 1455-1458.
- Hernandez, Y., Nicolosi, V., Lotya, M., Blighe, F. M., Sun, Z., De, S., McGovern, I. T., Holland, B., Byrne, M., Gun'ko, Y. K., Boland, J. J., Niraj, P., Duesberg, G., Krishnamurthy, S., Goodhue, R., Hutchison, J., Scardaci, V., Ferrari, A. C. & Coleman, J. N. (2008) High-yield production of graphene by liquid-phase exfoliation of graphite. *Nat Nano*, 3, 563-568.
- Hesjedal, T. (2011) Continuous roll-to-roll growth of graphene films by chemical vapor deposition. *Applied Physics Letters*, 98, 133106-3.
- Hu, B., Ago, H., Ito, Y., Kawahara, K., Tsuji, M., Magome, E., Sumitani, K., Mizuta, N., Ikeda, K.-I. & Mizuno, S. (2012a) Epitaxial growth of large-area single-layer graphene over Cu(111)/sapphire by atmospheric pressure CVD. *Carbon*, 50, 57-65.
- Hu, B., Ago, H., Orofeo, C. M., Ogawa, Y. & Tsuji, M. (2012b) On the nucleation of graphene by chemical vapor deposition. *New Journal of Chemistry*, 36, 73-77.
- Hu, S., Guan, Y., Wang, Y. & Han, H. (2011) Nano-magnetic catalyst KF/CaO-Fe<sub>3</sub>O<sub>4</sub> for biodiesel production. *Applied Energy*, 88, 2685-2690.
- Hummers, W. S. & Offeman, R. E. (1958) Preparation of graphitic oxide. *Journal of the American Chemical Society*, 80, 1339-1339.
- Hwang, C., Yoo, K., Kim, S. J., Seo, E. K., Yu, H. & Biró, L. P. (2011) Initial stage of graphene growth on a Cu substrate. *The Journal of Physical Chemistry C*, 115, 22369-22374.
- Iijima, S. (1991) Helical microtubules of graphitic carbon. *Nature*, 354, 56-58.
- IPCC (2007) Fourth Assessment Report: Climate Change 2007 [Online] [Accessed January 2016]  
Available from World Wide Web  
[https://www.ipcc.ch/publications\\_and\\_data/ar4/wg1/en/ch2s2-10-2.html](https://www.ipcc.ch/publications_and_data/ar4/wg1/en/ch2s2-10-2.html)
- Ishigami, M., Chen, J. H., Cullen, W. G., Fuhrer, M. S. & Williams, E. D. (2007) atomic structure of graphene on SiO<sub>2</sub>. *Nano Letters*, 7, 1643-1648.

- Ishihara, M., Koga, Y., Kim, J., Tsugawa, K. & Hasegawa, M. (2011) Direct evidence of advantage of Cu(111) for graphene synthesis by using Raman mapping and electron backscatter diffraction. *Materials Letters*, 65, 2864-2867.
- Iwasaki, T., Park, H. J., Konuma, M., Lee, D. S., Smet, J. H. & Starke, U. (2011) Long-range ordered single-crystal graphene on high-quality heteroepitaxial Ni thin films grown on MgO(111). *Nano Letters*, 11, 79-84.
- Jacobson, P., Stöger, B., Garhofer, A., Parkinson, G. S., Schmid, M., Caudillo, R., Mittendorfer, F., Redinger, J. & Diebold, U. (2012a) Disorder and defect healing in graphene on Ni(111). *The Journal of Physical Chemistry Letters*, 3, 136-139.
- Jacobson, P., Stöger, B., Garhofer, A., Parkinson, G. S., Schmid, M., Caudillo, R., Mittendorfer, F., Redinger, J. & Diebold, U. (2012b) Nickel carbide as a source of grain rotation in epitaxial graphene. *ACS Nano*, 6, 3564-3572.
- Jeon, I., Yang, H., Lee, S.-H., Heo, J., Seo, D. H., Shin, J., Chung, U. I., Kim, Z. G., Chung, H.-J. & Seo, S. (2011) Passivation of metal surface states: microscopic origin for uniform monolayer graphene by low temperature chemical vapor deposition. *ACS Nano*, 5, 1915-1920.
- Jeong, H. J., Kim, H. Y., Jeong, S. Y., Han, J. T., Baeg, K.-J., Hwang, J. Y. & Lee, G.-W. (2014) Improved transfer of chemical-vapor-deposited graphene through modification of intermolecular interactions and solubility of poly(methylmethacrylate) layers. *Carbon*, 66, 612-618.
- Ji, H., Hao, Y., Ren, Y., Charlton, M., Lee, W. H., Wu, Q., Li, H., Zhu, Y., Wu, Y., Piner, R. & Ruoff, R. S. (2011) Graphene growth using a solid carbon feedstock and hydrogen. *ACS Nano*, 5, 7656-7661.
- Jiang, J. (2009), SingNano – Singapore nanotechnology network newsletter [Online], [Accessed July 2015]  
Available from World Wide Web  
[http://www.nano-globe.biz/SingNano/SingNano\\_newsletter4.pdf](http://www.nano-globe.biz/SingNano/SingNano_newsletter4.pdf)
- Jiao, L., Fan, B., Xian, X., Wu, Z., Zhang, J. & Liu, Z. (2008) Creation of nanostructures with poly(methyl methacrylate)-mediated nanotransfer printing. *Journal of the American Chemical Society*, 130, 12612-12613.
- Jobst, J., Waldmann, D., Speck, F., Hirner, R., Maude, D. K., Seyller, T. & Weber, H. B. (2010) Quantum oscillations and quantum Hall effect in epitaxial graphene. *Physical Review B*, 81, 195434.
- Jung, W., Kim, D., Lee, M., Kim, S., Kim, J.-H. & Han, C.-S. (2014) Ultraconformal Contact Transfer of Monolayer Graphene on Metal to Various Substrates. *Advanced Materials*, 26, 6394-6400
- Kalbac, M., Frank, O. & Kavan, L. (2012) The control of graphene double-layer formation in copper-catalyzed chemical vapor deposition. *Carbon*, 50, 3682-3687.

- Kalita, G., Wakita, K. & Umeno, M. (2012) Low temperature growth of graphene film by microwave assisted surface wave plasma CVD for transparent electrode application. *RSC Advances*, 2, 2815-2820.
- Kang, B. J., Mun, J. H., Hwang, C. Y. & Cho, B. J. (2009) Monolayer graphene growth on sputtered thin film platinum. *Journal of Applied Physics*, 106, 104309-6.
- Kang, J., Hwang, S., Kim, J. H., Kim M. H., Ryu J., Seo, S. J., Hong, B. H., Kim, M. K. & Choi, J.-B. (2012) Efficient transfer of large-area graphene films onto rigid substrates by hot pressing. *ACS Nano*, 6, 5360-5365.
- Karoui, S., Amara, H., Bichara, C. & Ducastelle, F. (2010) Nickel-assisted healing of defective graphene. *ACS Nano*, 4, 6114-6120.
- Khasha, G (2015) Graphene, 2D Materials and Carbon Nanotubes: Markets, Technologies and Opportunities 2015-2025 [online][Accessed December 2015] Available from World Wide Web  
<http://www.idtechex.com/research/reports/graphene-2d-materials-and-carbon-nanotubes-markets-technologies-and-opportunities-2015-2025-000440.asp>
- Kim, C., Woo, J. Y., Choi, J., Park, J. & Han, C.-S. (2012a) Direct transfer of graphene without the removal of a metal substrate using a liquid polymer. *Scripta Materialia*, 66, 535-537.
- Kim, H., Mattevi, C., Calvo, M. R., Oberg, J. C., Artiglia, L., Agnoli, S., Hirjibehedin, C. F., Chhowalla, M. & SAIZ, E. (2012b) Activation energy paths for graphene nucleation and growth on Cu. *ACS Nano*, 6, 3614-3623.
- Kim, H. H., Chung, Y., Lee E., Lee, S. & Cho, K. (2014) Water-free transfer method for CVD-grown graphene and its application to flexible air-stable graphene transistors. *Advanced Materials*, 26, 3213-3217.
- Kim, J., Park, H., Hannon, J. B., Bedell, S. W., Fogel, K., Sadana, D. K. & Dimitrakopoulos, C. (2013a) Layer-resolved graphene transfer via engineered strain layers. *Science*, 342, 833-836.
- Kim K. S., Zhao, Y., Jang, H., Lee, S. Y., Kim, J. M., Kim, K. S., Ahn, J.-H., Kim, P., Choi, J.-Y. & Hong, B. H. (2009) Large-scale pattern growth of graphene films for stretchable transparent electrodes. *Nature*, 457, 706-710.
- Kim M., An, H., Lee W.-J. & Jung, J. (2013b) Low damage-transfer of graphene using epoxy bonding. *Electronic Materials Letters*, 9, 517-521.
- Kim, Y. J., Kim, S. J., Jung, M. H., Choi, K. Y., Bae, S., Lee, S. K., Lee, Y., Shin, D., Lee, B., Shin, H., Choi, M., Park, K., Ahn, J. H. & Hong, B. H. (2012c) Low-temperature growth and direct transfer of graphene-graphitic carbon films on flexible plastic substrates. *Nanotechnology*, 23.
- Kishi, N., Fukaya, A., Sugita, R., Kado, T., Soga, T. & Jimbo, T. (2012) Synthesis of graphenes on Ni foils by chemical vapor deposition of alcohol with IR-lamp heating. *Materials Letters*, 79, 21-24.

- Kroto, H.W., Heath, J.R., O'Brien, S.C., Curl, R.F. & Smalley, R.E. (1985) C<sub>60</sub>: Buckminsterfullerene. *Nature*, 318, 162 - 163.
- Kumar, A., Voevodin, A. A., Zemlyanov, D., Zakharov, D. N. & Fisher, T. S. (2012) Rapid synthesis of few-layer graphene over Cu foil. *Carbon*, 50, 1546-1553.
- Lacovig, P., Pozzo, M., Alfè, D., Vilmercati, P., Baraldi, A. & Lizzit, S. (2009) Growth of dome-shaped carbon nanoislands on Ir(111): The intermediate between carbidic clusters and quasi-free-standing graphene. *Physical Review Letters*, 103, 166101.
- Lahiri, J., Miller, T., Adamska, L., Oleynik, I. I. & Batzill, M. (2011a) Graphene growth on Ni(111) by transformation of a surface carbide. *Nano Letters*, 11, 518-522.
- Lahiri, J., Miller, T. S., Ross, A. J., Adamska, L., Oleynik, I. I. & Batzill, M. (2011b) Graphene growth and stability at nickel surfaces. *New Journal of Physics*, 13.
- Land, T. A., Michely, T., Behm, R. J., Hemminger, J. C. & Comsa, G. (1992) STM investigation of single layer graphite structures produced on Pt(111) by hydrocarbon decomposition. *Surface Science*, 264, 261-270.
- Lavan, D. A., McGuire, T. & Langer, R. (2003) Small-scale systems for in vivo drug delivery. *Nature biotechnology*, 21, 1184-1191.
- Lee, C., Wei, X., Kysar, J. W. & Hone, J. (2008) Measurement of lene. *Science*, 321, 385-388.
- Lee J., Kim, Y., Shin, H.-J., Lee, C., Lee, D., Lee, S., Moon, C.-Y., Lee, S. U., Kim, S. J., Ji, J. H., Yoon, H. S. & Jun, S. C. (2014) Crack-release transfer method of wafer-scale grown graphene onto large-area substrates. *ACS Applied Materials & Interfaces*, 6, 12588-9.
- Lee, J., Kim, Y., Shin, H.-J., Lee, C., Lee, D., Moon, C.-Y., Lim, J. & Chan Jun, S. (2013) Clean transfer of graphene and its effect on contact resistance. *Applied Physics Letters*, 103, -.
- Lee, J. H., Shin, D. W., Makotchenko, V. G., Nazarov, A. S., Fedorov, V. E., Kim, Y. H., Choi, J.-Y., Kim, J. M. & Yoo, J.-B. (2009) One-step exfoliation synthesis of easily soluble graphite and transparent conducting graphene sheets. *Advanced Materials*, 21, 4383-4387.
- Lee, S., Lee, K. & Zhong, Z. (2010a) Wafer scale homogeneous bilayer graphene films by chemical vapor deposition. *Nano Letters*, 10, 4702-4707.
- Lee, W. H., Suk, J. W., Lee, J., Hao, Y., Park, J., Yang, J. W., Ha, H.-W., Murali, S., Chou, H., Akinwande, D., Kim, K. S. & Ruoff, R. S. (2012) Simultaneous transfer and doping of cvd-grown graphene by fluoropolymer for transparent conductive films on plastic. *ACS Nano*, 6, 1284-1290.

- Lee, Y.-H. & Lee, J.-H. (2010) Scalable growth of free-standing graphene wafers with copper(Cu) catalyst on SiO<sub>2</sub>/Si substrate: Thermal conductivity of the wafers. *Applied Physics Letters*, 96, 083101-3.
- Lee, Y., Bae, S., Jang, H., Jang, S., Zhu, S.-E., Sim, S. H., Song, Y. I., Hong B. H. & Ahn, J.-H. (2010b) Wafer-scale synthesis and transfer of graphene films. *Nano Letters*, 10, 490-493.
- Levchenko, I., Volotskova, O., Shashurin, A., Raitses, Y., Ostrikov, K. & Keidar, M. (2010) The large-scale production of graphene flakes using magnetically-enhanced arc discharge between carbon electrodes. *Carbon*, 48, 4570-4574.
- Levendorf, M. P., Ruiz-VargaS, C. S., Garg, S. & PArk, J. (2009) Transfer-free batch fabrication of single layer graphene transistors. *Nano Letters*, 9, 4479-4483.
- Li, H., Wu, J., Huang, X., Yin, Z., Liu, J. & Zhang, H. (2014) A universal, rapid method for clean transfer of nanostructures onto various substrates. *ACS Nano*.8(7):6563-70., 8, 6563-70.
- Li, X., Cai, W., An, J., Kim, S., Nah, J., Yang, D., Piner, R., Velamakanni, A., Jung, I., Tutuc, E., Banerjee, S. K., Colombo, L. & Ruoff, R. S. (2009a) Large-area synthesis of high-quality and uniform graphene films on copper foils. *Science*, 324, 1312-1314.
- Li, X., Cai, W., Colombo, L. & Ruoff, R. S. (2009b) Evolution of graphene growth on ni and cu by carbon isotope labeling. *Nano Letters*, 9, 4268-4272.
- Li, X., Magnuson, C. W., Venugopal, A., An, J., Suk, J. W., Han, B., Borysiak, M., Cai, W., Velamakanni, A., Zhu, Y., Fu, L., Vogel, E. M., Voelkl, E., Colombo, L. & Ruoff, R. S. (2010) Graphene films with large domain size by a two-step chemical vapor deposition process. *Nano Letters*, 10, 4328-4334.
- Li, X., Magnuson, C. W., Venugopal, A., Tromp, R. M., Hannon, J. B., Vogel, E. M., Colombo, L. & Ruoff, R. S. (2011a) Large-area graphene single crystals grown by low-pressure chemical vapor deposition of methane on copper. *Journal of the American Chemical Society*, 133, 2816-2819.
- Li, X., Zhu, Y., Cai, W., Borysiak, M., Han, B., Chen, D., Piner, R. D., Cl, L. & Ruoff, R. S. (2009c) Transfer of large-area graphene films for high-performance transparent conductive electrodes. *Nano Letters*, 9, 4359-4363.
- Li, Z., Wu, P., Wang, C., Fan, X., Zhang, W., Zhai, X., Zeng, C., Li, Z., Yang, J. & Hou, J. (2011b) Low-temperature growth of graphene by chemical vapor deposition using solid and liquid carbon sources. *ACS Nano*, 5, 3385-3390.
- Liang, X., Chang, A. S. P., Zhang, Y., Harteneck, B. D., Choo, H., Olynick, D. L. & Cabrini, S. (2009) Electrostatic force assisted exfoliation of prepatterned few-layer graphenes into device sites. *Nano Letters*, 9, 467-472.
- Liang, X., Sperling, B. A., Calizo, I., Cheng, G., Hacker, C. A., Zhang, Q., Obeng, Y., Yan, K., Peng, H., Li, Q., Zhu, X., Yuan, H., Hight walker, A. R., Liu, Z., Peng,



- L.-M. & Richter, C. A. (2011) Toward clean and crackless transfer of graphene. *ACS Nano*, 5, 9144-9153.
- Liang, Y. T. & Hersam, M. C. (2010) Highly Concentrated graphene solutions via polymer enhanced solvent exfoliation and iterative solvent exchange. *Journal of the American Chemical Society*, 132, 17661-17663.
- Liao, C.-D., Lu, Y.-Y., Tamalampudi, S. R., Cheng, H.-C. & Chen, Y.-T. (2013) Chemical vapor deposition synthesis and raman spectroscopic characterization of large-area graphene sheets. *The Journal of Physical Chemistry A*, 117, 9454-9461.
- Lin, W.-H., Chen, T.-H., Chang, J.-K., Taur, J.-I., Lo, Y.-Y. & Lee, W.-L. (2014) A Direct and polymer-free method for transferring graphene grown by chemical vapor deposition to any substrate. *ACS Nano*, 8, 1784-91.
- Lin, Y.-C., Jin, C., Lee, J.-C., Jen, S.-F., Suenaga, K. & Chiu, P.-W. (2011) Clean transfer of graphene for isolation and suspension. *ACS Nano*, 5, 2362-2368.
- Lin, Y.-C., Lu C.-C., Yeh, C.-H., Jin, C., Suenaga, K. & Chiu, P.-W. (2012) Graphene annealing: How clean can it be? *Nano Letters*, 12, 414-419.
- Lin, Y.-M., Jenkins, K. A., Valdes-Garcia, A., Small, J. P., Farmer, D. B. & Avouris, P. (2008) Operation of graphene transistors at gigahertz frequencies. *Nano Letters*, 9, 422-426.
- Liu, N., Fu, L., Dai, B., Yan, K., Liu, X., Zhao, R., Zhang, Y. & Liu, Z. (2011a) Universal segregation growth approach to wafer-size graphene from non-noble metals. *Nano Letters*, 11, 297-303.
- Liu, N., Pan, Z., Fu, L., Zhang, C., Dai, B. & Liu, Z. (2011b) The origin of wrinkles on transferred graphene. *Nano Research*, 4, 996-1004.
- Liu, W., Li, H., Xu, C., KhatamI, Y. & Banerjee, K. (2011c) Synthesis of high-quality monolayer and bilayer graphene on copper using chemical vapor deposition. *Carbon*, 49, 4122-4130.
- Liu, X., Fi, L., Liu, N., Gao, T., Zhang, Y., Liao, L. & Liu, Z. (2011d) Segregation growth of graphene on Cu-Ni alloy for precise layer control. *The Journal of Physical Chemistry C*, 115, 11976-11982.
- Liu, X., Wang, C. Z., Yao, Y. X., Lu, W. C., Hupalo, M., Tringides, M. C. & Ho, K. M. (2011e) Bonding and charge transfer by metal adatom adsorption on graphene. *Physical Review B*, 83, 235411.
- Loginova, E., Bartelt, N. C., Feibelman, P. J. & McCarty, K. F. (2008) Evidence for graphene growth by C cluster attachment. *New Journal of Physics*, 10.
- Loginova, E., Bartelt, N. C., Feibelman, P. J. & McCarty, K. F. (2009a) Factors influencing graphene growth on metal surfaces. *New Journal of Physics*, 11.

- Loginova, E., Bartelt, N. C., Feibelman, P. J. & McCarty, K. F. (2009b) Defects of graphene on Ir(111): Rotational domains and ridges. *Physical Review B*, 80, 085430.
- López, G. A. & Mittemeijer, E. J. (2004) The solubility of C in solid Cu. *Scripta Materialia*, 51, 1-5.
- Losurdo, M., Giangregorio, M. M., Capezzuto, P. & Bruno, G. (2011) Graphene CVD growth on copper and nickel: role of hydrogen in kinetics and structure. *Physical Chemistry Chemical Physics*, 13, 20836-20843.
- Luo, Z., Kim, S., Kawamoto, N., Rappe, A. M. & Johnson, A. T. C. (2011) Growth mechanism of hexagonal-shape graphene flakes with zigzag edges. *ACS Nano*, 5, 9154-9160.
- Martins, L., Song, Y., Zeng, T., Dresselhaus, M., Kong, J. & Araujo, P. (2013.) Direct transfer of graphene onto flexible substrates. *Proceedings of the National Academy of Sciences*.
- Mattevi, C., Kim, H. & Chhowalla, M. (2011) A review of chemical vapour deposition of graphene on copper. *Journal of Materials Chemistry*, 21, 3324-3334.
- McAllister, M. J., Li, J.-L., Adamson, D. H., Schniepp, H. C., Abdala, A. A., Liu, J., Herrera-Alonso, M., Milius, D. L., Car, R., Prud'homme, R. K. & Aksay, I. A. (2007) Single sheet functionalized graphene by oxidation and thermal expansion of graphite. *Chemistry of Materials*, 19, 4396-4404.
- Memon, N. K., Kear, B. H. & Tse, S. D. (2013a) Transition between graphene-film and carbon-nanotube growth on Nickel alloys in open-atmosphere flame synthesis. *Chemical Physics Letters*, 570, 90-94.
- Memon, N. K., Tse, S. D., Chhowalla, M. & Kear, B. H. (2013b) Role of substrate, temperature, and hydrogen on the flame synthesis of graphene films. *Proceedings of the Combustion Institute*, 34, 2163-2170.
- Meng, L., Sun, Q., Wang, J. & Ding, F. (2012) Molecular dynamics simulation of chemical vapor deposition graphene growth on Ni (111) surface. *The Journal of Physical Chemistry C*, 116, 6097-6102.
- Merino, P., Švec, M., Pinaridi, A. L., Otero, G. & Martín-Gago, J. A. (2011) Strain-driven moiré superstructures of epitaxial graphene on transition metal surfaces. *ACS Nano*, 5, 5627-5634.
- Meyer, J. C., Girit, C. O., Crommie, M. F. & Zettl, A. (2008) Hydrocarbon lithography on graphene membranes. *Applied Physics Letters*, 92, 123110-3.
- Mittendorfer, F., Garhofer, A., Redinger, J., Klimeš, J., Harl, J. & Kresse, G. (2011) Graphene on Ni(111): Strong interaction and weak adsorption. *Physical Review B*, 84, 201401.

- Morozov, S. V., Novoselov, K. S., Schedin, F., Jiang, D., Firsov, A. A. & Geim, A. K. (2005) Two-dimensional electron and hole gases at the surface of graphite. *Physical Review B*, 72, 201401.
- Murata, Y., Petrova, V., Kappes, B. B., Ebnonnasir, A., Petrov, I., Xie, Y.-H., Ciobanu, C. V. & Kodambaka, S. (2010) Moiré Superstructures of graphene on faceted nickel islands. *ACS Nano*, 4, 6509-6514.
- N'diaye, A. T., Bleikamp, S., Feibelman, P. J. & Michely, T. (2006) Two-dimensional Ir Cluster lattice on a graphene moiré on Ir(111). *Physical Review Letters*, 97, 215501.
- N'diaye, A. T., Coraux, J., Plasa, T. N., Busse, C. & Michely, T. (2008) Structure of epitaxial graphene on Ir(111). *New Journal of Physics*, 10.
- Nandamuri, G., Roumimov, S. & Solanki, R. (2011) Chemical vapor deposition of graphene films *Nanotechnology*, 21, 145604.
- Nie, S., Walter, A. L., Bartelt, N. C., Starodub, E., Bostwick, A., Rotenberg, E. & McCarty, K. F. (2011a) Growth from below: Graphene bilayers on Ir(111). *ACS Nano*, 5, 2298-2306.
- Nie, S., Wofford, J. M., Bartelt, N. C., Dubon, O. D. & McCarty, K. F. (2011b) Origin of the mosaicity in graphene grown on Cu(111). *Physical Review B*, 84, 155425.
- Nilsson, L., Andersen, M., Bjerre, J., Balog, R., Hammer, B., Hornekær, L. & Stensgaard, I. (2012) Preservation of the Pt(100) surface reconstruction after growth of a continuous layer of graphene. *Surface Science*, 606, 464-469.
- Novoselov, K. S., Geim, A. K., Morozov, S. V., Jiang, D., Katsnelson, M. I., Grigorieva, I. V., Dubonos, S. V. & Firsov, A. A. (2005) Two-dimensional gas of massless Dirac fermions in graphene. *Nature*, 438, 197-200.
- Novoselov, K. S., Geim, A. K., Morozov, S. V., Jiang, D., Zhang, Y., Dubonos, S. V., Grigorieva, I. V. & Firsov, A. A. (2004) Electric field effect in atomically thin carbon films. *Science*, 306, 666-669.
- Novoselov, K. S., Morozov, S. V., Mohinddin, T. M. G., Ponomarenko, L. A., Elias, D. C., Yang, R., Barbolina, I. I., Blake, P., Booth, t. J., Jiang, D., Giesbers, J., Hill, E. W. & Geim, A. K. (2007) Electronic properties of graphene. *physica status solidi (b)*, 244, 4106-4111.
- Obraztsov, A. N., Obraztsova, E. A., Tyurnina, A. V. & Zolotukhin, A. A. (2007) Chemical vapor deposition of thin graphite films of nanometer thickness. *Carbon*, 45, 2017-2021.
- Odahara, G., Hibino, H., Nakayama, N., Shimbata, T., Oshima, C., Otani, S., Suzuki, M., Yasue, T. & Koshikawa, T. (2012) Macroscopic single-domain graphene growth on polycrystalline nickel surface. *Applied Physics Express*, 5.

- Odahara, G., Otani, S., Oshima, C., Suzuki, M., Yasue, T. & Koshikawa, T. (2011) Macroscopic single-domain graphene sheet on Ni(111). *Surface and Interface Analysis*, 43, 1491-1493.
- Ogawa, Y., Hu, B., Orofeo, C. M., Tsuji, M., Ikeda, K.-I., Mizuno, S., Hibino, H. & Ago, H. (2012) Domain structure and boundary in single-layer graphene grown on Cu(111) and Cu(100) films. *The Journal of Physical Chemistry Letters*, 3, 219-226.
- Oganov, A.R., Hemley, R. Hanzen, R.M., & Jones, A.P. (2013) Structure, bonding, and mineralogy of carbon at extreme conditions. *Review Minerals Geochemistry*, 75, 47-77.
- Ohta, T., Bostwick, A., Seyller, T., Horn, K. & Rotenberg, E. (2006) Controlling the Electronic Structure of Bilayer Graphene. *Science*, 313, 951-954.
- Panagiotopoulos, N. T., Diamanti, E. K., Koutsokeras, L. E., Baikousi, M., Kordatos, E., Matikas, T. E., Gournis, D. & Patsalas, P. (2012) Nanocomposite catalysts producing durable, super-black carbon nanotube systems: Applications in solar thermal harvesting. *ACS Nano*, 6, 10475-10485.
- Panchal, V., Cedergren, K., Yakimova, R., Tzalenchuk, A., Kubatkin, S. & Kazakova, O. (2012) Small epitaxial graphene devices for magnetosensing applications. *Journal of Applied Physics*, 111, 07E509-3.
- Pantelic, R. S., Suk, J. W., Magnuson, C. W., Meyer, J. C., Wachsmuth, P., Kaiser, U., Ruoff, R. S. & Stahlberg, H. (2011) Graphene: Substrate preparation and introduction. *Journal of Structural Biology*, 174, 234-238.
- Park, H. J., Meyer, J., Roth, S. & Skákalová, V. (2010) Growth and properties of few-layer graphene prepared by chemical vapor deposition. *Carbon*, 48, 1088-1094.
- Park, J.-H., Jung, W., Cho, D., Seo, J.-T., Moon, Y., Woo, S. H., Lee, C., Park, C.-Y. & Ahn, J. R. (2013) Simple, green, and clean removal of a poly(methyl methacrylate) film on chemical vapor deposited graphene. *Applied Physics Letters*, 103, -.
- Pei, S. & Cheng, H.-M. (2012) The reduction of graphene oxide. *Carbon*, 50, 3210-3228
- Peng, Z., Somodi, F., Helveg, S., Kisielowski, C., Specht, P. & Bell, A. T. (2012a) High-resolution in situ and ex situ TEM studies on graphene formation and growth on Pt nanoparticles. *Journal of Catalysis*, 286, 22-29.
- Peng, Z., Yan, Z., Sun, Z. & Tour, J. M. (2012b) Direct growth of bilayer graphene on SiO<sub>2</sub> substrates by carbon diffusion through nickel. *ACS Nano*, 5, 8241-8247.
- Petrone, N., Dean, C. R., Meric, I., Van Der Zande, A. M., Huang, P. Y., Wang, L., Muller, D., Shepard, K. L. & Hone, J. Chemical vapor deposition-derived graphene with electrical performance of exfoliated graphene. *Nano Letters*, 12, 2751-2756.

- Pettes, M. T., Jo, I., Yao, Z. & Shi, L. (2011) Influence of polymeric residue on the thermal conductivity of suspended bilayer graphene. *Nano Letters*, 11, 1195-1200.
- Pirchler, T. (2011) Unraveling electron chirality in graphene. *Physics* 4, 9.
- Pletikosić, I., Kralj, M., Pervan, P., Brako, R., Coraux, J., N'diaye, A. T., Busse, C. & Michely, T. (2009) Dirac cones and minigaps for graphene on Ir(111). *Physical Review Letters*, 102, 056808.
- Politano, A., Marino, A. R. & Chiarello, G. (2012) Phonon dispersion of quasi-freestanding graphene on Pt(111). *Journal of Physics: Condensed Matter*, 24, 104025.
- Power, S. R. & Ferreira, M. S. (2011) Electronic structure of graphene beyond the linear dispersion regime. *Physical Review B*, 83, 155432.
- Preobrajenski, A. B., Ng, M. L., Vinogradov, A. S. & Mårtensson, N. (2008) Controlling graphene corrugation on lattice-mismatched substrates. *Physical Review B*, 78, 073401.
- Qi, J. L., Zheng, W. T., Zheng, X. H., Wang, X. & Tian, H. W. (2011) Relatively low temperature synthesis of graphene by radio frequency plasma enhanced chemical vapor deposition. *Applied Surface Science*, 257, 6531-6534.
- Radhakrishnan, G., Adams, P. M., Stapleton, A. D., Muller, H. G. & Foran, B. J. (2011) Large single-crystal monolayer graphene by decomposition of methanol. *Applied Physics A: Materials Science and Processing*, 105, 31-37.
- Rasool, H. I., Song, E. B., Allen, M. J., Wassei, J. K., Kaner, R. B., Wang, K. L., Weiller, B. H. & Gimzewski, J. K. (2011a) Continuity of Graphene on Polycrystalline Copper. *Nano Letters*, 11, 251-256.
- Rasool, H. I., Song, E. B., Mecklenburg, M., Regan, B. C., Wang, K. L., Weiller, B. H. & Gimzewski, J. K. (2011b) Atomic-scale characterization of graphene grown on copper (100) single crystals. *Journal of the American Chemical Society*, 133, 12536-12543.
- Ray, A. K., Sahu, R. K., Rajinikanth, V., Bapari, H., Ghosh, M. & Paul, P. (2012) Preparation and characterization of graphene and Ni-decorated graphene using flower petals as the precursor material. *Carbon*, 50, 4123-4129.
- Reddy, K. M., Gledhill, A. D., Chen, C.-H., Drexler, J. M. & Padture, N. P. (2011) High quality, transferrable graphene grown on single crystal Cu(111) thin films on basal-plane sapphire. *Applied Physics Letters*, 98, 113117-3.
- Regan, W., Alem, N., Aleman, B., Geng, B., Girit, C., Maserati, L., Wang, F., Crommie, M. & Zettl, A. (2010) A direct transfer of layer-area graphene. *Applied Physics Letters*, 96, 113102-3.

- Regmi, M., Chisholm, M. F. & Eres, G. (2012) The effect of growth parameters on the intrinsic properties of large-area single layer graphene grown by chemical vapor deposition on Cu. *Carbon*, 50, 134-141.
- Reina, A., Jia, X., Ho, J., Nezich, D., Son, H., Bulovic, V., Dresselhaus, M. S. & Kong, J. (2008a) Large area, few-layer graphene films on arbitrary substrates by chemical vapor deposition. *Nano Letters*, 9, 30-35.
- Reina, A., Son, H., Jiao, L., Fan, B., Dresselhaus, M. S., Liu, Z. & kong, J. (2008b) Transferring and identification of single- and few-layer graphene on arbitrary substrates. *The Journal of Physical Chemistry C*, 112, 17741-17744.
- Reina, A., Thiele, S., Jia, X., Bhaviripudi, S., Dresselhaus, M. S., Schaefer, J. A. & Kong, J. (2009) Growth of large-area single- and bi-layer graphene by controlled carbon precipitation on polycrystalline Ni surfaces. *Nano Res.*, 2, 509-516.
- Report Linker (2015), Nanotechnology Market Outlook 2020 [Online], [Accessed January 2016]  
Available from World Wide Web  
<http://www.reportlinker.com/p02162665/Nanotechnology-Market-Outlook.html>
- Riedl, C., Coletti, C. & Starke, U. (2010) Structural and electronic properties of epitaxial Graphene on SiC(0001): A review of growth, characterization, transfer doping and hydrogen intercalation. *Journal of Physics D: Applied Physics*, 43.
- Robertson, A. W. & Warner, J. H. (2011) Hexagonal Single Crystal Domains of Few-Layer Graphene on Copper Foils. *Nano Letters*, 11, 1182-1189.
- Robinson, J., Weng, X., Trumbull, K., Cavalero, R., Wetherington, M., Frantz, E., Labella, M., Hughes, Z., Fanton, M. & Snyder, D. (2009) Nucleation of epitaxial graphene on SiC(0001). *ACS Nano*, 4, 153-158.
- Robinson, Z. R., Tyagi, P., Murray, T. M., Ventrice, J. C. A., Chen, S., Munson, A., Magnuson, C. W. & Ruoff, R. S. (2012) Substrate grain size and orientation of Cu and Cu--Ni foils used for the growth of graphene films. *Journal of Vacuum Science & Technology A: Vacuum, Surfaces, and Films*, 30, 011401-7.
- Ruan, G., Sun, Z., Peng, Z. & Tour, J. M. (2011) Growth of graphene from food, insects, and waste. *ACS Nano*, 5, 7601-7607.
- Rümmeli, M. H., Rocha, C. G., Ortmann, F., Ibrahim, I., Sevincli, H., Börrnert, F., Kunstmann, J., Bachmatiuk, A., Pötschke, M., Shiraishi, M., Meyyappa, M., Büchner, B., Roche, S. & Cuniberti, G. (2011) Graphene: Piecing it together. *Advanced Materials*, 23, 4471-4490.
- Sackett, W. M. (1995) The thermal stability of methane from 600 to 1000°C. *Organic Geochemistry*, 23, 403-406.
- Schedin, F., Geim, A. K., Morozov, S. V., Hill, E. W., Blake, P., Katsnelson, M. I. & Novoselov, K. S. (2007) Detection of individual gas molecules adsorbed on graphene. *Nature Materials*, 6, 652-655.

- Seah, C.-M., Chai, S.-P. & Mohamed, A. R. (2014) Mechanisms of graphene growth by chemical vapour deposition on transition metals. . *Carbon*, 70, 1-21.
- Seah, C.-M., Chai, S.-P. & Mohamed, A. R. (2011a) Synthesis of aligned carbon nanotubes. *Carbon*, 49, 4613-4635.
- Seah, C., Chai, S., Ichikawa, S. & Mohamed, A. R. (2012) Synthesis of single-walled carbon nanotubes over a spin-coated Fe catalyst in an ethanol-PEG colloidal solution. . *Carbon*, 50, 960-967.
- Seah, C., Chai, S., Ichikawa, S. & Mohamed, A. R. (2013) Parametric study of methane catalytic CVD into single-walled carbon nanotubes using spin-coated iron nanoparticles. *Chemical Vapor Deposition*, 19, 53-60.
- Selman, G. L., Ellison, P. J. & Darling, A. S. (1970) Carbon in platinum and palladium- solubility determinations and diffusion at high temperatures. *Platinum Metals Review*, 14, 14-20.
- Seo, J. H., Lee, H. W., Kim, J.-K., Kim, D.-G., Kang, J.-W., Kang, M.-S. & Kim, C. S. (2012) Few layer graphene synthesized by filtered vacuum arc system using solid carbon source. *Current Applied Physics*, 12, Supplement 2, S131-S133.
- Shelton, J. C., Patil, H. R. & Blakely, J. M. (1974) Equilibrium segregation of carbon to a nickel (111) surface: A surface phase transition. *Surface Science*, 43, 493-520.
- Shi, X., Yin, Q. & Wei, Y. (2012) A theoretical analysis of the surface dependent binding, peeling and folding of graphene on single crystal copper. *Carbon*, 50, 3055-3063.
- Shi, Y., Kim, K. K., Reina, A., Hofmann, M., Li, L.-J. & Kong, J. (2010) Work function engineering of graphene electrode via chemical doping. *ACS Nano*, 4, 2689-2694.
- Shishir, R. S. & Ferry, D. K. (2009) Velocity saturation in intrinsic graphene. *Journal of Physics: Condensed Matter*, 21, 232204.
- Shu, H., Chen, X., Tao, X. & Ding, F. (2012) Edge structural stability and kinetics of graphene chemical vapor deposition growth. *ACS Nano*, 6, 3243-3250.
- Siller, R. H., Oates, W. A. & McClellan, R. B. (1968) The solubility of carbon in palladium and platinum. *Journal of the Less Common Metals*, 16, 71-73.
- Singh, M. K., Singh, P. P., Titus, E., Misra, D. S. & Lenormand, F. (2002) High density of multiwalled carbon nanotubes observed on nickel electroplated copper substrates by microwave plasma chemical vapor deposition. *Chemical Physics Letters*, 354, 331-336.
- Singh, M. K., Titus, E., Tyagi, P. K., Palnitkar, U., Misra, D. S., Roy, M., Dua, A. K., Cojocar, C. S. & Le Normand, F. (2003) Ni and Ni/Pt filling inside multiwalled carbon nanotubes. *Journal of Nanoscience and Nanotechnology*, 3, 165-170.

- Singleton, M. & Nash, P. (1989) The C-Ni (Carbon-Nickel) system. *Bulletin of Alloy Phase Diagrams*, 10, 121-126.
- Son, I. H., Song, H. J., Kwon, S., Bachmatiuk, A., Lee, S. J., Benayad, A., Park, J. H., Choi, J.-Y., Chang, H. & Rummeli, M. H. (2014) CO<sub>2</sub> Enhanced chemical vapor deposition growth of few-layer graphene over NiOx. *ACS Nano*, 8, 9224-9232.
- Sonde, S., Vecchio, C., Giannazzo, F., Yakimova, R., Raineri, V. & Rimini, E. (2012) Effect of graphene/4H-SiC(0001) interface on electrostatic properties in graphene. *Physica E: Low-dimensional Systems and Nanostructures*, 44, 993-996.
- Song, J., Kam, F.-Y., Png, R.-Q., Seah, W.-L., Zhuo, J.-M., Lim, G.-K., Ho, P. K. H. & Chua, L.-L. (2013) A general method for transferring graphene onto soft surfaces. *Nat Nano*, 8, 356-362.
- Song, L., Ci, L., Gao, W. & Ajayan, P. M. (2009) Transfer printing of graphene using gold film. *ACS Nano*, 3, 1353-1356.
- Srivastava, A., Galande, C., Ci, L., Song, L., Rai, C., Jariwala, D., Kelly, K. F. & Ajayan, P. M. (2010) Novel liquid precursor-based facile synthesis of large-area continuous, single, and few-layer graphene films. *Chemistry of Materials*, 22, 3457-3461.
- Staudenmaier, L. (1898) Verfahren zur Darstellung der Graphitsäure. *Berichte der deutschen chemischen Gesellschaft*, 31, 1481-1487.
- Su, C.-Y., Lu, A.-Y., Wu, C.-Y., Li, Y.-T., Liu, K.-K., Zhang, W., Lin, S.-Y., Juang, Z.-Y., Zhong, Y.-L., Chen, F.-R. & Li, L.-J. (2011) Direct formation of wafer scale graphene thin layers on insulating substrates by chemical vapor deposition. *Nano Letters*, 11, 3612-3616.
- Suk, J. W., Kitt, A., Magnuson, C. W., Hao, Y., Ahmed, S., An, J., Swan, A. K., Goldberg, B. B. & Ruoff, R. S. (2011) Transfer of CVD-grown monolayer graphene onto arbitrary substrates. *ACS Nano*, 5, 6916-6924.
- Sun, J., Hannon, J. B., Tromp, R. M., Johari, P., Bol, A. A., Shenoy, V. B. & Pohl, K. (2010a) Spatially-resolved structure and electronic properties of graphene on polycrystalline Ni. *ACS Nano*, 4, 7073-7077.
- Sun, Z., James, D. & Tour, J. (2011) Graphene chemistry: Synthesis and manipulation. *The Journal of Physical Chemistry Letters*, 2, 2425-2432.
- Sun, Z., Yan, Z., Yao, J., Beitler, E., Zhu, Y. & Tour, J. M. (2010b) Growth of graphene from solid carbon sources. *Nature*, 468, 549-552.
- Sutter, E., Albrecht, P. & Sutter, P. (2009a) Graphene growth on polycrystalline Ru thin films. *Applied Physics Letters*, 95.
- Sutter, P., Hybertsen, M. S., Sadowski, J. T. & Sutter, E. (2009b) Electronic structure of few-layer epitaxial graphene on Ru(0001). *Nano Letters*, 9, 2654-2660.



- Sutter, P., Sadowski, J. T. & Sutter, E. (2009c) Graphene on Pt(111): Growth and substrate interaction. *Physical Review B*, 80, 245411.
- Sutter, P. W., Albrecht, P. M. & Sutter, E. A. (2010) Graphene growth on epitaxial Ru thin films on sapphire. *Applied Physics Letters*, 97.
- Sutter, P. W., Flege, J. I. & Sutter, E. A. (2008) Epitaxial graphene on ruthenium. *Nature Materials*, 7, 406-411.
- Suzuki, S., Orofeo, C. M., Wang, S., Maeda, F., Takamura, M. & Hibino, H. (2013) Structural instability of transferred graphene grown by chemical vapor deposition against heating. *The Journal of Physical Chemistry C*, 117, 22123-22130.
- Takahashi, K., Yamada, K., Kato, H., Hibino, H. & Homma, Y. (2012) In situ scanning electron microscopy of graphene growth on polycrystalline Ni substrate. *Surface Science*, 606, 728-732.
- Tan, Y. Y., Jayawardena, K. D. G. I., Adikaari, A. A. D. T., Tan, L. W., Anguita, J. V., Henley, S. J., Stolojan, V., Carey, J. D. & Silva, S. R. P. (2012) Photo-thermal chemical vapor deposition growth of graphene. *Carbon*, 50, 668-673.
- Taniguchi, N. (1974). On the basic concept of 'nano-technology'. Proceedings of the International Conference on Production Engineering, Tokyo, 1974, Part II (Japan Society of Precision Engineering).
- Tao, L., Lee, J., Chou, H., Holt, M., Ruoff, R. S. & Akinwande, D. (2012) Synthesis of high quality monolayer graphene at reduced temperature on hydrogen-enriched evaporated copper (111) films. *ACS Nano*, 6, 2319-2325.
- Tedesco, J. L., Vanmil, B. L., Myers-Ward, R. L., McCrate, J. M., Kitt, S. A., Campbell, P. M., Jernigan, G. G., Culbertson, J. C., Eddy, J. C. R. & Gaskill, D. K. (2009) Hall effect mobility of epitaxial graphene grown on silicon carbide. *Applied Physics Letters*, 95, 122102-3.
- Terasawa, T.-O. & Saiki, K. (2012) Growth of graphene on Cu by plasma enhanced chemical vapor deposition. *Carbon*, 50, 869-874.
- Tetlow, H., Posthuma De Boer, J., Ford, I. J., Vvedensky, D. D., Coraux, J. & Kantorovich, L. (2014) Growth of epitaxial graphene: Theory and experiment. *Physics Reports*, 542, 195-295.
- Tyagi, P., Robinson, Z. R., Munson, A., Magnuson, C. W., Chen, S., McNeilan, J. D., Moore, R. L., Piner, R. D., Ruoff, R. S. & Ventrice JR, C. A. (2015) Characterization of graphene films grown on CuNi foil substrates. *Surface Science*, 634, 16-24.
- Tzalenchuk, A., Lara-Avila, S., Kalaboukhov, A., Paolillo, S., Syvajarvi, M., Yakimova, R., Kazakova, O., Janssen, T. J. B. M., Fal'ko, V. & Kubatkin, S. (2010) Towards a quantum resistance standard based on epitaxial graphene. *Nat Nano*, 5, 186-189.

- Ugeda, M. M., Fernández-Torre, D., Brihuega, I., Pou, P., Martínez-Galera, A. J., Pérez, R. & Gómez-Rodríguez, J. M. (2011) Point Defects on graphene on metals. *Physical Review Letters*, 107, 116803.
- Unarunotai, S., Koepke, J. C., Tsai, C.-L., Du, F., Chialvo, C. E., Murata, Y., Haasch, R., Petrov, I., Mason, N., Shim, M., Lyding, J. & Rogers, J. A. (2010) Layer-by-layer transfer of multiple, large area sheets of graphene grown in multilayer stacks on a single SiC wafer. *ACS Nano*, 4, 5591-5598.
- Unarunotai, S., Murata, Y., Chialvo, C. E., Kim, H.-S., Maclaren, S., Mason, N., Petrov, I. & Rogers, J. A. (2009) Transfer of graphene layers grown on SiC wafers to other substrates and their integration into field effect transistors. *Applied Physics Letters*, 95, 202101-3.
- Economic Planning Unit, (2006) Ninth malaysia plan [Online] [Accessed July 2015] Available from World Wide Web [www.epu.gov.my/html/themes/epu/html/rm9/html/english.htm](http://www.epu.gov.my/html/themes/epu/html/rm9/html/english.htm)
- Vanin, M., Mortensen, J. J., Kelkkanen, A. K., Garcia-Lastra, J. M., Thygesen, K. S. & Jacobsen, K. W. (2010) Graphene on metals: A van der Waals density functional study. *Physical Review B*, 81, 081408.
- Varchon, F., Feng, R., Hass, J., Li, X., Nguyen, B. N., Naud, C., Mallet, P., Veullen, J. Y., Berger, C., Conrad, E. H. & Magaud, L. (2007) Electronic Structure of epitaxial graphene layers on SiC: Effect of the substrate. *Physical Review Letters*, 99, 126805.
- Viñes, F., Neyman, K. M. & Görling, A. (2009) Carbon on platinum substrates: from carbidic to graphitic phases on the (111) surface and on nanoparticles. *The Journal of Physical Chemistry A*, 113, 11963-11973.
- Vlassioug, I., Regmi, M., Fulvio, P., Dai, S., Datskos, P., Eres, G. & Smirnov, S. (2011a) Role of Hydrogen in Chemical Vapor Deposition Growth of Large Single-Crystal Graphene. *ACS Nano*, 5, 6069-6076.
- Vlassioug, I., Smirnov, S., Ivanov, I., Fulvio, P. F., Dai, S., Meyer, H., Chi, M., Hensley, D., Datskos, P. & Lavrik, N. V. (2011b) Electrical and thermal conductivity of low temperature CVD graphene: The effect of disorder. *Nanotechnology*, 22.
- Vlassioug, I., Smirnov, S., Regmi, M., Surwade, S. P., Srivastava, N., Feenstra, R., Eres, G., Parish, C., Lavrik, N., Datskos, P., Dai, S. & Fulvio, P. (2013) Graphene nucleation density on copper: fundamental role of background pressure. *The Journal of Physical Chemistry C*, 117, 18919-18926.
- Volotskova, O., Levchenko, I., Shashurin, A., Raitsev, Y., Ostrikov, K. & Keidar, M. (2010) Single-step synthesis and magnetic separation of graphene and carbon nanotubes in arc discharge plasmas. *Nanoscale*, 2, 2281-2285.
- Walter, A. L., Nie, S., Bostwick, A., Kim, K. S., Moreschini, L., Chang, Y. J., Innocenti, D., Horn, K., McCarty, K. F. & Rotenberg, E. (2011) Electronic

- structure of graphene on single-crystal copper substrates. *Physical Review B*, 84, 195443.
- Wan, D., Lin, T., Bi, H., Huang, F., Xie, X., Chen, I. W. & Jiang, M. (2012) Autonomously controlled homogenous growth of wafer-sized high-quality graphene via a smart janus substrate. *Advanced Functional Materials*, 22, 1033-1039.
- Wang, D.-Y., Huang, I. S., Ho, P.-H., Li, S.-S., Yeh, Y.-C., Wang, D.-W., Chen, W.-L., Lee, Y.-Y., Chang, Y.-M., Chen, C.-C., Liang, C.-T. & Chen, C.-W. (2013) Clean-lifting transfer of large-area residual-free graphene films. *Advanced Materials*, 25, 4521-4526.
- Wang, X., Zhi, L. & Mullen, K. (2007) Transparent, conductive graphene electrodes for dye-sensitized solar cells. *Nano Letters*, 8, 323-327.
- Wang, Y., Page, A. J., Nishimoto, Y., Qian, H.-J., Morokuma, K. & Irlle, S. (2011a) Template effect in the competition between haeckelite and graphene growth on Ni(111): Quantum chemical molecular dynamics simulations. *Journal of the American Chemical Society*, 133, 18837-18842.
- Wang, Y., Yang, R., Shi, Z., Zhang, L., Shi, D., Wang, E. & Zhang, G. (2011b) Super-elastic graphene ripples for flexible strain sensors. *ACS Nano*, 5, 3645-3650.
- Wang, Y., Zheng, Y., Xu, X., Dubuisson, E., Bao, Q., Lu, J. & Loh, K. P. (2011c) electrochemical delamination of cvd-grown graphene film: Toward the recyclable use of copper catalyst. *ACS Nano*, 5, 9927-9933.
- Weatherup, R. S., Baetz, C., Dlubak, B., Bayer, B. C., Kidambi, P. R., Blume, R., Schloegl, R. & Hofmann, S. (2013) Introducing carbon diffusion barriers for uniform, high-quality graphene growth from solid sources. *Nano Letters*, 13, 4624-4631.
- Weatherup, R. S., Bayer, B. C., Blume, R., Ducati, C., Baetz, C., Schloegl, R. & Hofmann, S. (2011) In situ characterization of alloy catalysts for low-temperature graphene growth. *Nano Letters*, 11, 4154-4160.
- Weingart, S., Bock, C., Kunze, U., Emtsev, K. V., Seyller, T. & Ley, L. (2010) Influence of the growth conditions of epitaxial graphene on the film topography and the electron transport properties. *Physica E: Low-dimensional Systems and Nanostructures*, 42, 687-690.
- Wofford, J. M., Nie, S., McCarty, K. F., Bartelt, N. C. & Dubon, O. D. (2010) Graphene islands on Cu foils: The interplay between shape, orientation, and defects. *Nano Letters*, 10, 4890-4896.
- Woo, Y. S., Seo, D. H., Yeon, D.-H., Heo, J., Chung, H.-J., Benayad, A., Chung, J.-G., Han, H., Lee, H.-S., Seo, S. & Choi, J.-Y. (2013) Low temperature growth of complete monolayer graphene films on Ni-doped copper and gold catalysts by a self-limiting surface reaction. *Carbon*, 64, 315-323.

- Wood, J. D., Schmucker, S. W., Lyons, A. S., Pop, E. & Lyding, J. W. (2011) Effects of polycrystalline Cu substrate on graphene growth by chemical vapor deposition. *Nano Letters*, 11, 4547-4554.
- Wu, P., Jiang, H., Zhang, W., Li, Z., Hou, Z. & Yang, J. (2012a) Lattice mismatch induced nonlinear growth of graphene. *Journal of the American Chemical Society*, 134, 6045-6051.
- Wu, W., Jauregui, L. A., Su, Z., Liu, Z., Bao, J., Chen, Y. P. & Yu, Q. (2011a) Growth of single crystal graphene arrays by locally controlling nucleation on polycrystalline Cu using chemical vapor deposition. *Advanced Materials*, 23, 4898-4903.
- Wu, Y., Chou, H., Ji, H., Wu, Q., Chen, S., Jiang, W., Hao, Y., Kang, J., Ren, Y., Piner, R. D. & Ruoff, R. S. (2012b) Growth mechanism and controlled synthesis of AB-stacked bilayer graphene on Cu-Ni alloy foils. *ACS Nano*, 6, 7731-7738.
- Wu, Y. A., Fan, Y., Speller, S., Creeth, G. L., Sadowski, J. T., He, K., Robertson, A. W., Allen, C. S. & Warner, J. H. (2012c) Large single crystals of graphene on melted copper using chemical vapor deposition. *ACS Nano*, 6, 5010-5017.
- Wu, Y. A., Robertson, A. W., Schäffel, F., Speller, S. C. & Warner, J. H. (2011b) Aligned rectangular few-layer graphene domains on copper surfaces. *Chemistry of Materials*, 23, 4543-4547.
- Xu, M., Fujita, D., Sagisaka, K., Watanabe, E. & Hanagata, N. (2011) Production of extended single-layer graphene. *ACS Nano*, 5, 1522-1528.
- Xue, Y., Wu, B., Jiang, L., Guo, Y., Huang, L., Chen, J., Tan, J., Geng, D., Luo, B., Hu, W., Yu, G. & Liu, Y. (2012) Low temperature growth of highly nitrogen-doped single crystal graphene arrays by chemical vapor deposition. *Journal of the American Chemical Society*, 134, 11060-11063.
- Yamada, T., Ishihara, M., Kim, J., Hasegawa, M. & Iijima, S. (2012) A roll-to-roll microwave plasma chemical vapor deposition process for the production of 294mm width graphene films at low temperature. *Carbon*, 50, 2615-2619.
- Yamaguchi, H., EDA, G., Mattevi, C., Kim, H. & Chhowalla, M. (2010) Highly uniform 300 mm wafer-scale deposition of single and multilayered chemically derived graphene thin films. *ACS Nano*, 4, 524-528.
- Yan, K., Peng, H., Zhou, Y., Li, H. & Liu, Z. (2011a) Formation of bilayer bernal graphene: layer-by-layer epitaxy via chemical vapor deposition. *Nano Letters*, 11, 1106-1110.
- Yan, Z., Peng, Z., Sun, Z., Yao, J., Zhu, Y., Liu, Z., Ajayan, P. M. & Tour, J. M. (2011b) Growth of bilayer graphene on insulating substrates. *ACS Nano*, 5, 8187-8192.
- Yang, X., Peng, H., Xie, Q., Zhou, Y. & Liu, Z. (2012) Clean and efficient transfer of CVD-grown graphene by electrochemical etching of metal substrate. *Journal of Electroanalytical Chemistry*.

- Yao, Y., Li, Z., L<sup>in</sup>, Z., Moon, K.-S., Agar, J. & Wong, C. (2011) Controlled Growth of multilayer, few-layer, and single-layer graphene on metal substrates. *The Journal of Physical Chemistry C*, 115, 5232-5238.
- Yazyev, O. V. & Pasquarello, A. (2008) Effect of metal elements in catalytic growth of carbon nanotubes. *Physical Review Letters*, 100, 156102.
- Yi, P., Shi, D. & Gao, H. J. (2007) Formation of graphene on Ru(0001) surface. *Chinese Physics B*, 16, 3151-3153.
- Yong, V. & Hahn, H. T. (2011) Graphene growth with giant domains using chemical vapor deposition. *CrystEngComm*, 13, 6933-6936.
- Yoon, T., Shin, W. C., Kim, T. Y., Mun, J. H., Kim, T. S. & Cho, B. J. (2012) Direct measurement of adhesion energy of monolayer graphene as-grown on copper and its application to renewable transfer process. *Nano Letters*, 12, 1448-1452.
- Yu, Q., Jauregui, L. A., Wu, W., Colby, R., Tian, J., Su, Z., Cao, H., Liu, Z., Pandey, D., Wei, D., Chung, T. F., Peng, P., Guisinger, N. P., Stach, E. A., Bao, J., Pei, S.-S. & Chen, Y. P. (2011) Control and characterization of individual grains and grain boundaries in graphene grown by chemical vapour deposition. *Nat Mater*, 10, 443-449.
- Yu, Q., Lian, J., Siriponglert, S., Li, H., Chen, Y. P. & Pei, S.-S. (2008) Graphene segregated on Ni surfaces and transferred to insulators. *Applied Physics Letters*, 93, 113103-3.
- Yuan, S., Meng, L. & Wang, J. (2013) Greatly improved methane dehydrogenation via ni adsorbed Cu(100) surface. *The Journal of Physical Chemistry C*, 117, 14796-14803.
- Zhang, H., Fu, Q., Cui, Y., Tan, D. & Bao, X. (2009a) Growth mechanism of graphene on Ru(0001) and O<sub>2</sub> adsorption on the graphene/Ru(0001) surface. *The Journal of Physical Chemistry C*, 113, 8296-8301.
- Zhang, J., Hu, P., Wang, X. & Wang, Z. (2012a) Structural evolution and growth mechanism of graphene domains on copper foil by ambient pressure chemical vapor deposition. *Chemical Physics Letters*, 536, 123-128.
- Zhang, L., Liang, J., Huang, Y., Ma, Y., Wang, Y. & Chen, Y. (2009b) Size-controlled synthesis of graphene oxide sheets on a large scale using chemical exfoliation. *Carbon*, 47, 3365-3368.
- Zhang, Q., Han, B., Tang, X., Heier, K., Li, J. X., Hoffman, J., Lin, M., Britton, S. L., Derecskei-Kovacs, A. & Cheng, H. (2012b) On the mechanisms of carbon formation reaction on Ni(111) surface. *The Journal of Physical Chemistry C*, 116, 16522-16531.
- Zhang, Y., Gomez, L., Ishikawa, F. N., Madaria, A., Ryu, K., Wang, C., Badmaev, A. & Zhou, C. (2010) Comparison of graphene growth on single-crystalline and polycrystalline Ni by chemical vapor deposition. *The Journal of Physical Chemistry Letters*, 1, 3101-3107.

- Zhang, Y., Li, Z., Kim, P., Zhang, L. & Zhou, C. (2012c) Anisotropic hydrogen etching of chemical vapor deposited graphene. *ACS Nano*, 6, 126-132.
- Zhang, Y., Tan, Y.-W., Stormer, H. L. & Kim, P. (2005) Experimental observation of the quantum Hall effect and Berry's phase in graphene. *Nature*, 438, 201-204.
- Zhang, Y., Zhang, L., Kim, P., Ge, M., Li, Z. & Zhou, C. (2012d) Vapor trapping growth of single-crystalline graphene flowers: Synthesis, Morphology, and electronic properties. *Nano Letters*, 12, 2810-2816.
- Zhao, L., Rim, K. T., Zhou, H., He, R., Heinz, T. F., Pinczuk, A., Flynn, G. W. & Pasupathy, A. N. (2011) Influence of copper crystal surface on the CVD growth of large area monolayer graphene. *Solid State Communications*, 151, 509-513.
- Zheng, M., Takei, K., Hsia, B., Fang, H., Zhang, X., Ferralis, N., Ko, H., Chueh, Y.-L., Zhang, Y., Maboudian, R. & Javey, A. (2010) Metal-catalyzed crystallization of amorphous carbon to graphene. *Applied Physics Letters*, 96, 063110-3.
- Zhou, S. Y., Gweon, G. H., Fedorov, A. V., First, P. N., De Heer, W. A., Lee, D. H., Guinea, F., Castro Neto, A. H. & Lanzara, A. (2007) Substrate-induced bandgap opening in epitaxial graphene. *Nat Mater*, 6, 770-775.
- Zhu, Y., Murali, S., Cai, W., Li, X., Suk, J. W., Potts, J. R. & Ruoff, R. S. (2010) Graphene and graphene oxide: Synthesis, Properties, and applications. *Advanced Materials*, 22, 3906-3924.



# Choon-Ming SEAH

## Synthèse de graphène mono-couche sur nickel et catalyseur bi-métallique Ni-Cu et réutilisation du catalyseur.

Thèse en Co-Tutelle  
(Université de Lorraine – Universiti Sains Malaysia)

Date de soutenance : Mardi 15 décembre 2015

Devant le jury composé de :

**Prof. Abdul Rahman Mohamed** (Supervisor, School of Chemical Engineering, Universiti Sains Malaysia, Nibong Tebal, Malaysia)

**Dr. Brigitte Vigolo** (Supervisor UL, Institut Jean Lamour, Nancy, France)

**Prof. Noraishah Saidina Amin** (External reviewer, Faculty of Chemical Engineering, Universiti Teknologi Malaysia, Johor, Malaysia)

**Dr. Johann Coraux** (External reviewer, Institut NÉEL Grenoble, France)

Invité:

**Assoc Prof Dr Chai Siang Piao** (Co-supervisor, Monash University Sunway Campus, Malaysia)





## SOMMAIRE

INTRODUCTION	p.182
<b>I. Généralités sur le graphène</b>	p.183
<i>I.1. Structure et propriétés</i>	p.183
<i>I.2. Méthodes de synthèse et objectifs du travail de thèse</i>	p.184
<b>II. Partie expérimentale</b>	p.185
<i>II.1. Montage expérimental utilisé pour la synthèse</i>	p.185
<i>II.2. Techniques expérimentales principales</i>	p.185
<b>III. Résultats et discussion</b>	p.186
<i>III.1. Synthèse de graphène monocouche par CVD à pression atmosphérique</i>	p.186
<i>III.2. Séparation du graphène et recyclage du catalyseur</i>	p.191
CONCLUSIONS ET PERSPECTIVES	p.195
Quelques références importantes	p.196

## INTRODUCTION

Le graphène est une couche de carbone d'une épaisseur atomique au sein de laquelle les atomes de carbone sont hybridés  $sp^2$ . Depuis sa découverte en 2004, le graphène devient l'un des sujets les plus importants de la recherche dans le monde. L'attractivité du graphène est principalement attribuable à ses propriétés remarquables : mécaniques, optiques, thermiques et électriques, permettant au graphène d'être potentiellement utilisé pour diverses applications. Le graphène peut être synthétisé par exfoliation mécanique, réduction de l'oxyde de graphène, la sublimation du SiC et le dépôt chimique en phase vapeur (CVD). Parmi ces techniques, la sublimation du SiC et les méthodes CVD sont deux méthodes prometteuses pour produire du graphène monocouche ; et la technique CVD en particulier, car elle permet une séparation facile du graphène à partir du substrat catalytique nécessaire à sa croissance. L'objectif général de la thèse concerne la préparation de graphène de façon contrôlée avec une méthode de croissance bas-coût. Pour cela, nous avons choisi de travailler à la pression atmosphérique avec des métaux catalytiques polycristallins. Dans ce travail de thèse, une attention particulière a été portée à la caractérisation des échantillons synthétisés afin de pouvoir apprécier le contrôle des croissances réalisées. Par ailleurs, la synthèse de graphène monocouche qui possède les propriétés et le potentiel d'application les plus élevées a été investie. Pour cela, dans les conditions utilisées un nouveau dispositif a été développé, il permet de créer une barrière efficace à l'excès d'apport de carbone à la surface des métaux utilisés. La dernière partie du travail s'intéresse au problème récurrent de séparation du graphène de son substrat de croissance. La réutilisation du catalyseur pour réaliser plusieurs croissances de graphène successives avec la même feuille métallique a également été étudiée. Dans ce mémoire succinct, après une description du graphène et quelques données expérimentales, les principaux résultats concernant chacun des aspects abordés seront donnés.

## I. Généralités sur le graphène

### *I.1. Structure et propriétés*

Le carbone peut présenter plusieurs formes allotropiques (figure 1). Le graphène est donc un film mince composé seulement d'atomes de carbone hybridés  $sp^2$  et organisés en réseau hexagonal. Il s'agit du plus fin cristal connu, qui se trouve à l'état naturel dans le graphite. Le graphène a été isolé à l'université de Manchester en 2004 par Sir Andre Geim et Novoselov Sir Kostya, découverte qui leur valu le prix Nobel de physique en 2010.

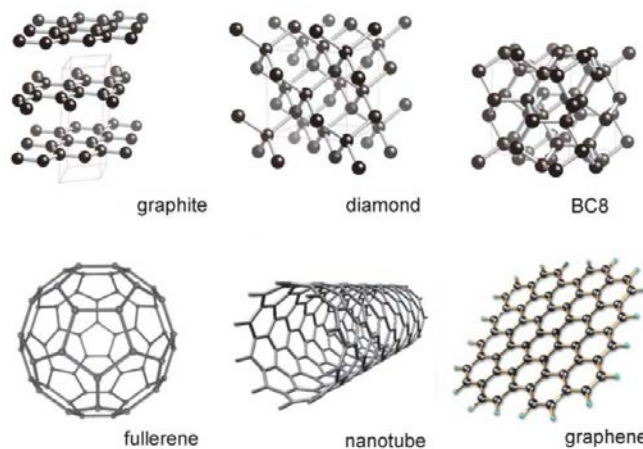


Figure 1. Structure de plusieurs allotropes du carbone.

Depuis lors, le graphène suscite un grand intérêt dans le domaine de la recherche, les premières études sur ce matériau fascinent toutes les communautés scientifiques. Le graphène a une très bonne résistance (avec son module d'Young de 1 TPa) et se révèle être un excellent conducteur d'électricité. Il possède une excellente mobilité de porteurs de charge qui dépasse  $200\,000\text{ cm}^2\cdot\text{V}^{-1}\cdot\text{s}^{-1}$ . Par ailleurs, c'est le meilleur conducteur thermique connu aujourd'hui. Il peut évacuer 5300 watts par mètre et par kelvin à température ambiante. Ses propriétés optiques sont également très convoitées puisqu'il transmet 97 % de la lumière visible. Ces propriétés font du graphène, un matériau idéal pour l'industrie électronique en vue de son utilisation dans de nombreux domaines.

### *1.2. Méthodes de synthèse et objectifs du travail de thèse*

Dans ces conditions, la synthèse de graphène est un domaine très important. En effet, le déficit actuel est de pouvoir préparer des échantillons de graphène de façon contrôlée et dont la qualité structurale et les caractéristiques morphologiques sont reproductibles. Le contrôle du nombre de couches est primordiale puisque les propriétés physiques sont largement affectées dès que le nombre de couche est supérieur à 2 et elles sont complètement perdues pour 3 couches et au-delà.

La méthode de l'exfoliation mécanique utilisée par Novoselov et collaborateurs est simple et permet d'obtenir du graphène de très bonne qualité. Néanmoins, elle n'est pas adaptée à la production à grande échelle. Les méthodes d'exfoliation chimique consistent à utiliser un agent chimique qui peut s'intercaler entre les feuillets de graphène du graphite ou du graphite expansé en voie liquide. La séparation des feuillets est induite après intercalation par ultrasons par exemple. Elles permettent d'obtenir un mélange de plusieurs types de graphène (nombre de couches variable souvent jusqu'à plus de 10 couches) en relativement grande quantité mais la prolongation aux traitements chimiques agressifs et/ou aux ultrasons induit l'introduction d'une quantité non négligeable de défauts dans le graphène produit. Les méthodes de croissance épitaxiale à partir du carbure de silicium (SiC) et CVD sont également très étudiées parce qu'elles permettent de faire croître du graphène possédant un nombre couche limité, d'une bonne qualité structurale et sur des dimensions compatibles avec une intégration dans des composants électroniques et écrans plats par exemple. La méthode à partir de SiC présente l'inconvénient de rendre très difficile la séparation du graphène synthétisé du substrat utilisé pour sa croissance. La méthode de synthèse CVD qui permet de faire croître du graphène par un mécanisme de dissociation d'un composé carboné (un hydrocarbure le plus souvent) sur un catalyseur métallique a montré plusieurs avantages. Il s'agit d'une méthode flexible puisque les conditions expérimentales (nature du précurseur carboné et du catalyseur, température, pression, etc..) peuvent être adaptées aux caractéristiques du graphène voulu. Par ailleurs, la séparation du graphène après sa croissance peut être réalisée avec succès c'est-à-dire sans induire d'endommagement au graphène séparé. Afin de limiter le nombre de couches dans le graphène, la synthèse est généralement réalisée sous pression réduite afin de limiter l'apport de carbone à la surface du catalyseur. De plus, des substrats métalliques monocristallins sont souvent préférées parce qu'ils permettent un bon contrôle de l'uniformité du graphène obtenu. Ces contraintes de vide et de métaux

monocristallins impliquent des dispositifs expérimentaux complexes et un coût général de synthèse élevé.

Dans cette thèse, nous nous sommes intéressés à la synthèse par CVD sous atmosphère atmosphérique et en utilisant des substrats métalliques polycristallins afin de proposer une méthode de synthèse du graphène simple et peu coûteuse.

## II. Partie expérimentale

### II.1. Montage expérimental utilisé pour la synthèse CVD

Pour la synthèse, après une purge ( $N_2$ ) du réacteur placé dans un four tubulaire, le gaz (mélange  $CH_4/H_2$ ) est introduit (figure 2). La température du four est alors maintenue à la température voulue. La croissance du graphène a lieu sur le substrat placé dans une nacelle de quartz. Le refroidissement rapide est réalisé en déplaçant rapidement la nacelle de la zone chaude du four à l'extérieur du dispositif. La vitesse de refroidissement atteint ainsi plus de  $700^\circ C/min$ .

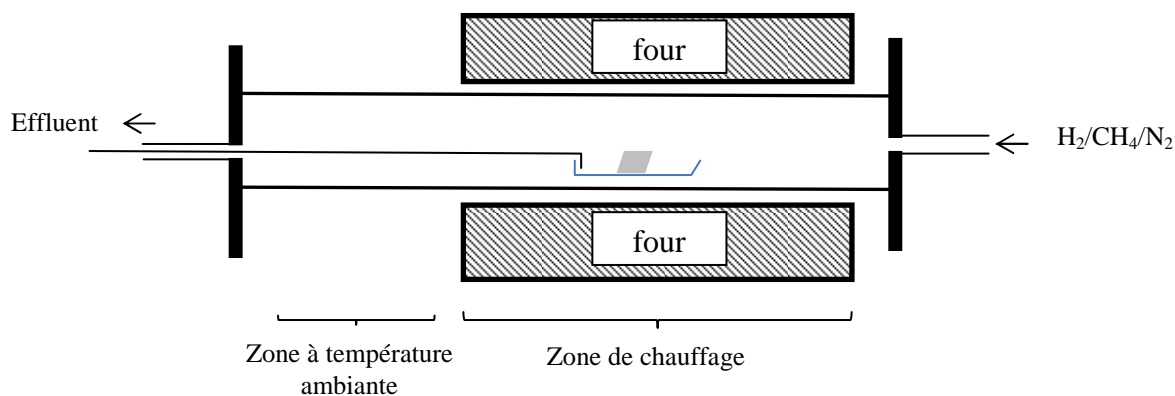


Figure 2. Schéma simplifié du dispositif CVD utilisé pour la synthèse du graphène.

### II.2. Techniques expérimentales principales

La caractérisation du graphène s'intéresse à plusieurs aspects :

- le nombre de couche ;
- la qualité structurale moyenne, présence de défauts dans la structure carbonée  $sp^2$  ;
- l'uniformité du nombre de couches et de la qualité structurale sur des dimensions (relativement) grandes (plusieurs dizaines de microns).

La microscopie optique permet d’apprécier sur une dimension relativement large l’homogénéité des échantillons de graphène. Un faible contraste d’image garantit une bonne uniformité du nombre de couches et de l’absence de défauts (rides, fractures). Au contraire, un contraste apparent indique des échantillons abimés ou avec des inhomogénéités d’épaisseur.

La microscopie électronique à transmission haute résolution (METHR) est une technique de choix largement utilisée pour la caractérisation du graphène notamment parce que même si c’est une technique locale, elle permet de mettre en évidence le nombre de couches du graphène.

La spectroscopie Raman, soit réalisée en plusieurs points de façon aléatoire soit par balayage sur plusieurs dizaines de microns sur l’échantillon, est sensible au nombre de couches de graphène et à sa qualité structurale. De caractère plus ‘macroscopique’, sa complémentarité avec le METHR est nécessaire.

### III. Résultats et discussion

#### III.1. Synthèse de graphène monocouche par CVD à pression atmosphérique

Le cuivre et le nickel sont les 2 catalyseurs les plus communs pour la synthèse de graphène par CVD. Si l’on se fonde sur les diagrammes de phase des composés massifs, la solubilité du carbone est significativement plus importante dans le nickel que dans le cuivre. Les mécanismes de croissance sont différents puisque il a été montré que le mécanisme était à caractéristique volumique dans le nickel et de surface dans le cas du cuivre (figure 3).

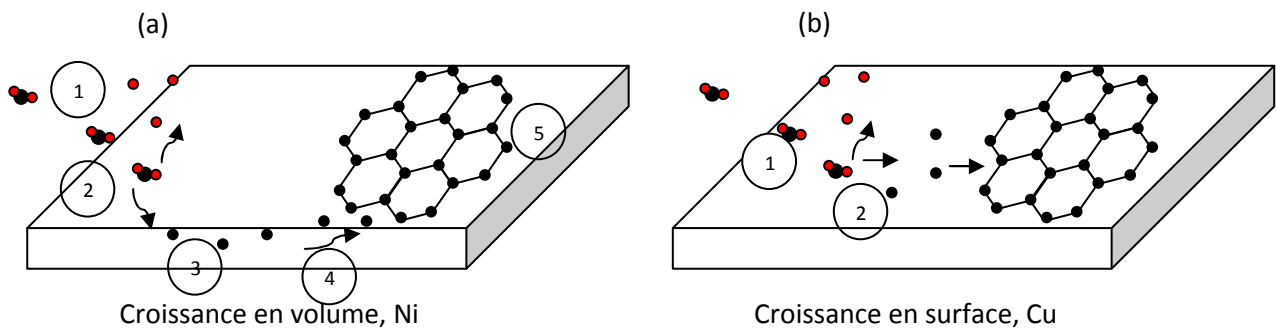


Figure 3. Mécanismes de formation du graphène par (a) le Ni et (b) le Cu.

Pour la synthèse de graphène sur nickel, il faut utiliser des conditions drastiques pour réduire l'apport de carbone indispensable pour limiter le nombre de couches. Il est connu que la croissance de graphène multicouche est favorisée sur le nickel ; c'est la raison pour laquelle il a actuellement perdu de son attractivité au profit du cuivre pour la croissance CVD de graphène avec un nombre de couches réduit.

Un travail d'optimisation des conditions expérimentales favorables à la croissance de graphène par CVD à pression atmosphérique a été réalisé. Les paramètres expérimentaux de durée, de température et de pression partielle de méthane ont été variés sur une large gamme. En utilisant le cuivre, nous n'avons pas pu obtenir de graphène dans notre réacteur CVD à pression atmosphérique. En ce qui concerne le nickel, du graphène monocouche a pu être obtenu après optimisation des conditions expérimentales et l'utilisation d'un refroidissement rapide permettant une trempe de la réaction. Les températures utilisées étaient 800, 850, 900, 950 et 1000 °C, la durée de réaction de 1 à 8 min et le flux de méthane de 10, 20, 30, 40, 50 et 60 sccm, dilué dans la quantité adéquate d'hydrogène pour que sa pression partielle varie entre 0,1 et 0,6 atm. Dans ce mémoire succinct, nous avons choisi de présenter les résultats obtenus en fonction de la pression partielle pour une température fixée à 850°C et une durée de réaction de 5 min. Les spectres de spectroscopie Raman sont présentés figure 4.

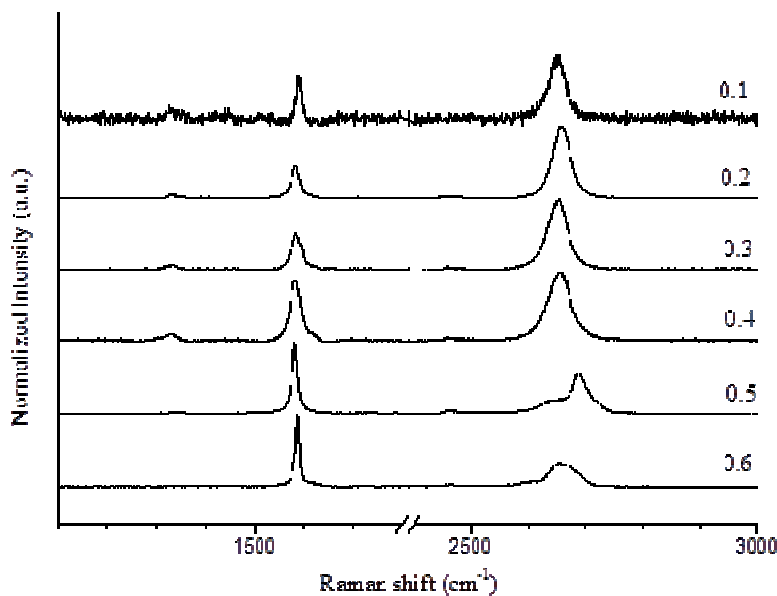


Figure 4. Spectres Raman des échantillons de graphène synthétisés à 850°C pour une durée de 5 min pour des pressions partielles de méthane variable de 0,1 à 0,6 atm.



Entre 0,1 et 0,3 atm de méthane, la croissance donne lieu à du graphène monocouche. L'intensité de bande 2D est plus importante que celle de la bande G et le rapport  $I_{2D}/I_G$  signe la présence de graphène monocouche. Néanmoins, à 0,1 atm le graphène ne couvrait pas totalement la feuille de nickel. C'est seulement à 0,2 et 0,3 atm de méthane que le graphène en couvrait toute la surface. A partir de 0,4 atm, la bande G devient plus importante et du graphène contenant plus de 2 couches a été synthétisé.

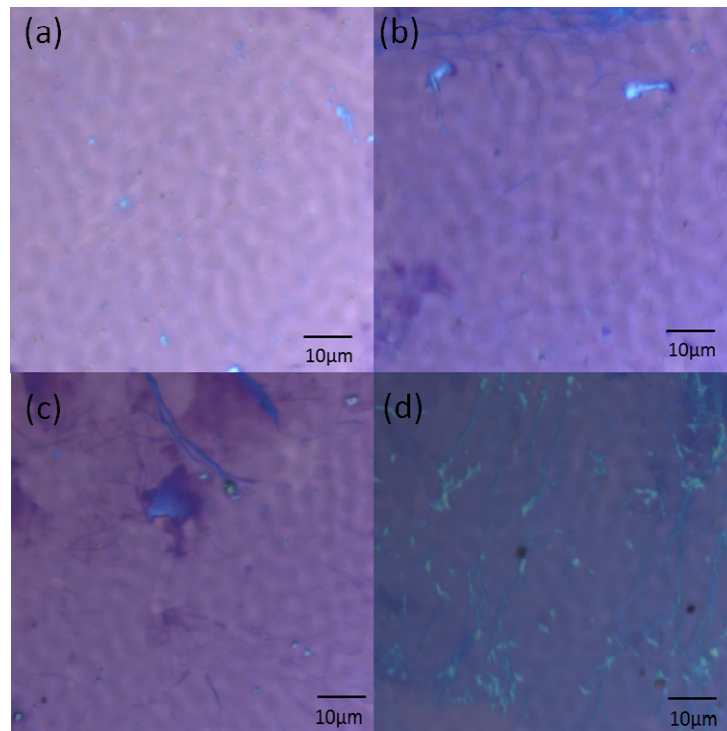


Figure 5. Images de microscopie optique des échantillons de graphène synthétisés à 850°C pendant 5 min avec une pression partielle de méthane de (a) 0,1 atm, (b) 0,2 atm, (c) 0,3 atm, (d) 0,4 atm.

L'observation des images de microscopie optique (figure 5) montre que l'uniformité du graphène devient de moins en moins bonne lorsque la pression partielle de méthane augmente dans le réacteur. Des zones de contraste (couleur) différent apparaissent de plus en plus nombreuses lorsque la quantité de méthane augmente. Cet effet est classiquement rapporté comme dû à l'accumulation de carbone aux joints de grain du nickel polycristallin. C'est la raison pour laquelle, nous avons modifié le catalyseur pour réduire et homogénéiser l'apport de carbone à la surface du métal.

Le système de catalyseur utilisé pour la suite ce travail de thèse met en œuvre le nickel et le cuivre ; il est simplement réalisé en enveloppant une feuille polycristalline de cuivre autour d'une feuille polycristalline de nickel (figure 6).

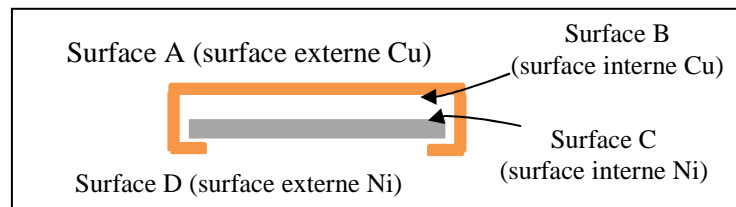


Figure 6. Système catalytique utilisé pour synthétiser du graphène monocouche par CVD à pression atmosphérique.

Les caractérisations par spectroscopie Raman et METHR du graphène obtenu qui mettent en évidence le graphène monocouche sont présentées sur les figures 7 et 8.

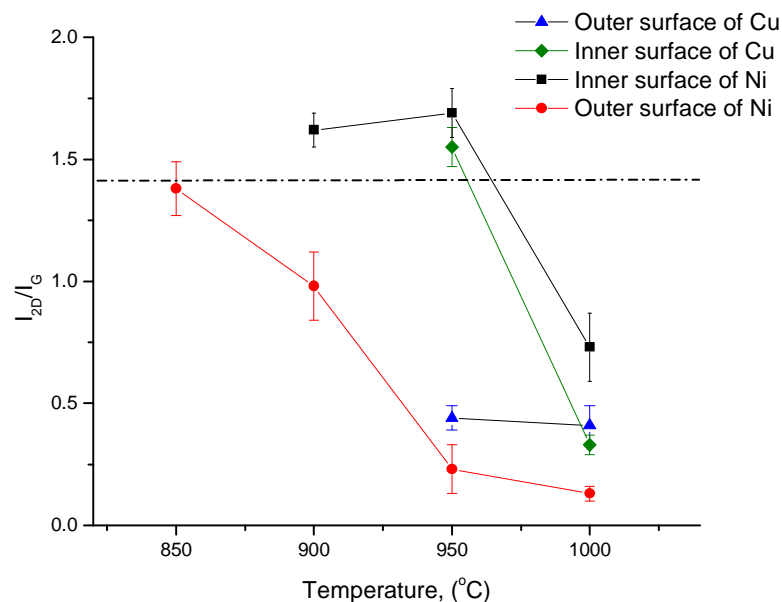


Figure 7.  $I_{2D}/I_G$  calculé à partir des spectres Raman des échantillons de graphène obtenu sur les 4 surfaces du catalyseur bimétallique Ni-Cu.

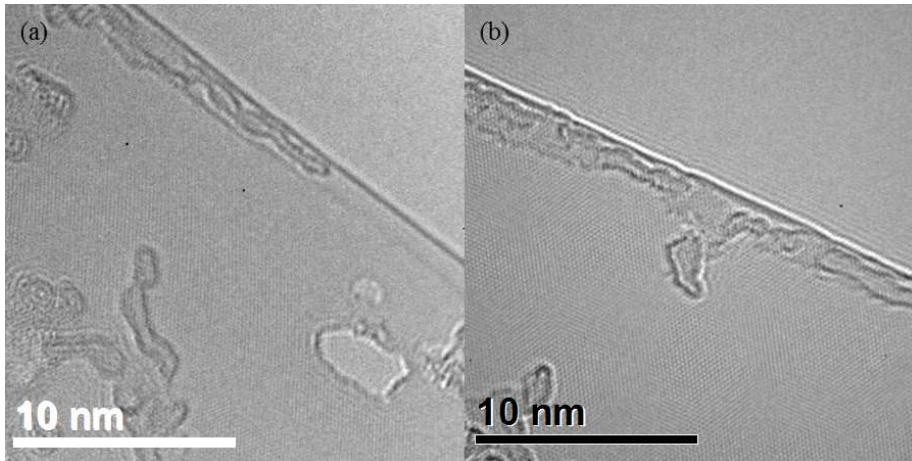


Figure 8. Images obtenues par METHR du graphène obtenu sur les surfaces internes (a) du nickel et (b) du cuivre.

$I_{2D}/I_G$  est supérieur à 1.4 (figure 7), signature de graphène monocouche, pour le graphène obtenu sur les surfaces internes du nickel et du cuivre pour des températures de 900-950°C, la croissance ayant eu lieu pendant 5 min à 0.2 atm de méthane. La présence de graphène monocouche est confirmée par METHR (figure 8) qui montre une bordure avec une seule ligne.

Le dispositif catalytique utilisé permet de limiter efficacement l'accès du carbone à la surface interne du nickel grâce au cuivre qui joue le rôle de bouclier. Le mécanisme de croissance propose que l'excès de carbone est drainé par les joints de grains du nickel polycristallin. Par ailleurs, la forte épaisseur de la feuille de nickel induit un gradient moyen de concentration en carbone, ce qui provoque une force de diffusion du carbone par les grains eux-mêmes, ce qui permet d'homogénéiser l'apport de carbone à la surface interne du nickel (figure 9, à gauche). Par ailleurs, le carbone présent à l'interface nickel-cuivre permet d'obtenir du graphène monocouche sur les 2 surfaces internes (celle du nickel et celle du cuivre). Pour les conditions de température, de durée et de pression partielle de méthane pour lesquelles l'apport de carbone devient trop important, du graphène multicouche est obtenu (figure 9, à droite).

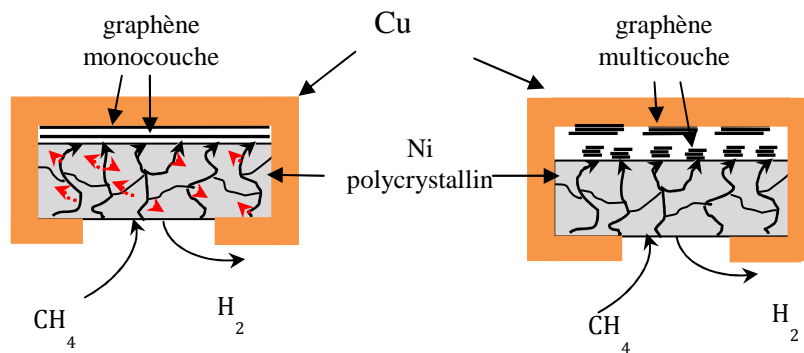


Figure 9. Mécanisme proposé pour la croissance de graphène monocouche avec le dispositif bi-métallique développé.

Des conditions optimales pour la croissance de graphène monocouche ont pu être trouvées dans le cas d'un réacteur de croissance soumis à une pression atmosphérique et avec des catalyseurs polycristallins.

### III.2. Séparation du graphène et recyclage du catalyseur

La séparation du graphène de la surface du catalyseur qui a été utilisé pour sa croissance est une question très importante pour plusieurs raisons. Il a été largement montré que le catalyseur métallique a souvent une interaction très forte avec le graphène. Si bien que les propriétés et les caractéristiques du graphène peuvent être affectées par la présence du substrat métallique. Sa séparation et dépôt sur des substrats plus neutres est donc nécessaire pour d'une part pouvoir étudier de façon fiable le graphène et d'autre part espérer l'intégrer à des dispositifs pour une utilisation pratique. De nombreuses méthodes ont été développées pour séparer le graphène de son catalyseur. La limitation de l'endommagement et de la contamination du graphène séparé est au cœur des préoccupations. Un procédé chimique couramment utilisé consiste à solubiliser complètement le métal dans une solution d'acide (acide nitrique par exemple). Dans ce cas, le catalyseur est utilisé une seule fois, ce qui augmente le coût de production du graphène. Dans ce travail, nous avons utilisé un agent chimique peu agressif (le nitrate de fer(III)) afin de pouvoir réutiliser la même feuille métallique de nickel plusieurs fois. Le travail d'optimisation a permis de mettre en évidence l'importance de la faible rugosité de la surface du catalyseur ainsi que l'absence de contamination pour un bon contrôle des caractéristiques du graphène obtenu. Alors que la

séparation en utilisant une solution de nitrate de fer(III) n'a pas pu être réalisée avec du graphène monocouche et multicouche, du graphène bicouche préparé a pu être séparé avec succès sans subir d'endommagement, ni être contaminé. Après optimisation de la concentration de la solution de nitrate de fer afin d'obtenir un détachement du graphène dans des délais raisonnables (2 jours) en limitant d'une part la contamination du graphène et d'autre part la consommation de la feuille de nickel ; cette dernière a pu être réutilisée 6 fois sans que les échantillons de graphène obtenu à chaque cycle ne montrent de différence significative. La figure 10 montre (en haut) la progression de la séparation du graphène bicouche dans les conditions utilisées, (en bas, à gauche) les 6 échantillons de graphène séparés et déposés sur des substrats de silicium et (en bas, à droite) une image typique de METHR du graphène bicouche obtenu à la 6ème croissance. La caractérisation par spectroscopie Raman permet de confirmer que les échantillons de graphène produit à chaque cycle ont des caractéristiques similaires (figure 11).

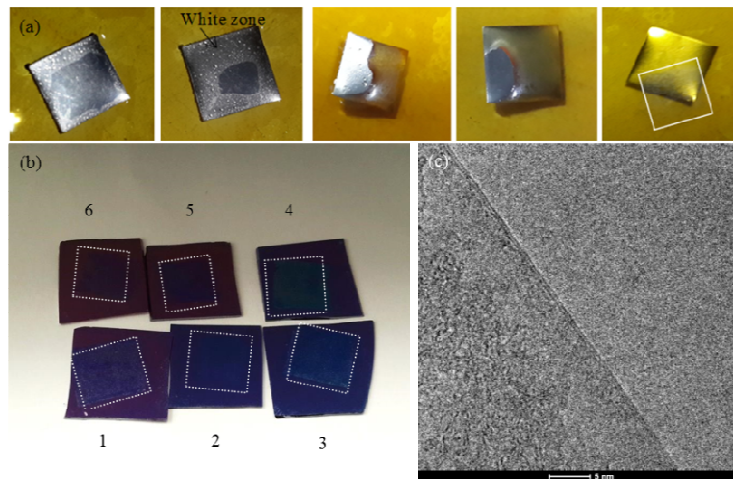


Figure 10. Progression de la séparation du graphène bicouche dans la solution de nitrate de fer(III) (en haut), les 6 échantillons de graphène séparés et déposés sur des substrats de silicium (en bas, à gauche) et image typique de METHR du graphène bicouche obtenu à la 6ème croissance (en bas, à droite).

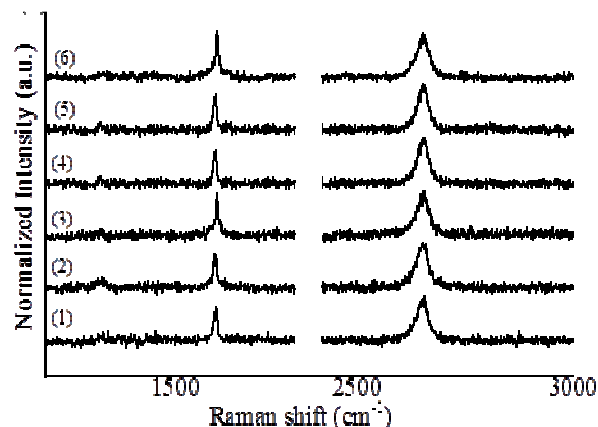


Figure 11. Spectres Raman des 6 graphènes synthétisés sur la même feuille de nickel dans les mêmes conditions.

Les observations visuelles du processus de séparation du graphène lors de sa mise en présence avec la solution de nitrate de fer(III) ont permis de soupçonner un phénomène d'intercalation jouant un rôle primordial pour séparer le graphène du nickel et permettre la réutilisation du nickel. La figure 12 montre les diffractogrammes obtenus par diffraction des rayons X du nickel après croissance et après séparation, ils mettent en évidence la présence de carbure de nickel ( $\text{Ni}_3\text{C}$ ) qui est rarement observé lors de la croissance de graphène.

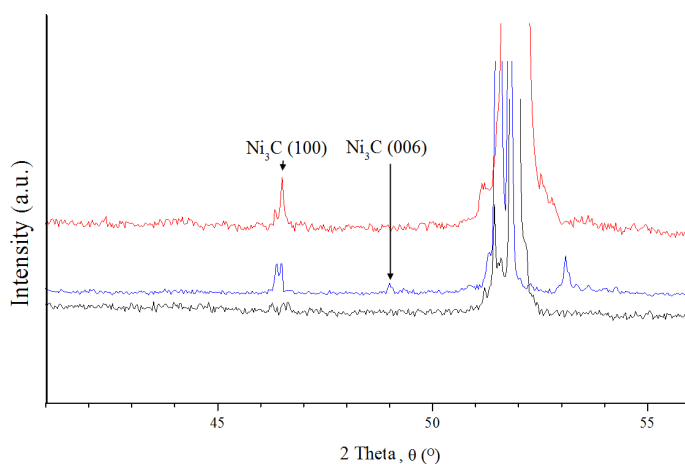


Figure 12. Diffractogrammes des substrats catalytiques après croissance (rouge) et après croissance et séparation en utilisant une solution de nitrate de fer (bleu) et une acide nitrique (noir).

Le carbure de nickel est connu pour ses propriétés anti-corrosion. Nous pensons qu'en couche fine à la surface du nickel, il peut être à l'origine de sa relativement bonne préservation lors de l'utilisation du nitrate de fer. Par contre, l'acide nitrique qui est un agent chimique plus fort peut attaquer  $Ni_3C$  (figure 12) qui se retrouve largement moins visible qu'après utilisation de la solution de nitrate de fer. Par ailleurs, cette couche de carbure de nickel facilite la séparation du graphène d'avec la surface de son substrat catalytique. Le  $Ni_3C$  formé joue ainsi un rôle important dans la réutilisation de la feuille de nickel. Sa formation est induite par la trempe de la réaction CVD. En effet, les atomes de carbone se retrouvent piégés en relativement grande quantité dans le nickel, ce qui permet la formation de  $Ni_3C$  (figure 13).

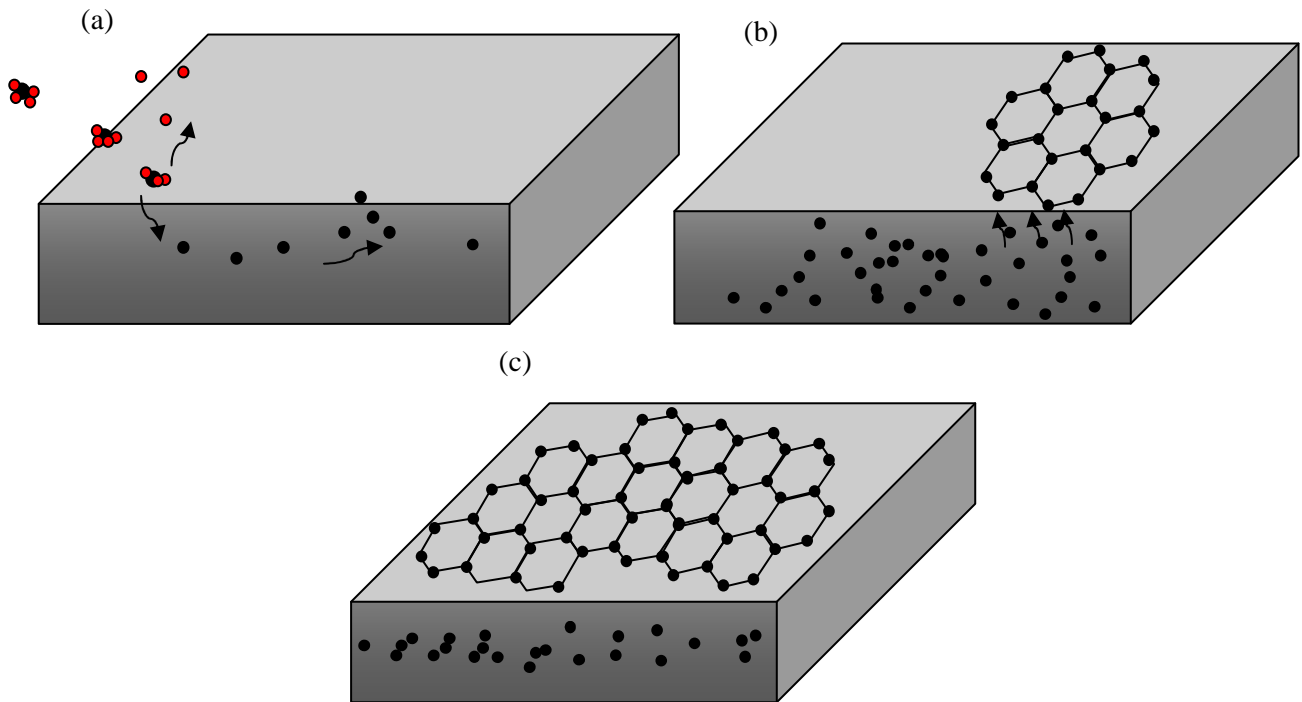


Figure 13. Mécanisme de formation du graphène et du  $Ni_3C$ . (a) A température, le méthane se décompose à la surface du catalyseur et les atomes de carbone se solubilisent dans le feuille de Ni. (b) Formation du graphène par ségrégation du carbone au-dessus du seuil de solubilité (c) Trempe: inhibition de la diffusion du carbone à la surface du Ni. L'hydrogène est en rouge et le carbone en noir.

## CONCLUSIONS ET PERSPECTIVES

Ce travail de thèse avait pour objectif de proposer des conditions expérimentales simples pour réaliser la croissance graphène monocouche par CVD sous pression atmosphérique sur un métal catalytique polycristallin, ce qui permet de diminuer fortement le coût de synthèse du graphène. Le travail expérimental d'optimisation réalisé sur le cuivre et le nickel de façon séparé a permis de trouver la gamme dans laquelle les conditions de température, de durée de réaction et de pression partielle de méthane devaient être variées.

Alors que sur le Cu, nous n'avons pas pu obtenir du graphène monocouche dans notre réacteur CVD, du graphène monocouche homogène a pu croître sur le nickel dans des conditions expérimentales peu contraignantes (par exemple, 850°C, 5 min, 0,2 atm de méthane). Néanmoins, comme souvent observé sur le nickel, une accumulation de carbone aux joints de grains de la feuille catalytique conduit à du graphène multicouche. Afin d'améliorer l'homogénéité du graphène, un nouveau dispositif catalytique a été proposé. Il est simplement constitué de deux feuilles de Cu et de Ni assemblés en bicouche métallique. Il permet de limiter efficacement et d'homogénéiser l'apport de carbone à l'interface Ni/Cu. La haute uniformité et qualité cristalline du graphène monocouche obtenu ont été mises en évidence par les caractérisations réalisées par spectroscopie Raman et METHR.

Dans les conditions utilisées, le refroidissement rapide du catalyseur en fin de synthèse est primordial d'une part pour obtenir du graphène monocouche et d'autre part pour faciliter la séparation du graphène de son substrat métallique. Nous avons montré que le Ni<sub>3</sub>C formé lors de la trempe de la réaction agit comme une couche protectrice du nickel et permet un phénomène d'intercalation de l'agent chimique utilisé pour séparer le graphène. La réutilisation de la feuille de Ni a pu ainsi être envisagée pour la synthèse de graphène bicouche. Elle a pu être réutilisée 6 fois sans causer d'écart significatif de la qualité et l'uniformité du graphène bicouche formé. Le Ni<sub>3</sub>C est en effet capable de limiter l'effet de gravure de la feuille de Ni. Ce travail a donc démontré avec succès que le coût moyen pour synthétiser du graphène avec un nombre limité de couches (1 ou 2) de haute qualité de façon contrôlée pouvait être réduit grâce à des procédés simples à mettre en œuvre.



### **Quelques références importantes**

Allen, M. J., Tung, V. C. & Kaner, R. B. (2009) Honeycomb carbon: A review of graphene. *chemical reviews*, 110, 132-145.

Batzill, M. (2012) The surface science of graphene: Metal interfaces, CVD synthesis, nanoribbons, chemical modifications, and defects. *Surface Science Reports*, 67, 83-115.

Bianco, A., Cheng, H.-M., Enoki, T., Gogotsi, Y., Hurt, R. H., Koratkar, N., Kyotani, T., Monthieux, M., Park, C. R., Tascon, J. M. D. & Zhang, J. (2013) All in the graphene family: A recommended nomenclature for two-dimensional carbon materials. *Carbon*, 65, 1-6.

Chen, S., Cai, W., Piner, R. D., Suk, J. W., Wu, Y., Ren, Y., Kang, J. & Ruoff, R. S. (2011) Synthesis and characterization of large-area graphene and graphite films on commercial Cu-Ni alloy foils. *Nano Letters*, 11, 3519-3525.

Dahal, A. & Batzill, M. (2014) Graphene-nickel interfaces: a review. *Nanoscale*, 6, 2548-2562.

Ferrari, A. C., Meyer, J. C., Scardaci, V., Casiraghi, C., Lazzeri, M., Mauri, F., Piscanec, S., Jiang, D., Novoselov, K. S., Roth, S. & Geim, A. K. (2006) Raman Spectrum of Graphene and Graphene Layers. *Physical Review Letters*, 97, 187401.

Gao, L., Guest, J. R. & Guisinger, N. P. (2010) Epitaxial graphene on Cu(111). *Nano Letters*, 10, 3512-3516.

Gao, L., Ren, W., Xu, H., Jin, L., Wang, Z., Ma, T., Ma, L.-P., Zhang, Z., Fu, Q., Peng, L.-M., Bao, X. & Cheng, H.-M. (2012) Repeated growth and bubbling transfer of graphene with millimetre-size single-crystal grains using platinum. *Nat Commun*, 3, 699.

Geim, A. K. & Novoselov, K. S. (2007) The rise of graphene. *Nature Materials*, 6, 183-191.

Li, X., Cai, W., Colombo, L. & Ruoff, R. S. (2009) Evolution of graphene growth on ni and cu by carbon isotope labeling. *Nano Letters*, 9, 4268-4272.

Liao, C.-D., Lu, Y.-Y., Tamalampudi, S. R., Cheng, H.-C. & Chen, Y.-T. (2013) Chemical vapor deposition synthesis and raman spectroscopic characterization of large-area graphene sheets. *The Journal of Physical Chemistry A*, 117, 9454-9461.

Losurdo, M., Giangregorio, M. M., Capezzuto, P. & Bruno, G. (2011) Graphene CVD growth on copper and nickel: role of hydrogen in kinetics and structure. *Physical Chemistry Chemical Physics*, 13, 20836-20843.

Novoselov, K. S., Geim, A. K., Morozov, S. V., Jiang, D., Katsnelson, M. I., Grigorieva, I. V., Dubonos, S. V. & Firsov, A. A. (2005) Two-dimensional gas of massless Dirac fermions in graphene. *Nature*, 438, 197-200.

Novoselov, K. S., Geim, A. K., Morozov, S. V., Jiang, D., Zhang, Y., Dubonos, S. V., Grigorieva, I. V. & Firsov, A. A. (2004) Electric field effect in atomically thin carbon films. *Science*, 306, 666-669.

Peng, Z., Yan, Z., Sun, Z. & Tour, J. M. (2012) Direct growth of bilayer graphene on SiO<sub>2</sub> substrates by carbon diffusion through nickel. *ACS Nano*, 5, 8241-8247.

Reina, A., Jia, X., Ho, J., Nezich, D., Son, H., Bulovic, V., Dresselhaus, M. S. & Kong, J. (2008) Large area, few-layer graphene films on arbitrary substrates by chemical vapor deposition. *Nano Letters*, 9, 30-35.

Singleton, M. & Nash, P. (1989) The C-Ni (Carbon-Nickel) system. *Bulletin of Alloy Phase Diagrams*, 10, 121-126.

Son, I. H., Song, H. J., Kwon, S., Bachmatiuk, A., Lee, S. J., Benayad, A., Park, J. H., Choi, J.-Y., Chang, H. & Rummeli, M. H. (2014) CO<sub>2</sub> Enhanced chemical vapor deposition growth of few-layer graphene over NiO<sub>x</sub>. *ACS Nano*, 8, 9224-9232.

Tyagi, P., Robinson, Z. R., Munson, A., Magnuson, C. W., Chen, S., McNeilan, J. D., Moore, R. L., Piner, R. D., Ruoff, R. S. & Ventrice JR, C. A. (2015) Characterization of graphene films grown on CuNi foil substrates. *Surface Science*, 634, 16-24.

Wang, Y., Zheng, Y., Xu, X., Dubuisson, E., Bao, Q., Lu, J. & Loh, K. P. (2011) electrochemical delamination of cvd-grown graphene film: Toward the recyclable use of copper catalyst. *ACS Nano*, 5, 9927-9933.

Wu, Y., Chou, H., Ji, H., Wu, Q., Chen, S., Jiang, W., Hao, Y., Kang, J., Ren, Y., Piner, R. D. & Ruoff, R. S. (2012) Growth mechanism and controlled synthesis of AB-stacked bilayer graphene on Cu-Ni alloy foils. *ACS Nano*, 6, 7731-7738.

Xu, M., Fujita, D., Sagisaka, K., Watanabe, E. & Hanagata, N. (2011) Production of extended single-layer graphene. *ACS Nano*, 5, 1522-1528.

Yan, Z., Peng, Z., Sun, Z., Yao, J., Zhu, Y., Liu, Z., Ajayan, P. M. & Tour, J. M. (2011) Growth of bilayer graphene on insulating substrates. *ACS Nano*, 5, 8187-8192.

Yu, Q., Jauregui, L. A., Wu, W., Colby, R., Tian, J., Su, Z., Cao, H., Liu, Z., Pandey, D., Wei, D., Chung, T. F., Peng, P., Guisinger, N. P., Stach, E. A., Bao, J., Pei, S.-S. & Chen, Y. P. (2011) Control and characterization of individual grains and grain boundaries in graphene grown by chemical vapour deposition. *Nat Mater*, 10, 443-449.

Zhang, Y., Gomez, L., Ishikawa, F. N., Madaria, A., Ryu, K., Wang, C., Badmaev, A. & Zhou, C. (2010) Comparison of graphene growth on single-crystalline and polycrystalline Ni by chemical vapor deposition. *The Journal of Physical Chemistry Letters*, 1, 3101-3107.

Zhu, Y., Murali, S., Cai, W., Li, X., Suk, J. W., Potts, J. R. & Ruoff, R. S. (2010) Graphene and graphene oxide: Synthesis, Properties, and applications. *Advanced Materials*, 22, 3906-3924.



## **Abstract**

Graphene is a layer of  $sp^2$  hybridized carbon atoms with a thickness of only one atom. It possesses various magnificent properties that are not shared by other materials. To date, Chemical Vapor Deposition (CVD) is a promising method to produce wafer-scale graphene. From our study, monolayer graphene was grown directly on polycrystalline Ni foil under simple atmospheric pressure CVD with the assist of fast cooling. On the other hand, another facile technique was successful to grow uniform monolayer graphene simultaneously on both polycrystalline Ni and Cu foils using a Ni-Cu bilayer catalyst. The application of post-CVD fast cooling encourages the formation of  $Ni_3C$  within the Ni foil, which subsequently enables the Ni foil to be reused again up to 6 cycles without causing a huge deviation. This work has successfully demonstrated a simple, novel and cost effective route to synthesize monolayer graphene with high quality.

## **Résumé**

Le graphène est une couche de carbone d'une épaisseur atomique pour laquelle les atomes de carbone sont hybridés  $sp^2$ . Il possède diverses propriétés remarquables supérieures à celles des autres matériaux connus. Le dépôt chimique en phase vapeur (CVD) est une méthode prometteuse pour produire du graphène monocouche. Dans cette étude, du graphène monocouche a pu être synthétisé directement sur une feuille de Ni polycristallin par CVD sous pression atmosphérique à l'aide d'un refroidissement rapide. Par ailleurs, nous proposons une technique simple pour préparer du graphène monocouche homogène dont la croissance est réalisée simultanément sur deux feuilles de Cu et de Ni assemblés en bicouche métallique. L'application du refroidissement rapide induit la formation de  $Ni_3C$ , qui permet de réutiliser la feuille de Ni jusqu'à 6 fois sans causer d'écart significatif de la qualité et l'uniformité du graphène produit. Ce travail a donc démontré avec succès que le coût moyen pour synthétiser une monocouche de graphène de haute qualité pouvait être réduit avec des procédés simples à mettre en œuvre.